

UNIVERSITY OF KWAZULU-NATAL

**BINARY VAPOUR-LIQUID EQUILIBRIA FOR OXYGEN-  
CONTAINING COMPOUNDS**

**Jeremy Clive Pillay**

**2009**

## PREFACE

The work presented in this dissertation entitled “Binary Vapour-Liquid Equilibria for Oxygen-Containing Compounds” was performed at the School of Chemical Engineering, University of KwaZulu-Natal, Howard College Campus, from January 2007 to December 2009. The work was supervised by Professor D. Ramjugernath and Dr. P. Naidoo and has been submitted in fulfillment of the academic requirements for the degree of Master of Science in Engineering at the School of Chemical Engineering, University of KwaZulu-Natal, Durban

## DECLARATION

I, Jeremy Clive Pillay, declare that

- (i) The research reported in this dissertation/thesis, except where otherwise indicated, is my original work.
- (ii) This dissertation/thesis has not been submitted for any degree or examination at any other university.
- (iii) This dissertation/thesis does not contain other persons’ data, pictures, graphs or other information, unless specifically acknowledged as being sourced from other persons.
- (iv) This dissertation/thesis does not contain other persons’ writing, unless specifically acknowledged as being sourced from other researchers. Where other written sources have been quoted, then:
  - a) their words have been re-written but the general information attributed to them has been referenced;
  - b) where their exact words have been used, their writing has been placed inside quotation marks, and referenced.
- (v) Where I have reproduced a publication of which I am an author, co-author or editor, I have indicated in detail which part of the publication was actually written by myself alone and have fully referenced such publications.

- (vi) This dissertation/thesis does not contain text, graphics or tables copied and pasted from the Internet, unless specifically acknowledged, and the source being detailed in the dissertation/thesis and in the References sections.

Signed:

\_\_\_\_\_  
J.C. Pillay

\_\_\_\_\_  
Date

As the candidate's supervisor, I agree/do not agree to the submission of this thesis.

\_\_\_\_\_  
Prof. D. Ramjugernath

Date\_\_\_\_\_

## **ACKNOWLEDGEMENTS**

I would like to take this opportunity to acknowledge and thank the people and organizations who have made a significant contribution to this project:

- My supervisors, Prof. D. Ramjugernath, Dr. P. Naidoo and Prof. J.D. Raal for their support and guidance during this study
- Dr. B. Van Dyk for his assistance with Aspen, and his guidance and motivation
- The workshop and laboratory staff at UKZN
- Sasol Limited for financial assistance during my degree
- My dear friend, Cameel Baichan, for continuous support and motivation during this study

## ABSTRACT

In this study, there was a need for VLE data for systems of oxygen-containing organic compounds. Experimental VLE data are presented for the following binary systems:

- a) 2-propanone (1) + 2-butanol (2) at 333.15K, 353.15K and 373.15K
- b) 2-propanone (1) + n-propanoic acid (2) at 333.15K, 353.15K and 373.15K
- c) 1-propanol (1) + n-butanoic acid (2) at 333.15K and 353.15K

A test system (cyclohexane + ethanol at 323.15K) was measured to confirm the accuracy of the method and apparatus. With the exception of the test system, data for all the other binary systems investigated in this study are currently not available in the open literature.

The dynamic recirculating stills of Joseph (2001) and Reddy (2006) were utilised to undertake the measurements. The experimental vapour pressure data measured in this study and the results obtained for the highly non-ideal test system were in excellent agreement with the literature data. It was thus concluded that the apparatus and operating procedures used were capable of producing highly accurate VLE data and confidence in the new data measured was obtained.

Thermodynamic consistency testing was performed on the experimental VLE data using the point test (Van Ness et al., 1973), which provided an indication of the data's quality and reliability. The data were thereafter subjected to data correlation to enable interpolation of the data and extrapolation to conditions other than those measured. Appropriate thermodynamic models (taking into account vapour-phase association in particular) were correlated to the data using the combined approach to VLE ( $\gamma$ - $\Phi$  method). For the calculation of the fugacity coefficients, three methods were used viz. the virial EOS and the Hayden-O'Connell correlation (1975); chemical theory and the Nothnagel et al. Formulation (1973); and the VPA/IK-CAPE EOS (Abbott and Van Ness, 1992). Three activity coefficients models were also used viz. the Wilson (1964) model; the NRTL model (Renon and Prausnitz, 1968); and the UNIQUAC model (Abrams and Prausnitz, 1975). In general, the models fitted the data well and the model parameters that were acquired are included. Theoretical developments involving associating components are ongoing.

## TABLE OF CONTENTS

	<b>Page</b>
<b>PREFACE</b> .....	ii
<b>ACKNOWLEDGEMENTS</b> .....	iv
<b>ABSTRACT</b> .....	v
<b>TABLE OF CONTENTS</b> .....	vi
<b>LIST OF FIGURES</b> .....	x
<b>LIST OF TABLES</b> .....	xxi
<b>NOMENCLATURE</b> .....	xxv
<b>CHAPTER 1: INTRODUCTION</b> .....	1
<b>CHAPTER 2: BINARY SYSTEMS CHOSEN FOR EXPERIMENTATION</b> .....	3
<b>2.1. Carboxylic acids</b> .....	4
<b>2.2. Alcohols</b> .....	7
<b>2.3. Ketones</b> .....	8
<b>CHAPTER 3: THE THEORETICAL TREATMENT OF VLE DATA</b> .....	9
<b>3.1. Fundamental thermodynamic relationships and equations</b> .....	9
<b>3.2. Chemical potential</b> .....	11
<b>3.3. Fugacity and fugacity coefficients</b> .....	12
<b>3.4. Activity and activity coefficients</b> .....	14
<b>3.5. Theoretical VLE methods</b> .....	16
<b>3.5.1. The combined method (gamma-phi approach, activity coefficient approach)</b> .....	17

<b>3.5.2. The direct method (phi-phi approach, equation of state approach)</b>	20
<b>3.6. Thermodynamic models</b>	21
<b>3.6.1. Equations-of-state</b>	21
3.6.1.1. The virial EOS and the Hayden-O'Connell correlation (HOC)	21
3.6.1.2. Chemical theory and the Nothnagel et al. formulation (NTH)	22
3.6.1.3. The VPA/IK-CAPE EOS (VPA)	24
3.6.1.4. The Statistical Associating Fluid Theory (SAFT) and Cubic Plus Association (CPA) Models	25
<b>3.6.2. Activity coefficient/Gibbs excess (<math>G^E</math>) models</b>	26
3.6.2.1. The Wilson (1964) model	27
3.6.2.2. The NRTL (1968) model	29
3.6.2.3. The UNIQUAC (1975) model	30
<b>3.7. Thermodynamic consistency testing</b>	33
<b>3.7.1. The Gibbs-Duhem equation</b>	34
<b>3.7.2. Slope/Differential test</b>	36
<b>3.7.3. Area/Integral test</b>	37
<b>3.7.4. Point/Residual (Van Ness-Byer-Gibbs) test</b>	40
<b>3.7.5 Direct test</b>	43
<b>CHAPTER 4: EQUIPMENT DESCRIPTION</b>	46
<b>4.1. The VLE apparatus of Joseph (2001)</b>	46
<b>4.2. The VLE apparatus of Reddy (2006)</b>	49
<b>4.3. Auxiliary equipment</b>	53
<b>4.3.1. Auxiliary equipment on the apparatus of Joseph (2001)</b>	53
4.3.1.1. Pressure measurement and stabilization/control	53
4.3.1.2. Temperature measurement and control	54
<b>4.3.2. Auxiliary equipment on the apparatus of Reddy (2006)</b>	54
4.3.2.1. Pressure measurement and stabilization/control	54
4.3.2.2. Temperature measurement and control	55
<b>4.3.3 Sampling and composition analysis</b>	55

<b>CHAPTER 5: EXPERIMENTAL PROCEDURE.....</b>	<b>57</b>
<b>5.1. Preparation of experimental apparatus.....</b>	<b>57</b>
5.1.1 Cleaning of the VLE still .....	57
5.1.2 Leak detection.....	57
<b>5.2. Temperature, pressure and composition calibrations.....</b>	<b>58</b>
5.2.1. Pressure transmitter calibration.....	58
5.2.2. Temperature sensor calibration.....	58
5.2.3. Gas chromatograph detector calibration.....	59
<b>5.3. Operating procedures.....</b>	<b>60</b>
<b>5.3.1. Isobaric operation.....</b>	<b>60</b>
5.3.1.1. Start-up procedure.....	60
5.3.1.2. Determination of equilibrium .....	62
5.3.1.3. Phase composition determinations.....	64
5.3.1.4. Effecting composition changes within the VLE apparatus.....	64
5.3.1.5. Shut-down procedure.....	65
<b>5.3.2. Isothermal operation.....</b>	<b>65</b>
 <b>CHAPTER 6: EXPERIMENTAL RESULTS.....</b>	 <b>66</b>
<b>6.1. Purity of materials.....</b>	<b>66</b>
<b>6.2. Equipment calibrations and accuracy of measurements.....</b>	<b>68</b>
6.2.1. Pressure and temperature sensor calibrations.....	68
6.2.2. GC calibrations and operating conditions.....	71
<b>6.3. Systems measured.....</b>	<b>74</b>
<b>6.4. Pure component vapour pressure measurements.....</b>	<b>75</b>
<b>6.5. Binary vapour-liquid equilibrium measurements.....</b>	<b>83</b>
6.5.1. Results for the test system: cyclohexane (1) + ethanol (2) .....	83
6.5.2. Results for the system: 2-propanone (1) + 2-butanol (2) .....	86
6.5.3. Results for the system: 2-propanone (1) + n-propanoic acid (2) .....	92
6.5.4. Results for the system: 1-propanol (1) + n-butanoic acid (2) .....	98
 <b>CHAPTER 7: DATA ANALYSIS AND DISCUSSION.....</b>	 <b>103</b>
<b>7.1. Experimental vapour pressure data for pure components.....</b>	<b>103</b>

<b>7.2. Determination of experimental activity coefficients.....</b>	<b>105</b>
<b>7.3. Binary VLE data reduction.....</b>	<b>106</b>
<b>7.4. Thermodynamic consistency testing.....</b>	<b>106</b>
<b>7.4.1. Point test results: 2-propanone (1) + 2-butanol (2) .....</b>	<b>108</b>
<b>7.4.2. Point test results: 2-propanone (1) + n-propanoic acid (2) .....</b>	<b>115</b>
<b>7.4.3. Point test results: 1-propanol (1) + n-butanoic acid (2) .....</b>	<b>118</b>
<b>7.5. Final data reduction analyses.....</b>	<b>120</b>
<b>7.5.1 Final regression results: 2-propanone (1) + 2-butanol (2) .....</b>	<b>120</b>
<b>7.5.2 Final regression results: 2-propanone (1) + n-propanoic acid (2) ....</b>	<b>129</b>
<b>7.5.3 Final regression results: 1-propanol (1) + n-butanoic acid (2) .....</b>	<b>137</b>
<b>7.6. The effect of excluded data points on model parameters obtained.....</b>	<b>143</b>
<b>CHAPTER 8: CONCLUSIONS.....</b>	<b>147</b>
<b>8.1. Experimental aspects.....</b>	<b>147</b>
<b>8.2. Theoretical aspects.....</b>	<b>148</b>
<b>CHAPTER 9: RECOMMENDATIONS AND FUTURE WORK.....</b>	<b>150</b>
<b>REFERENCES.....</b>	<b>152</b>
<b>Appendix A.....</b>	<b>160</b>
<b>A.1. The criterion for equilibrium: .....</b>	<b>160</b>
<b>A.2. Fugacity of a pure liquid: .....</b>	<b>163</b>
<b>Appendix B (Residuals for the point test) .....</b>	<b>165</b>

## LIST OF FIGURES

- Figure 2-1 The carboxyl functional group
- Figure 2-2 Structures of carboxylic acids used in this study
- Figure 2-3 Dimer formation in carboxylic acids through hydrogen bonding
- Figure 2-4 The hydroxyl functional group
- Figure 2-5 Hydrogen bonding in alcohols
- Figure 2-6 The generalized structure of a ketone
- Figure 3-1 Typical plot for the area test
- Figure 4-1 Schematic diagram of the glass VLE still taken from Joseph (2001)
- Figure 4-2 Schematic Block diagram of the glass VLE apparatus of Joseph (2001)
- Figure 4-3 Schematic diagram of the stainless steel VLE still taken from Reddy (2006)
- Figure 4-4 Schematic diagram of the equipment layout of the steel apparatus taken from Reddy (2006)
- Figure 5-1 Typical temperature response curve illustrating the “plateau region” for a “well-behaved compound”
- Figure 6-1 Calibration plot for the pressure transmitter on the apparatus of Joseph (2001) for the 0 to 10KPa pressure range

- Figure 6-2 Calibration plot for the pressure transmitter on the apparatus of Joseph (2001) for the 10 to 100KPa pressure range
- Figure 6-3 Calibration plot for the temperature sensor on the apparatus of Joseph (2001)
- Figure 6-4 Calibration plot for the temperature sensor on the apparatus of Reddy (2006)
- Figure 6-5 Vapour pressure curve for 2-butanol
- Figure 6-6 Vapour pressure curve for 1-propanol
- Figure 6-7 Vapour pressure curve for n-butanoic acid
- Figure 6-8 Vapour pressure curve for n-propanoic acid
- Figure 6-9 Vapour pressure curve for 2-propanone
- Figure 6-10 Vapour pressure curve for cyclohexane
- Figure 6-11 GC calibration plot for cyclohexane (1) + ethanol (2) in the ethanol rich region
- Figure 6-12 GC calibration plot for cyclohexane (1) + ethanol (2) in the cyclohexane rich region
- Figure 6-13 Experimental P- $x_1$ - $y_1$  data for the cyclohexane (1)+ ethanol (2) system at 323.15K
- Figure 6-14  $x_1$ - $y_1$  data for the cyclohexane (1)+ ethanol (2) system at 323.15K
- Figure 6-15 GC calibration plot for 2-propanone (1) + 2-butanol (2) in the 2-butanol rich region

- Figure 6-16 GC calibration plot for 2-propanone (1) + 2-butanol (2) in the 2-propanone rich region
- Figure 6-17 Experimental P- $x_1$ - $y_1$  data for the 2-propanone (1) + 2-butanol (2) system at 333.15K
- Figure 6-18  $x_1$ - $y_1$  data for the 2-propanone (1) + 2-butanol (2) system at 333.15K
- Figure 6-19 Experimental P- $x_1$ - $y_1$  data for the 2-propanone (1) + 2-butanol (2) system at 353.15K
- Figure 6-20  $x_1$ - $y_1$  data for the 2-propanone (1) + 2-butanol (2) system at 353.15K
- Figure 6-21 Experimental P- $x_1$ - $y_1$  data for the 2-propanone (1) + 2-butanol (2) system at 373.15K
- Figure 6-22  $x_1$ - $y_1$  data for the 2-propanone (1) + 2-butanol (2) system at 373.15K
- Figure 6-23 GC calibration plot for 2-propanone (1) + n-propanoic acid (2) in the n-propanoic acid rich region
- Figure 6-24 GC calibration plot for 2-propanone (1) + n-propanoic acid (2) in the 2-propanone rich region
- Figure 6-25 Experimental P- $x_1$ - $y_1$  data for the 2-propanone (1) + n-propanoic acid (2) system at 333.15K
- Figure 6-26  $x_1$ - $y_1$  data for the 2-propanone (1) + n-propanoic acid (2) system at 333.15K
- Figure 6-27 Experimental P- $x_1$ - $y_1$  data for the 2-propanone (1) + n-propanoic acid (2) system at 353.15K
- Figure 6-28  $x_1$ - $y_1$  data for the 2-propanone (1) + n-propanoic acid (2) system at 353.15K

- Figure 6-29 Experimental P- $x_1$ - $y_1$  data for the 2-propanone (1) + n-propanoic acid (2) system at 373.15K
- Figure 6-30  $x_1$ - $y_1$  data for the 2-propanone (1) + n-propanoic acid (2) system at 373.15K
- Figure 6-31 GC calibration plot with a linear fit to the data for 1-propanol (1) + n-butanoic acid (2) in the n-butanoic acid rich region
- Figure 6-32 GC calibration plot with a linear fit to the data for 1-propanol (1) + n-butanoic acid (2) in the 1-propanol rich region
- Figure 6-33 GC calibration plot with a quadratic fit to the data for 1-propanol (1) + n-butanoic acid (2) in the n-butanoic acid rich region
- Figure 6-34 GC calibration plot with a quadratic fit to the data for 1-propanol (1) + n-butanoic acid (2) in the 1-propanol rich region
- Figure 6-35 Experimental P- $x_1$ - $y_1$  data for the 1-propanol (1) + n-butanoic acid (2) system at 333.15K
- Figure 6-36  $x_1$ - $y_1$  data for the 1-propanol (1) + n-butanoic acid (2) system at 333.15K
- Figure 6-37 Experimental P- $x_1$ - $y_1$  data for the 1-propanol (1) + n-butanoic acid (2) system at 353.15K
- Figure 6-38  $x_1$ - $y_1$  data for the 1-propanol (1) + n-butanoic acid (2) system at 353.15K
- Figure 7-1 Experimental liquid-phase activity coefficients for the 2-propanone (1) + n-propanoic acid (2) system at 333.15K using the conventional method
- Figure 7-2 Point test (varying EOS): pressure-residual for the 2-propanone (1) + 2-butanol (2) system at 333.15K

- Figure 7-3 Point test (varying EOS):  $\Delta y_1$  for the 2-propanone (1) + 2-butanol (2) system at 333.15K
- Figure 7-4 Point test (varying activity coefficient model): pressure-residual for the 2-propanone (1) + 2-butanol (2) system at 333.15K
- Figure 7-5 Point test (varying activity coefficient model):  $\Delta y_1$  for the 2-propanone (1) + 2-butanol (2) system at 333.15K
- Figure 7-6 Comparison between HOC, VPA and NTH model fits to P- $x_1$ - $y_1$  data for the 2-propanone (1) + 2-butanol (2) system at 333.15K
- Figure 7-7 Comparison between HOC, VPA and NTH model fits to  $x_1$ - $y_1$  data for the 2-propanone (1) + 2-butanol (2) system at 333.15K
- Figure 7-8 Comparison between NRTL, WILSON and UNIQUAC model fits to P- $x_1$ - $y_1$  data for the 2-propanone (1) + 2-butanol (2) system at 333.15K
- Figure 7-9 Comparison between NRTL, WILSON and UNIQUAC model fits to  $x_1$ - $y_1$  data for the 2-propanone (1) + 2-butanol (2) system at 333.15K
- Figure 7-10 Comparison between HOC, VPA and NTH model fits to P- $x_1$ - $y_1$  data for the 2-propanone (1) + 2-butanol (2) system at 353.15K
- Figure 7-11 Comparison between HOC, VPA and NTH model fits to  $x_1$ - $y_1$  data for the 2-propanone (1) + 2-butanol (2) system at 353.15K
- Figure 7-12 Comparison between NRTL, WILSON and UNIQUAC model fits to experimental P- $x_1$ - $y_1$  data for the 2-propanone (1) + 2-butanol (2) system at 353.15K

- Figure 7-13 Comparison between NRTL, WILSON and UNIQUAC model fits to experimental  $x_1$ - $y_1$  data for the 2-propanone (1) + 2-butanol (2) system at 353.15K
- Figure 7-14 Comparison between HOC, VPA and NTH model fits to P- $x_1$ - $y_1$  data for the 2-propanone (1) + 2-butanol (2) system at 373.15K
- Figure 7-15 Comparison between HOC, VPA and NTH model fits to  $x_1$ - $y_1$  data for the 2-propanone (1) + 2-butanol (2) system at 373.15K
- Figure 7-16 Comparison between NRTL, WILSON and UNIQUAC model fits to experimental P- $x_1$ - $y_1$  data for the 2-propanone (1) + 2-butanol (2) system at 373.15K
- Figure 7-17 Comparison between NRTL, WILSON and UNIQUAC model fits to experimental  $x_1$ - $y_1$  data for the 2-propanone (1) + 2-butanol (2) system at 373.15K
- Figure 7-18 Comparison between HOC, VPA and NTH model fits to P- $x_1$ - $y_1$  data for the 2-propanone (1) + n-propanoic acid (2) system at 333.15K
- Figure 7-19 Comparison between HOC, VPA and NTH model fits to  $x_1$ - $y_1$  data for the 2-propanone (1) + n-propanoic acid (2) system at 333.15K
- Figure 7-20 Comparison between NRTL, WILSON and UNIQUAC model fits to experimental P- $x_1$ - $y_1$  data for the 2-propanone (1) + n-propanoic acid (2) system at 333.15K
- Figure 7-21 Comparison between NRTL, WILSON and UNIQUAC model fits to experimental  $x_1$ - $y_1$  data for the 2-propanone (1) + n-propanoic acid (2) system at 333.15K

- Figure 7-22 Comparison between HOC, VPA and NTH model fits to P- $x_1$ - $y_1$  data for the 2-propanone (1) + n-propanoic acid (2) system at 353.15K
- Figure 7-23 Comparison between HOC, VPA and NTH model fits to  $x_1$ - $y_1$  data for the 2-propanone (1) + n-propanoic acid (2) system at 353.15K
- Figure 7-24 Comparison between NRTL, WILSON and UNIQUAC model fits to experimental P- $x_1$ - $y_1$  data for the 2-propanone (1) + n-propanoic acid (2) system at 353.15K
- Figure 7-25 Comparison between NRTL, WILSON and UNIQUAC model fits to experimental  $x_1$ - $y_1$  data for the 2-propanone (1) + n-propanoic acid (2) system at 353.15K
- Figure 7-26 Comparison between HOC, VPA and NTH model fits to P- $x_1$ - $y_1$  data for the 2-propanone (1) + n-propanoic acid (2) system at 373.15K
- Figure 7-27 Comparison between HOC, VPA and NTH model fits to  $x_1$ - $y_1$  data for the 2-propanone (1) + n-propanoic acid (2) system at 373.15K
- Figure 7-28 Comparison between NRTL, WILSON and UNIQUAC model fits to experimental P- $x_1$ - $y_1$  data for the 2-propanone (1) + n-propanoic acid (2) system at 373.15K
- Figure 7-29 Comparison between NRTL, WILSON and UNIQUAC model fits to experimental  $x_1$ - $y_1$  data for the 2-propanone (1) + n-propanoic acid (2) system at 373.15K
- Figure 7-30 Comparison between HOC, VPA and NTH model fits to P- $x_1$ - $y_1$  data for the 1-propanol (1) + n-butanoic acid (2) system at 333.15K
- Figure 7-31 Comparison between HOC, VPA and NTH model fits to  $x_1$ - $y_1$  data for the 1-propanol (1) + n-butanoic acid (2) system at 333.15K

- Figure 7-32 Comparison between NRTL, WILSON and UNIQUAC model fits to experimental  $P$ - $x_1$ - $y_1$  data for the 1-propanol (1) + n-butanoic acid (2) system at 333.15K
- Figure 7-33 Comparison between NRTL, WILSON and UNIQUAC model fits to experimental  $x_1$ - $y_1$  data for the 1-propanol (1) + n-butanoic acid (2) system at 333.15K
- Figure 7-34 Comparison between HOC, VPA and NTH model fits to  $P$ - $x_1$ - $y_1$  data for the 1-propanol (1) + n-butanoic acid (2) system at 353.15K
- Figure 7-35 Comparison between HOC, VPA and NTH model fits to  $x_1$ - $y_1$  data for the 1-propanol (1) + n-butanoic acid (2) system at 353.15K
- Figure 7-36 Comparison between NRTL, WILSON and UNIQUAC model fits to experimental  $P$ - $x_1$ - $y_1$  data for the 1-propanol (1) + n-butanoic acid (2) system at 353.15K
- Figure 7-37 Comparison between NRTL, WILSON and UNIQUAC model fits to experimental  $x_1$ - $y_1$  data for the 1-propanol (1) + n-butanoic acid (2) system at 353.15K
- Figure B-1 Point test (varying EOS): pressure-residual for the 2-propanone (1) + 2-butanol (2) system at 333.15K
- Figure B-2 Point test (varying EOS):  $\Delta y_1$  for the 2-propanone (1) + 2-butanol (2) system at 333.15K
- Figure B-3 Point test (varying activity coefficient model): pressure-residual for the 2-propanone (1) + 2-butanol (2) system at 333.15K

- Figure B-4 Point test (varying activity coefficient model):  $\Delta y_1$  for the 2-propanone (1) + 2-butanol (2) system at 333.15K
- Figure B-5 Point test (varying EOS): pressure-residual for the 2-propanone (1) + 2-butanol (2) system at 353.15K
- Figure B-6 Point test (varying EOS):  $\Delta y_1$  for the 2-propanone (1) + 2-butanol (2) system at 353.15K
- Figure B-7 Point test (varying activity coefficient model): pressure-residual for the 2-propanone (1) + 2-butanol (2) system at 353.15K
- Figure B-8 Point test (varying activity coefficient model):  $\Delta y_1$  for the 2-propanone (1) + 2-butanol (2) system at 353.15K
- Figure B-9 Point test (varying EOS): pressure-residual for the 2-propanone (1) + 2-butanol (2) system at 373.15K
- Figure B-10 Point test (varying EOS):  $\Delta y_1$  for the 2-propanone (1) + 2-butanol (2) system at 373.15K
- Figure B-11 Point test (varying activity coefficient model): pressure-residual for the 2-propanone (1) + 2-butanol (2) system at 373.15K
- Figure B-12 Point test (varying activity coefficient model):  $\Delta y_1$  for the 2-propanone (1) + 2-butanol (2) system at 373.15K
- Figure B-13 Point test (varying EOS): pressure-residual for the 2-propanone (1) + n-propanoic acid (2) system at 333.15K
- Figure B-14 Point test (varying EOS):  $\Delta y_1$  for the 2-propanone (1) + n-propanoic acid (2) system at 333.15K

- Figure B-15 Point test (varying activity coefficient model): pressure-residual for the 2-propanone (1) + n-propanoic acid (2) system at 333.15K
- Figure B-16 Point test (varying activity coefficient model):  $\Delta y_1$  for the 2-propanone (1) + n-propanoic acid (2) system at 333.15K
- Figure B-17 Point test (varying EOS): pressure-residual for the 2-propanone (1) + n-propanoic acid (2) system at 353.15K
- Figure B-18 Point test (varying EOS):  $\Delta y_1$  for the 2-propanone (1) + n-propanoic acid (2) system at 353.15K
- Figure B-19 Point test (varying activity coefficient model): pressure-residual for the 2-propanone (1) + n-propanoic acid (2) system at 353.15K
- Figure B-20 Point test (varying activity coefficient model):  $\Delta y_1$  for the 2-propanone (1) + n-propanoic acid (2) system at 353.15K
- Figure B-21 Point test (varying EOS): pressure-residual for the 2-propanone (1) + n-propanoic acid (2) system at 373.15K
- Figure B-22 Point test (varying EOS):  $\Delta y_1$  for the 2-propanone (1) + n-propanoic acid (2) system at 373.15K
- Figure B-23 Point test (varying activity coefficient model): pressure-residual for the 2-propanone (1) + n-propanoic acid (2) system at 373.15K
- Figure B-24 Point test (varying activity coefficient model):  $\Delta y_1$  for the 2-propanone (1) + n-propanoic acid (2) system at 373.15K
- Figure B-25 Point test (varying EOS): pressure-residual for the 1-propanol (1) + n-butanoic acid (2) system at 333.15K

- Figure B-26 Point test (varying EOS):  $\Delta y_1$  for the 1-propanol (1) + n-butanoic acid (2) system at 333.15K
- Figure B-27 Point test (varying activity coefficient model): pressure-residual for the 1-propanol (1) + n-butanoic acid (2) system at 333.15K
- Figure B-28 Point test (varying activity coefficient model):  $\Delta y_1$  for the 1-propanol (1) + n-butanoic acid (2) system at 333.15K
- Figure B-29 Point test (varying EOS): pressure-residual for the 1-propanol (1) + n-butanoic acid (2) system at 353.15K
- Figure B-30 Point test (varying EOS):  $\Delta y_1$  for the 1-propanol (1) + n-butanoic acid (2) system at 353.15K
- Figure B-31 Point test (varying activity coefficient model): pressure-residual for the 1-propanol (1) + n-butanoic acid (2) system at 353.15K
- Figure B-32 Point test (varying activity coefficient model):  $\Delta y_1$  for the 1-propanol (1) + n-butanoic acid (2) system at 353.15K

## LIST OF TABLES

Table 2-1	Comparison of boiling points for carboxylic acids, alcohols and alkanes of similar molecular weights (taken from Clifford, 2004)
Table 3-1	Categories of data assessment according to Smith (1984)
Table 3-2	Consistency Index for VLE data for the direct test (Van Ness, 1995)
Table 6-1	List of chemicals used and their respective purities
Table 6-2	Estimated accuracy of measured system variables
Table 6-3	Operating conditions for the Shimadzu 2014 gas chromatograph
Table 6-4	Operating conditions for the Shimadzu 2010 gas chromatograph
Table 6-5	Available specifications for columns used for GC analyses
Table 6-6	Summary of response factor ratios obtained from slopes of linear GC calibration plots
Table 6-7	Vapour pressure measurements undertaken on the apparatus of Joseph (2001)
Table 6-8	Vapour pressure measurements undertaken on the apparatus of Reddy (2006)
Table 6-9	Overview of the binary VLE measurements conducted on each of the apparatuses used in this project
Table 6-10	Vapour pressure data for 2-butanol
Table 6-11	Vapour pressure data for 1-propanol

Table 6-12	Vapour pressure data for n-butanoic acid
Table 6-13	Vapour pressure data for n-propanoic acid
Table 6-14	Vapour pressure data for 2-propanone
Table 6-15	Vapour pressure data for cyclohexane
Table 6-16	P-x <sub>1</sub> -y <sub>1</sub> data for cyclohexane (1) + ethanol (2) at 323.15K
Table 6-17	P-x <sub>1</sub> -y <sub>1</sub> data for 2-propanone (1) + 2-butanol (2) at 333.15K
Table 6-18	P-x <sub>1</sub> -y <sub>1</sub> data for 2-propanone (1) + 2-butanol (2) at 353.15K
Table 6-19	P-x <sub>1</sub> -y <sub>1</sub> data for 2-propanone (1) + 2-butanol (2) at 373.15K
Table 6-20	P-x <sub>1</sub> -y <sub>1</sub> data for 2-propanone (1) + n-propanoic acid (2) at 333.15K
Table 6-21	P-x <sub>1</sub> -y <sub>1</sub> data for 2-propanone (1) + n-propanoic acid (2) at 353.15K
Table 6-22	P-x <sub>1</sub> -y <sub>1</sub> data for 2-propanone (1) + n-propanoic acid (2) at 373.15K
Table 6-23	P-x <sub>1</sub> -y <sub>1</sub> data for 1-propanol (1) + n-butanoic acid (2)
Table 7-1	Comparison between literature and experimental vapour pressure data
Table 7-2	Parameters for the Antoine equation (this work)
Table 7-3	Average deviations for the point test: 2-propanone (1) + 2-butanol (2) at 333.15K

Table 7-4	Average deviations for the point test: 2-propanone (1) + 2-butanol (2) – 353.15K
Table 7-5	Average deviations for the point test: 2-propanone (1) + 2-butanol (2) – 373.15K
Table 7-6	Average deviations for the point test: 2-propanone (1) + n-propanoic acid (2) – 333.15K
Table 7-7	Average deviations for the point test: 2-propanone (1) + n-propanoic acid (2) – 353.15K
Table 7-8	Average deviations for the point test: 2-propanone (1) + n-propanoic acid (2) – 373.15K
Table 7-9	Average deviations for the point test: 1-propanol (1) + n-butanoic acid (2) – 333.15K
Table 7-10	Average deviations for the point test: 1-propanol (1) + n-butanoic acid (2)– 353.15K
Table 7-11	Best fit models for the 2-propanone (1) + 2-butanol (2) system
Table 7-12	Model Parameters for the 2-propanone (1) + 2-butanol (2) system
Table 7-13	Best fit models for the 2-propanone (1) + n-propanoic acid (2) system
Table 7-14	Model Parameters for the 2-propanone (1) + n-propanoic acid (2) system
Table 7-15	Best fit models for the 1-propanol (1) + n-butanoic acid (2) system
Table 7-16	Model Parameters for the 1-propanol (1) + n-butanoic acid (2) system

Table 7-17	Number of data points not included in final regression analyses
Table 7-18	Model Parameters obtained for the 2-propanone (1) + 2-butanol (2) system at 373.15K using the full set of data and only those for which the point test passes
Table 7-19	Model Parameters obtained for the 2-propanone (1) + n-propanoic acid (2) system at 373.15K using the full set of data and only those for which the point test passes
Table 7-20	Model Parameters for the 1-propanol (1) + n-butanoic acid (2) system at 333.15K using the full set of data and only those for which the point test passes
Table 8-1	Best-fit models for the systems in this study

## NOMENCLATURE

### English Letters

$a_i$	Activity of a liquid
$A_i$	Constant in the Antoine equation
$a_{ij}$	Constants for temperature dependency of model parameters
$B_i$	Constant in the Antoine equation
$B_{ii}$	Second virial coefficient of pure component $i$ [ $\text{cm}^3/\text{mol}$ ]
$b_{ij}$	Constants for temperature dependency of model parameters
$B_{ij}$	Second virial coefficient for species $i$ – species $j$ interaction [ $\text{cm}^3/\text{mol}$ ]
$C_i$	Constant in the Antoine equation
$c_{ij}$	Constants for temperature dependency of model parameters
$d_{ij}$	Constants for temperature dependency of model parameters
$e_{ij}$	Constants for temperature dependency of model parameters
$f$	Fugacity [kPa]
$f_i^0$	Fugacity of the pure component $i$ in a standard (or reference) state
$\hat{f}_i$	Fugacity in solution of component $i$ [kPa]
$F$	Degrees of freedom of the system (Gibbs phase rule)
$f_{ij}$	Constants for temperature dependency for model parameters
$g_{ij}$ – $g_{ii}$	Parameter in NRTL (1968) model representing interactions between species
$G$	Molar or specific Gibbs energy [J/mol]
$\bar{G}_i$	Partial molar Gibbs free energy
$H$	Molar or specific Enthalpy [J/mol]
$K_i$	Chemical equilibrium constant for association equilibria
$l_i$	Parameter in the UNIQUAC (1975) model
$n_i$	Number of moles of component $i$
$N$	Number of chemical species or components present in a system
$P$	System pressure [kPa]
$q_i$	Pure component area parameter in the UNIQUAC (1975) model
$Q$	Energy transferred as heat energy
$r_i$	Pure component volume parameter in the UNIQUAC (1975) model

$R$	Universal gas constant [J/mol.K]
$S$	Molar or specific entropy
$T$	System temperature [ $^{\circ}$ C or K]
$U$	Molar or specific internal energy
$V$	Molar or specific volume [cm <sup>3</sup> /mol]
$V_m$	Molar volume [cm <sup>3</sup> /mol]
$w$	Normalizing factor
$W$	Work done on a system
$x_i$	Mole fraction of component $i$ in the liquid phase
$y_i$	Mole fraction of component $i$ in the vapour phase
$z$	Co-ordination number in the UNIQUAC (1975) model
$z_{in}$	True species concentration for component $i$
$z_{Mij}$	True concentration of cross-dimers of component $i$ and $j$
$Z$	Compressibility factor

### Greek Letters

$\alpha_{12}$	Non-randomness parameter in NRTL (1968) model
$\gamma_i$	Activity coefficient of component $i$
$\delta$	Denotes a residual (e.g. $\delta P$ )
$\Delta$	Denotes the residual for the point test
$\eta$	Solvation (unlike species) and association (pure species) parameters (HOC)
$\theta_i$ and $\theta'_i$	Area fractions in UNIQUAC (1975) equation
$\Theta$	Constant of integration in Equation 3.16
$\Theta_i$	Segment fractions in UNIQUAC (1975) equation
$\lambda_{ii}$	Parameter representing interactions between species in the Wilson (1964) model
$A_{ij}$	Parameter in Wilson (1964) model
$\mu_i$	Chemical potential of component $i$
$\pi$	Number of phases present in a system (Gibbs phase rule)
$\tau_{ij}$	Parameter in the NRTL (1968) model and UNIQUAC (1975) model
$\phi$	Fugacity coefficient
$\hat{\phi}$	Fugacity coefficient in solution

$\Phi$	Ratio of fugacity coefficients, with the pointing correction factor
$\varphi_i$	True species fugacity coefficient

### Superscripts

exp	Denotes values calculated from experimental data
<i>E</i>	Denotes an excess property
<i>id</i>	Denotes an ideal solution
<i>L</i>	Denotes the liquid phase
Lit	Refers to literature data
<i>Sat</i>	Denotes a saturated value
<i>V</i>	Denotes the vapour phase

### Subscripts

1	Denotes component 1 (the more volatile component in a binary mixture)
2	Denotes component 2 (the less volatile component in a binary mixture)
avg	Denotes an average value
c	Denotes a critical property
rev	Denotes reversible processes

# CHAPTER 1

## INTRODUCTION

This study was initiated out of the need for vapour-liquid equilibrium (VLE) data for mixtures of oxygen-containing compounds by the petrochemical company Sasol Limited. Alcohols, ketones and carboxylic acids are all examples of oxygen-containing compounds since their chemical structures contain at least one oxygen atom. These classes of compounds are often formed as by-products in industrial processes and frequently appear in aqueous waste streams. They are found in Sasol's Fischer-Tropsch product streams and knowledge on their phase behaviour is essential in designing and optimizing the chemical processes and equipment in which they are found. There is the potential of considerable savings in both capital and operating costs through the recovery and purification of these useful components which would have otherwise been discarded. Knowledge of the relations between the temperature, pressure, and composition of co-existing phases is essential not only in the case of distillation and other contacting equipment, but also in heat transfer and fluid flow equipment, where complete or partial vapourization and condensation occurs. The exact process stream data and specifications that were provided by Sasol cannot be divulged in this work owing to the confidential nature of the information.

Vapour-liquid equilibria can be obtained either by experimental measurements or via predictive methods. Most systems of industrial importance are non-ideal since they usually involve chemicals of dissimilar chemical nature (as opposed to members of the same homologous series). Attempts to predict the equilibrium compositions of such mixtures from theoretical considerations alone can prove to be extremely unreliable in certain instances and such data is therefore best determined experimentally. However, the data obtained must be shown to be accurate and reliable before it can be confidently used in the design and development of industrial processes. Working with polar compounds is particularly challenging because of their ability to form hydrogen bonds and to agglomerate into clusters of two or more molecules.

The experimental techniques and modeling aspects are not straightforward when dealing with such systems of dissimilar components. For this work, the dynamic recirculating stills of Joseph (2001) and Reddy (2006) were utilized to undertake the measurements. There are numerous

models available in literature to correlate and predict the phase equilibrium, however, not many literature sources have shown to model the systems studied in this work. The binary VLE data obtained in this work were regressed using the combined method for VLE applying various thermodynamic model combinations to the data (taking into account vapour-phase association in particular). Theoretical developments involving associating components are ongoing.

## CHAPTER 2

### BINARY SYSTEMS CHOSEN FOR EXPERIMENTATION

In this study, isothermal VLE measurements were undertaken for the following four binary systems:

- a) cyclohexane (1) + ethanol (2) at 323.15 K
- b) 2-propanone (1) + 2-butanol (2) at 333.15 K, 353.15 K and 373.15 K
- c) 2-propanone (1) + n-propanoic acid (2) at 333.15 K, 353.15 K and 373.15 K
- d) 1-propanol (1) + n-butanoic acid (2) at 333.15 K and 353.15 K

The cyclohexane (1) + ethanol (2) system is the only one from those listed above which has been measured previously (i.e. data exists in the open literature). It was measured as a test system to confirm the accuracy of the apparatus (and calibrations) and experimental procedure by comparing the data measured in this study to that reported in the open literature. This system was chosen as a test system for the following reasons (Clifford, 2004):

- System is very non-ideal
- Thermodynamically consistent literature data is available for comparison
- System chemicals are available at a sufficiently high purity (>99%)
- Chemicals are not excessively expensive, toxic or unstable

The remaining binary systems measured were made up of components for which Sasol required VLE data. Each binary is made up of either a carboxylic acid, alcohol or ketone. There is relatively little data available pertaining to polar compounds. This is probably due to the complicated VLE systems that they form, since they associate to a large degree. A search through the available literature and databanks such as the Dortmund Data Bank (DDB, 2008) revealed that the binary systems listed above (excluding the test system) all constitute new data. A brief description of some of the properties of the classes of chemical compounds utilised in this study is given in the following sections.

## 2.1. Carboxylic acids

Carboxylic acids are compounds which contain the carboxyl functional group (-COOH) that is depicted in Figure 2-1. The structures of the two carboxylic acids worked with in this study, n-propanoic acid and n-butanoic acid, are shown in Figure 2-2.

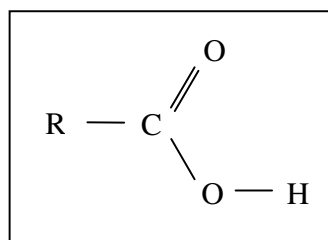


**Figure 2-1 The carboxyl functional group**

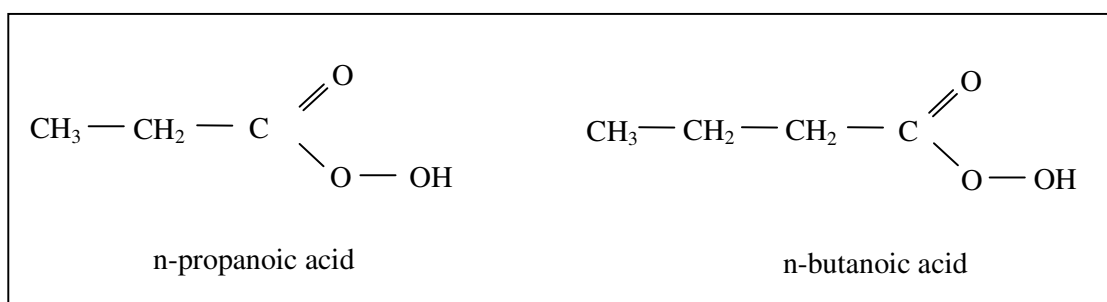


**Figure 2-2 Structures of carboxylic acids used in this study**

The carboxyl functional group is the active portion of the carboxylic acid responsible for its chemistry. One of the most important properties of carboxylic acids (and the one that is responsible for naming them) is their acidity. Carboxylic acids are weak acids relative to most mineral acids such as sulphuric acid and nitric acid since they only partially dissociate into H<sup>+</sup> cations and RCOO<sup>-</sup> anions in aqueous solutions. However, when compared to phenols and ketones their acidity is far superior.

Carboxylic acids undergo many different types of reactions. They react easily with bases (weak or strong) and with pure metals (such as sodium and magnesium). Both these reactions would result in the formation of a metal-carboxylate salt (e.g. sodium ethanoate) and water. With

extremely powerful reducing agents (such as  $\text{LiAlH}_4$ ), carboxylic acids can also undergo reduction reactions and may be reduced to an aldehyde or even to a primary alcohol.

An important reaction is the esterification reaction involving a carboxylic acid and an alcohol to produce their ester derivative and water (a condensation reaction). This is an exceedingly slow reaction and therefore requires catalysis and heating in order to increase the reaction rate. The esterification reaction can be forced forward by removing the water molecule that is formed.

A distinguishing feature of carboxylic acids is the fact that they tend to associate significantly in the vapour phase, forming oligomers consisting of two or more molecules held closely together by hydrogen bonds (see Figure 2-3). The effect of the vapour-phase association of the carboxylic acids on the activity coefficients has been recognized dating back to the work by Dolezalek (1908). It is usually difficult to measure and interpret the carboxylic acid vapour-phase data because of difficult sample purification and unwanted reactions at temperatures of interest (Vawdrey et al., 2004). These difficulties and considerable complexity in the analysis and interpretation of their VLE data have led to a scarcity of reliable data for carboxylic acids. The stronger the acid, the greater the tendency toward scission of the original O-H bond and hence the greater will be the tendency toward dissociation of the dimer (Landee and Johns, 1941). Thus, for strong acids the degree of association should be relatively less than for weak acids.

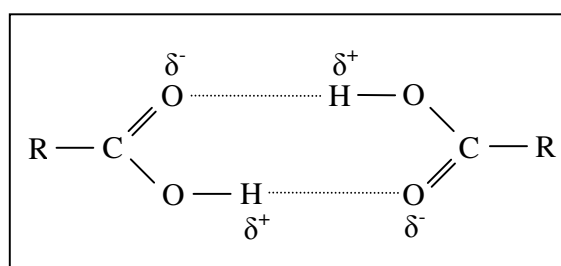


**Figure 2-3 Dimer formation in carboxylic acids through hydrogen bonding**

Several authors claim that only monomers and dimers are present in a carboxylic acid vapour. Weltner (1955) made such a claim based on vapour heat capacity measurements. Taylor and Bruton (1952) also state that no higher polymerization is indicated, however the maximum pressure in their experiments was 36 mm Hg and the formation of trimers is small at lower pressures. Various authors have suggested that in addition to dimerization, higher

polymerization reactions are also plausible. Johnson and Nash (1950) have shown that trimers must exist in acetic acid and in tri-methyl acetic acid vapours. The same conclusion was reached by Lundin et al. (1952) for butyric acid. More recently, Vawdrey et al. (2004) made use of density functional theory (DFT) calculations to quantify the size and distribution of oligomers present in *n*-aliphatic carboxylic acid vapours. They have shown that the dimer species is the only significant one in the vapour-phase of carboxylic acids, even at modest temperatures and pressures. This is in accordance with the findings of Curtiss and co-workers (1980) who used thermal conductivity measurements to determine which oligomers are present in acetic acid. Furthermore, according to Le Chateliers principle, the dimer fraction decreases with increasing temperature and increases with increasing pressure. As the pressure approaches zero, the fraction of associated species approaches zero.

The association of carboxylic acids is one of the reasons why this class of compounds has significantly higher boiling points than alcohols, aldehydes, hydrocarbons and ketones of the same molecular weight. Two carboxylic acid molecules are able to form two hydrogen bonds with each other as opposed to two alcohol molecules which can only form one hydrogen bond between each other. Owing to dimer formation, carboxylic acids require additional heat energy to boil than the corresponding alcohol. In addition to the higher actual molecular weight, extra heat is required to sever the strong hydrogen bonds to break down the dimers or trimers. Table 2-1 provides a comparison between the boiling points of carboxylic acids, alcohols and alkanes of similar molecular weights.

**Table 2-1 Comparison of boiling points for carboxylic acids, alcohols and alkanes of similar molecular weights (taken from Clifford, 2004)**

<b>Compound</b>	<b>Molecular Weight</b>	<b>Boiling Point/°C</b>	<b>Intermolecular Force</b>
butane	58	-1	dispersion
methyl ethyl ether	60	6	weak dipole
propionaldehyde	58	49	strong dipole
1-propanol	60	97	hydrogen bonds
acetic acid	60	118	dimers

## 2.2. Alcohols

Alcohols are compounds which contain the hydroxyl functional group (OH; see Figure 2-4). They are polar compounds and the hydroxyl groups (like the carboxyl groups) are able to hydrogen bond to each other or to other compounds (see Figure 2-5).

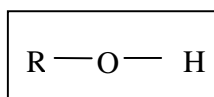


**Figure 2-4 The hydroxyl functional group**

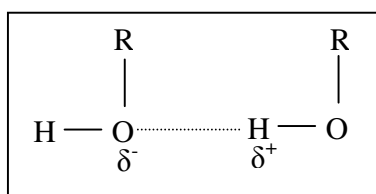


**Figure 2-5 Hydrogen bonding in alcohols**

Alcohols display two opposing solubility trends:

- The hydroxyl group's tendency to promote solubility in water.
- The carbon chains tendency to resist solubility in water.

Therefore depending on the particular chemistry of the alcohol, it can display either one or a mixture of the solubility trends. For example, methanol, ethanol and propanol are miscible in water due to the stronger effect of the hydroxyl group over the short carbon chain. Butanol on the other hand, has four carbon atoms, and hence displays moderate solubility due to the combination of the two solubility trends. Alcohols containing more than five carbon atoms are insoluble in water due to the carbon chain dominating over the hydroxyl group. However, all simple alcohols are miscible in organic solvents. The ability of alcohols to hydrogen bond results in them having higher boiling points compared to hydrocarbons and ethers of the same molecular weight (see Table 2-1).

Alcohols can display either acidic or basic properties at the hydroxyl group. They are generally weak acids ( $pK_a \sim 16-19$ ), slightly weaker than water. Although weak, they can react with strong bases and reactive metals such as sodium. The lone pair of unbonded electrons on the oxygen atom makes the alcohol a weak base in the presence of strong acids such as sulphuric acid. Alcohols can undergo oxidation and dehydration reactions. Oxidation of alcohols produces aldehydes, ketones or carboxylic acids whereas the dehydration of alcohols produces alkenes. As mentioned above, alcohols can also react with carboxylic acids to produce esters.

### 2.3. Ketones

The functional group on aldehydes and ketones is a carbonyl group ( $C=O$ ). The difference between the two is that in aldehydes the carbonyl group is on the "end" of a carbon chain, while in ketones it is in the "middle" of a carbon chain – i.e. bonded to two other carbons (see Figure 2-6). Ketones, like alcohols and carboxylic acids, are also polar compounds making them soluble in water. They do not have the ability to self-associate like alcohols and carboxylic acids and are more volatile than alcohols and carboxylic acids of similar molecular weight (see Table 2-1).

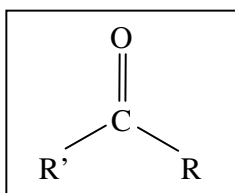


**Figure 2-6** The generalized structure of a ketone

## CHAPTER 3

### THE THEORETICAL TREATMENT OF VLE DATA

This chapter deals with the thermodynamic treatment of the acquired experimental data, especially that relevant to associating compounds such as carboxylic acids and alcohols. Theoretical aspects of vapour-liquid phase equilibria, in particular data in the low to moderate pressure region, are included and data correlation using suitable thermodynamic models which enables interpolation of the data and extrapolation to conditions other than those measured are also described. This review describes the  $\gamma$ - $\Phi$  formulation (combined method) of VLE, with the associated activity coefficient models and equations-of-state, as well as modelling of VLE data by the  $\Phi$ - $\Phi$  (direct) method using the equations-of-state to describe both the liquid and vapour phases. The methods proposed for the evaluation of the fugacity and activity coefficients are examined and the chapter concludes with a discussion on the various thermodynamic consistency tests for VLE data. For a greater coverage of the subject and a more detailed discussion of the relations presented here, the following excellent texts are recommended: Walas (1985), Malanowski and Anderko (1992), Raal and Mühlbauer (1998), Sandler (1999), Prausnitz et al. (1999) and Smith et al. (1996, 2001).

#### 3.1. Fundamental thermodynamic relationships and equations

Thermodynamics is the branch of science that embodies the principles of energy transformation in macroscopic systems. The general restrictions which experience has shown to apply to all such transformations are known as the *laws of thermodynamics*. These laws are primitive and cannot be derived from anything more basic (Perry, 1997).

The *first law of thermodynamics* is a statement of the conservation of energy. For a closed system (but not necessarily isolated), it may be stated mathematically for a reversible process as:

$$d(nU) = dQ_{rev} - dW_{rev} \quad (3.1)$$

It can be written for a change in total entropy for a reversible process (defining equation for entropy):

$$d(nS) = \frac{dQ_{rev}}{T} \quad (3.2)$$

A succinct statement of the *second law of thermodynamics* is (Raal and Mühlbauer, 1998):

$$\Delta S_{total} \geq 0 \quad (3.3)$$

i.e. no process is possible in which the total entropy decreases; the total entropy either increases or, in the limit where the system has reached an equilibrium state and is operating reversibly, remains constant.

For closed PVT systems, the work of a reversible process may always be calculated from (Perry, 1997):

$$dW_{rev} = Pd(nV) \quad (3.4)$$

This equation follows directly from the definition of mechanical work.

Combining the *first and second laws of thermodynamics* with Equation 3.4, it is easily shown that the internal energy of a closed (constant mass), homogenous (single phase), non-reacting system containing  $n$  moles of material can be expressed as:

$$d(nU) = Td(nS) - Pd(nV) \quad (3.5)$$

Although derived for a reversible process, this equation relates properties only and is valid for any change between equilibrium states in a closed system. Equation 3.5 restated for changes to a unit number of moles ( $n = 1$ ) of a homogenous fluid between two equilibrium states gives:

$$dU = TdS - PdV \quad (3.6)$$

The calculation of energy (U) using Equation 3.6 requires expressions explicit in entropy (S) and volume (V) to integrate the terms on the right hand side. Rearrangement of Equation 3.6 enables the calculation of energy using expressions explicit in temperature and pressure (measurable

quantities). From the definitions of the convenience state functions (additional primary functions) of enthalpy (H), Gibbs free energy (G), and the Helmholtz free energy (A), and some elementary manipulation, the following differentials can be found:

$$dH = TdS + VdP \quad (3.7)$$

$$dG = VdP - SdT \quad (3.8)$$

$$dA = -PdV - SdT \quad (3.9)$$

The Gibbs free energy is immediately useful because of its functional relation to temperature (T) and pressure (P), variables which are of primary interest in chemical processing. For phase equilibrium studies it is even more useful since the temperature and pressure do not change for a phase change, and hence the Gibbs free energy change is zero (constant T and P in Equation 3.8):

$$dG_{T,P} = 0 \quad (3.10)$$

i.e. the Gibbs free energy per unit mass is a minimum and is the same in both phases.

### 3.2. Chemical potential

In a mixture, an important driving force for mass transfer of individual components is the gradient of the chemical potential ( $\mu_i$ ) of each component present. Equivalent expressions for  $\mu_i$  (an intensive property) may be written as:

$$\mu_i \equiv \left( \frac{\partial(nG)}{\partial n_i} \right)_{P,T,n_j} \equiv \left( \frac{\partial(nH)}{\partial n_i} \right)_{P,nS,n_j} \equiv \left( \frac{\partial(nU)}{\partial n_i} \right)_{S,nV,n_j} \equiv \left( \frac{\partial(nA)}{\partial n_i} \right)_{T,nV,n_j} \quad (3.11)$$

The first identity is used by some authors to define  $\mu_i$ . The expression  $\left( \frac{\partial(nG)}{\partial n_i} \right)_{P,T,n_j}$  is a partial

molar quantity due to the defining constraints of constant T, P and  $n_j$  – i.e.,  $\mu_i = \overline{G}_i$  (partial molar Gibbs free energy). This relationship is important in the development of the activity coefficient, which is discussed in Section 3.4. The general *criterion for equilibrium* for  $\pi$  phases with  $N$  chemical components is (see Appendix A.1 for the derivation):

$$\mu_i^\alpha = \mu_i^\beta = \dots = \mu_i^\pi \quad (i = 1, 2, \dots, N) \quad (3.12)$$

i.e. the chemical potential of each species is equal for each phase throughout the system. The use of the chemical potential, however, is impractical since it is an abstract concept and not easily related to measurable quantities. To be useful, the thermodynamic relationships for a system must be in terms of quantities that can be measured experimentally (Gess et al., 1991). In the case of phase equilibrium, temperature and pressure can be measured directly and the chemical potential cannot. This problem was solved by expressing the chemical potential in terms of experimentally accessible quantities via the introduction of fugacity.

### 3.3. Fugacity and fugacity coefficients

According to Smith et al. (2001) the concept of fugacity was introduced by G.N. Lewis and is physically more meaningful than chemical potential (fugacity has the dimension of pressure). For a pure species the definition of fugacity is:

$$dG_i = RTd \ln f_i \quad (\text{constant T}) \quad (3.13)$$

$$\lim_{P \rightarrow 0} \frac{f}{P} = 1$$

and the fugacity coefficient,  $\phi$ , is defined as:

$$\phi = \frac{f}{P} \quad (\text{dimensionless}) \quad (3.14)$$

For a component in mixture,

$$d\bar{G}_i = RTd \ln \hat{f}_i \quad (\text{constant T}) \quad (3.15)$$

$$\lim_{P \rightarrow 0} \frac{\hat{f}_i}{x_i P} = 1$$

Where  $\bar{G}_i$  is the partial molar Gibbs free energy and  $\hat{f}_i$  is the fugacity of species  $i$  in solution.

Furthermore, for a species  $i$  in a mixture:

$$\widehat{\phi}_i^V = \frac{\widehat{f}_i^V}{y_i P} \quad (\text{vapour phase}) \quad (3.16)$$

$$\widehat{\phi}_i^L = \frac{\widehat{f}_i^L}{x_i P} \quad (\text{liquid phase}) \quad (3.17)$$

Since  $\mu_i = \overline{G}_i$ , Equation 3.15 becomes:

$$d\mu_i = RT d \ln \widehat{f}_i \quad (\text{constant T}) \quad (3.18)$$

Integrating Equation 3.18 at constant temperature gives:

$$\mu_i = RT \ln \widehat{f}_i + \Theta_i(T) \quad (3.19)$$

Since  $\Theta_i$  is a function of temperature only, and all phases in equilibrium with each other are at the same temperature, substitution of Equation 3.19 into Equation 3.12 provides an alternative criterion for equilibrium in terms of  $\widehat{f}_i$ :

$$\widehat{f}_i^\alpha = \widehat{f}_i^\beta = \dots = \widehat{f}_i^\pi \quad (i = 1, 2, \dots, N) \quad (3.20)$$

i.e. for a liquid (L) phase in equilibrium with its vapour (V) phase, in addition to uniform temperature and pressure,

$$\widehat{f}_i^V = \widehat{f}_i^L \quad (3.21)$$

Although fugacity is still an abstract quantity, it is more readily related to measurable quantities such as temperature (T), pressure (P) and molar volume (V) and is evaluated from a suitable

equation of state (EOS). The fugacity coefficient is evaluated using the compressibility factor ( $Z$ ) defined as:

$$Z = \frac{PV}{RT} \quad (3.22)$$

It can be shown that (Smith et al., 2001):

$$\ln \hat{\phi}_i = \int_0^P \left( \frac{\partial(nZ - n)}{\partial n_i} \right)_{P,T,n_j} \frac{dP}{P} \quad (3.23)$$

$$\ln \phi_i^{sat} = \int_0^{P_i^{sat}} (Z - 1) \frac{dP}{P} \quad (3.24)$$

The fugacity coefficient for a pure species (Equation 3.24) and the fugacity coefficient for a species in solution (Equation 3.23) can be calculated from an appropriate expression for the compressibility factor. A short discussion on some of these equations-of-state (from where  $Z$  is obtained) is given in Section 3.6.1.

### 3.4. Activity and activity coefficients

Lewis and Randall (1923) define activity,  $a$ , as the relative fugacity, or the ratio between the fugacity of the substance in solution and a standard state fugacity (its fugacity as a pure liquid). Thus,

$$a_i = \frac{\hat{f}_i}{f_i^0} \quad (3.25)$$

where  $a_i$  is the activity of the pure liquid and  $f_i^0$  is the fugacity of the pure component  $i$  in a standard (or reference) state. Activity coefficients  $\gamma_i$  are simply the activities divided by their respective mole fractions,

$$\gamma_i = \frac{a_i}{x_i} = \frac{\hat{f}_i}{x_i f_i^0} \quad (3.26)$$

For systems with condensable components, the activity coefficient is normalized as:

$$\lim_{x_i \rightarrow 1} \gamma_i = 1 \quad (3.27)$$

Thus, as the composition tends towards that of a pure component,  $\hat{f}_i^L \rightarrow x_i f_i^0$ . This convention is referred to as symmetric normalization. A useful reference (or standard) state for  $f_i^0$  is the saturated liquid at the system temperature.

For non-condensable components, an unsymmetrical convention is used involving Henry's constant ( $H_i$ ) as the standard state fugacity for the component in the dilute region.

$$H_i = \lim_{x_i \rightarrow 0} \frac{\hat{f}_i}{x_i} = f_i^0 \quad (3.28)$$

$$\hat{f}_i^{id} = x_i H_i \quad (3.29)$$

Liquid-phase behaviour is conveniently described using the concept of activity coefficients to represent the departure of a solution from ideality. Equation 3.19 can be written for an ideal solution:

$$\mu_i^{id} = \bar{G}_i^{id} = RT \ln \hat{f}_i^{id} + \Theta_i(T) \quad (3.30)$$

The Lewis/Randall rule provides a simple equation for the fugacity of a species in an ideal solution:

$$\hat{f}_i^{id} = x_i f_i \quad (3.31)$$

Therefore, for an ideal solution, Equation 3.30 becomes:

$$\bar{G}_i^{id} = RT \ln x_i f_i + \Theta_i(T) \quad (3.32)$$

Subtraction of Equation 3.32 from Equation 3.19 gives an expression for the partial molar *excess* Gibbs energy  $\bar{G}_i^E$ :

$$\bar{G}_i - \bar{G}_i^{id} = \bar{G}_i^E = RT \ln \frac{\hat{f}_i}{x_i f_i} \quad (3.33)$$

The activity coefficient by definition is:

$$\gamma_i = \frac{\hat{f}_i}{x_i f_i} \quad (3.34)$$

Therefore,

$$\bar{G}_i^E = RT \ln \gamma_i \quad \text{or} \quad \mu_i^E = RT \ln \gamma_i \quad (3.35)$$

$\mu_i^E$  represents changes in chemical potentials in excess of the changes for an ideal solution (Barker, 1953). Carlson and Colburn (1942) differentiate between positive and negative deviations from ideality. The large proportion of non-ideal systems show positive deviations from ideality (meaning the values of  $\log \gamma_i$  are positive i.e., the values of  $\gamma$  are above unity). Some systems, however, do have negative deviations ( $\gamma_i$  is fractional) (e.g. acetone-chloroform). Negative deviations occur in electrolytes and other liquids where association or compound formation of some type reduces the volatility. A short discussion on some of the models used to correlate activity coefficients is given in Section 3.6.2.

### 3.5. Theoretical VLE methods

The reduction of VLE data allows for the following:

- large amounts of data to be summarized comprehensively and compactly
- the accurate interpolation of data and limited amount of extrapolation

- thermodynamic consistency testing of certain data
- the extension of binary VLE data to predict multi-component VLE
- the creation and refinement of predictive VLE methods

There are many techniques for the computation of phase equilibria; some are more common than others due to their reliability and ease of application. The following two theoretical methods will be briefly discussed in this chapter:

1. the  $\gamma_i - \Phi_i$  (combined) method
2. the  $\Phi_i - \Phi_i$  (direct) method

Raal and Mühlbauer (1998) give an excellent review on the two theoretical methods above and describe in detail the procedures of both.

### 3.5.1. The combined method (gamma-phi approach, activity coefficient approach)

The combined method for VLE uses two distinct and separate auxiliary functions to describe the non-ideality in the equilibrium phases. The phase non-idealities are determined from:

- i.) the fugacity coefficient of component  $i$  in solution ( $\hat{\phi}_i$ ) in the vapour phase (calculated using an EOS), and,
- ii.) the activity coefficient of component  $i$  in solution ( $\gamma_i$ ) in the liquid phase (calculated from an activity coefficient model).

Equation 3.21 (the equilibrium criterion) can then be expanded from the definitions for the fugacity and activity coefficients (Equations 3.16 and 3.34 respectively) as:

$$y_i \hat{\phi}_i^V P = x_i \gamma_i f_i \quad (3.36)$$

The pure component liquid-phase fugacity ( $f_i$ ) is given by (see Appendix A.2 for derivation):

$$f_i = \phi_i^{sat} P_i^{sat} \exp\left[\frac{V_i^L(P - P_i^{sat})}{RT}\right] \quad (3.37)$$

(NB: Saturated conditions = pure component equilibrium)

The exponential term is referred to as the Poynting correction factor and describes the effect of pressure on liquid phase fugacity. Substituting for  $f_i$  into Equation 3.36 gives

$$y_i \Phi_i P = x_i \gamma_i P_i^{sat} \quad (3.38)$$

where

$$\Phi_i = \frac{\hat{\phi}_i}{\phi_i^{sat}} \exp\left[\frac{-V_i^L(P - P_i^{sat})}{RT}\right] \quad (3.39)$$

The exponential term is usually set equal to 1 for low to moderate pressures, introducing an error of about 0.01% on  $\log \gamma_i$  (Sebastiani & Lacquaniti, 1967). According to Smith et al. (2001), the Poynting factor differs from unity by only a few parts per thousand at low to moderate pressures and thus its omission introduces negligible error. This assumption is reasonable for non-polar molecules at low pressure but becomes unacceptable for mixtures containing polar or associating molecules especially carboxylic acids (Prausnitz et al., 1980).

Equation 3.38 is a very useful general equation that relates liquid and vapour phases at equilibrium. In an ideal system, the vapour phase is represented by an ideal gas and the liquid phase by an ideal solution. Such a system displays the simplest possible VLE relation and is known as Raoult's Law (Smith et al., 2001). In special cases, where  $\Phi_i$  and  $\gamma_i$  are both equal to one, Equation 3.38 simplifies to Raoult's law. In general though, equations-of-state (such as those discussed in Section 3.6.1) are used to describe the fugacity coefficients and Gibbs excess ( $G^E$ ) models (such as those discussed in Section 3.6.2) are used to describe the activity coefficients. In addition, a dependable correlation for evaluating the saturated liquid molar

volume  $V_i^L$  (if not experimentally determined) must be selected. Generally, the Rackett (1970) equation is employed for this purpose:

$$V_r = \frac{V_i^L}{V_c} = Z_c^{(1-T_r)^{2/7}} \quad (3.40)$$

where  $Z$  is the compressibility factor, the subscript  $c$  indicates the critical point and  $(T_r)_i$  is the reduced temperature defined as  $T/(T_c)_i$ . The Rackett (1970) equation is not applicable to carboxylic acids and the modified form of the Rackett equation (Spencer and Adler, 1978), which includes parameters for carboxylic acids, is more suitable when they are present.

Finally, a suitable procedure or algorithm for obtaining the model parameters via regression must be chosen. The first model-dependent data reduction method was described by Barker (1953) and a similar method was used in this work. The regression procedure is normally conducted by minimizing the error between the experimental and model values for a particular quantity. Van Ness et al. (1978) defined the difference between the two values (model and corresponding experimental value) as a residual and is denoted by the symbol  $\delta$ . The primary residuals are defined:

$$\delta y_i = y_i^{\text{exp}} - y_i^{\text{calculated}} \quad (3.41)$$

$$\delta P_i = P_i^{\text{exp}} - P_i^{\text{calculated}} \quad (3.42)$$

The above are referred to as primary residuals as all other residuals (such as  $\delta\gamma_i$ ) may be written in terms of  $\delta P$  and  $\delta y$  (Van Ness and Abbott, 1982). The residuals form the basis for the data reduction since the quantity selected for minimization (objective function) is usually written in terms of  $\delta P$  and  $\delta y$ . Barker (1953) minimized the objective function of the form:

$$\text{Objective Function} = \sum (\delta P_i)^2 \quad (3.43)$$

in the determination of the unknown parameters (where the summation  $\Sigma$  is taken over all experimental points). Many forms of the objective function for controlling the regression have been suggested in the literature. The objective function used for isobaric data developed by Gmehling and Onken (1977) for the Dechema VLE and LLE data collection is:

$$\text{Objective Function} = \sum \left( 1 - \frac{\gamma_i^{\text{calc}}}{\gamma_i^{\text{exp}}} \right)^2 \quad (3.44)$$

For this study, an objective function combining both the P and  $y_1$  residuals were used. When two parameters residuals are minimized simultaneously, they are usually normalized using normalizing factors for example:

$$\text{Objective Function} = \sum \left( \frac{\delta P}{w_p} \right)^2 + \left( \frac{\delta y_1}{w_y} \right)^2 \quad (3.45)$$

where the normalizing factors  $w_p$  and  $w_y$  used are often the RMS values obtained from the minimization of  $\Sigma(\delta y_1)^2$  and  $\Sigma(\delta P)^2$  respectively.

Since a specific model is sometimes better suited to a particular system, it is common practice to analyse a system with more than one model to determine which provides the best fit of the data (Clifford, 2004). The method of data reduction therefore requires that a number of models be fitted to experimental data until the model that yields no systematic discrepancies is found (i.e. the fit does not show a positive or negative bias). The adjustable parameters obtained from isothermal data are true constants (i.e. they apply throughout the concentration range for an isotherm). This is not the case for isobaric data since the temperature varies across the composition range. Once the parameters are obtained, T-P- $x_i$ - $y_i$  plots can be constructed at any desired condition. However, caution must be exercised when the extrapolating far outside of the temperature/pressure range of the data set.

### 3.5.2. The direct method (phi-phi approach, equation of state approach)

The direct method offers an alternative to the combined method for data reduction. In this method, fugacity coefficients (from an EOS) are used to describe non-idealities in both the

vapour and liquid phases. The equilibrium criterion (Equation 3.21) can then be expanded from the definition for the fugacity coefficient (Equations 3.16) for both the liquid and vapour phases as:

$$y_i \hat{\phi}_i^V = x_i \hat{\phi}_i^L \quad (3.46)$$

A suitable EOS needs to be used to determine  $\hat{\phi}_i^V$  and  $\hat{\phi}_i^L$ . Similar to the method described for the combined method above, a regression procedure is used to find the best fit for the data.

### 3.6. Thermodynamic models

In this section the thermodynamic models utilized in this study will be briefly discussed.

#### 3.6.1. Equations-of-state

##### 3.6.1.1. The virial EOS and the Hayden-O'Connell correlation (HOC)

At low to moderate pressures, the virial EOS (truncated at the second term) is used by most to evaluate fugacity coefficients:

$$Z = 1 + \frac{BP}{RT} \quad (3.47)$$

The second virial coefficient, B, is calculated from the composition and the pure component ( $B_{ii}(T)$ ) and mixture ( $B_{ij}(T)$ ) virial coefficients:

$$B = \sum_i \sum_j x_i x_j B_{ij}(T) \quad (3.48)$$

Hayden and O'Connell (1975) published a well-accepted method for calculating second virial coefficients for a large range of compounds (applicable to nonpolar, polar and associating compounds). Their formulation incorporates the chemical theory of dimerization and accounts for strong association and solvation effects, including those found in systems containing organic acids. The method and calculation procedure consists of many complex equations and the discussion presented in this work will include only the most relevant. The reader is referred to

the publication of Hayden and O'Connell (1975) for more detail (the calculation procedure is also detailed in Appendix A of Prausnitz et al., 1980). The virial coefficient is calculated from Equation 3.48 with  $B_{ij}(T)$  calculated from (Hayden and O'Connell, 1975):

$$B_{ij}(T) = (B_{free-nonpolar})_{ij} + (B_{free-polar})_{ij} + (B_{metastable})_{ij} + (B_{bound})_{ij} + (B_{chem})_{ij} \quad (3.49)$$

were  $(B_{free-nonpolar})_{ij}$  and  $(B_{free-polar})_{ij}$  are contributions by free pairs (non-polar, non-associating species) and  $(B_{metastable})_{ij}$ ,  $(B_{bound})_{ij}$  and  $(B_{chem})_{ij}$  are contributions by chemically bonding species. Parameters involved in the calculation include the pure component properties such as the critical pressure, critical temperature, mean radius of gyration, dipole moment as well as solvation and association parameters. The chemical bonding contributions are functions of the association parameter,  $\eta$  (binary parameter). The method of Hayden and O'Connell (1975) only considers dimerization and is the common EOS of choice for carboxylic acids at low to moderate pressures. At higher pressures, however, the accuracy of the truncated virial equation of state becomes questionable.

### 3.6.1.2. Chemical theory and the Nothnagel et al. formulation (NTH)

Nothnagel et al. (1973) presented a method for determining fugacity coefficients based on a chemical theory of imperfections. The Nothnagel EOS is based on the ideal gas law and incorporates a volume exclusion term owing to the finite size of the molecules:

$$P = \frac{RT}{V_m - b} \quad (3.50)$$

Where  $V_m$  is the molar volume of the mixture (total volume divided by true total number of moles) and  $b$  is the molar excluded volume due to the finite size of molecules (a mixture of monomers and dimers):

$$b = \sum y_i b_i + \sum_i \sum_j y_{ij} b_{ij} \quad (3.51)$$

$$b_{ij} = \frac{(b_i^{1/3} + b_j^{1/3})^3}{8}$$

At low to moderate pressures, chemical theory assumes that the following reversible dimerization reactions occur in the vapour phase:



Hence, individual species present in the mixture will include the monomers ( $A_1$  and  $B_1$ ) and the dimers ( $A_2$  and  $B_2$ ).  $K_A$  and  $K_B$  are the chemical equilibrium constants for the formation of the dimers from the monomers and is expressed (on a pressure basis) as:

$$K_A = \frac{z_{A_2} \phi_{A_2}}{z_{A_1}^2 P \phi_{A_1}^2} \quad (3.54)$$

$$K_B = \frac{z_{B_2} \phi_{B_2}}{z_{B_1}^2 P \phi_{B_1}^2} \quad (3.55)$$

Where  $P$  is the total system pressure;  $z_i$  ( $i=A_1, A_2, B_1, B_2$ ) represents the “true species” mole fractions in the vapour phase; and  $\phi_i$  is the “true species” fugacity coefficient of component  $i$ . The total number of moles depends on the equilibrium constant and the pressure. Nothnagel et al. (1973) have shown that  $\phi_i$  can be calculated from:

$$\phi_i = \frac{z_i \phi_i}{y_i} \quad (3.56)$$

where  $y_i$  is the apparent vapour phase mole fraction of species  $i$ . Furthermore, the true species fugacity coefficients are found from (Nothnagel et al., 1973):

$$\varphi_i = \exp \frac{b_i P}{RT} \quad (3.57)$$

The  $K_i$  values are assumed to be dependent solely on temperature:

$$K_i = A_i + \frac{B_i}{T} \quad (3.58)$$

For the association between two different components (cross association or hetero-dimerization), the equilibrium constant is calculated from the pure component dimerization constants from (Prausnitz, 1969):

$$K_{ij} = 2\sqrt{K_i K_j} \quad (3.59)$$

Christian (1957) has shown that Equation 3.59 is the appropriate expression since it leads to the correct entropy change of  $R \ln 2$ .

Equation 3.50 can be rewritten as:

$$Z = \frac{PV_m}{RT} = 1 + \frac{Pb}{RT} \quad (3.61)$$

Equation 3.61 is similar to the virial EOS above and numerous authors (including Nothnagel et al., 1973) have shown that the chemical theory of gas imperfections leads to an EOS of the virial form in the limit where the fraction of molecules dimerized approaches zero.

### 3.6.1.3. The VPA/IK-CAPE EOS (VPA)

The VPA/IK-CAPE EOS is a vapour phase association (VPA) model published by IK-CAPE, a German consortium that develops property models for computer-aided process engineering (CAPE). In a manner similar to the formulation of Nothnagel (1973), the VPA/IK-CAPE model is based on the ideal gas law but allows for the formation of tetramers and hexamers in addition to the formation of dimers. The main assumption of the model is that all vapour phase non-ideality is due to molecular association. Attractive forces between the molecules and the

complexes are neglected (Aspen Plus help file). Acetic acid is known to form tetramers (Johnson and Nash, 1950) as well as dimers, but normally tetramerization can be safely ignored. For this study only the formation of dimers were considered. Once again, the equations and calculation methods for this method are extremely complex and only the more important equations are shown here. The reader is referred to the Aspen Plus help files for more detail and references.

As with the Nothnagel formulation (1973) discussed above, the VPA/IK-CAPE EOS also makes use of Equations 3.52, 3.53, 3.58 and 3.59. The true concentration of each species is solved from a system of non-linear equations obtained from the total and individual species mass balances coupled with the dimerization equilibrium condition. Once the true species concentrations are calculated, the following EOS is used:

$$V = \frac{RT}{P} \frac{1}{\sum_i \sum_n n z_{in} + 2 \sum_i \sum_{j>i} z_{Mij}} \quad (3.61)$$

where  $n$  is the degree of association ( $n=2$  for dimerization);  $z_{in}$  is the true species concentration for component  $i$  and degree of dimerization  $n$ ;  $z_{Mij}$  is the true concentration of cross-dimers of component  $i$  and  $j$ .

The fugacity coefficient is calculated from Equation 3.56 with all  $\phi_i$  set equal to zero since the mixture of true species are assumed to behave ideally (all non ideality in the vapour phase is attributed solely to the dimerization).

#### **3.6.1.4. The Statistical Associating Fluid Theory (SAFT) and Cubic Plus Association (CPA) Models**

Although they have not been used in this project, it is worth mentioning a few of the developments with associating models that have applied the principles of statistical mechanics. Chapman et al. (1990) developed the statistical associating fluid theory (SAFT) model based on Wertheim's first-order thermodynamic perturbation theory. In this model, pure fluids are treated as chains of equal-sized spherical segments. In order to describe association, molecules are assigned bonding sites, and the interactions between these sites are modeled using the square-well potential (Wolbach and Sandler, 1997). One of the restrictions of this model is that for

molecules that have one bonding site (i.e. carboxylic acids), only dimers are allowed to form. That is, both the vapour and liquid phases are restricted to being composed of only monomers and dimers.

Many modifications of the SAFT model have been suggested over the years. One of the most successful models has been that suggested by Huang and Radosz (1990), who applied a dispersion term in the SAFT framework. Gross and Sadowski (2001) developed the perturbed-chain SAFT (PC-SAFT) EOS by applying a second order perturbation theory to the original SAFT formulation. The PC-SAFT model is so named because a hard-chain fluid serves as a reference for the perturbation theory rather than spherical molecules, as in the earlier SAFT modifications. Gross and Sadowski (2001) found that their modification improved the pure-component representation when compared to the SAFT version of Huang and Radosz (1990).

Kontogeorgis et al. (1996) developed an equation-of-state for associating fluids by combining the physical term of the cubic SRK EOS (Soave, 1972) with the chemical (association) term taken from SAFT. The result is what is known as the Cubic Plus Association (CPA) EOS. Kontogeorgis et al. (1996) aimed to combine the simplicity of a cubic EOS with the theoretical background of the perturbation theory. In chemical equations of state, the association is expressed through the equilibrium constant  $K$ , which is independent of density. In the perturbation EOS (SAFT & CPA), the association strength is expressed through a function of the reduced density and association volume – the difference in definitions of these two properties being the difference between CPA and SAFT (Kontogeorgis et al., 1996).

### 3.6.2. Activity coefficient/Gibbs excess ( $G^E$ ) models

Many equations have been proposed correlating activity coefficients with composition (and to a lesser extent, temperature). The liquid activity coefficient models are often reported as functions for the excess Gibbs energy ( $G^E$ ), as these functions are linked by:

$$\ln \gamma_i = \frac{\partial}{\partial n_i} \left( \frac{n_T G^E}{RT} \right)_{P,T,n_j} \quad (3.61)$$

$$\frac{G^E}{RT} = \sum_i x_i \ln \gamma_i \quad (3.62)$$

In this study, only the three most widely used liquid activity coefficient (gamma) models were utilised and will be discussed here: viz. the Wilson (1964) model; the NRTL (Non-Random Two Liquid) model (Renon and Prausnitz, 1968); and the UNIQUAC (Universal Quasi-Chemical Theory) model (Abrams and Prausnitz, 1975). Raal and Mühlbauer (1998) provide a more detailed review on activity coefficient models.

### 3.6.2.1. The Wilson (1964) model

Wilson (1964) proposed a model based on the concept of local compositions. Local compositions within a liquid solution (different from the overall mixture composition) are presumed to account for the short-range order and non-random molecular orientation that results from differences in molecular size and inter molecular forces (Hwengwere, 2005). The local composition theory uses a probability model (Boltzmann distribution) to determine the average composition around any molecule in the liquid.

The Wilson expression for the excess Gibbs energy for a system consisting of  $m$  components is:

$$\frac{G^E}{RT} = -\sum_{i=1}^m x_i \ln \left( \sum_{j=1}^m x_j \Lambda_{ij} \right) \quad (3.63)$$

where  $\Lambda_{ij}$  and  $\Lambda_{ji}$  are the adjustable Wilson parameters which are related to the pure component liquid volumes by:

$$\Lambda_{ij} = \frac{V_j}{V_i} \exp \left[ -\frac{\lambda_{ij} - \lambda_{ii}}{RT} \right] \quad (3.64)$$

$$\Lambda_{ii} = 1 \quad (3.65)$$

The version of the Wilson model implemented in Aspen Plus (which was used for the data regression in this study) does not use the liquid molar volumes; instead  $\Lambda_{ij}$  is a function of temperature only:

$$\Lambda_{ij} = \exp \left( a_{ij} + \frac{b_{ij}}{T} + c_{ij} \ln T + d_{ij} T \right) \quad (3.66)$$

This variation of the Wilson model tends to fit VLE data better, particularly over wide temperature ranges (Van Dyk, 2005). The activity coefficient for any component  $k$  is given by:

$$\ln \gamma_k = -\ln \left( \sum_{j=1}^m x_j \Lambda_{kj} \right) + 1 - \sum_{i=1}^m \frac{x_i \Lambda_{ik}}{\sum_{j=1}^m x_j \Lambda_{ij}} \quad (3.67)$$

The advantages of the Wilson (1964) model include:

1. accurate representation of data with only a few parameters. A system of  $n$  components can be fitted with  $n(n-1)$  parameters obtained from the binaries.
2. accurate predictions of multi-component properties from binary data

According to Wilson (1964), for a binary system,  $A_{12}$  and  $A_{21}$  (the two adjustable parameters) are positive if the deviation from ideality is positive, and negative if the deviation from ideality is negative. In some cases the parameters will have opposite signs and the deviation from ideality will depend on which has the greatest effect and may change sign. Values greater than or equal to one produce imaginary numbers for  $G^E$  at certain compositions. Only values less than unity are needed in actual use with a value of unity indicating zero interaction between molecules.

A few limitations to the Wilson (1964) model are:

1. it cannot be used for partially miscible systems – i.e. it cannot predict the separation of two liquid phases.
2. it cannot be used for systems exhibiting activity coefficients extrema (a maximum or minimum). The Wilson equation always predicts that the activity coefficient increases monotonically as  $x_i$  approaches infinite dilution. Although relatively rare, some real systems do exhibit maxima.
3. systems with negative deviations from ideality are apparently not represented as well as with systems with positive deviations from ideality
4. expressions for  $H^E$  and  $S^E$  (heat of mixing and excess entropy) derived from the Wilson don't have the same analytical form of the equation for  $G^E$ .

Pairs of  $A_{12}$  and  $A_{21}$  parameters are not unique and a range of values will fit the data equally well (Barniki, 2002). The actual pair determined in the regression calculation depends on the

algorithm and initial guesses. Unfortunately,  $\Lambda_{ij}$  values have no real physical significance, so they are hard to guess *a priori*. Typical values range from about 3500 to -500 with little observable pattern based on type of system or deviations from ideality (Barniki, 2002).

### 3.6.2.2. The NRTL (1968) model

Renon and Prausnitz (1968) proposed an improved local composition model known as the Non-Random Two Liquid (NRTL) equation. It is based on the two-liquid model of Scott (1956) and an assumption of non-randomness similar to that used by Wilson (1964). A major difference between the Wilson (1964) and NRTL model is that the latter is also applicable to partially miscible systems. The NRTL equation for a system consisting of  $m$  components is expressed as:

$$\frac{G^E}{RT} = \sum_{i=1}^m x_i \frac{\sum_{j=1}^m \tau_{ji} G_{ji} x_j}{\sum_{l=1}^m G_{li} x_l} \quad (3.68)$$

where

$$G_{ij} = \exp(-\alpha_{ij} \tau_{ij}) \quad (3.69)$$

$$\tau_{ij} = \frac{g_{ij} - g_{ji}}{RT} \quad (3.70a)$$

In Aspen Plus, the  $\tau_{ij}$  parameter is defined in a similar manner as the  $\Lambda_{ij}$  for the Wilson:

$$\tau_{ij} = a_{ij} + \frac{b_{ij}}{T} + e_{ij} \ln T + f_{ij} T \quad (3.70b)$$

The activity coefficient for any component  $i$  is given by:

$$\ln \gamma_i = \frac{\sum_{j=1}^m \tau_{ji} G_{ji} x_j}{\sum_{l=1}^m G_{li} x_l} + \sum_{j=1}^m \frac{x_j G_{ij}}{\sum_{l=1}^m G_{lj} x_l} \left( \tau_{ij} - \frac{\sum_{r=1}^m x_r \tau_{rj} G_{rj}}{\sum_{l=1}^m G_{lj} x_l} \right) \quad (3.71)$$

The NRTL equation consists of the following three parameters:  $(g_{ij}-g_{jj})$ ,  $(g_{ji}-g_{ii})$  and  $\alpha_{ij}$ . The  $(g_{ij}-g_{jj})$  and  $(g_{ji}-g_{ii})$  parameters represent the interaction between species  $i$  and  $j$ . The parameter  $\alpha_{ij}$  (so-called non-randomness factor) is a constant that is characteristic of the randomness of the mixture, where a value of zero indicates that the mixture is completely random. It has become accepted that suitable values for  $\alpha_{ij}$  fall in the range of -1 to 0.5, since the activity coefficients are relatively insensitive to values of  $\alpha_{ij}$  within this range. The value of  $\alpha_{ij}$  is often fixed arbitrarily at a value between 0.2 and 0.47. Walas (1985) suggest that values for  $\alpha_{ij}$  (based on regression values of the Dechema data set) should be approximately 0.3 for non-aqueous mixtures and approximately 0.4 for aqueous organic systems. However, Raal and Mühlbauer (1998) have found these suggestions to be inconclusive and mention that a suitable value for  $\alpha_{ij}$  should be found from the reduction of experimental data (if sufficient data is available).

Similar to the Wilson model, only binary parameters are used in the NRTL model and parameters fit only on binary data may be used for multi-component systems, often with good accuracy. The NRTL model however, more so than Wilson, does not have a unique parameter set that best fits any binary system.

### 3.6.2.3. The UNIQUAC (1975) model

From the derivation of NRTL, it can be seen that this model is more suitable as an  $H^E$  model than a  $G^E$ -model (Prausnitz et al., 1999). The UNIQUAC (Universal Quasi-Chemical) model was developed by Abrams and Prausnitz (1975) in searching for a two parameter model that would retain at least some of the advantages of the Wilson model, but that would also be applicable to partly miscible systems. It consists of two parts, a *combinatorial part* due to molecular size and shape,  $G_{Comb}^E$ , and a *residual part* primarily for intermolecular energy interactions,  $G_{Res}^E$ . The combinatorial part depends only on pure component properties (requires volume and area parameters), while the residual part depends on the properties of the binary mixture and includes the two interaction parameters per binary. The UNIQUAC model also includes a third parameter, the coordination number ( $z$ ). This is almost always fixed at a value of 10.

The UNIQUAC model has a wide range of applicability (to miscible and immiscible solutions) and incorporates parameter temperature dependence; however, the equations are more complex than the activity coefficient models discussed above. Anderson and Prausnitz (1978) introduced a slightly modified form of the UNIQUAC equation. The equation takes the form:

$$G^E = G_{Combinatorial}^E + G_{Residual}^E \quad (3.72)$$

Where, for a binary mixture:

$$\frac{G_{Combinatorial}^E}{RT} = x_1 \ln \frac{\Theta_1}{x_1} + x_2 \ln \frac{\Theta_2}{x_2} + \frac{z}{2} \left[ q_1 x_1 \ln \frac{\theta_1}{\Phi_1} + q_2 x_2 \ln \frac{\theta_2}{\Phi_2} \right] \quad (3.73)$$

$$\frac{G_{Residual}^E}{RT} = -q_1' x_1 \ln [\theta_1' + \theta_2' \tau_{21}] - q_2' x_2 \ln [\theta_2' + \theta_1' \tau_{12}] \quad (3.74)$$

In Equations 3.73 and 3.74 the segment fractions ( $\Theta_i$ ) and area fractions ( $\theta_i$  and  $\theta_i'$ ) are given by:

$$\Theta_i = \frac{x_i r_i}{\sum_j x_j r_j} \quad (\text{summation over all components}) \quad (3.75)$$

$$\theta_i = \frac{x_i q_i}{\sum_j x_j q_j} \quad (\text{summation over all components}) \quad (3.76)$$

$$\theta_i' = \frac{x_i q_i'}{\sum_j x_j q_j'} \quad (\text{summation over all components}) \quad (3.77)$$

In the original formulation of Abrams and Prausnitz (1975), the parameters  $q_i$  and  $q_i'$  were identical. Anderson and Prausnitz (1978) recommended empirically adjusted values for  $q_i$  (denoted by  $q_i'$ ) to improve the performance of the UNIQUAC equation for systems containing water and alcohols. For fluids other than water or alcohols,  $q_i = q_i'$ . The parameters,  $r_i$  and  $q_i$  are the pure component volume and area structural parameters respectively. They are tabulated in Prausnitz et al. (1980) for 92 fluids. However, when unavailable, they are evaluated from molecular structure contributions for various groups and subgroups ( $r$  and  $q$ ). This group contribution method used in determining  $r_i$  and  $q_i$  is discussed in Raal and Mühlbauer (1998) and Fredensland et al. (1977).

The two adjustable model parameters,  $\tau_{12}$  and  $\tau_{21}$ , in Equation 3.74 are determined by data reduction and are defined by:

$$\tau_{ij} = \exp\left[\frac{-(u_{ij} - u_{jj})}{RT}\right] \quad (3.78)$$

As with the Wilson model, the version of the UNIQUAC model implemented in Aspen Plus differs in their definition of the adjustable parameters. In Aspen Plus, the adjustable model parameters,  $\tau_{ij}$ , are defined as:

$$\tau_{ij} = \exp\left(a_{ij} + \frac{b_{ij}}{T} + c_{ij} \ln T + d_{ij} T + \frac{e_{ij}}{T^2}\right) \quad (3.79)$$

Since the  $G^E$  expression consists of two terms, the analogous activity coefficient expression equation must also contain a combinatorial and residual part:

$$\ln \gamma_i = \ln \gamma_i^C + \ln \gamma_i^R \quad (3.80)$$

where

$$\ln \gamma_i^C = \ln \frac{\Phi_i}{x_i} + \frac{z}{2} q_i \ln \frac{\theta}{\Phi_i} + \Phi_j \left[ l_i - \frac{r_i}{r_j} l_j \right] \quad (3.81)$$

$$\ln \gamma_i^R = -q_i' \ln [\theta_i' + \theta_j' \tau_{ji}] + \theta_j' q_i' \left[ \frac{\tau_{ji}}{\theta_i' + \theta_j' \tau_{ji}} - \frac{\tau_{ji}}{\theta_j' + \theta_i' \tau_{ij}} \right] \quad (3.82)$$

with

$$l_i = \frac{z}{2} [r_i - q_i] - [r_i - 1] \quad (3.83)$$

The UNIQUAC equation has the advantages of the previous models (predicting immiscibility and activity coefficient extrema) and is also superior in representing mixtures of widely different molecular sizes (Walas, 1985). It is applicable to highly non-ideal chemical systems including mixtures of polar or non-polar, but non-electrolyte components. Like the NRTL model, regressing UNIQUAC to binary data does not yield a unique set of parameters. One of the greatest advantages of the UNIQUAC equation is its extension to predicting system parameters from pure component data via the group-contribution method UNIFAC method (Clifford, 2004). The reader is referred to Smith et al. (1996) and Fredenslund et al. (1977) for a full description of this (UNIFAC) technique.

According to Walas (1985), the main drawbacks to the UNIQUAC model are its greater algebraic complexity as compared to the NRTL and Wilson equations and the fact that often the representation of the VLE is poorer than for some simpler equations.

### 3.7. Thermodynamic consistency testing

It is tempting to accept published data or regression analyses of such data at face value, however, there is no guarantee on such data's quality. The graphical consistency of VLE data i.e. points on a smooth curve can in many instances be misleading as to the quality of the data, as systematic errors (positive or negative bias to any correlating equation) can easily be masked (Reddy, 2006). It is therefore important to spend some effort assuring that experimental VLE data are of acceptable quality before further use.

The Gibbs phase rule for non-reacting systems (Smith et al., 2001) provides the *degrees of freedom* for a system:

$$F = 2 - \pi + N \quad (3.84)$$

where  $\pi$  is the number of phases present,  $N$  is the number of chemical species (components) present, and  $F$  is called the degrees of freedom of the system. For a binary VLE system (two components, two phases), the Gibbs phase rule provides for two independent intensive variables ( $F=2$ ) so that when either the pressure  $P$ , or the temperature  $T$  is fixed, the composition of the liquid  $x_i$  and that of the vapour  $y_i$  cannot be changed without variation of  $T$  and  $P$  respectively. It is therefore not necessary to measure all four variables of experimental VLE data ( $T$ ,  $P$ ,  $x_i$  and  $y_i$ )

as the fourth property can easily be obtained from other three using solution thermodynamics. Measuring the fourth variable inevitably over-specifies the system; however there is a distinct advantage to measuring all four since the fourth variable can then be used to test for thermodynamic consistency. Consistency tests may be applied when redundant experimental data is available in conjunction with a set of mathematical relationships which inter-relate them. If a measurement can be predicted by other measured variables and mathematical relationships, then consistency can be claimed if the predicted and experimental values match to within experimental uncertainty (Jackson & Wilsak, 1995). Hence, thermodynamic consistency tests can only be applied to a full set of VLE data – i.e. P, T,  $x_i$  and  $y_i$ . For VLE data, the Gibbs-Duhem equation (which inter-relates the activity coefficients of all components in a mixture) forms the basis for many consistency tests including the following which are briefly described in this section:

- Slope test
- Area Test
- Point Test
- Direct Test

The point test was applied in this study.

### 3.7.1. The Gibbs-Duhem equation

The Gibbs-Duhem equation is an important thermodynamic relation which gives the constraint to how partial molar properties change with pressure and temperature and has traditionally served as one of the most important thermodynamic relations employed for validating the thermodynamic consistency of a VLE data set. Different thermodynamic consistency tests can be obtained by different manipulations of the Gibbs-Duhem equation. A derivation is provided below:

The summability of partial molar properties written for the activity coefficient for one mole of a binary system is:

$$\left(\frac{G^E}{RT}\right) = x_1 \ln \gamma_1 + x_2 \ln \gamma_2 \quad (3.85)$$

It follows that:

$$d\left(\frac{G^E}{RT}\right) = x_1 d \ln \gamma_1 + x_2 d \ln \gamma_2 + \ln \frac{\gamma_1}{\gamma_2} dx_1 \quad (3.86)$$

The fundamental excess property relation for one mole of a binary mixture is given by

$$d\left(\frac{G^E}{RT}\right) = \frac{V^E}{RT} dP - \frac{H^E}{RT^2} dT + \ln \frac{\gamma_1}{\gamma_2} dx_1 \quad (3.87)$$

Van Ness (1995) rewrites Equation 3.87 as:

$$\frac{d\left(G^E/RT\right)}{dx_1} = \ln \frac{\gamma_1}{\gamma_2} + \varepsilon \quad (3.88)$$

where

$$\varepsilon \equiv \varepsilon_T + \varepsilon_P \quad (3.89)$$

$$\varepsilon_T \equiv -\frac{H^E}{RT^2} \frac{dT}{dx_1} \text{ and } \varepsilon_P \equiv \frac{V^E}{RT} \frac{dP}{dx_1} \quad (3.90)$$

Binary VLE data are always measured either isobarically ( $\varepsilon_P = 0$ ) or isothermally ( $\varepsilon_T = 0$ ). Hence, only one  $\varepsilon$  term is required in the equations derived. For the isothermal case the heat of mixing term drops out of Equation 3.88 (zero change in temperature as well as enthalpy being a function of temperature only) ( $\varepsilon_T = 0$ ) and it is often justifiable to assume that the activity coefficient values have a weak dependency on pressure at low pressures (the excess volume term is usually negligible - typically 4 % of the magnitude of the activity coefficient according to Van Ness and Abbott, 1982). Therefore,  $\varepsilon_P = 0$  and the following is obtained:

$$\frac{d(G^E/RT)}{dx_1} = \ln \frac{\gamma_1}{\gamma_2} \quad (3.91)$$

The Gibbs-Duhem equation can also be written as:

$$\sum x_i d \ln \gamma_i = \frac{V^E}{RT} dP - \frac{H^E}{RT^2} dT \quad \text{or} \quad (3.92)$$

$$x_1 \frac{d \ln \gamma_1}{dx_1} + x_2 \frac{d \ln \gamma_2}{dx_1} - \varepsilon = 0 \quad (3.93)$$

It is interesting to note that  $\sum x_i d \ln \gamma_i = 0$  at constant temperature and pressure and

$$x_1 \frac{d \ln \gamma_1}{dx_1} = x_2 \frac{d \ln \gamma_2}{dx_2} \quad (\text{Constant T, P}) \quad (3.94)$$

There are two important applications for the Gibbs-Duhem equation:

1. In the absence of complete experimental data or the properties of a mixture, the Gibbs Duhem equation may be used to calculate additional properties.
2. If experimental data are available for each component over some composition range, it is possible to check the data for thermodynamic consistency. If the data satisfy the Gibbs-Duhem equation (or one derived from it), then they are thermodynamically consistent and it is likely that they are reliable.

When satisfying the Gibbs-Duhem equation it is likely, but by no means guaranteed that they are correct, since it is possible that an incorrect data set could fortuitously satisfy the Gibbs-Duhem equation.

### 3.7.2. Slope/Differential test

Implicit in the Gibbs-Duhem equation is the slope test for thermodynamic consistency. It is a theoretically simple test drawn directly from Equation 3.94 above. This test compares slopes of curves drawn to fit data points on plots of  $\ln \gamma_1$  and  $\ln \gamma_2$  versus  $x_1$ . These slopes may be

measured and are then substituted into Equation 3.94 at various compositions to see if the Gibbs-Duhem equation is satisfied. While this test appears to be both simple and exact, it is of little practical value since it is difficult to measure slopes with sufficient accuracy. Van Ness (1995) regards the test as tedious and uncertain, and as such, it has never found serious application. Hence, the “slope method” provides at best a rough measure of thermodynamic consistency which can only be applied in a semi quantitative manner. It can however be used to detect serious errors in the equilibrium data. For example, at a given composition, if  $\frac{d \ln \gamma_1}{dx_1}$  is positive then  $\frac{d \ln \gamma_2}{dx_2}$  must also be positive and likewise if  $\frac{d \ln \gamma_1}{dx_1}$  is zero (representing a maximum or minimum activity coefficient) then  $\frac{d \ln \gamma_2}{dx_2}$  must also be zero (Prausnitz, 1969). It should be noted this method is not recommended for systems that undergo phenomena such as self or cross-association at some part of the composition range (Jackson & Wilsak, 1995) and so is not applicable to systems containing alcohols and carboxylic acids.

### 3.7.3. Area/Integral test

For quantitative purposes, it is much more practical to use an integral (area) test rather than a differential (slope) test (Prausnitz, 1969). The area test was proposed independently by Herington (1947) and Redlich and Kister (1948) and involves the integration of Equation 3.88 over the entire composition range:

$$\int_0^1 \left( \frac{G^E}{RT} \right) dx_1 = \int_0^1 \left( \ln \frac{\gamma_1}{\gamma_2} + \varepsilon \right) dx_1 \quad (3.95)$$

$\left( \frac{G^E}{RT} \right) = 0$  at  $x_1=0$  and  $x_1=1$ , therefore Equation 3.95 reduces to:

$$\int_0^1 \left( \ln \frac{\gamma_1}{\gamma_2} + \varepsilon \right) dx_1 = 0 \quad (3.96)$$

To perform the test, one plots  $\left( \ln \frac{\gamma_1^{\text{exp}}}{\gamma_2^{\text{exp}}} + \varepsilon \right)$  against  $x_1$ . Figure 3-1 illustrates a typical curve obtained when this is done.

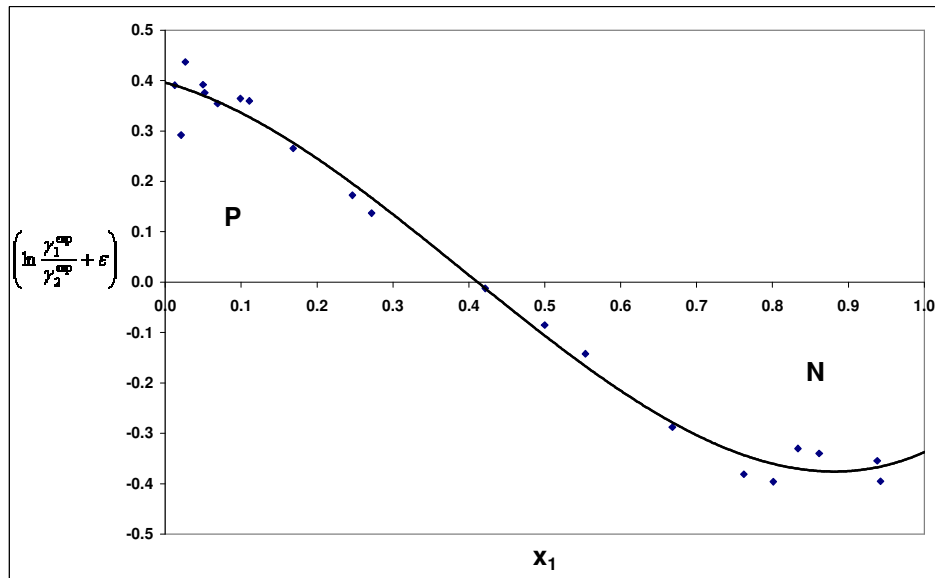


**Figure 3-1 Typical plot for the area test (data plotted for the 2-propanone (1) + 2-butanol (2) system at 333.15 K; measured in this study).**

$\varepsilon$  is often and incorrectly ignored when applying the area test to both isothermal and isobaric data sets (Van Ness, 1995). The value of the logarithmic function passes from positive to negative as the composition space is traversed and the plot must result in a net area of zero for the data to be consistent by this test – i.e. the negative area of the integral (N) should be equal to the positive area (P). In general it is acceptable that the difference between the positive and negative areas should be less than a few percentage points. i.e.

$$\frac{P - |N|}{P + |N|} \leq 10\% \quad (\text{van Ness, 1995; Gmehling and Onken, 1977})$$

Smith (1984) (cited in Jackson and Wilsak, 1995) employed the use of the ratios of the area P and N (of the area above the abscissa to that below or its reciprocal) as a measure of the

consistency of the data. Smith devised five categories for the assessment of the data on the basis of the outcome of the test (see Table3-1).

**Table 3-1 Categories of data assessment according to Smith (1984)**

Area ratio	Data assessment
0-0.6	totally unacceptable
0.6-0.8	marginal
0.8-0.9	fair
0.9-0.95	good
0.95-1	excellent

This test, though widely used in earlier studies, is of very little use in determining the thermodynamic consistency of a data set, as has been pointed out by many authors (including Raal and Mühlbauer, 1998). Van Ness et al. (1973, 1995) state that the area test is a necessary but not sufficient condition for consistency as it is considered to be too mild. At best it can only be concluded that data failing the test are thermodynamically inconsistent. The following limitations/concerns of the area test contribute to this:

1.  $\varepsilon$  is usually omitted (due to the unavailability of data) - which is a satisfactory approximation for isothermal data, but not in the case of isobaric data where the excess enthalpy (heat of mixing) is often a significant quantity. Heats of mixing ( $H^E$ ) over the temperature range of isobaric data sets is an important variable to take into consideration.
2. the consistency criterion of the net area  $\leq 10\%$  of the total area is not a stringent requirement – the data as a whole is tested rather than point by point.
3. the integral nature of the tests mean that the area under the  $\ln \frac{\gamma_1}{\gamma_2}$  versus  $x_1$  curve may appear correct but may have many compensating errors which can mask inadequacies and cause inconsistent data sets to pass.
4. more seriously, the greatest criticism on the area test is with regards to the pressure variable. From the  $\gamma-\Phi$  representation of VLE the ratio of the activity coefficients are:

$$\frac{\gamma_1}{\gamma_2} = \frac{y_1 P \Phi_1 / x_1 P_1^{sat}}{y_2 P \Phi_2 / x_2 P_2^{sat}} = \frac{y_1 \Phi_1 x_2 P_2^{sat}}{y_2 \Phi_2 x_1 P_1^{sat}} \quad (3.97)$$

Van Ness (1973) showed that when determining the ratio of  $\frac{\gamma_1^{\text{exp}}}{\gamma_2^{\text{exp}}}$  (as required by the area test), the measured total pressure cancels out and disappears from examination. Its remaining minor influence is only in the ratio  $\frac{\Phi_1}{\Phi_2}$ . Thus the area test does not make use of experimental pressure data (one of the most important and most accurately measured variables is lost) and is inconclusive in many instances. This test would sometimes pass data sets that are inconsistent while failing data sets that actually were consistent. The area test is therefore extremely sensitive to the values used for the pure component vapour pressures, as all it is testing is whether  $\frac{P_2^{\text{sat}}}{P_1^{\text{sat}}}$  is appropriate to the  $x_i$ - $y_i$  subset – i.e. assesses only the consistency of the  $x_i$ - $y_i$  data set at the given temperature.

The area test has been a very popular test and was readily accepted due to its simplicity. It is, however, a necessary condition that consistent data pass the area test but not a sufficient one (Van Ness, 1995). The problems mentioned above are avoided in the test utilized in this work to check for consistency of VLE data: the point test.

#### **3.7.4. Point/Residual (Van Ness-Byer-Gibbs) test**

Van Ness et al. (1973 & 1982) outline a point-to-point test that measures the internal consistency of the data. They put forward a more stringent test (compared to the slope and area tests) for the assessment of data consistency. As mentioned earlier, the four measurable variables of experimental VLE data T, P,  $x_i$  and  $y_i$  present an over specification of variables according to the phase rule of Gibbs. Thus when T is fixed, for any value of  $x_i$ , we can calculate values of  $y_i$  and P. In general the vapour phase compositions ( $y_i$ -data) introduce the most error (Smith et al., 2001); thus they are the most logical variable to be used when testing for thermodynamic consistency since if the  $y_i$ -values are consistent, then T, P and  $x_i$  should also be consistent. It is therefore common practice when testing a set of isothermal P- $x_i$ - $y_i$  data to compute  $y_i$  from the P- $x_i$  data alone using data reduction and then to compare the calculated  $y_i$  values with those measured. This procedure requires that the regression be performed using Barker's method

(discussed earlier) with only the pressure residual in the objective function. The latter ensures that the pressure residual scatters about zero (Van Ness, 1982). Systematic errors are transferred to the vapour composition residual, which scatters about zero for consistent data. The thermodynamic consistency of the system is judged by the deviations between the predicted and experimental  $y$  values ( $\Delta y = y_1^{\text{exp}} - y_1^{\text{calc}}$ ). The quantity  $\Delta y$  is calculated for each data point and an average value established. To successfully pass this test, the following two criteria must be met:

1. A quantitative, but still somewhat subjective criterion for acceptance is given by Christiansen and Fredenslund (1975),

$$|\Delta y| \leq \delta x + \delta y$$

Where  $\delta x$  and  $\delta y$  are the estimated uncertainties in the  $x$  and  $y$  measurements. A reasonable value for the RHS is about 0.01 (Raal and Mühlbauer, 1998). It is further suggested that the data are probably internally consistent when the average absolute deviation in the vapour mole fractions ( $|\Delta y_{1\text{avg}}|$ ) is less than or equal to about 0.01. (Fredenslund et al., 1977; Gmehling and Onken, 1977 & Gess et al., 1991).

2. If the data are truly random, the values of  $\Delta y$  must randomly scatter about  $\Delta y=0$  (the origin) as determined from a plot of  $\Delta y_1$  versus  $x_1$ . Otherwise, there may be a systematic error in either the experimental technique, or a poor fit of the activity coefficient, fugacity coefficient, and/or vapour pressure models. Outliers are easy to identify. At times, a few points might not meet this criterion, but the overall set may still be of adequate quality.

When testing of the experimental data requires the selection of a suitable thermodynamic model, Bradshaw (1985) pointed out that the chosen model must meet the following criteria:

1. errors introduced by the model must be considerably less than the errors in the experimental measurements.
2. model must be flexible enough to ensure that there is no loss of accuracy in the translation of experimental measurements into a set of model parameters.

For the point test in particular, the excess Gibbs energy model must be flexible enough to allow the pressure residual to scatter about zero. In addition, the pure component vapour pressures must be measured carefully as incorrect values introduce systematic errors in  $\Delta y$ . If these criteria

are not met, then failure of a consistency test could be attributed to the inability of the chosen model to adequately describe the data, and not only to systematic error in the data itself.

Jackson and Wilsak (1995) strongly recommend that the following three plots be reviewed in interpreting the results from this test before drawing conclusions:

1. Pressure-composition diagram displaying the experimental data and the model
2. P-residual plot
3. y-residual plot

The first two plots are useful for determining whether or not the P- $x_i$  data have been successfully modeled, and if this so, then the last plot will clearly show if bias exists in the y-residuals. Even though it is one of the most definitive thermodynamic consistency tests available, it is not without shortcomings (extracted from Jackson and Wilsak, 1995):

1. a proper model must be chosen *a priori*. An inappropriate choice will be manifested as a bias in one or more of the three plots mentioned above, and may lead an inexperienced user to the premature conclusion that the data are of poor quality. Moreover, if the appropriate model cannot be found, this test cannot be utilized.
2. emphasis is placed squarely on the discrete location of the experimental points. If an overly flexible model is fit to a data set that is sparse in one region of the pressure-composition diagram, it is possible for the model to show anomalous behaviour between the points in the sparse region. This is one important reason for viewing the data and the model on the pressure-composition diagram, as such anomalous behaviour will not be noticed on the residual plots.
3. the regressions employed for this test usually conform to the recommendation of Barker (1953) rather than taking into account experimental uncertainty in all the measured variables, as would be the case if a maximum likelihood regression were used. A statistically insignificant variation of a measured variable in a highly sensitive region can induce biased results. Indeed, Barker's approach, which assumes no error associated with either the temperature or the liquid phase measurements, was used in the present investigation during the regressions.
4. poor results can sometimes be difficult to interpret. If the data in a region where the standard assumptions are in doubt, the inconsistencies may be an indication of bad data,

an inappropriate model, or both. Using only this test, it can sometimes be difficult to determine why the inconsistencies are present.

5. Finally, problems can be encountered in getting the regressions to converge for some systems, while for others the number of adjustable parameters in the model may exceed the number of data points available. In such cases, the test cannot be used at all.

### 3.7.5 Direct test

The area test is based on  $\left( \ln \frac{\gamma_1^{\text{exp}}}{\gamma_2^{\text{exp}}} + \varepsilon \right)$  and as discussed earlier it was found to be lacking as a consistency test. Van Ness (1995) developed the direct test. He noted that the residual  $\delta \ln(\gamma_1 / \gamma_2)$  offered a unique opportunity for consistency testing.

Differentiating Equation 3.85 (the summability of partial properties) with respect to  $x_1$ :

$$\frac{d(G^E/RT)^{\text{exp}}}{dx_1} = x_1 \frac{d \ln \gamma_1^{\text{exp}}}{dx_1} + \ln \gamma_1^{\text{exp}} + x_2 \frac{d \ln \gamma_2^{\text{exp}}}{dx_1} - \ln \gamma_2^{\text{exp}} \quad (3.98)$$

Equation 3.98 may be written for experimental data as:

$$\frac{d(G^E/RT)^{\text{exp}}}{dx_1} = \ln \frac{\gamma_1^{\text{exp}}}{\gamma_2^{\text{exp}}} + \varepsilon + x_1 \frac{d \ln \gamma_1^{\text{exp}}}{dx_1} + x_2 \frac{d \ln \gamma_2^{\text{exp}}}{dx_1} - \varepsilon \quad (3.99)$$

and for the regressed data as:

$$\frac{d(G^E/RT)}{dx_1} = \ln \frac{\gamma_1}{\gamma_2} + \varepsilon + x_1 \frac{d \ln \gamma_1}{dx_1} + x_2 \frac{d \ln \gamma_2}{dx_1} - \varepsilon \quad (3.100)$$

where the appropriate equation for  $\varepsilon$  is selected depending on whether the VLE data have been measured isobarically or isothermally. The excess Gibbs energy residual results when Equation

3.100 is subtracted from Equation 3.99. Re-writing in terms of residuals (with  $\delta = \text{exp-calc}$ ) leads to:

$$\frac{d(\delta G^E/RT)}{dx_1} = \delta \ln \frac{\gamma_1}{\gamma_2} - \left( x_1 \frac{d \ln \gamma_1^{\text{exp}}}{dx_1} + x_2 \frac{d \ln \gamma_2^{\text{exp}}}{dx_1} - \varepsilon \right) \quad (3.101)$$

When a data set (isobaric or isothermal) is reduced using an objective function which minimizes the excess Gibbs energy residual (e.g.  $\sum \delta \frac{G^E}{RT}$  or  $\sum \left( \delta \frac{G^E}{RT} \right)^2$ ) (so as to force the Gibbs excess residuals to scatter about zero), the excess Gibbs energy residual should scatter about zero and Equation 3.101 becomes:

$$\delta \ln \frac{\gamma_1}{\gamma_2} = x_1 \frac{d \ln \gamma_1^{\text{exp}}}{dx_1} + x_2 \frac{d \ln \gamma_2^{\text{exp}}}{dx_1} - \varepsilon \quad (3.102)$$

The Gibbs-Duhem equation requires that the RHS of Equation 3.102 to be equal to zero provided that the experimental VLE data are consistent and the LHS is a direct measure of the deviation of the experimental data from the Gibbs-Duhem equation. The direct test, therefore, requires that the residual  $\delta \ln \frac{\gamma_1}{\gamma_2}$  for thermodynamically consistent data, scatter about zero when the data are reduced minimizing an objective function which minimizes the excess Gibbs energy residual. The extent to which the residual values scatter about the x-axis provides a measure of the departure of the data from thermodynamic consistency. Van Ness (1995) suggests a scale based on the root mean square (RMS) of the residual  $\delta \ln \frac{\gamma_1}{\gamma_2}$  to quantify the degree to which the data departs from consistency (Table 3-2). A value of “1” is assigned to data of the highest quality and 10 for a highly unsatisfactory or poor data set.

**Table 3-2 Consistency Index for VLE data for the direct test (Van Ness, 1995)**

Index	RMS $\delta \ln \frac{\gamma_1}{\gamma_2}$	
1	>0	$\leq 0.025$
2	>0.025	$\leq 0.050$
3	>0.050	$\leq 0.075$
4	>0.075	$\leq 0.100$
5	>0.100	$\leq 0.125$
6	>0.125	$\leq 0.150$
7	>0.150	$\leq 0.175$
8	>0.175	$\leq 0.200$
9	>0.200	$\leq 0.225$
10	>0.225	

## CHAPTER 4

### EQUIPMENT DESCRIPTION

This chapter provides a description of the experimental equipment which were utilized for this project i.e. the dynamic recirculating stills of Joseph (2001) and Reddy (2006) (Figure 4-1 and Figure 4-3 respectively). Joseph (2001) made structural improvements to the glass apparatus of Raal (Raal & Mühlbauer, 1998) and developed a computer-aided control strategy for the control of temperature and pressure. The apparatus of Joseph (2001) imposes a constraint on the upper limit of pressure (and hence, temperature) as it is not capable of withstanding pressures higher than atmospheric pressure. Furthermore, the still itself was not designed for high temperature work because the septa used on the still (for liquid and vapour sampling) degrade at temperatures above 180 °C. The stainless steel design of Reddy (2006) was based on the design by Harris (2004) which, for the most part, was also based on the glass still design of Raal (Raal & Mühlbauer, 1998). The apparatus of Reddy (2006) enabled measurements above atmospheric pressure to be undertaken, however, it was unable to achieve stability at pressures lower than about 10 kPa. The apparatus of Joseph (2001) was found to operate well at pressures as low as a few kilopascals and provided greater precision with respect to the pressure measurements. This chapter also discusses the auxiliary equipment involved with the pressure measurement and stabilization, temperature measurement, as well as those involved with the sampling and analysis of the equilibrium phases.

#### **4.1. The VLE apparatus of Joseph (2001)**

The glass VLE apparatus utilized in this project has been used recently by Clifford (2004) and Hwengwere (2005) and is described in great detail by Joseph (2001) and Reddy (2006). Figure 4-1 shows a schematic diagram of the glass VLE still of Joseph (2001) and a schematic block diagram of the experimental setup is provided in Figure 4-2.

The reboiler was charged with a liquid sample and the internal and external heaters were used to bring the sample to a boil. The external heater consisted of nichrome wire wrapped around the boiling chamber, which compensated for heat losses to the environment, while the internal heater consisted of a heater cartridge that provided the actual impetus for boiling. The internal heater

was positioned within the boiling chamber, and further provided nucleation sites for smooth boiling and facilitates the precise control of the circulation rate, while inducing rapid boiling. As the mixture boils, slugs of liquid are carried up by the vapour through the Cottrell tube (G) via the vapour-liquid lift mechanism. The vapour/liquid mixture exits the Cottrell tube at its top end and discharges onto 3 mm rolled 316 stainless steel wire mesh cylinders present in the equilibrium chamber (A). The vapour and liquid phases flow downwards co-currently through the packing and reach a state of thermodynamic equilibrium. Thereafter, the phases are separated to allow for the withdrawal of small (1 $\mu$ l) samples and subsequent analysis, before the phases are mixed and reintroduced into the boiling chamber.

A further innovative feature of this still design is that the Cottrell tube is vacuum insulated to prevent the transfer of heat from the slightly superheated mixture in the Cottrell tube to the equilibrium chamber. The entire equilibrium chamber is also surrounded by a vacuum jacket to further ensure adiabatic operation of the chamber. The disengaged vapour phase is condensed before sampling. An ethylene glycol solution, which is used as the cooling medium, is circulated through the condenser from a water bath containing a temperature controller and a cooling coil unit which facilitates the attainment of sub-ambient temperatures in the condenser. The liquid and vapour condensate streams are returned separately to the boiling chamber in their respective return lines. Any backflow into the sample traps was compensated for in the design of Joseph (2001), which features a "siphon break" tube to prevent the above. There is also a capillary section (J) at the base of the reboiler, which serves to reduce backflow and allows for the smooth flow of the returning stream into the boiling chamber. Since the still is constructed from glass, it is limited to measurements at or below atmospheric pressure. There is an efficient pressure-regulating system present (connected to the condenser) to maintain a constant pressure within the apparatus.

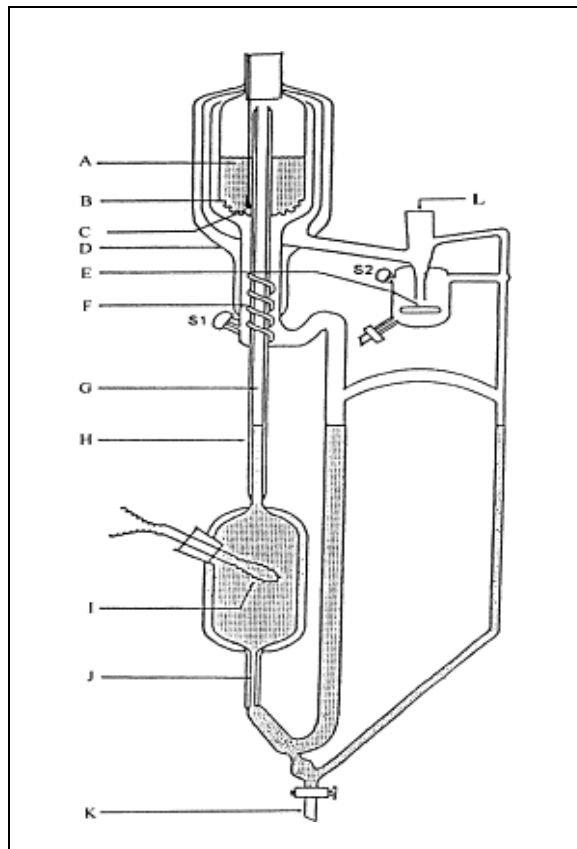


**Figure 4-1 Schematic diagram of the glass VLE still taken from Joseph (2001)**

A: SS wire mesh packing; B: drain holes; C: Pt-100 bulb; D: vacuum jacket; E: magnetic stirrer; F: SS mixing spiral; G: insulated Cottrell pump; H: vacuum jacket; I: internal heater; J: capillary; K: drain valve; S1: liquid sampling point; S2: vapour sampling point; L: condenser is attached here.

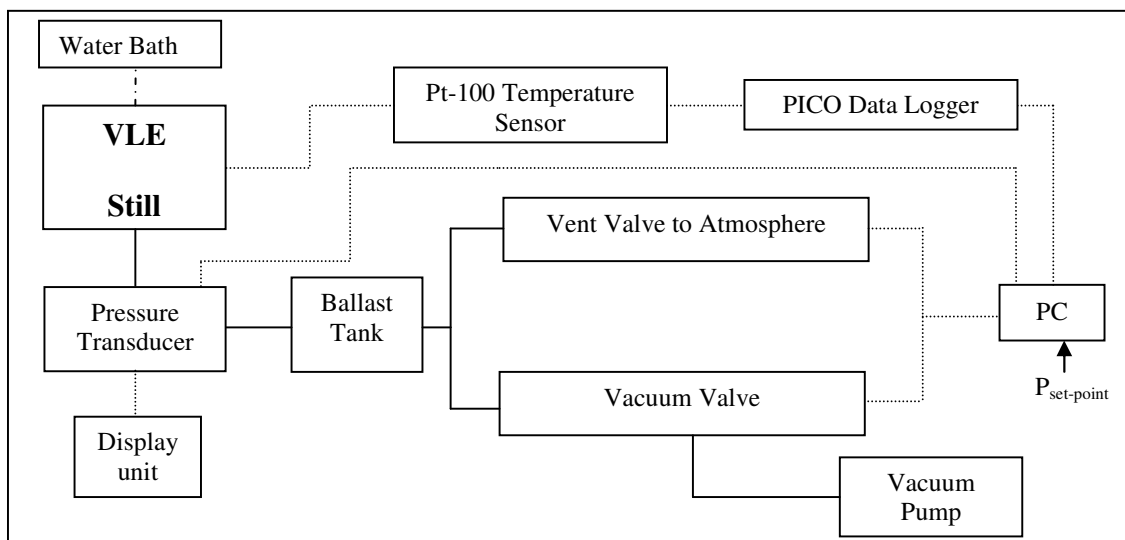


**Figure 4-2 Schematic Block diagram of the glass VLE apparatus of Joseph (2001)**

..... electronic lines; - - - - - water lines; ————— pneumatic lines.

#### **4.2. The VLE apparatus of Reddy (2006)**

The stainless steel dynamic equilibrium still of Reddy (2006) is similar to the design of Joseph (2001) with the additional capabilities of withstanding higher pressures and temperatures. Reddy critically evaluated the design of Harris (2004) and addressed some of the principal flaws of the previous design to develop the more efficient design used for this project. The maximum temperature and pressure limits for safe operation are 750kPa and 600K respectively.

A schematic diagram of the apparatus, as reproduced from the dissertation of Reddy (2006), is shown in Figure 4-3. The bulk of the apparatus was constructed from 316 stainless steel. The design of the reboiler (A), equilibrium chamber (C) and sample traps (G & I) incorporated the use of flanges and graphite-based gaskets, which have good sealing properties and resilience. Significantly thinner walls were used in the construction of this apparatus in comparison to those used in the design of Harris (2004). The large mass of stainless steel with a large heat capacity resulted in a slow thermal response in the apparatus of Harris and made the attainment of a thermal equilibrium very difficult. Although a reduction in the wall thickness resulted in a lower maximum operating pressure limit, it assists in attaining thermal equilibrium, and improves the thermal response of the apparatus to a change in the heat input. This also reduces the general operating time by resulting in shorter start-up, shut-down and equilibrium times.

The operation of the still by Reddy (2006) is similar to operating procedure described by Joseph (2001) for the low-pressure VLE glass still. Similar to the low pressure still, the apparatus of Reddy (2006) has two heaters present in the reboiler – an internal heater H1 (in the form of a 200 W heater cartridge within a machined insert at the base of the reboiler) and an external heater (H2) in the form of a custom-made 900 W Supernozzle heater. The external heater contributes to the boiling of the mixture and together with a refractory cement casing on its upper flange and an insulation layer of graphite and glass wool tape, it compensates for heat losses to the environment. The internal heater is centrally positioned within the boiling chamber and permits rapid boiling and precise control of the circulation rate. The surface of the heater cartridge cavity in contact with the reboiler contents was roughened to promote smooth boiling and efficient transfer of heat to the mixture. As an improvement to the design of Harris (2004), mechanical agitation was also incorporated into the boiling chamber of the apparatus in the form of a magnetically coupled stirrer. The stirrer was machined from 306 SS and rotated upon a ball-bearing mechanism.

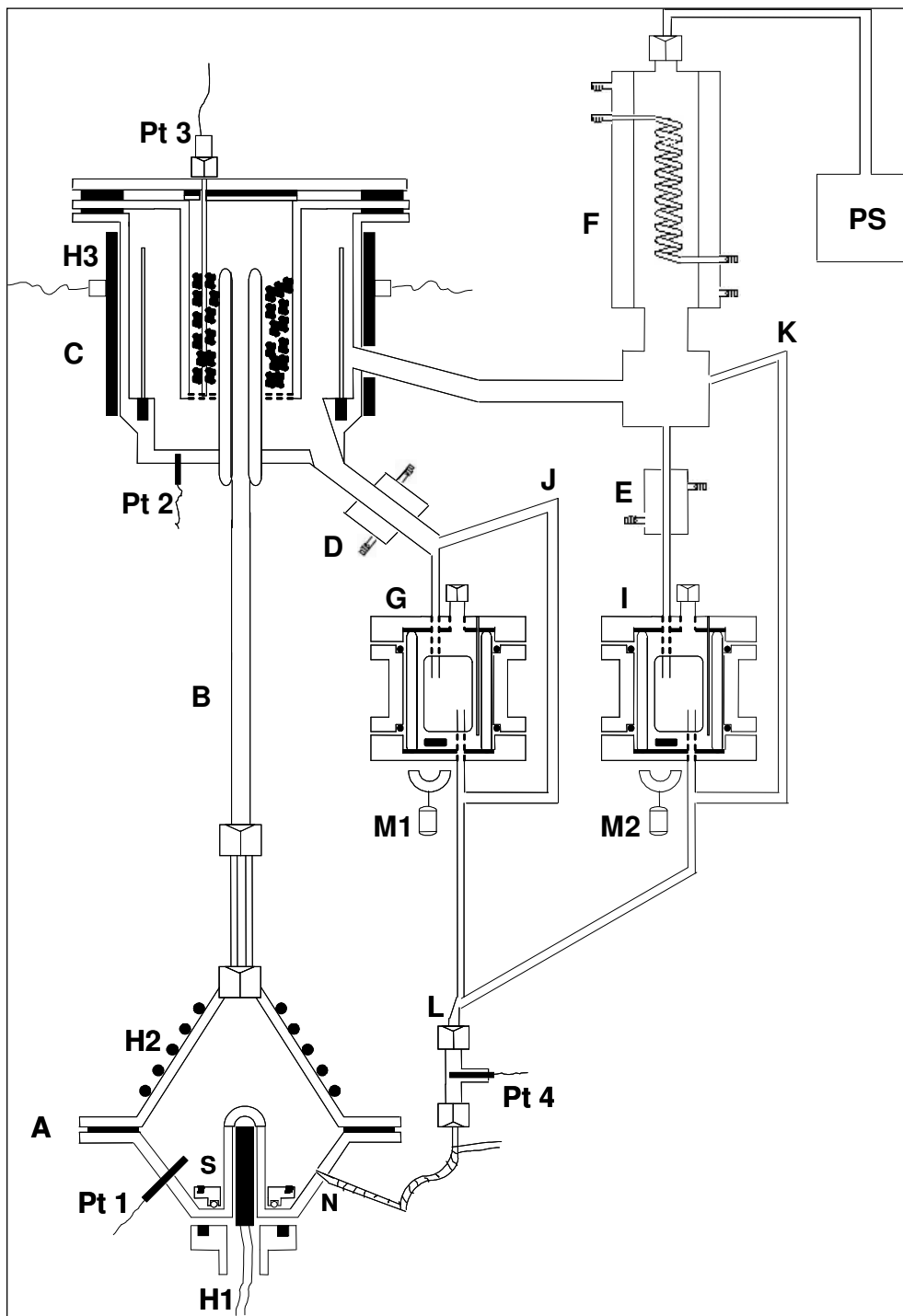
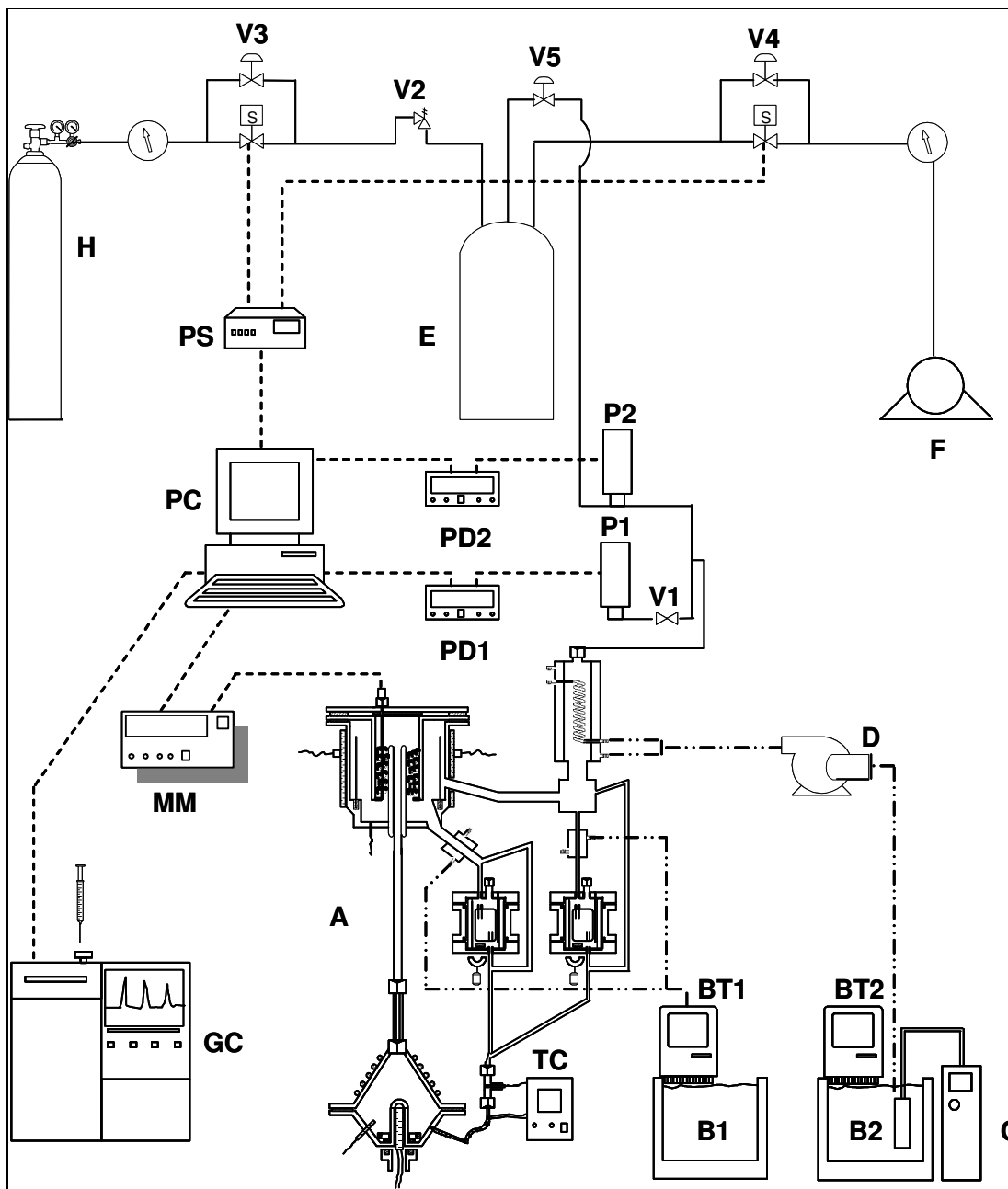


Figure 4-3 Schematic diagram of the stainless steel VLE still taken from Reddy (2006)

A: reboiler; B: Cottrell tube; C: equilibrium chamber; D: liquid cooler; E: vapour condensate cooler; F: condenser; G: liquid sample trap; H1, H2, H3: heaters; I: vapour condensate sample trap; J: liquid trap pressure equalizer tube; K: vapour condensate sample trap equalizer tube; L: return line union; M1, M2: motor-shaft mounted magnets; N: capillary; PS: pressure stabilization system; Pt1, Pt2, Pt3, Pt4: platinum temperature resistors; S: reboiler stirrer.



**Figure 4-4 Schematic diagram of the equipment layout of the steel apparatus taken from Reddy (2006)**

A: VLE still; B1,B2: waterbaths; BT1, BT2: thermostats/circulator pumps; C: refrigeration apparatus; D: coolant fluid pump; E: ballast tank; F: vacuum pump; GC: gas chromatograph; H: gas cylinder; MM: multimeter; P1: pressure transducer (Sensotec); P2: pressure transmitter (Wika); PC: personal computer; PD1, PD2: pressure displays; PS: power supply unit; TC: temperature controller; V1: shut-off valve; V2: safety relief valve; V3,V4,V5: control valves; - - - - - electronic lines; - - - - - water lines; \_\_\_\_\_ pneumatic lines.

**Other important features of the design of Reddy (2006) include the following:**

- (a) Transparent sections in the Cottrell tube (B) and in the sample traps (G and I). This allowed for the general fluid flow and circulation rate to be monitored. In the Cottrell tube it is important to ensure that there is continuous transport of slugs of vapour and liquid. In the sample traps, transparency allows for an observation of the occurrence of any backflow into the sample trap and an observation of the circulation rate in the form of a drop count.
- (b) Magnetic stirrers were used to eliminate any concentration gradients in the traps.
- (c) The use of an indirect pulley drive system to couple the magnetized stirrer in the reboiler to an external rotating magnetic field.
- (d) The lines immediately before the sample traps are jacketed to allow for the flow of a cooling medium (D and E) – which is to be used at elevated temperatures to prevent damage to the Teflon<sup>®</sup> and Viton<sup>®</sup> sealing materials.
- (e) Additional tubes (J and K) were used across sample traps to allow for pressure equalization and a minimal holdup of the phases exiting the sample traps.
- (f) In order to facilitate some pre-mixing of the returning equilibrium phases, the vapour condensate line and liquid phase return line are combined into a single line (L) a fair distance away from the entry point of the combined phases into the reboiler.
- (g) The combined returning streams can be pre-heated with the use of nichrome wire windings around the respective section and a CN-40 temperature controller, before re-entering the reboiler.
- (h) In addition to the temperature sensor used to measure the equilibrium temperature, other Pt-100 sensors are used to monitor the thermal profiles of the reboiler and wall of the equilibrium chamber to assist in preventing the superheating of the mixture.

**Innovative features common to the designs of Joseph (2001) and Reddy (2006) include the following:**

- (a) Packing in the equilibrium chamber (A) increases the interfacial area for mass transfer allowing for intimate contact and the quick attainment of equilibrium between the vapour and liquid phases during each pass through the chamber, even for species with a high relative volatility

- (b) The packing (miniature 3mm SS cylinders constructed from hollow wire mesh) is easily accessible and the volume of packing can be adjusted if required. The open structure of the packing minimizes the pressure drop through the packing.
- (c) The equilibrium chamber is angularly symmetric about the Cottrell tube which prevents the formation of temperature or concentration gradients since there is no preferred radial direction for the equilibrating mixture of vapour and liquid to pass through.
- (d) The concentric design around the packed section of the equilibrium chamber minimizes liquid drop entrainment in the vapour phase and forces the vapour to surround the equilibrium chamber, serving as a thermal lagging.
- (e) Mechanical agitation is present in the boiling chambers which provide nucleation sites for boiling (in addition to the housing for the internal heater) and also ensures that the returning vapour condensate is mixed properly with the returning liquid. The condensed vapour is at a lower temperature and contains a higher mole fraction of the more volatile components and if the phases are not properly mixed in the reboiler this could result in the occurrence of non-equilibrium vapourization or flashing.

### **4.3. Auxiliary equipment**

Figure 4-2 and Figure 4-4 illustrate the auxiliary equipment utilized in this project including how they are connected to the VLE still and each other in the equipment of Joseph (2001) and Reddy (2006) respectively. The major auxiliary sections will be described in the proceeding paragraphs.

#### **4.3.1. Auxiliary equipment on the apparatus of Joseph (2001)**

##### **4.3.1.1. Pressure measurement and stabilization/control**

A WIKA P-10 (0 to 2.5 bar abs) model pressure transmitter is located in line between the VLE apparatus and the ballast tank (Figure 4-2). The pressure was displayed on a WIKA DI35 display unit and controlled via a PC using the Shinko ACS01M controller which actuated one of two Clippard solenoid valves.

The large ballast tank serves as a pressure reservoir to dampen the effects of pressure fluctuations and trap any condensable vapours should the condenser fail. The ballast tank may be opened to the atmosphere (high-pressure source) or to an Edwards model 3 vacuum pump (low-pressure source) with inline solenoid valves. The solenoid valves are “normally closed” unless actuated

by the PC (via the Shinko software) to either increase or decrease the pressure as required. They allow for a very small admittance of flow and are arranged in a by-pass loop configuration to allow for faster pressurization and evacuation of the ballast tank when needed.

The pressure accuracy was estimated as  $\pm 0.03$  kPa and controlled to within 0.01 kPa for isobaric operation.

#### **4.3.1.2. Temperature measurement and control**

Joseph (2001) made use of a Pt-100 sensor connected to a Hewlett-Packard 6-1/2 digit multimeter to display its resistance. In this project, the Pt-100 sensor was connected to a PICO PT104 Pt100 converter which enabled the logging and plotting of the temperature profiles on a PC. The sensor was positioned at the bottom of the packing to ensure that the temperature is measured reliably at a point after equilibrium has been established (label “C” in Figure 4-1).

During isothermal operation, the temperature was controlled manually by carefully adjusting the system pressure; by increasing or decreasing the pressure, the system temperature would increase or decrease respectively. The accuracy of the measured temperature was estimated as  $\pm 0.02^\circ\text{C}$  and the temperature control varied between  $\pm 0.01^\circ\text{C}$  and  $\pm 0.05^\circ\text{C}$  depending on the chemical system being investigated and the composition range.

#### **4.3.2. Auxiliary equipment on the apparatus of Reddy (2006)**

##### **4.3.2.1. Pressure measurement and stabilization/control**

Two pressure sensors were fitted to the apparatus of Reddy (P1 and P2 in Figure 4-4), i.e. the original Sensotec Super TJE pressure transmitter of Harris (2004), as well as a more recent WIKA P-10 pressure transmitter which can be used for applications going up to 10 bar. In this project, the system pressure was measured using the WIKA sensor alone and was controlled via a PC (using the VALVECON program of Harris (2004) as modified by Reddy (2006) to incorporate the WIKA pressure sensor) which, as in the case of Joseph’s apparatus, actuated one of two Clippard solenoid valves.

The apparatus also has a 113.4 litre ballast tank (E) serving the same purpose as in the glass apparatus. In this arrangement, the ballast tank is connected to a high pressure source (H,

nitrogen delivered from a high pressure cylinder) and a low pressure source (F, an Edwards Speedivac vacuum pump) with inline solenoid valves. These solenoid valves are also arranged in a by-pass loop configuration to allow for faster pressurization and evacuation of the ballast tank when needed and are “normally closed” unless actuated by the PC (via the VALVECON program) to either increase or decrease the pressure as required.

The pressure accuracy was estimated as  $\pm 0.1$  kPa and controlled to within 0.1 kPa for isobaric operation.

#### **4.3.2.2. Temperature measurement and control**

The equilibrium temperature was measured using a 4-wire 1/10 DIN Pt-100 sensor (supplied by WIKA Instruments) connected to an Agilent 34401A multimeter. The sensor was positioned at the bottom of the packing to ensure that a reliable and accurate temperature of the equilibrated sample/mixture was obtained (Pt3 in Figure 4-1).

During isothermal operation, the temperature was controlled in the same manner as with the glass apparatus i.e. via the manual manipulation of the system pressure. The accuracy of the measured temperature was estimated as  $\pm 0.02$  °C and was controlled to within  $\pm 0.01$  °C.

#### **4.3.3 Sampling and composition analysis**

Of the several methods available to analyse the composition of samples, gas chromatography was chosen because of its convenience. Gas chromatographs have the advantages of having small sample sizes (below 1 $\mu$ l), excellent detection limits and reproducibility, and relatively simple operating procedures. For both equipment, samples were withdrawn using a 1  $\mu$ l GC syringe directly from the sample traps through the chemically resistant septa used to seal the sampling ports. Depending on the chemical system, one of two gas chromatographs (A Shimadzu GC 2014 or Shimadzu GC 2010) was employed to accurately analyse the composition of the samples in this project. For some systems, the response of the detector on the Shimadzu 2014 GC (FID) to the constituent components was barely distinguishable from the background noise; furthermore, the packed Porapak Q column used with it was unable to sufficiently separate the components. These problems were rectified by switching to the Shimadzu 2010 GC fitted with a TCD detector and a Zebron ZB-WAXplus capillary column. This resulted in an excellent response to the chemicals and adequate separation (the polar phase in the column is well suited

for separating polar compounds); lower retention times were also observed when compared to when the packed column was used. The operating conditions for the two gas chromatographs used are presented in Section 6.2.2. The calculated species compositions were estimated to be accurate to  $\pm 0.002$  mole fraction.

## CHAPTER 5

### EXPERIMENTAL PROCEDURE

This chapter describes the general experimental procedures employed in measuring VLE data in this project and focuses on the preparation, calibration and operation of the experimental apparatuses involved.

#### 5.1. Preparation of experimental apparatus

##### 5.1.1 Cleaning of the VLE still

The importance of eliminating all impurities from the chemical systems and experimental apparatus before commencing with the calibration and experimental measurement procedures cannot be overstated. The presence of even the slightest impurity can have significant effects on the VLE behavior of the measured systems. Therefore, chemicals of the highest available purities were used (chemical purities of the chemicals used are listed in Chapter 6), and the VLE stills were cleaned thoroughly before undertaking measurements for each system.

Cleaning of the VLE stills was effected by repeatedly operating the still isobarically with a clean low-boiling solvent and draining in order to flush out the contaminants. Reddy (2006) utilized the more volatile component of the binary mixture under study as the cleaning solvent and this method was repeated in this work for both apparatuses. After three to four rinses with the cleaning solvent and the final draining, the pressure in the still was set as low as possible with the aid of a vacuum pump (about 0.1 kPa) and heated slightly in order to flash off any residual solvent and dry the still.

##### 5.1.2 Leak detection

The presence of leaks introduces instability in the pressure measurement and control, which results in a loss of material from the system which affects the phase composition measurements. Hence, the elimination of leaks from the experimental apparatus is another important aspect of its preparation. On the glass apparatus this was carried out by drawing a vacuum within the still with the aid of the vacuum pump and thereafter isolating the still from the ballast tank with the

vacuum pump and pressure controller switched off. An increase in the system pressure indicated the presence of leaks. Vacuum grease was applied to all ground glass joints and septa and valves were replaced if necessary. On the apparatus of Reddy (2006), leak detection was done by pressurizing the apparatus to about 2 bar and applying a soapy solution to the possible sources of leaks (such as the various tube fittings and joints). Bubbles were observed if a leak was present and the identified leaks were eliminated by applying a sealing agent to the area.

## **5.2. Temperature, pressure and composition calibrations**

In order to obtain accurate measurements, the equipment used to measure the pressure, temperature and composition of the system had to first be calibrated. This was essential so that they could be used to give true measurements of their respective variables by eliminating the sources of error introduced by the measuring equipment themselves. The calibration procedures are detailed below.

### **5.2.1. Pressure transmitter calibration**

On the apparatus of Reddy (2006), the WIKA P-10 pressure transmitter together with its display unit was sent to WIKA instruments to be calibrated such that the display reading was equal to the actual pressure it measured. The calibration of the WIKA P-10 pressure transmitter used on the glass still was achieved by using a standard reference pressure transmitter obtained from WIKA which was attached to the VLE still. The standard pressure transmitter (already calibrated by WIKA instruments) provides the true pressure reading within the still. With the aid of the pressure control system, the pressure in the still was varied. At each point in the progression, the pressure was allowed to stabilize for a few minutes before recording values for the true pressure (from the standard pressure sensor) and the values displayed for the WIKA P-10 sensor that was being calibrated. Plots of the true pressure versus the display reading for the pressure transducer were generated for two pressure ranges (0-10 kPa and 10-100 kPa), both of which yielded linear relationships as shown in Figures 6-1 and 6-2 (refer to Chapter 6). The accuracy of the measured pressure was estimated as  $\pm 0.03$  kPa and  $\pm 0.1$  kPa for the glass and steel apparatuses respectively.

### **5.2.2. Temperature sensor calibration**

As mentioned in Chapter 4, the Pt-100 temperature sensors used to obtain the equilibrium temperature were connected to a PICO PT104 Pt100 converter on the apparatus of Joseph (2001)

and to an Agilent 34401A multimeter on the apparatus of Reddy (2006). The PICO converter displayed the temperature in degrees Celsius on the PC and the Agilent multimeter indicated the resistance of the sensor in ohms. Both sensors were calibrated “in situ” by running the stills isobarically over a range of pressures with a chemical of very high purity (>99.5%). For each pressure, the corresponding equilibrium temperature was found using the experimental apparatus, and the true temperature of the system was calculated using the Antoine’s vapour pressure equation for the chemical used (coefficients obtained from Poling et al. 2001). Plots of the actual temperature against the display temperature or resistance of the sensor (whichever is applicable) yielded linear relationships, as shown in Figures 6-3 and 6-4 (refer to Chapter 6). The temperature accuracy was estimated as  $\pm 0.02$  °C in both cases.

### **5.2.3. Gas chromatograph detector calibration**

One of two Shimadzu GC’s (GC-2014 or GC-2010) was used to analyse the phase compositions. The operating conditions for each GC for each of the binary mixtures worked with are shown in Section 6.2.2. These were carefully determined to ensure adequate separation of components in the GC and are believed to be the most appropriate for the generation of separate sharp peaks for each system. The columns used were preconditioned to remove any contaminants present which will contribute to “ghost peaks” in the chromatograms and will adversely affect the column performance. This was done by heating the columns to about 20K below its maximum allowable temperature for approximately 15 hours with a steady flow of carrier gas flowing through the column.

The GC does not give absolute compositions, but rather it produces peak areas for each component present which are proportional to the amount of substance injected into the GC. The chromatogram area ratio method described by Raal and Mühlbauer (1998) for calibrating the GC was employed for this work. Defining  $F_i$  as the proportionality constant (known as the response factor) between the number of moles passing the detector ( $n_i$ ) and the peak area ( $A_i$ ) for each component, the following relationship exists:

$$n_i = A_i F_i \quad (5.1)$$

Raal and Mühlbauer (1998) work with area ratios as opposed to the absolute areas since the absolute areas depend on the amount of sample injected and are generally not very reproducible. For a binary mixture:

$$\frac{n_1}{n_2} = \left( \frac{A_1}{A_2} \right) \left( \frac{F_1}{F_2} \right) = \frac{x_1}{x_2} \quad (5.2)$$

Area ratios  $A_i/A_j$  are plotted against mole fraction ratios  $x_i/x_j$  at both ends of the composition range ( $x_i=0$  and  $x_i=1$ ). In the very dilute regions, the plots are usually linear and pass through the origin, and the response factor ratios are obtained from the slopes of the curves. If the response factor ratios are exactly constant, then the slope of the first plot should equal the inverse of the slope of the second plot. Conversely, if the slope of the first plot is equal to the inverse of the slope of the second plot (values within 1 % of each other will be considered acceptably close enough), then the response factor ratios can be assumed to be constant and a linear relationship assumed between the area ratios and mole fraction ratios.

The GC calibration curves were generated by gravimetrically preparing standard solutions from the pure starting materials and analyzing them to obtain the area ratios for the different mixtures spanning the entire composition range. The calibration curves for each of the binary systems worked with for this project were thereby constructed and can be found in Section 6.5. The calculated species compositions are estimated to be accurate to  $\pm 0.002$  of a mole fraction.

### **5.3. Operating procedures**

For the most part, the experimental procedures used by Joseph (2001) and Reddy (2006) were employed for this project and are described in the following sections. As stated in Chapter 4, isobaric and isothermal operation can be achieved using the computer control scheme which actuates either the solenoid valve to the vacuum pump or to the nitrogen tank at high pressure.

#### **5.3.1. Isobaric operation**

##### **5.3.1.1. Start-up procedure**

When commencing experiments the temperature and pressure display units, the motors for the magnetic stirrers and the computer were turned on, along with the cooling coil unit and the pump/temperature-controller for the water bath which is used for the condenser. On the steel

apparatus, the ballast tank and VLE still were evacuated to remove the air and other vapours that were present within the apparatus. This was achieved by switching on the vacuum pump with the pressure control system switched off. The solenoid valves were in their “normally closed” positions and the by-pass loop on the low-pressure side of the pressure control set-up was opened to allow for the rapid evacuation of the apparatus to occur. The evacuation process is complete when the pressure (observed on the pressure display unit) reaches a minimum value and stops decreasing, i.e. when further evacuation produces no measurable pressure change it is assumed that the system is free of foreign gases. Thereafter the by-pass loop on the low-pressure side was closed and nitrogen was allowed to flow into the ballast tank and VLE still via the by-pass loop on the high-pressure side of the pressure control set-up. A sufficient vacuum must exist in the still to be able to draw up the liquid mixture into the still through the drain/fill valve on the reboiler. It is also important that the pressure in the still be higher than the vapour pressure of the mixture at the still temperature to prevent the mixture from flashing upon entering the still.

The cleaned still was then charged with one of the pure components of the binary mixture (the glass still was simply charged at atmospheric pressure via the vapour condensate sampling point). The reboiler was filled to a level 3-4 cm above the top of the reboiler in both instances, which facilitates the lifting of the liquid mixture by the vapour up the Cottrell tube when the mixture begins to boil. Thereafter the pressure in the apparatus was set manually (somewhat close to the desired value) with the use of the by-pass loops, before the pressure control program was activated with the desired pressure set-point for precise pressure control via the two solenoid valves (as described in Chapter 4).

The still and its contents were then heated by switching on the internal and external heaters in the reboiler, as well as the equilibrium chamber external heater on the apparatus of Reddy (2006). The external heaters are used to compensate for heat losses to the environment and the reboiler internal heater is required for the principal heating of the mixture and for precise control of the circulation rate. The power supply to the heaters was gradually increased to prevent a thermal shock to the system and the temperature of the equilibrium chamber (and reboiler on the apparatus of Reddy (2006)) was monitored. Sufficient heat needs to be supplied to the reboiler to ensure smooth, continuous boiling (which is observed through the Cottrell tube) and a good circulation rate (judged by the drop count at the condenser). The increasing of the heat input was stopped and the system left to stabilize when there was a vigorous pumping action in the Cottrell

tube and steady flows of the liquid and vapour condensate phases in the respective traps were observed (approximately 120 drops per minute were observed in the vapour condensate trap).

### 5.3.1.2. Determination of equilibrium

Once the equipment has heated up and a steady-state operation has been achieved within the VLE still, there is still a relationship that exists between the measured temperature and the power input supplied to the reboiler (Kneisl et al. 1989). Kneisl et al. (1989) explained that the vapour/liquid mixture in the Cottrell tube is slightly superheated (due to the hydrostatic head acting on the fluid in the Cottrell tube) and that this superheat is relieved as the mixture is ejected from the Cottrell tube onto the packing in the equilibrium chamber. The mixture cools to its equilibrium temperature as a result of the occurrence of expansion of the mixture and also evaporation of a small quantity of the liquid phase upon entering the equilibrium chamber. Figure 5-1 illustrates a typical response of the measured equilibrium temperature to an increase in the energy input. Generally, at low heating rates, an increase in the energy input results in sharp rise in the measured equilibrium temperature to a broad “plateau region”. The sharp rise indicates that the heating rate in that region is not sufficient to superheat the liquid to a degree that offsets the subsequent cooling upon expansion in the equilibrium chamber (Kneisl et al. 1989). In the “plateau region”, small increases in the energy input have little or no effect on the measured temperature; the superheating balances off the cooling and the true equilibrium temperature is observed. Further heating (past the “plateau region”) results in the superheating exceeding the cooling effect, and the observed temperature once again increases with an increase in the energy input.

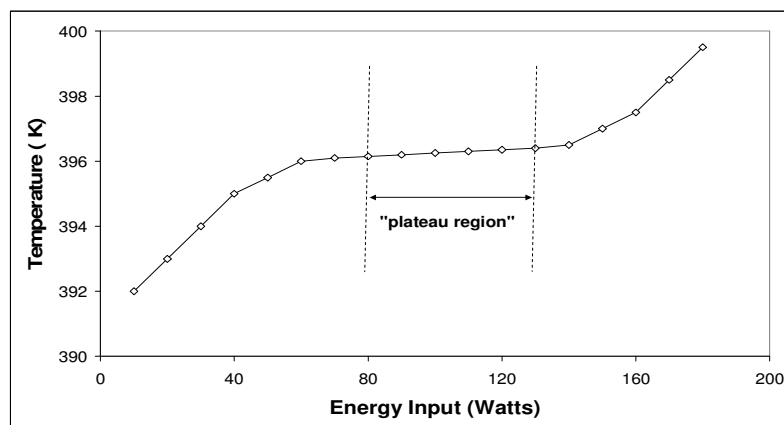


Figure 5-1 Typical temperature response curve illustrating the “plateau region” for a “well-behaved compound”.

Some of the “well-behaved” chemicals in the study by Kneisl et al. (1989) were found to have large and distinct plateau regions (such as for non-polar alkanes). The effect of the energy input on the measured temperature was found to be particularly strong for high boiling-point polar compounds (such as alcohols) which have very small plateau regions (appearing only as inflection points in some cases). Hence the “plateau region” is not always a flat region, but rather it is taken to be the region with the minimum slope and it is critical that measurements are undertaken in this region to obtain accurate boiling point measurements.

For each equilibrium point, the “plateau region” needed to be found. This was done by starting the still with lower heater settings and incrementally increasing the power input via the voltage setting of the internal heater. For each voltage increment, the still system was allowed to equilibrate and the measured temperature recorded. The initial power input was chosen as the lowest that resulted in an even boil as observed visually and the system was allowed to equilibrate for about 45 minutes on the steel apparatus and about 20 minutes on the glass apparatus. Thereafter, the voltage supply to the reboiler internal heater was increased in increments of 5 V and a further 15-20 minutes on the steel apparatus and about 10 minutes on the glass apparatus was required for equilibration at each subsequent increase in the power input.

Obtaining the plateau region was the first step in the determination of equilibrium. Once this had been reached, the system was allowed some time to attain a state of thermodynamic equilibrium (equilibration times of 45 minutes to an hour on the steel apparatus and 20 to 35 minutes on the glass apparatus were required). The equilibration times depend on the properties of the binary systems, particularly the relative volatility and the circulation rate in the still. A high circulation rate (indicated by the drop rate in the condenser) and the flow patterns of the equilibrium phases can be used as a second criterion to determine the equilibrium condition (continuous and steady “pumping” of slugs of vapour and liquid up the Cottrell tube are desirable). Constant phase compositions (for the binary mixtures) is the third criterion which indicates the attainment of thermodynamic equilibrium (i.e. simultaneous constancy of temperature, pressure and composition).

#### **5.3.1.3. Phase composition determinations**

Once it was certain that equilibrium was established, the temperature and pressure were recorded. Samples of the equilibrium phases were withdrawn from the sample traps through chemically resistant septa using a 1  $\mu$ l GC liquid syringe (supplied by DLD Scientific). The liquid samples were taken first, followed quickly by the condensed vapour as to minimize any disturbances to the equilibrium. The syringe was cleaned with acetone and flushed several times with the sample before a sample was withdrawn for analysis and injected directly into the GC. To ensure reproducibility, a minimum of three injections for each phase was made, ensuring that the average deviation for the area ratios was within a tolerance of 0.1 %. A deviation of  $\pm$  0.002 mole fraction between injections for a particular phase was considered an acceptable criterion for composition stability taking into account the uncertainty in the measuring apparatus and the calibration procedure (Reddy, 2006). Note that the chromatograms should be analysed for the presence of peaks in addition to those corresponding to the test components. Additional peaks may indicate the degradation of the test materials or the possible formation of reaction products or impurities.

#### **5.3.1.4. Effecting composition changes within the VLE apparatus**

With the exception of the 1-propanol + n-butanoic acid system, the experiments were started with one of the pure components of the binary mixtures that were measured. A change in the composition was effected by withdrawing a small volume of liquid from the still and replacing it with a similar volume of the second component. The procedures described in the previous sections were repeated to obtain the VLE data for about half of the composition range. Thereafter the operation of the still was stopped, the still was drained and cleaned before being charged with the second component of the binary mixture. VLE data for the second half of the composition range was then measured following the same procedures as for the first half. This method of measuring the VLE data from both ends of the composition range allows for many points in the dilute regions of both components to be measured and tests the measuring method since both halves of the phase equilibrium curves should meet without any discontinuity. With the 1-propanol + n-butanoic acid system, it was found that even without a catalyst, upon heating for extended periods of time, the components reacted to form the ester propyl butanoate and water (the reaction products were confirmed with a GCMS analysis). Hence for this system fresh chemicals had to be used for almost each equilibrium data point in order to keep the product impurity below 1 % (GC Area %).

#### **5.3.1.5. Shut-down procedure**

The heat input to the still was switched off by turning off the variacs, which are connected to the various heaters. The respective programs for pressure control were halted and the system maintained at the current pressure whilst the apparatus cooled down. The vacuum pump was closed off from the ballast tank before being switched off to prevent the pump oil from being sucked into the ballast tank via a pressure gradient once the pump is switched off. Thereafter the still was brought to atmospheric pressure. On the glass apparatus this was achieved by venting the equipment to the atmosphere. On the steel apparatus, if sub-atmospheric conditions were being used, nitrogen gas was allowed to flow into the apparatus via the by-pass loop until the pressure in the apparatus reached the atmospheric pressure. If pressures higher than atmospheric were used, then the pressure in the apparatus was reduced to atmospheric pressure using the by-pass loop on the low-pressure side of the pressure control set-up. Thereafter the contents of the still were emptied and the waste chemicals disposed off appropriately.

#### **5.3.2. Isothermal operation**

Isothermal operation relies upon the successful operation of the apparatus under isobaric conditions and manual control of the system temperature. The start-up, shut-down and phase composition determinations were as discussed for isobaric operation. In determining the equilibrium conditions, the temperature was maintained at a constant value by manipulating the pressure. The pressure was initially varied such that the corresponding equilibrium temperature (as determined for isobaric operation) was found to be close to the desired operating temperature. The temperature was then controlled manually by carefully adjusting the system pressure; by either increasing or decreasing the pressure, the system temperature would increase or decrease respectively. For each pressure set-point, the corresponding “plateau region” was found until the equilibrium temperature was the desired system temperature. The system pressure at that point was then recorded and the rest of the analysis was similar to the isobaric operation.

## CHAPTER 6

### EXPERIMENTAL RESULTS

This chapter presents the experimental results obtained during the course of the project. It includes the phase equilibrium data measured in this project, as well as the calibrations for the GC detectors and, pressure and temperature sensors. The uncertainty in the measured system variables of temperature, pressure and composition, along with the purity of chemicals used during experimentation, are important factors which influence the accuracy of the results obtained. These topics are therefore addressed in the preliminary sections of this chapter. Wherever possible, comparisons of data measured in this project with that available in the literature have been included.

#### 6.1. Purity of materials

The importance of eliminating all impurities from the chemical systems and apparatus before commencing with the apparatus calibrations and experimental measurements cannot be overstated. Only chemicals of the highest available purities were used in this study. Before the chemicals were used, their purities were checked against the manufacturer's claims via GC analyses of the pure components as well as measurements of their refractive indices. The refractive indices were measured using one of the high-precision refractometers available in the School (School of Chemical Engineering, UKZN) and provide a useful check of the purity. Table 6-1 lists the chemicals used in the experimental work; the chemical suppliers, stated purities, GC analyses and refractive indices are also stated. The GC analyses for 2-propanone and 2-butanol gave slightly lower purities compared to what was stated by the chemical suppliers. The refractive indices for these two chemicals, however, corresponded well with the literature values. For all of the remaining chemicals, the GC analyses revealed no significant impurities and the agreement between the refractive indices of each chemical measured in this work with those found in the literature was satisfactory. All chemicals were therefore used without further purification.

**Table 6-1 List of chemicals used and their respective purities**

Chemical (IUPAC name)	Synonyms	Supplier	Stated Minimum Purity (mass %) <sup>a</sup>	GC Analysis (peak area %)	Refractive Index Literature <sup>b</sup>	Refractive Index This work
n-heptane <sup>c</sup>	dipropyl methane	FLUKA	99.5%	99.9	1.3855 <sup>c</sup>	1.3854 <sup>c</sup>
n-octane <sup>c</sup>	-	MERCK	99.0%	99.9	1.3944 <sup>c</sup>	1.3944 <sup>c</sup>
cyclohexane	Hexahydrobenzene Hexamethylene Hexanaphthene hexanaphthylene	FLUKA	99.5%	99.9	1.4235 <sup>c</sup>	1.4234 <sup>c</sup>
ethanol	ethyl alcohol	SAARCHEM- MERCK	99.5%	99.9	1.3611 <sup>d</sup>	1.3612 <sup>d</sup>
1-propanol	n-propanol propyl alcohol 1-propyl alcohol	SAARCHEM- MERCK	99.0%	99.9	1.3850 <sup>d</sup>	1.3852 <sup>d</sup>
n-butanoic acid	n-butyric acid butyric acid ethyl acetic acid propyl formic acid	MERCK	99.0%	99.8	1.3980 <sup>d</sup>	1.3980 <sup>d</sup>
2-propanone	Acetone dimethyl ketone	SIGMA- ALDRICH	99.8%	99.2	1.3588 <sup>d</sup>	1.3588 <sup>d</sup>
2-butanol	sec-butanol sec-butyl alcohol 2-butyl alcohol 2-hydroxybutane methyl ethyl carbinol	FLUKA	99.5%	98.9	1.3978 <sup>d</sup>	1.3974 <sup>d</sup>
propanoic acid	propionic acid methyl acetic acid	FLUKA	99.0%	99.6	1.3809 <sup>d</sup>	1.3816 <sup>d</sup>

<sup>a</sup>As stated by the supplier

<sup>b</sup>CRC Handbook of Chemistry and Physics, 86<sup>th</sup> Edition (David R. Lide, 2005-2006)

<sup>c</sup>at 25 °C

<sup>d</sup>at 20 °C

<sup>e</sup>used to calibrate temperature sensors

## 6.2. Equipment calibrations and accuracy of measurements

Apart from the purity of the chemicals used during experimentation, there are other important factors which influence the accuracy of the results obtained. These include the uncertainty in the measured system variables of pressure, temperature and composition. The estimated accuracy of the measured variables for this project is summarized in Table 6-2.

**Table 6-2 Estimated accuracy of measured system variables**

	Apparatus of Joseph (2001)	Apparatus of Reddy (2006)
Temperature	$\pm 0.02$ °C	$\pm 0.02$ °C
Pressure	$\pm 0.03$ kPa	$\pm 0.1$ kPa
Composition	$\pm 0.002$ mole fraction	$\pm 0.002$ mole fraction

### 6.2.1. Pressure and temperature sensor calibrations

The calibrations of the pressure and temperature sensors are discussed in Chapter 5. As mentioned in Chapter 5, the pressure transmitter used on the apparatus of Reddy (2006) had been calibrated by WIKA instruments such that the reading taken off the display unit was equivalent to the actual system pressure. For the pressure transmitter on the apparatus of Joseph (2001), calibration plots were generated for two pressure ranges: 0 to 10 kPa and 10 to 100 kPa. The calibration curves for the pressure sensor on the apparatus of Joseph (2001) and for the temperature sensors located in the equilibrium chambers of both apparatuses used are presented in Figures 6-1 to 6-4.

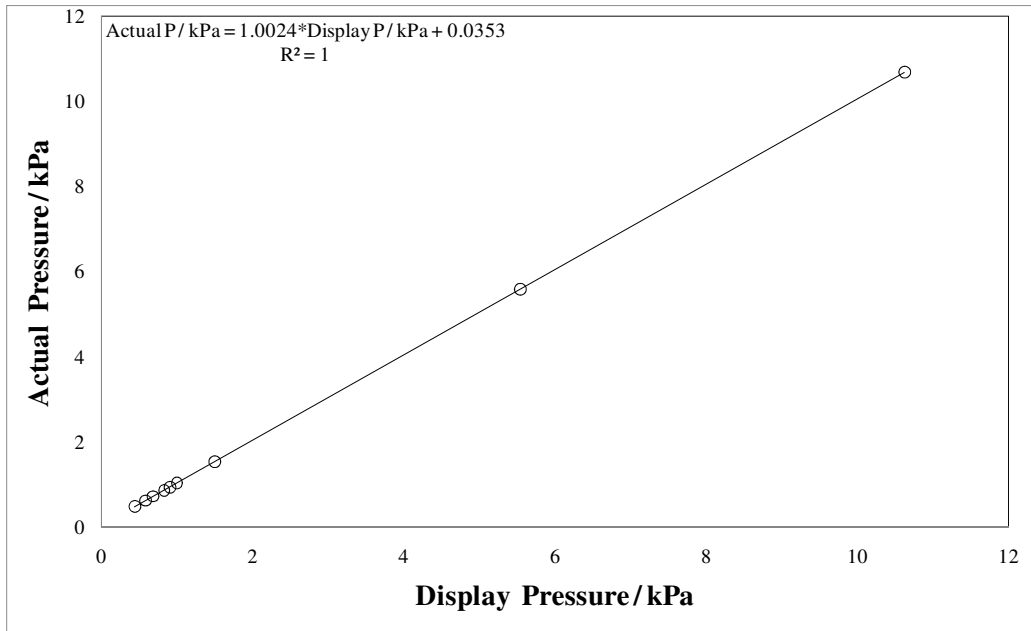


**Figure 6-1 Calibration plot for the pressure transmitter on the apparatus of Joseph (2001) for the 0 to 10 kPa pressure range**

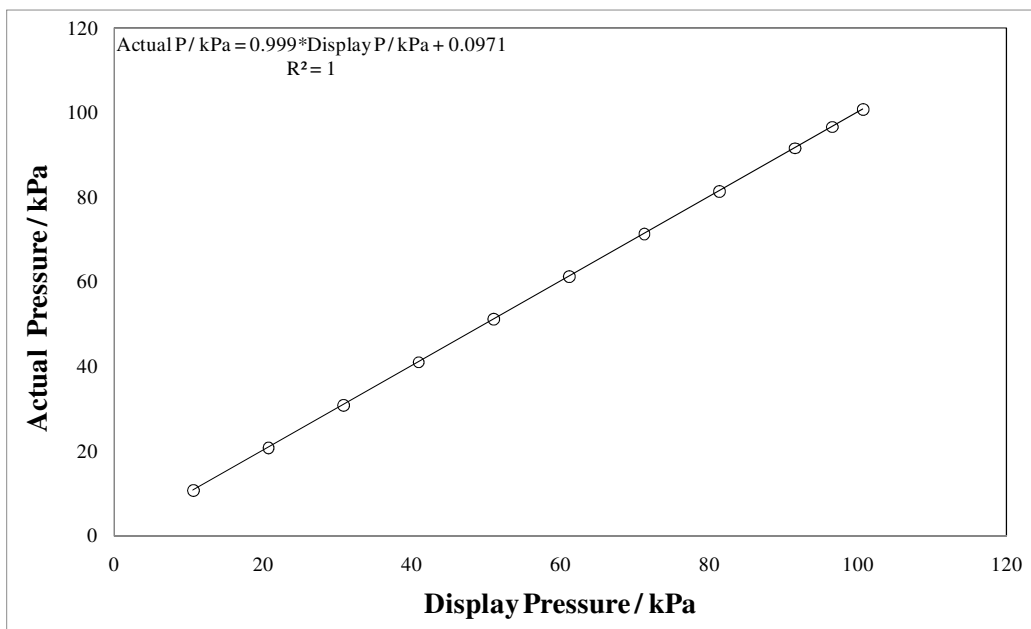


**Figure 6-2 Calibration plot for the pressure transmitter on the apparatus of Joseph (2001) for the 10 to 100 kPa pressure range**

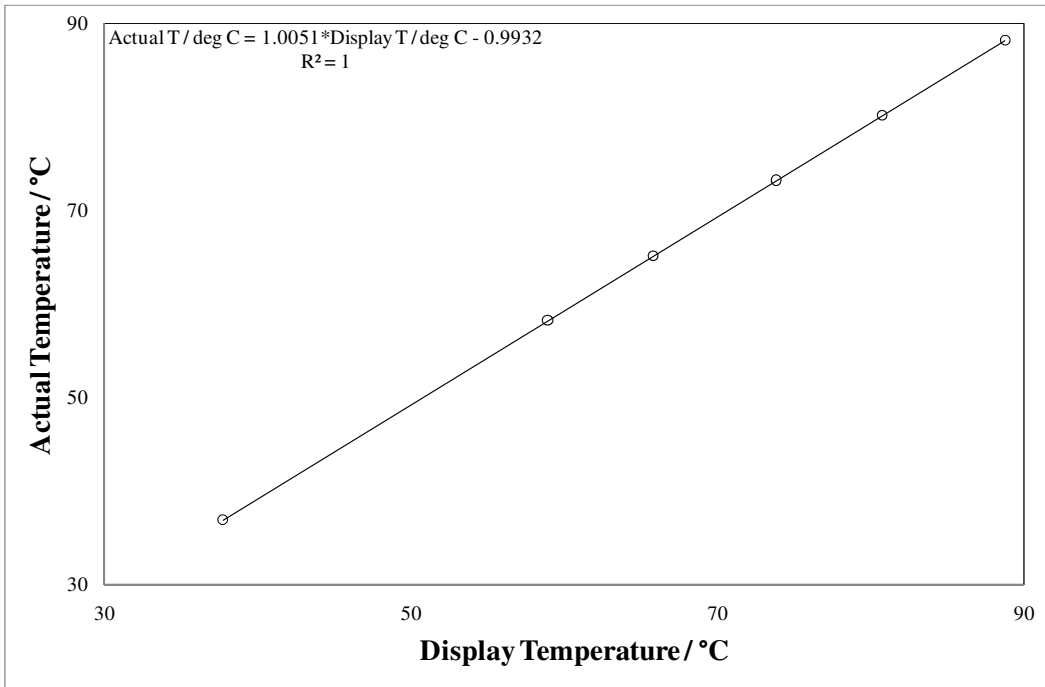


**Figure 6-3 Calibration plot for the temperature sensor on the apparatus of Joseph (2001)**

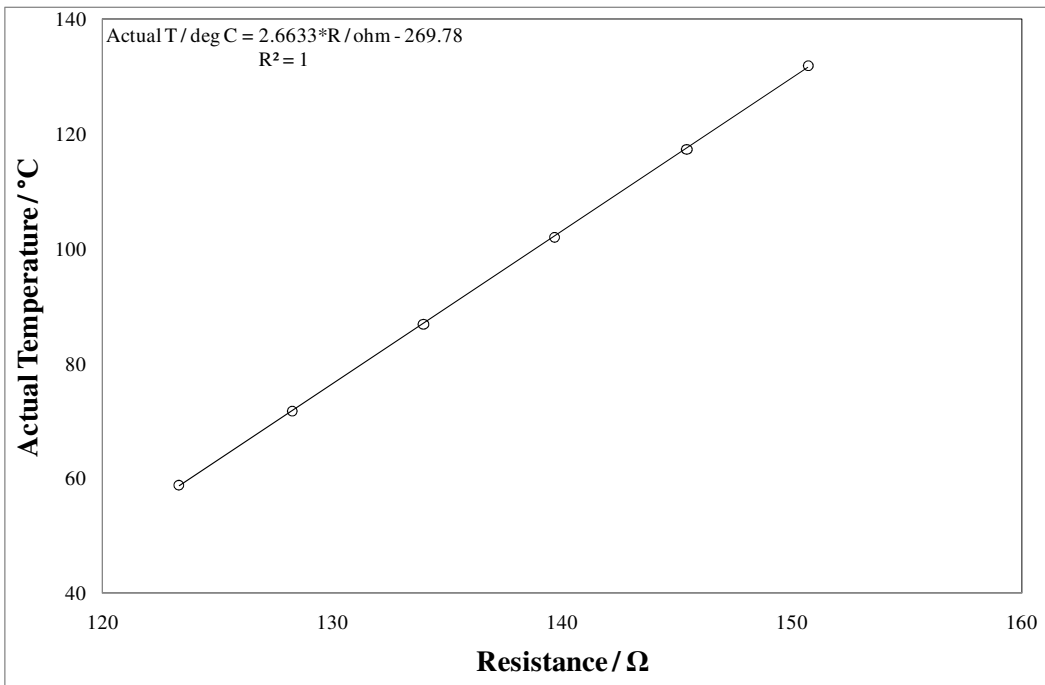


**Figure 6-4 Calibration plot for the temperature sensor on the apparatus of Reddy (2006)**

### 6.2.2. GC calibrations and operating conditions

The operating conditions for the gas chromatographs which ensured adequate separation of components and are believed to be the most appropriate for the generation of separate sharp peaks for each system are listed in Tables 6-3 and 6-4 for the two different gas chromatographs used during the project. These settings were used in obtaining the GC calibration graphs as well as the measured VLE results for the binary systems measured. The details of the columns used are given in Table 6-5.

**Table 6-3 Operating conditions for the Shimadzu 2014 gas chromatograph**

<b>Operating condition</b>	<b>Settings used in this work</b>	
<b>System</b>	cyclohexane (1) + ethanol (2)	1-propanol (1) + n-butanoic acid (2)
<b>Column used</b>	Porapak® Q	Porapak® Q
<b>Injector Profile</b>		
Injector temperature / °C	240	240
Carrier gas	helium	helium
Injection mode	split less	split less
Carrier gas flow rate / mL.min-1	30	30
Reference gas flow rate / mL.min-1	30	30
<b>Detector Profile</b>		
Detector type	FID	FID
Detector temperature / °C	240	240
<b>Oven Profile</b>		
Temperature control mode	isothermal	isothermal
Oven temperature / °C	200	230
<b>Elution Time / min</b>		
cyclohexane	6.5	
ethanol	1.8	
1-propanol		2.1
n-butanoic acid		6.4

**Table 6-4 Operating conditions for the Shimadzu 2010 gas chromatograph**

<b>Operating condition</b>	<b>Settings used in this work</b>	
<b>System</b>	2-propanone (1) + 2-butanol (2)	2-propanone (1) + n-propanoic acid (2)
<b>Column used</b>	Zebron ZB-WAXplus	Zebron ZB-WAXplus
<b>Injector Profile</b>		
Injector temperature / °C	240	240
Carrier gas	helium	helium
Injection mode	split	split
Split ratio (1:X)	5	20
Column pressure / kPa	81.9	81.9
Column flow / mL.min <sup>-1</sup>	1.2	0.6
Linear velocity / cm.sec <sup>-1</sup>	28.8	21.7
Total flow / mL.min <sup>-1</sup>	10.2	16.0
<b>Detector Profile</b>		
Detector type	TCD	TCD
Current / mA	90	90
Detector temperature / °C	240	240
Make up flow / mL.min <sup>-1</sup>	4	4
<b>Oven Profile</b>		
Temperature control mode	ramp	isothermal
Initial oven temperature / °C	30	170
Hold time for initial temp / min	1	-
Temperature ramp (rise) / °C.min <sup>-1</sup>	50	-
Final oven temperature / °C	100	170
Hold time for final temp / min	3.5	-
<b>Elution Time / min</b>		
2-propanone	3.07	2.60
2-butanol	4.59	
n-propanoic acid		4.39

**Table 6-5 Available specifications for columns used for GC analyses**

Column	Porapak® Q	Zebron ZB-WAXplus
serial number		146670
type	packed	capillary
max temp	250	250
Column length / m	2.5	30
film thickness / $\mu\text{m}$	-	0.25
material	stainless steel	
OD / mm	3.2	
ID / mm	2.2	
mesh range	50/80	

The GC detector calibration plots are presented together with the phase equilibrium data for each binary system in Section 6.5. As discussed in Section 5.2.3, two linear plots were generated for each binary system - one for each end of the composition range. If the slope of the first plot ( $F_2/F_1$ ) is equal to the inverse of the slope of the second plot ( $1/(F_1/F_2)$ ), then the response factor ratios can be assumed to be constant and a linear relationship assumed between the area ratios and mole fraction ratios across the entire mole fraction range. Table 6-6 summarizes the response factor ratios obtained from the slopes of the linear GC calibration plots for each system. With the exception of the 1-propanol (1) + n-butanoic acid (2) system, all other systems measured responded linearly and the gradients of  $A_1/A_2$  versus  $x_2/x_1$  were shown to be sufficiently close in value to the reciprocal of the gradient of  $A_2/A_1$  versus  $x_2/x_1$  (values within 1 % of each other were considered close enough to indicate the linear relationship).

**Table 6-6 Summary of response factor ratios obtained from slopes of linear GC calibration plots**

System	$F_1/F_2$	$F_2/F_1$	$1/(F_1/F_2)$	% difference	comment
cyclohexane (1) + ethanol (2)	0.2255	4.3901	4.4346	1.0	linear
2-propanone (1) + 2-butanol (2)	1.1996	0.8326	0.8336	0.1	linear
2-propanone (1) + n-propanoic acid (2)	1.1559	0.8636	0.8651	0.2	linear
1-propanol (1) + n-butanoic acid (2)	0.9865	0.9649	1.0137	5.1	not linear

### 6.3. Systems measured

The four binary systems for which isothermal phase equilibrium data were measured in this study were listed in Chapter 2. The cyclohexane (1) + ethanol (2) system was measured to confirm the accuracy of the apparatus (and calibrations) and experimental procedure. The remaining three binary systems constitute new data. Vapour pressure measurements for the pure components were made as they also serve as a preliminary test of the equipment (and calibrations) and experimental procedure. Tables 6-7 and 6-8 lists the range for which the vapour pressure measurements were made on the apparatuses of Joseph (2001) and Reddy (2006) respectively. An overview of the binary VLE measurements conducted on each of the apparatuses used in this project is provided in Table 6-9.

**Table 6-7 Vapour pressure measurements undertaken on the apparatus of Joseph (2001)**

Component	Temperature range/ °C	Pressure range/kPa
2-butanol	40.15 - 98.16	5.96 - 96.14
1-propanol	56.08 - 91.37	16.74 - 81.40
n-butanoic acid	68.45 - 89.41	1.59 - 5.64
n-propanoic acid	50.97 - 117.64	2.17 - 46.11

**Table 6-8 Vapour pressure measurements undertaken on the apparatus of Reddy (2006)**

Component	Temperature range / °C	Pressure range / kPa
2-propanone	49.13 - 110.40	79.9 - 479.7
cyclohexane	59.53 - 104.83	51.9 - 198.4

**Table 6-9 Overview of the binary VLE measurements conducted on each of the apparatuses used in this project**

System	Temperature / K	Pressure range / kPa	
		Apparatus used	
		Joseph (2001)	Reddy (2006)
cyclohexane + ethanol	333.15	29.74 - 57.65	-
	333.15	18.15 - 98.27	100.1 - 115.5
2-propanone + 2-butanol	353.15	46.38 - 160.20	59.5 - 213.8
	373.15	-	102.9 - 369.4
	333.15	3.64 - 98.89	91.7 - 115.5
2-propanone + n-propanoic acid	353.15	9.97 - 93.03	64.8 - 213.8
	373.15	23.65 - 80.42	86.5 - 369.4
	333.15	0.67 - 20.56	-
1-propanol + n-butanoic acid	373.15	3.54 - 51.30	-

#### 6.4. Pure component vapour pressure measurements

Vapour pressure data was measured for the components listed in Tables 6-7 and 6-8 as a preliminary test of the equipment and its calibrations. Wherever possible, the measured data was compared with data from two different sources in the literature. For a quantitative comparison, the following deviations between the experimentally measured data and the literature data were calculated:

Deviation of pressure (at the same temperature),  $\Delta P$

$$\Delta P = P^{Exp} - P^{Lit} \quad 6-1$$

% Deviation of pressure (at the same temperature),  $\Delta P\%$

$$\Delta P\% = 100 * \frac{P^{Exp} - P^{Lit}}{P^{Lit}} \quad 6-2$$

Deviation of temperature (at the same pressure),  $\Delta T$

$$\Delta T = T^{Exp} - T^{Lit} \quad 6-3$$

% Deviation of temperature (at the same pressure),  $\Delta T\%$

$$\Delta T\% = 100 * \frac{T^{Exp} - T^{Lit}}{T^{Lit}} \quad 6-4$$

where the superscripts “Exp” and “Lit” refer to the experimental data and the corresponding literature value respectively. The vapour pressure results and deviations from the literature values are presented in Tables 6-10 to 6-15 and illustrated graphically in Figures 6-5 to 6-10. The vapour pressure data was also regressed to obtain parameters for the Antoine equation (see Section 7.1).

**Table 6-10 Vapour pressure data for 2-butanol;  $\Delta X = X^{Exp} - X^{Lit}$  ;**

$$\Delta X \% = 100 * \frac{X^{Exp} - X^{Lit}}{X^{Lit}}$$

P / kPa	T / °C	$\Delta T / ^\circ C$		$\Delta T \%$		$\Delta P / \text{kPa}$		$\Delta P \%$	
		Lit <sup>a</sup>	Lit <sup>b</sup>	Lit <sup>a</sup>	Lit <sup>b</sup>	Lit <sup>a</sup>	Lit <sup>b</sup>	Lit <sup>a</sup>	Lit <sup>b</sup>
5.96	40.15	0.27	0.60	0.67	1.52	-0.10	-0.22	-1.60	-3.53
10.74	50.18	0.10	0.38	0.20	0.75	-0.06	-0.22	-0.55	-2.03
18.22	60.06	0.00	0.21	-0.01	0.35	0.00	-0.19	0.02	-1.05
29.84	70.19	0.00	0.17	0.00	0.24	0.00	-0.23	0.00	-0.77
46.82	80.24	0.01	0.16	0.02	0.19	-0.03	-0.31	-0.06	-0.67
70.47	90.11	0.03	0.19	0.03	0.21	-0.08	-0.53	-0.11	-0.74
96.14	98.16	0.05	0.26	0.05	0.26	-0.19	-0.94	-0.20	-0.97

<sup>a</sup>Poling et al., 2001

<sup>b</sup>DDB, 2008

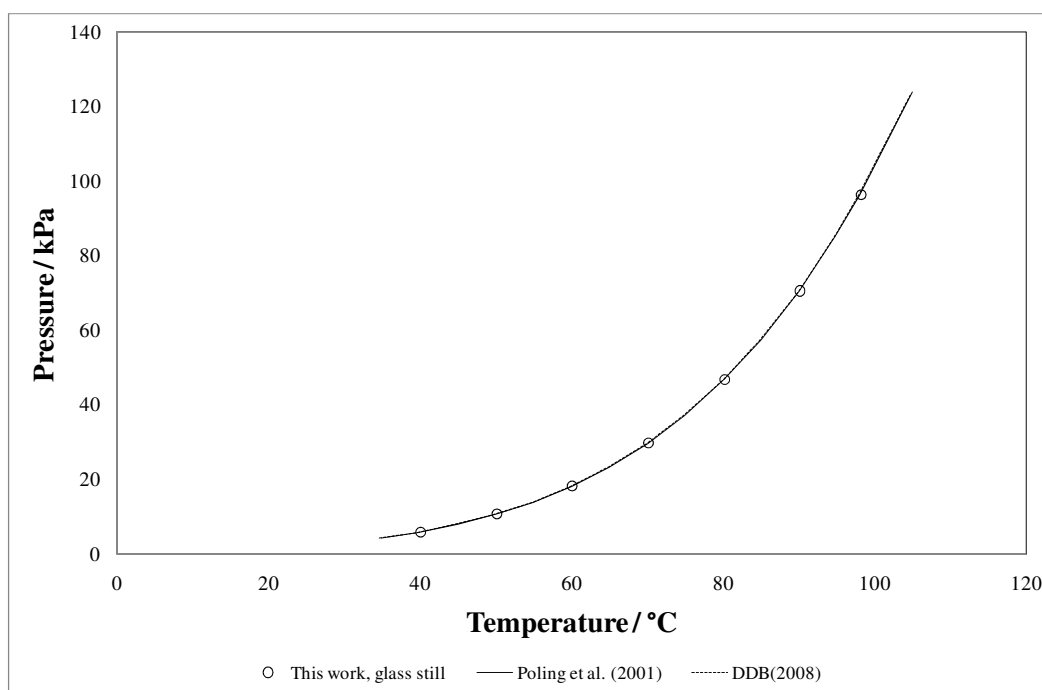


**Figure 6-5 Vapour pressure curve for 2-butanol**

**Table 6-11 Vapour pressure data for 1-propanol;  $\Delta X = X^{Exp} - X^{Lit}$  ;**

$$\Delta X \% = 100 * \frac{X^{Exp} - X^{Lit}}{X^{Lit}}$$

P / kPa T / °C	$\Delta T / ^\circ C$		$\Delta T \%$		$\Delta P / \text{kPa}$		$\Delta P \%$	
	Lit <sup>a</sup>	Lit <sup>b</sup>	Lit <sup>a</sup>	Lit <sup>b</sup>	Lit <sup>a</sup>	Lit <sup>b</sup>	Lit <sup>a</sup>	Lit <sup>b</sup>
16.74 56.08	-0.04	-0.39	-0.07	-0.69	0.04	0.33	0.21	1.99
20.56 60.00	-0.23	-0.58	-0.38	-0.95	0.23	0.58	1.14	2.89
32.97 70.00	-0.19	-0.48	-0.27	-0.68	0.28	0.72	0.87	2.23
41.09 75.01	-0.07	-0.30	-0.10	-0.40	0.13	0.55	0.33	1.35
51.30 80.00	-0.20	-0.34	-0.25	-0.42	0.44	0.75	0.87	1.48
81.40 91.37	-0.10	0.04	-0.11	0.05	0.32	-0.14	0.40	-0.17

<sup>a</sup>Poling et al., 2001

<sup>b</sup>DDB, 2008

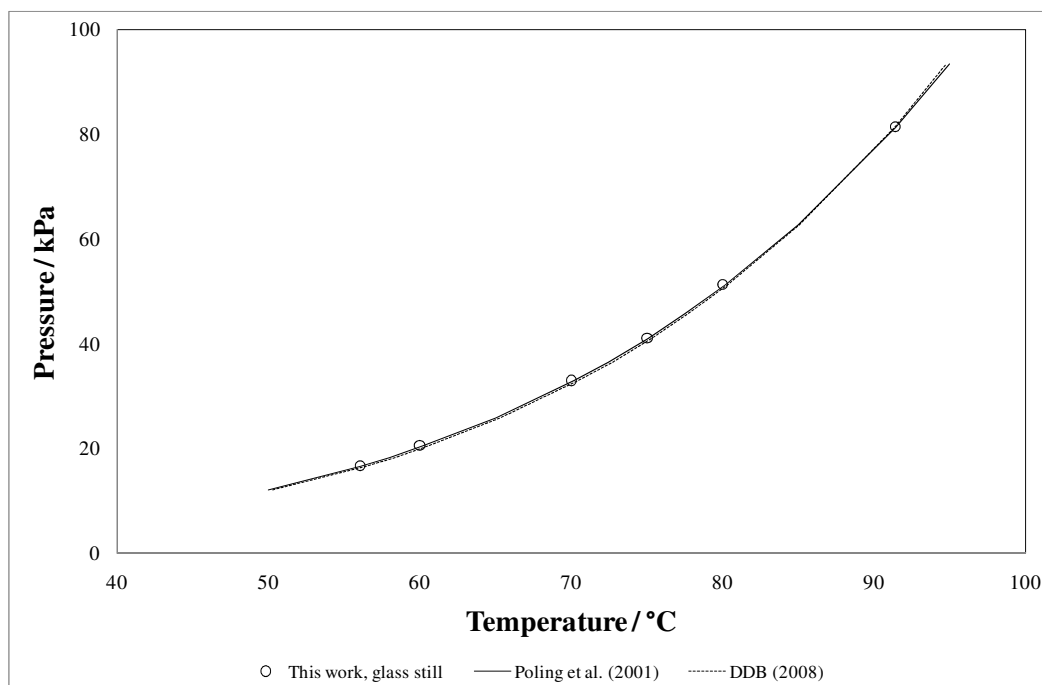


**Figure 6-6 Vapour pressure curve for 1-propanol**

**Table 6-12 Vapour pressure data for n-butanoic acid;  $\Delta X = X^{Exp} - X^{Lit}$ ;**

$$\Delta X \% = 100 * \frac{X^{Exp} - X^{Lit}}{X^{Lit}}$$

P / kPa	T / °C	$\Delta T$ / °C	$\Delta T$ %	$\Delta P$ / kPa	$\Delta P$ %
		Lit <sup>a</sup>	Lit <sup>a</sup>	Lit <sup>a</sup>	Lit <sup>a</sup>
1.59	68.45	*	*	*	*
2.61	74.90	0.55	0.75	-0.08	2.61
4.65	85.57	0.24	0.28	-0.06	4.65
5.64	89.41	0.18	0.20	-0.05	5.64

<sup>a</sup>Poling et al., 2001

\* out of range of source data

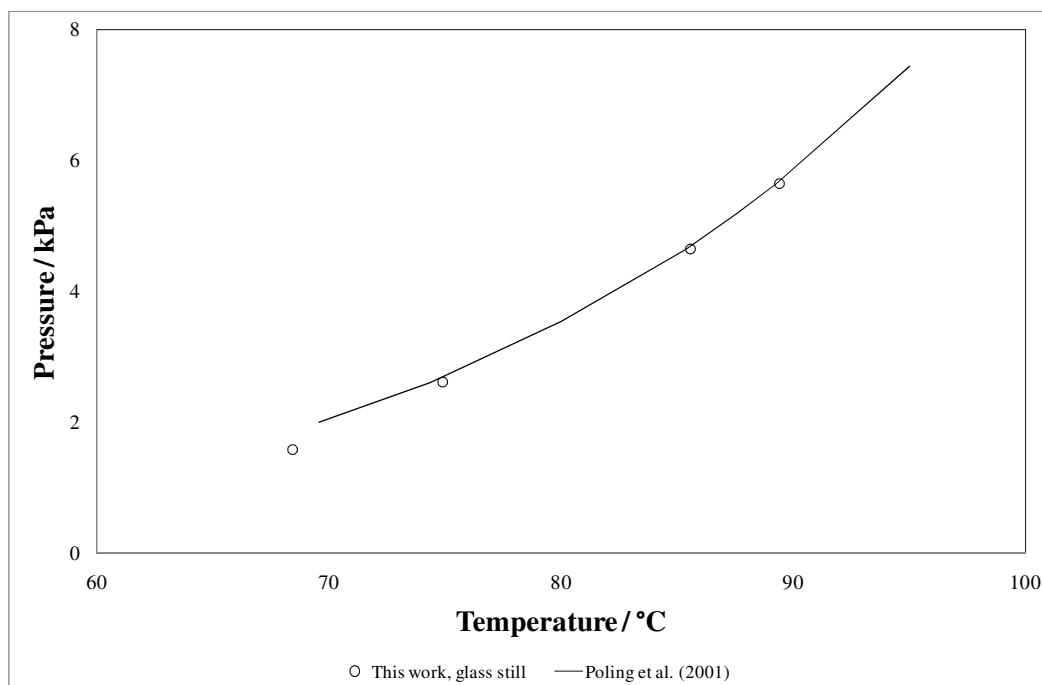


**Figure 6-7 Vapour pressure curve for n-butanoic acid**

**Table 6-13 Vapour pressure data for n-propanoic acid;  $\Delta X = X^{Exp} - X^{Lit}$  ;**

$$\Delta X \% = 100 * \frac{X^{Exp} - X^{Lit}}{X^{Lit}}$$

P / kPa	T / °C	$\Delta T / ^\circ C$		$\Delta T \%$		$\Delta P / \text{kPa}$		$\Delta P \%$	
		Lit <sup>a</sup>	Lit <sup>b</sup>	Lit <sup>a</sup>	Lit <sup>b</sup>	Lit <sup>a</sup>	Lit <sup>b</sup>	Lit <sup>a</sup>	Lit <sup>b</sup>
2.17	50.97	0.97	2.80	1.95	5.82	-0.12	-0.36	-5.37	-14.11
2.89	55.84	0.71	2.33	1.28	4.36	-0.11	-0.38	-3.78	-11.51
3.79	60.57	0.40	1.84	0.66	3.13	-0.08	-0.37	-2.06	-8.89
10.09	80.36	0.30	1.12	0.38	1.41	-0.14	-0.51	-1.37	-4.83
23.73	100.12	0.10	0.45	0.10	0.45	-0.09	-0.42	-0.38	-1.73
46.11	117.64	0.10	0.18	0.09	0.15	-0.17	-0.30	-0.37	-0.64

<sup>a</sup>Poling et al., 2001

<sup>b</sup>DDB, 2008

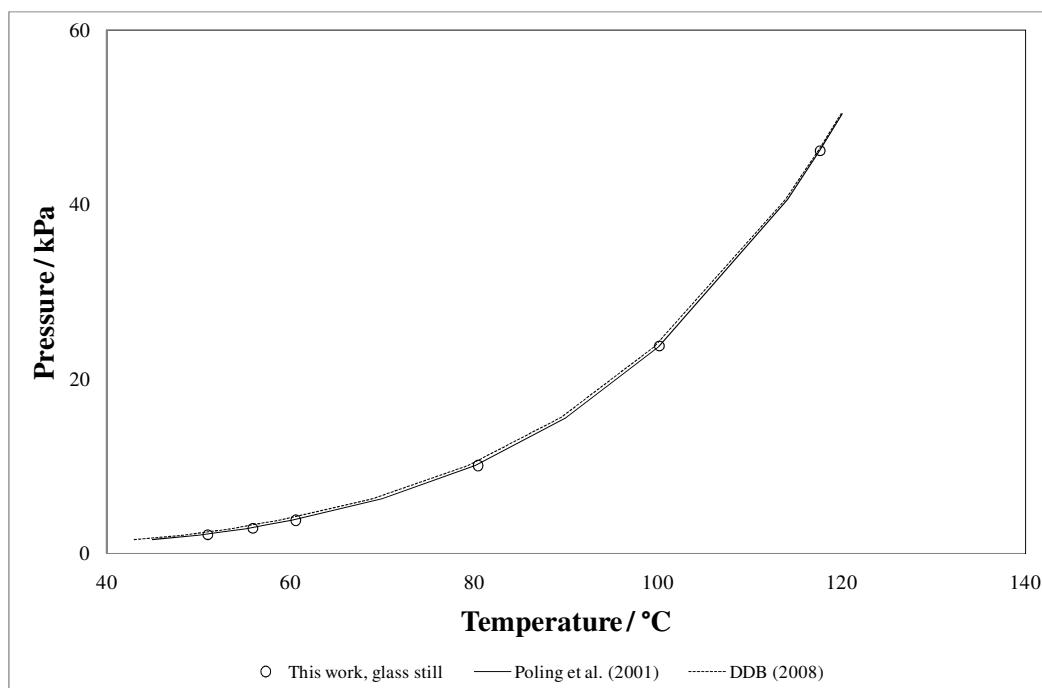


**Figure 6-8 Vapour pressure curve for n-propanoic acid**

**Table 6-14 Vapour pressure data for 2-propanone;  $\Delta X = X^{Exp} - X^{Lit}$ ;**

$$\Delta X \% = 100 * \frac{X^{Exp} - X^{Lit}}{X^{Lit}}$$

P / kPa	T / °C	$\Delta T / ^\circ C$		$\Delta T \%$		$\Delta P / \text{kPa}$		$\Delta P \%$	
		Lit <sup>a</sup>	Lit <sup>b</sup>	Lit <sup>a</sup>	Lit <sup>b</sup>	Lit <sup>a</sup>	Lit <sup>b</sup>	Lit <sup>a</sup>	Lit <sup>b</sup>
79.9	49.13	-0.16	-0.34	-0.33	-0.68	0.43	0.96	0.54	1.22
114.8	59.83	0.04	-0.17	0.06	-0.28	-0.09	0.65	-0.08	0.57
158.8	70.04	0.15	-0.48	0.22	-0.67	-0.72	2.29	-0.45	1.46
214.8	80.16	0.26	-0.54	0.33	-0.67	-1.65	3.34	-0.76	1.58
284.8	90.20	0.32	-0.58	0.35	-0.64	-2.49	4.48	-0.87	1.60
371.7	100.26	0.33	-0.60	0.33	-0.59	-3.19	5.69	-0.85	1.55
479.7	110.40	0.28	-0.62	0.26	-0.56	-3.28	7.22	-0.68	1.53

<sup>a</sup>Poling et al., 2001

<sup>b</sup>DDB, 2008

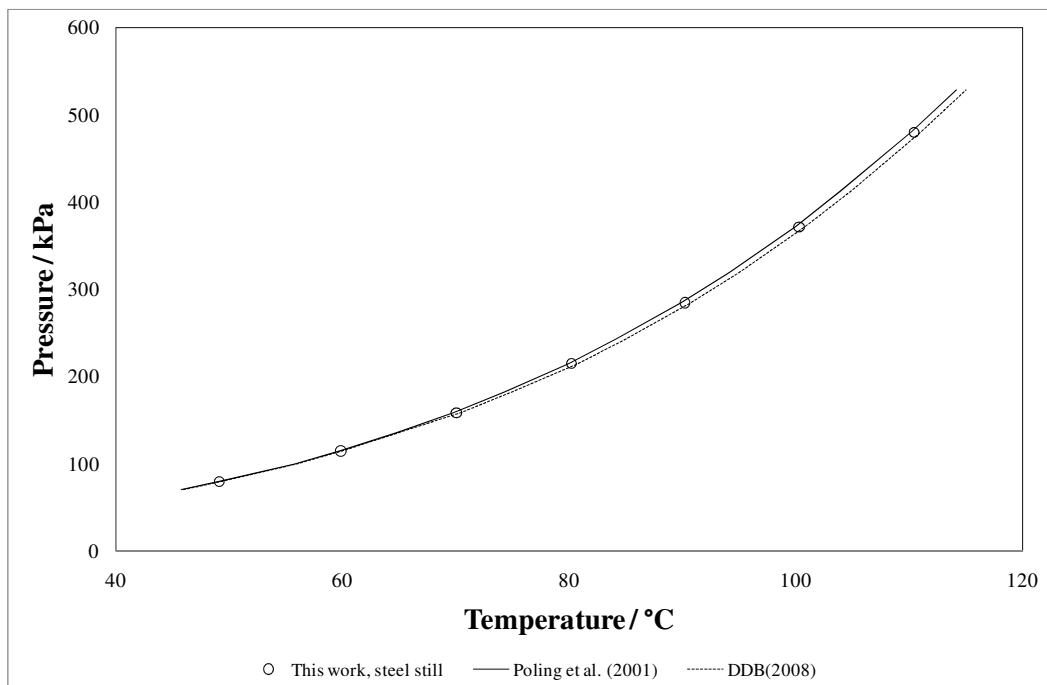


**Figure 6-9 Vapour pressure curve for 2-propanone**

**Table 6-15 Vapour pressure data for cyclohexane;  $\Delta X = X^{Exp} - X^{Lit}$  ;**

$$\Delta X \% = 100 * \frac{X^{Exp} - X^{Lit}}{X^{Lit}}$$

P / kPa	T / °C	$\Delta T / ^\circ C$		$\Delta T \%$		$\Delta P / \text{kPa}$		$\Delta P \%$	
		Lit <sup>a</sup>	Lit <sup>b</sup>	Lit <sup>a</sup>	Lit <sup>b</sup>	Lit <sup>a</sup>	Lit <sup>b</sup>	Lit <sup>a</sup>	Lit <sup>b</sup>
51.9	59.53	-0.47	-0.47	-0.79	-0.79	0.84	0.84	1.65	1.65
99.0	79.73	-0.27	-0.22	-0.34	-0.27	0.81	0.65	0.83	0.66
198.4	104.83	-0.17	-0.22	-0.16	-0.21	0.85	1.13	0.43	0.57

<sup>a</sup>Poling et al., 2001

<sup>b</sup>DDB, 2008

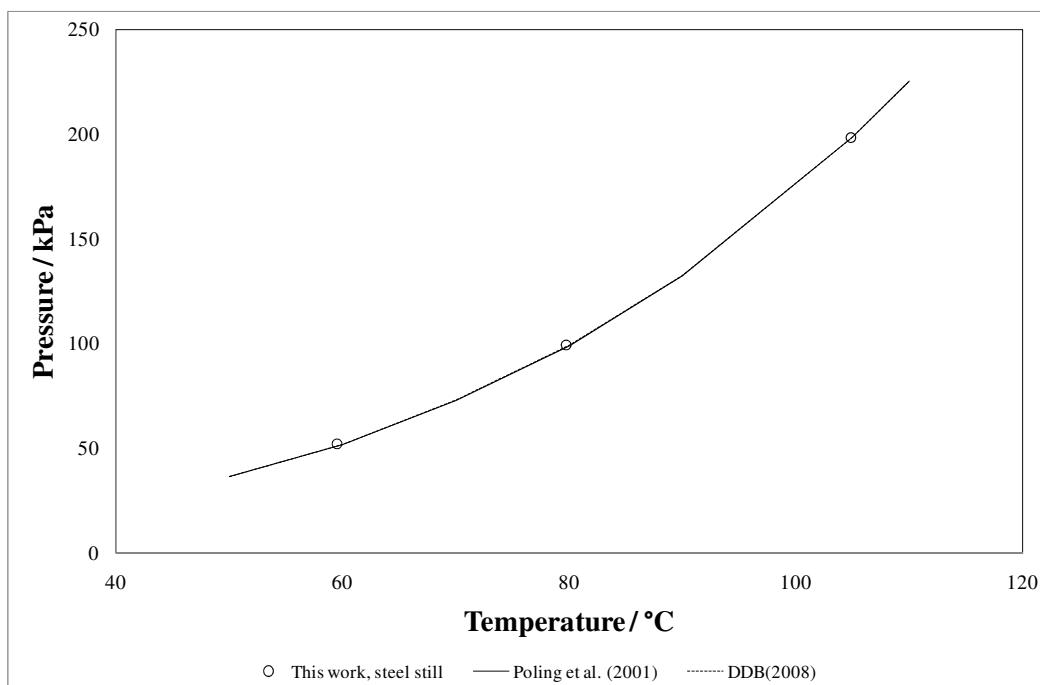


**Figure 6-10 Vapour pressure curve for cyclohexane**

## 6.5. Binary vapour-liquid equilibrium measurements

### 6.5.1. Results for the test system: cyclohexane (1) + ethanol (2)

Measurements for the cyclohexane (1) + ethanol (2) system at 323.15K were undertaken on the apparatus of Joseph (2001). The composition analysis was done using the Shimadzu 2014 GC fitted with a packed Porapak® Q column (described in Tables 6-3 and 6-5). The GC calibration plots are presented in Figures 6-11 and 6-12. The isothermal P-x<sub>1</sub>-y<sub>1</sub> data is listed in Table 6-16. Figures 6-13 and 6-14 compare the measured P-x<sub>1</sub>-y<sub>1</sub> and x<sub>1</sub>-y<sub>1</sub> data to that obtained by Joseph (2001) and Marachevsky et al., (1963) and illustrate the excellent agreement with literature data. After successfully reproducing the test system, the 2-propanone (1) + 2-butanol (2) system was measured on both the apparatuses of Joseph (2001) and Reddy (2006) and it was found that the data obtained using the different equipment were in good agreement with each other. With the additional vapour pressure data that was successfully measured as a test system, it was not deemed necessary to measure a further binary test system on the apparatus of Reddy (2006).

**Table 6-16 P-x<sub>1</sub>-y<sub>1</sub> data for cyclohexane (1) + ethanol (2) at 323.15K**

Measurements on apparatus of Joseph (2001)		
Pressure / kPa	x <sub>1</sub>	y <sub>1</sub>
29.74	0.000	0.000
35.16	0.019	0.143
41.39	0.047	0.290
45.87	0.076	0.375
50.74	0.131	0.460
54.71	0.224	0.527
56.32	0.327	0.564
57.43	0.560	0.597
57.65	0.634	0.603
57.43	0.716	0.610
57.31	0.754	0.614
57.15	0.797	0.623
56.53	0.869	0.639
54.91	0.921	0.660
54.20	0.937	0.673
36.51	1.000	1.000

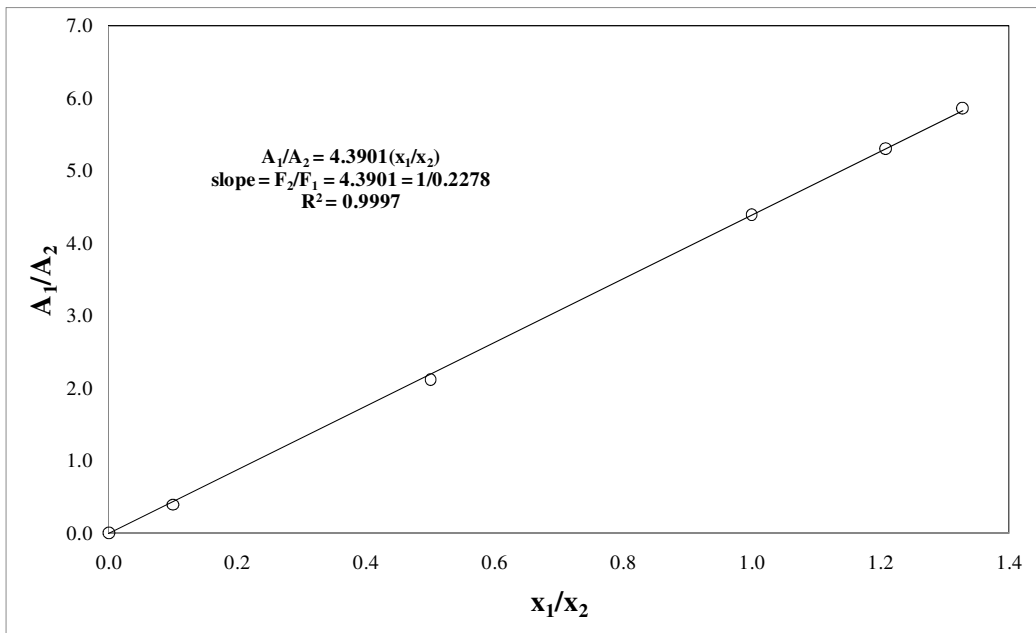


Figure 6-11 GC calibration plot for cyclohexane (1) + ethanol (2) in the ethanol rich region

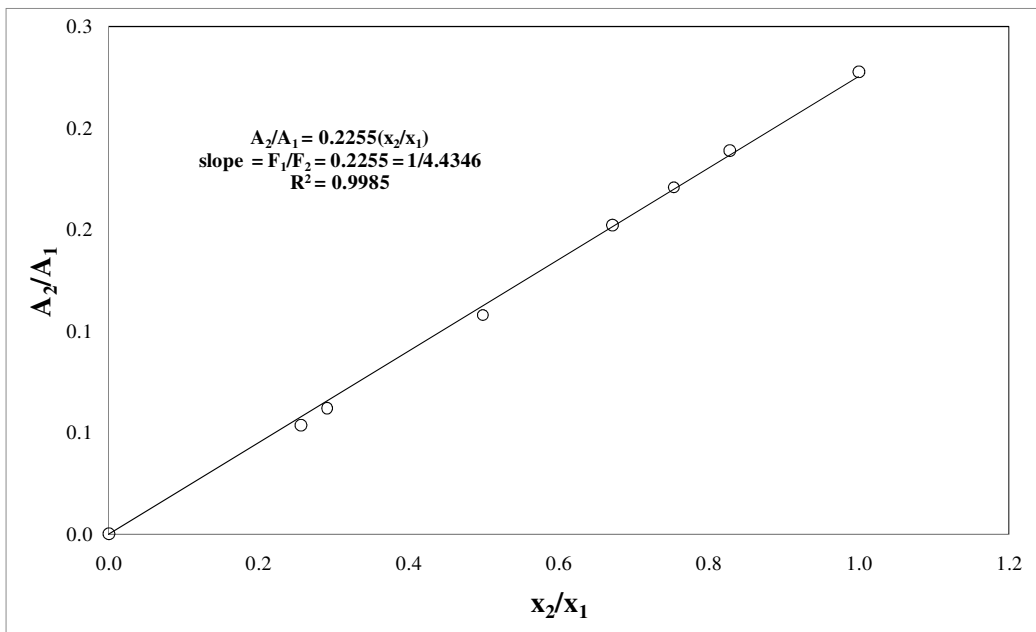
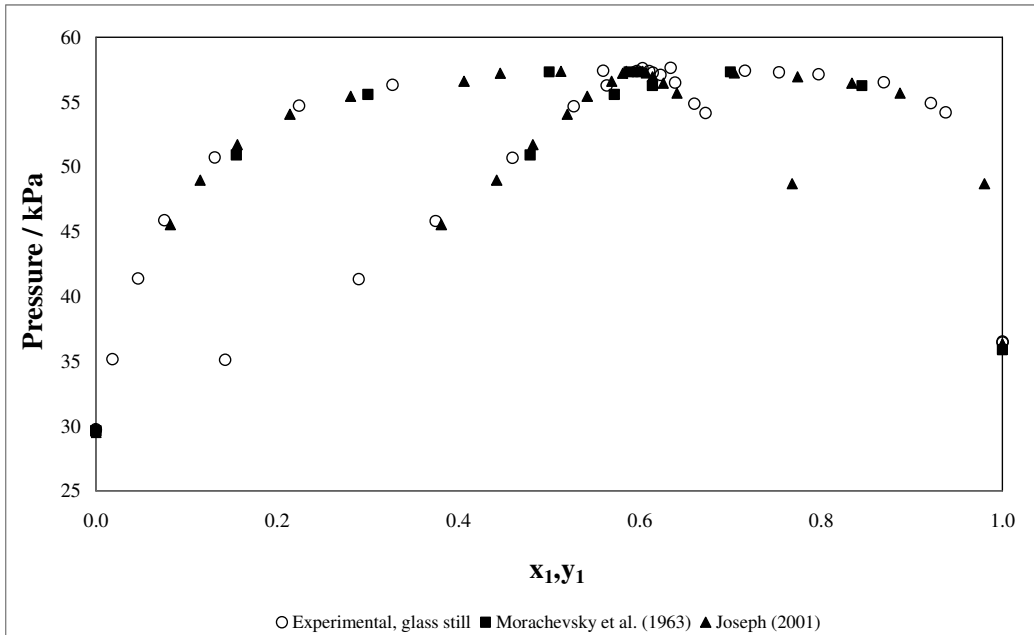
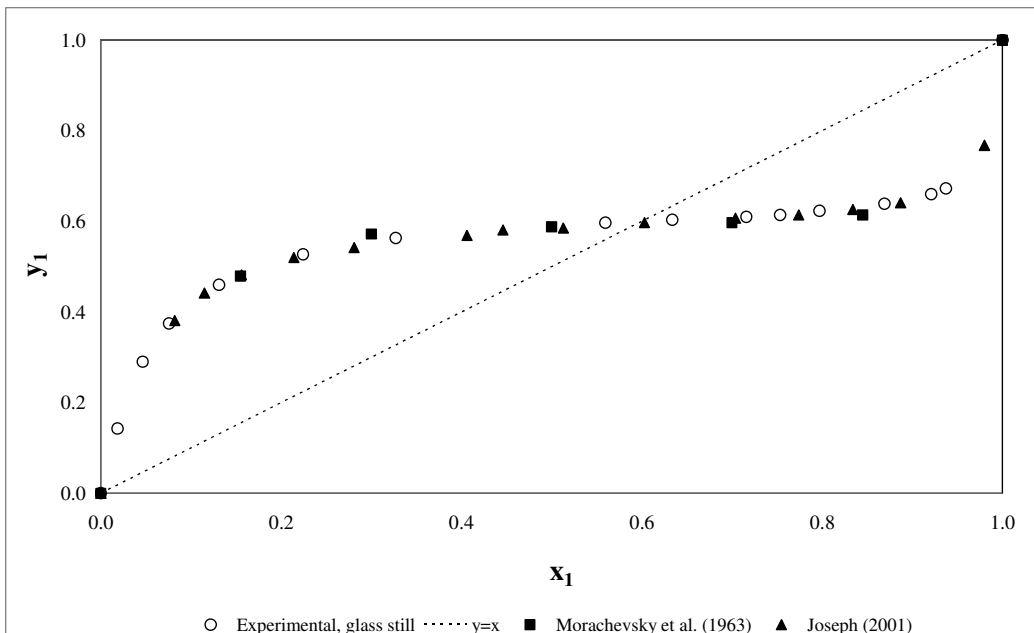


Figure 6-12 GC calibration plot for cyclohexane (1) + ethanol (2) in the cyclohexane rich region



**Figure 6-13 Experimental P- $x_1$ - $y_1$  data for the cyclohexane (1)+ ethanol (2) system at 323.15K**



**Figure 6-14  $x_1$ - $y_1$  data for the cyclohexane (1)+ ethanol (2) system at 323.15K**

### 6.5.2. Results for the system: 2-propanone (1) + 2-butanol (2)

Isothermal measurements were performed at 333.15K, 353.15K and 373.15K; all three sets of data represents new VLE data as this system has not previously been measured at these temperatures. The composition analysis was carried out using the Shimadzu 2010 GC fitted with the Zebron ZB-WAXplus capillary column (described in Tables 6-4 and 6-5). The calibration curves are presented in Figures 6-15 and 6-16 and the experimental VLE data points are listed in Tables 6-17 to 6-19. Graphical representations of the experimental data points for each isotherm are shown in Figures 6-17 to 6-22.

**Table 6-17 P-x<sub>1</sub>-y<sub>1</sub> data for 2-propanone (1) + 2-butanol (2) at 333.15K**

Measurements on apparatus of Joseph (2001)			Measurements on apparatus of Reddy (2006)		
Pressure / kPa	x <sub>1</sub>	y <sub>1</sub>	Pressure / kPa	x <sub>1</sub>	y <sub>1</sub>
18.15	0.000	0.000	100.1	0.834	0.958
20.26	0.012	0.105	102.3	0.862	0.966
21.36	0.021	0.152	109.3	0.938	0.985
22.85	0.026	0.211	109.5	0.942	0.986
26.40	0.050	0.330	115.5	1.000	1.000
26.34	0.052	0.335			
28.93	0.069	0.401			
33.15	0.099	0.500			
35.07	0.111	0.531			
42.48	0.169	0.626			
50.65	0.247	0.712			
53.19	0.272	0.731			
67.72	0.422	0.820			
74.06	0.500	0.853			
78.57	0.554	0.872			
87.65	0.668	0.905			
95.04	0.762	0.933			
98.27	0.801	0.945			

**Table 6-18 P-x<sub>1</sub>-y<sub>1</sub> data for 2-propanone (1) + 2-butanol (2) at 353.15K**

Measurements on apparatus of Joseph (2001)			Measurements on apparatus of Reddy (2006)		
Pressure / kPa	x <sub>1</sub>	y <sub>1</sub>	Pressure / kPa	x <sub>1</sub>	y <sub>1</sub>
46.38	0.000	0.000	59.5	0.063	0.270
50.7	0.018	0.093	174.8	0.762	0.916
51.29	0.020	0.107	185.1	0.829	0.943
55.18	0.036	0.175	190.5	0.864	0.956
60.18	0.057	0.258	202.6	0.937	0.981
67.19	0.089	0.355	203.4	0.943	0.983
78.01	0.141	0.469	213.8	1.000	1.000
80.26	0.151	0.489			
82.06	0.166	0.513			
92.24	0.214	0.576			
98.57	0.247	0.621			
129.3	0.440	0.761			
145.5	0.541	0.820			
160.2	0.632	0.859			

**Table 6-19 P-x<sub>1</sub>-y<sub>1</sub> data for 2-propanone (1) + 2-butanol (2) at 373.15K**

Measurements on apparatus of Reddy (2006)		
Pressure / kPa	x <sub>1</sub>	y <sub>1</sub>
102.9	0.000	0.000
114.0	0.037	0.128
123.7	0.069	0.219
225.2	0.415	0.697
245.2	0.495	0.747
257.7	0.546	0.789
272.3	0.618	0.819
305.1	0.777	0.899
321.0	0.829	0.929
331.6	0.865	0.946
347.2	0.925	0.972
352.1	0.942	0.978
369.4	1.000	1.000

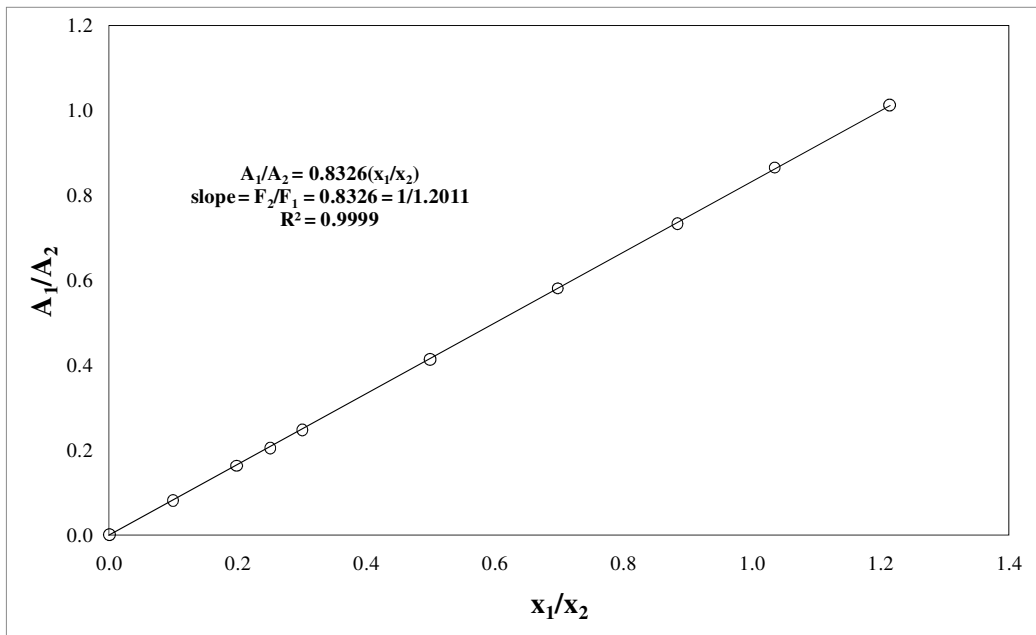


**Figure 6-15 GC calibration plot for 2-propanone (1) + 2-butanol (2) in the 2-butanol rich region**

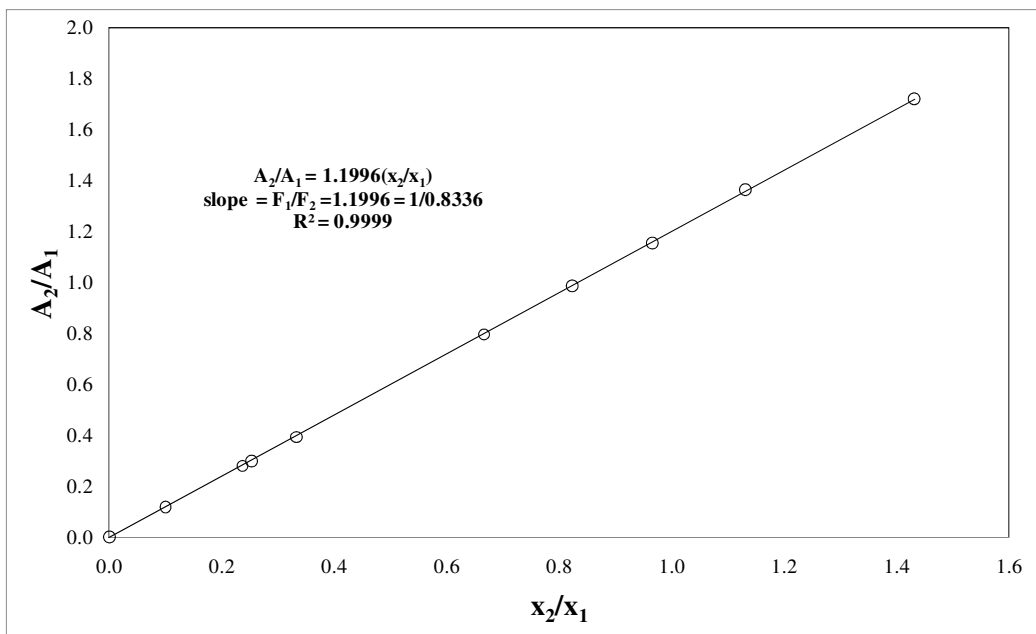


**Figure 6-16 GC calibration plot for 2-propanone (1) + 2-butanol (2) in the 2-propanone rich region**

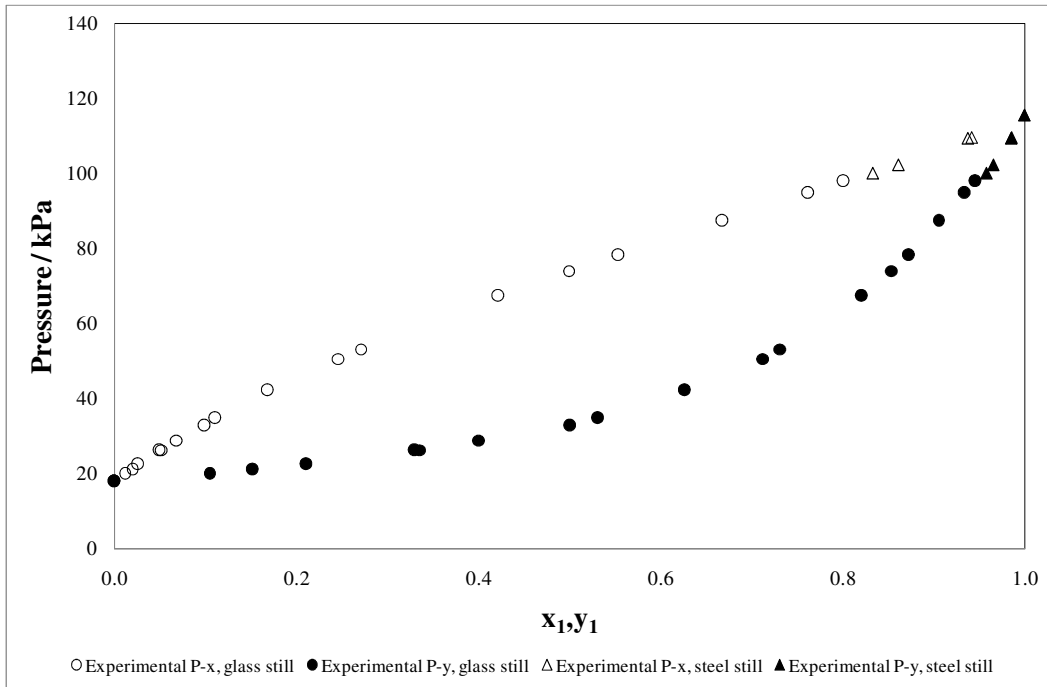


**Figure 6-17 Experimental P- $x_1$ - $y_1$  data for the 2-propanone (1) + 2-butanol (2) system at 333.15K**

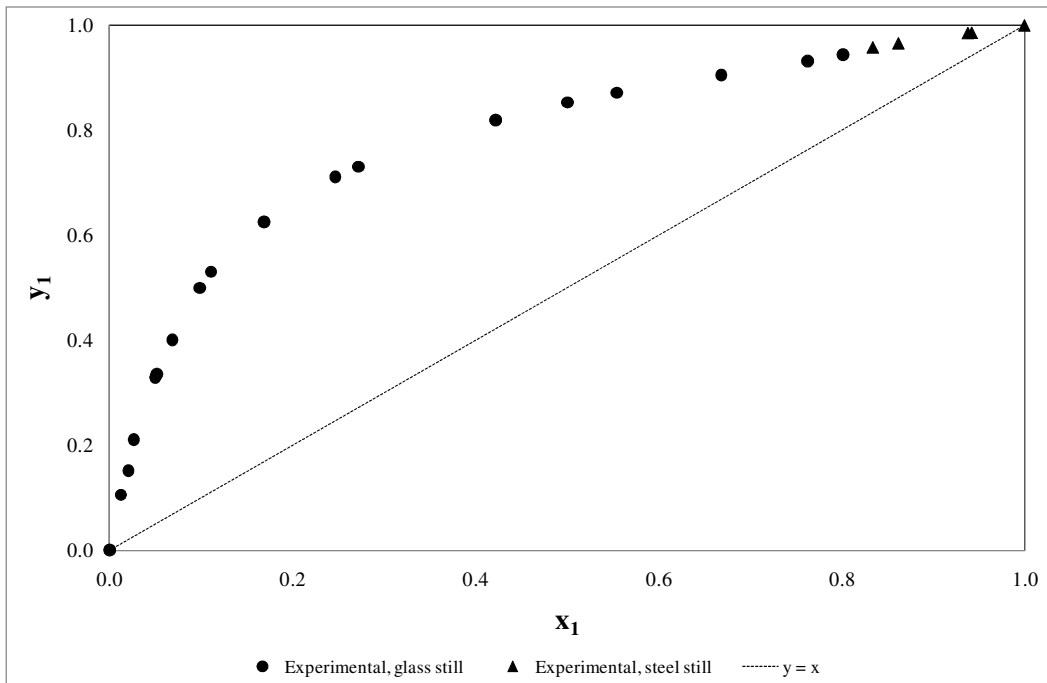


**Figure 6-18  $x_1$ - $y_1$  data for the 2-propanone (1) + 2-butanol (2) system at 333.15K**

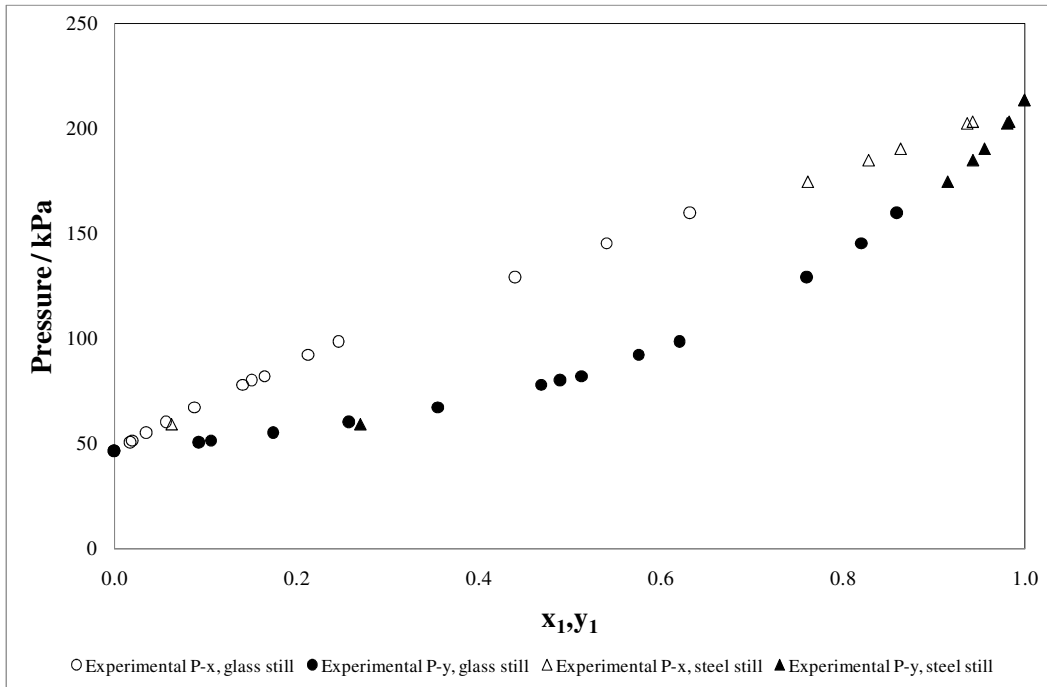


**Figure 6-19 Experimental P- $x_1$ - $y_1$  data for the 2-propanone (1) + 2-butanol (2) system at 353.15K**

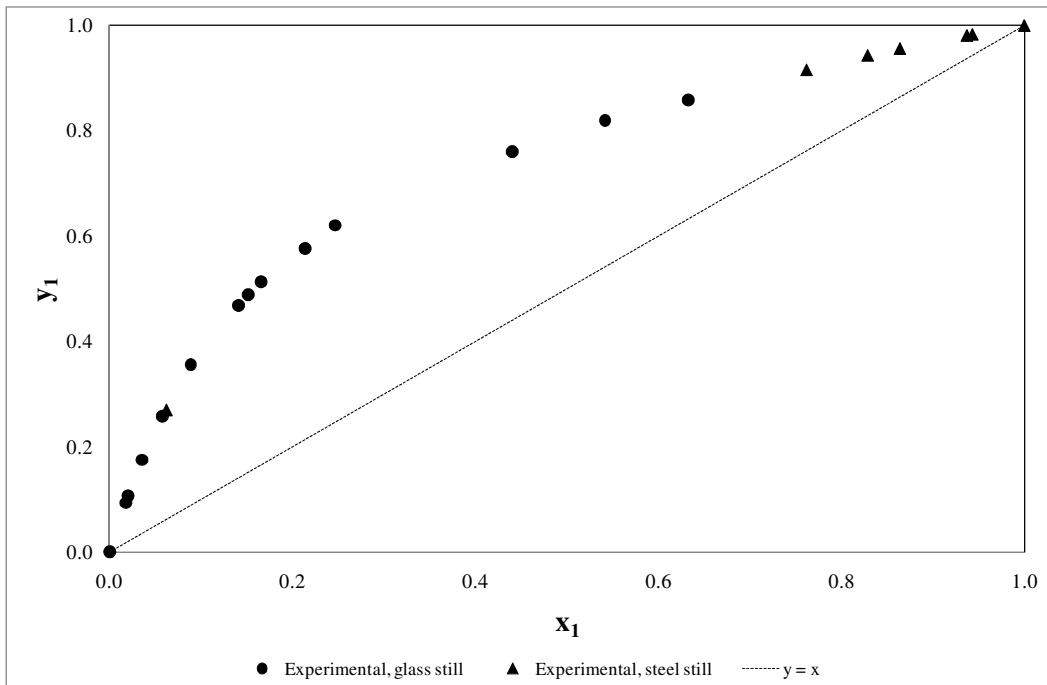


**Figure 6-20  $x_1$ - $y_1$  data for the 2-propanone (1) + 2-butanol (2) system at 353.15K**

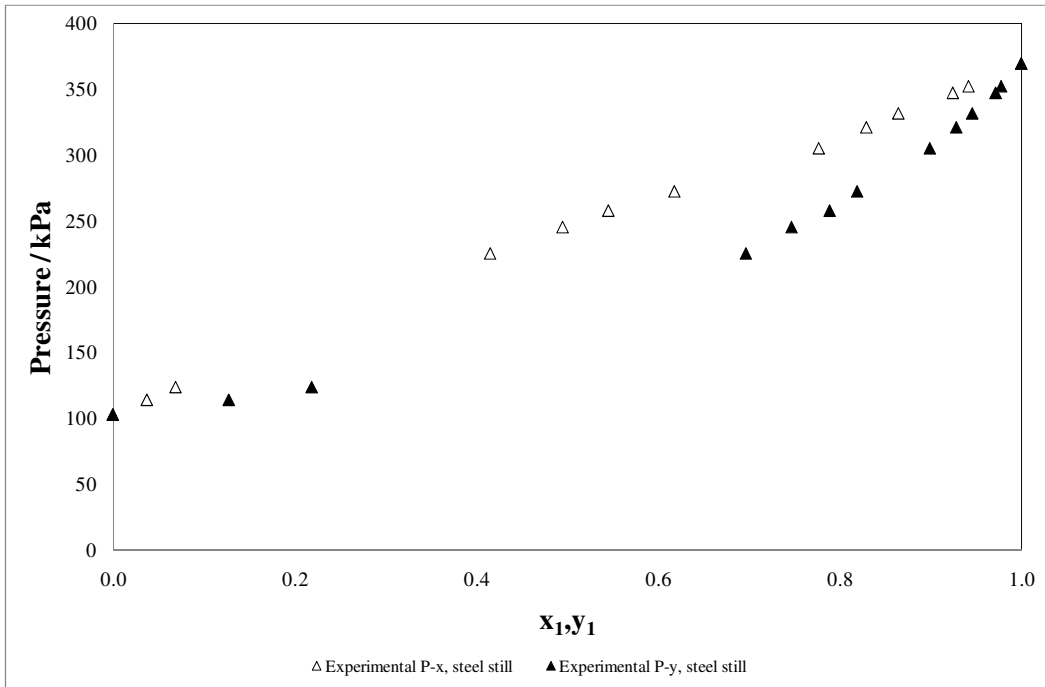


**Figure 6-21 Experimental P- $x_1$ - $y_1$  data for the 2-propanone (1) + 2-butanol (2) system at 373.15K**

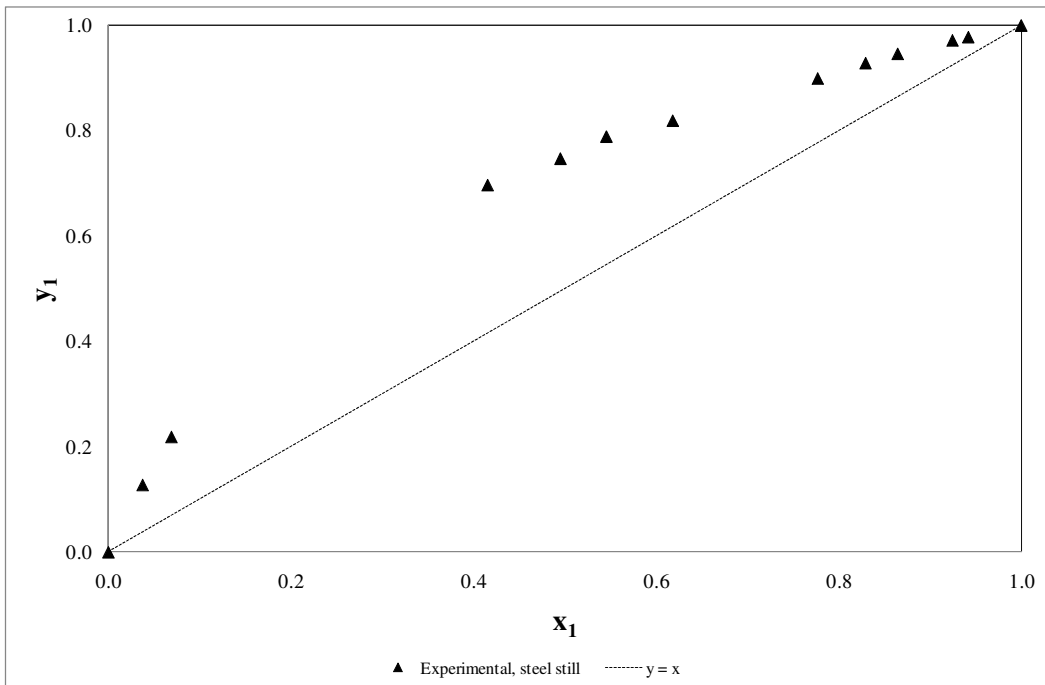


**Figure 6-22  $x_1$ - $y_1$  data for the 2-propanone (1) + 2-butanol (2) system at 373.15K**

### 6.5.3. Results for the system: 2-propanone (1) + n-propanoic acid (2)

Isothermal measurements were performed at 333.15K, 353.15K and 373.15K; once again all three sets of data represent new VLE data. The composition analysis was carried out using the Shimadzu 2010 GC fitted with the Zebron ZB-WAXplus capillary column (described in Tables 6-4 and 6-5). The calibration curves are presented in Figures 6-23 and 6-24 and the experimental VLE data points are listed in Tables 6-20 to 6-22. The equilibrium phase diagrams are presented in Figures 6-25 to 6-30. There is a slight discrepancy between the data obtained from the different equipment around  $x_1=0.3$ . This is probably due to the fact that on Reddy's (2006) still, there were larger temperature instabilities since the pressure control was only within  $\pm 0.1$  kPa, compared to the apparatus of Joseph (2001) which was controlled within  $\pm 0.01$  kPa. The data obtained on the apparatus of Joseph (2001) are considered to be more representative of this system in that region.

**Table 6-20 P- $x_1$ - $y_1$  data for 2-propanone (1) + n-propanoic acid (2) at 333.15K**

Measurements on apparatus of Joseph (2001)			Measurements on apparatus of Reddy (2006)		
Pressure / kPa	$x_1$	$y_1$	Pressure / kPa	$x_1$	$y_1$
3.64	0.000	0.000	91.7	0.800	0.992
3.73	0.001	0.025	98.7	0.859	0.995
3.74	0.003	0.022	103.1	0.893	0.997
4.29	0.005	0.077	108.9	0.935	0.997
4.43	0.005	0.103	115.5	1.000	1.000
6.62	0.025	0.397			
8.57	0.042	0.504			
11.65	0.070	0.637			
14.77	0.098	0.730			
18.32	0.134	0.810			
24.26	0.191	0.860			
29.62	0.237	0.892			
36.75	0.313	0.926			
44.89	0.391	0.944			
46.51	0.402	0.952			
63.35	0.541	0.974			
82.41	0.717	0.990			
91.7	0.801	0.993			
98.89	0.863	0.996			

**Table 6-21 P-x<sub>1</sub>-y<sub>1</sub> data for 2-propanone (1) + n-propanoic acid (2) at 353.15K**

Measurements on apparatus of Joseph (2001)			Measurements on apparatus of Reddy (2006)		
Pressure / kPa	x <sub>1</sub>	y <sub>1</sub>	Pressure / kPa	x <sub>1</sub>	y <sub>1</sub>
9.97	0.000	0.000	64.8	0.317	0.864
11.23	0.005	0.056	80.7	0.396	0.908
14.65	0.023	0.230	104	0.508	0.944
20.92	0.054	0.435	132.4	0.656	0.971
25.67	0.079	0.551	165.6	0.818	0.988
44.9	0.184	0.771	176.1	0.842	0.991
60.75	0.260	0.849	189.3	0.893	0.994
63.15	0.278	0.863	191.9	0.896	0.994
83.71	0.383	0.914	213.8	1.000	1.000
93.03	0.432	0.936			

**Table 6-22 P-x<sub>1</sub>-y<sub>1</sub> data for 2-propanone (1) + n-propanoic acid (2) at 373.15K**

Measurements on apparatus of Joseph (2001)			Measurements on apparatus of Reddy (2006)		
Pressure / kPa	x <sub>1</sub>	y <sub>1</sub>	Pressure / kPa	x <sub>1</sub>	y <sub>1</sub>
23.65	0.000	0.000	86.5	0.231	0.739
25.89	0.005	0.044	113.8	0.322	0.823
26.97	0.010	0.062	139.4	0.395	0.874
37.44	0.041	0.267	178.4	0.503	0.921
41.58	0.057	0.327	228.2	0.653	0.956
44.99	0.066	0.371	285.7	0.800	0.980
52.02	0.086	0.462	302.1	0.843	0.985
74.11	0.158	0.648	330.3	0.905	0.992
80.42	0.180	0.686	333.7	0.912	0.992
			339.4	0.925	0.994
			365.9	0.993	0.999
			369.4	1.000	1.000

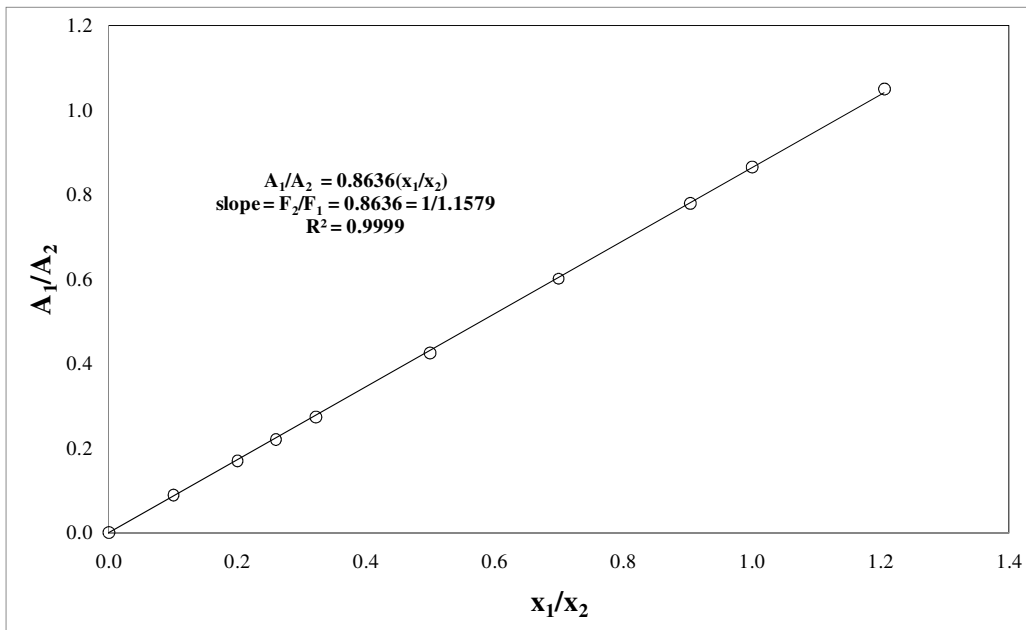


**Figure 6-23 GC calibration plot for 2-propanone (1) + n-propanoic acid (2) in the n-propanoic acid rich region**

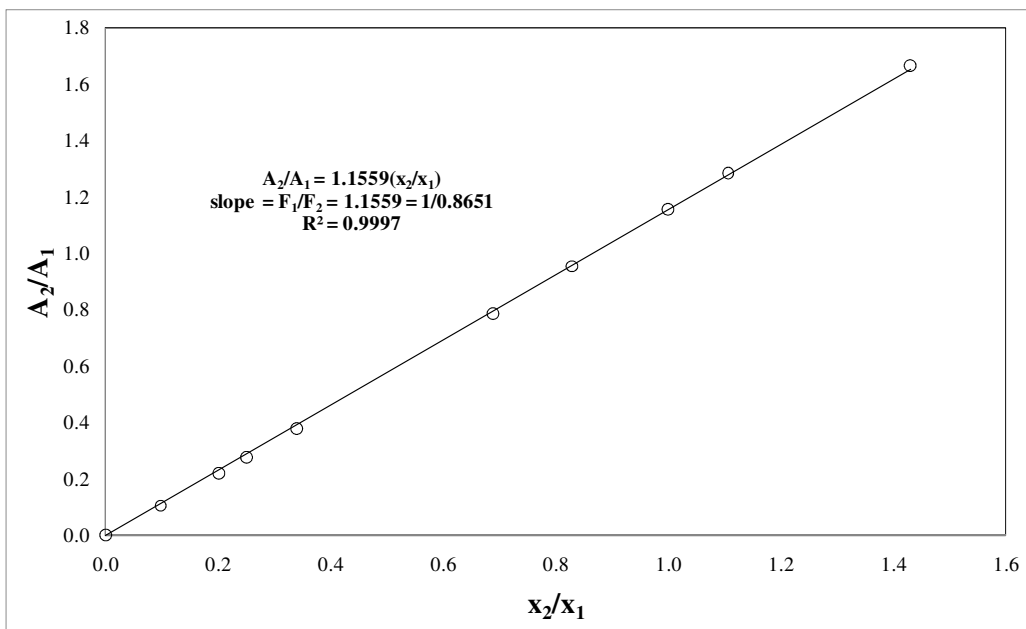


**Figure 6- 24 GC calibration plot for 2-propanone (1) + n-propanoic acid (2) in the 2-propanone rich region**

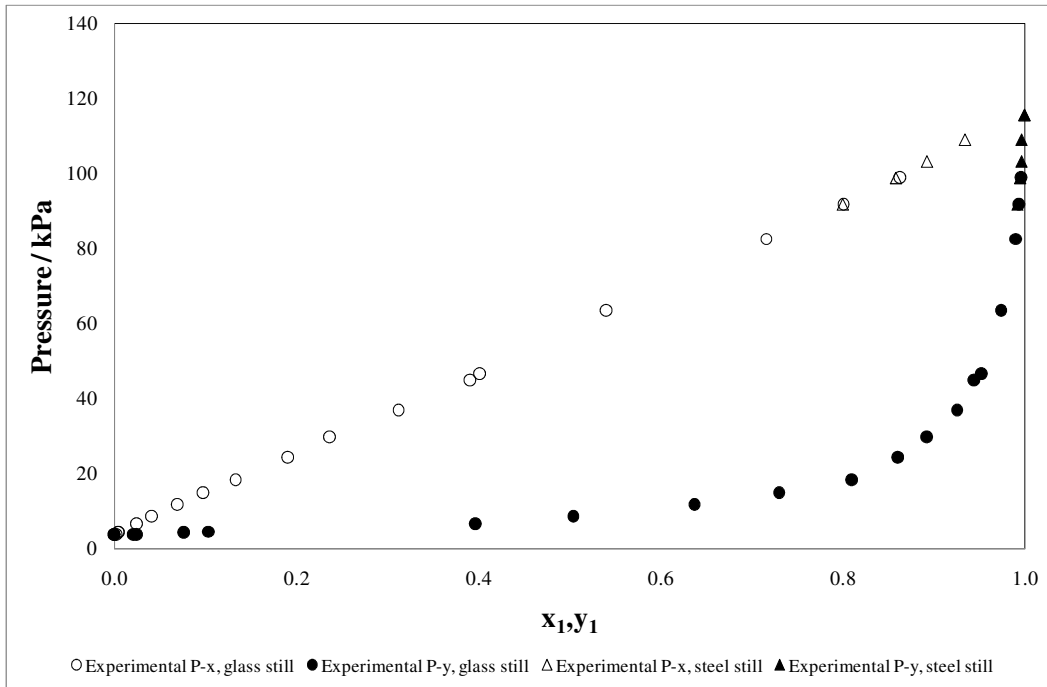


**Figure 6-25 Experimental P-x<sub>1</sub>-y<sub>1</sub> data for the 2-propanone (1) + n-propanoic acid (2) system at 333.15K**

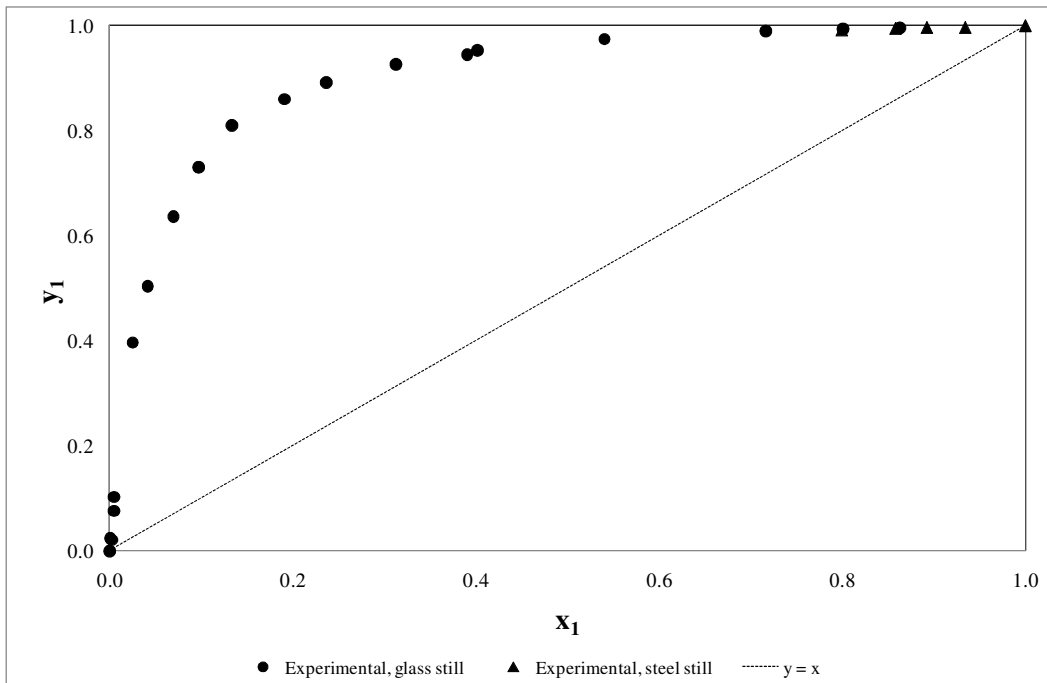


**Figure 6-26 x<sub>1</sub>-y<sub>1</sub> data for the 2-propanone (1) + n-propanoic acid (2) system at 333.15K**

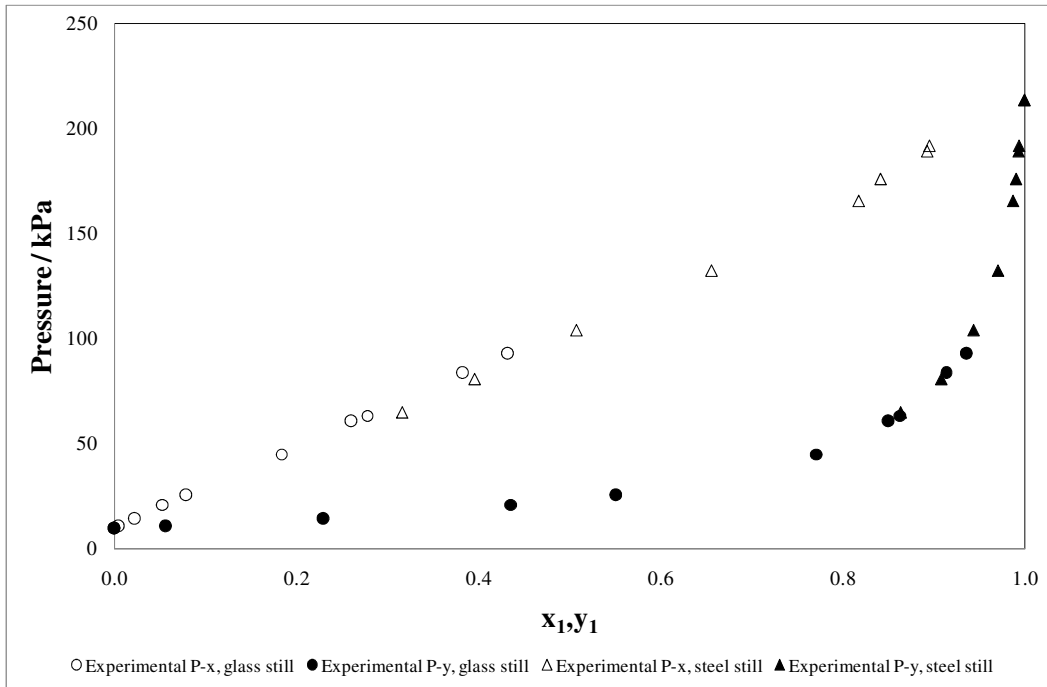


Figure 6-27 Experimental P- $x_1$ - $y_1$  data for the 2-propanone (1) + n-propanoic acid (2) system at 353.15K

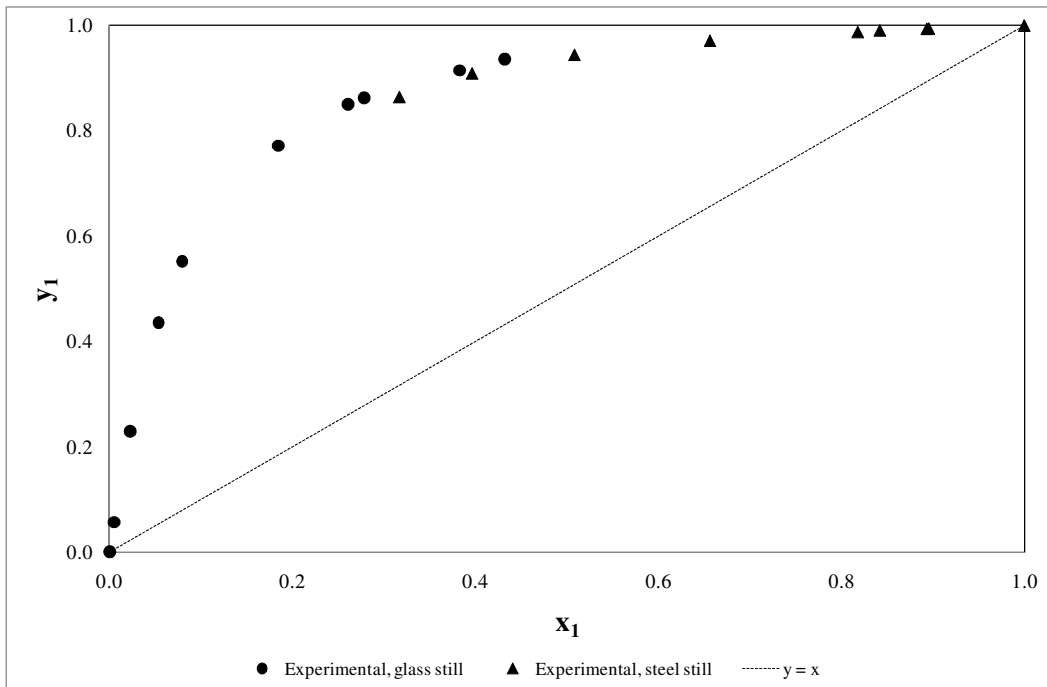
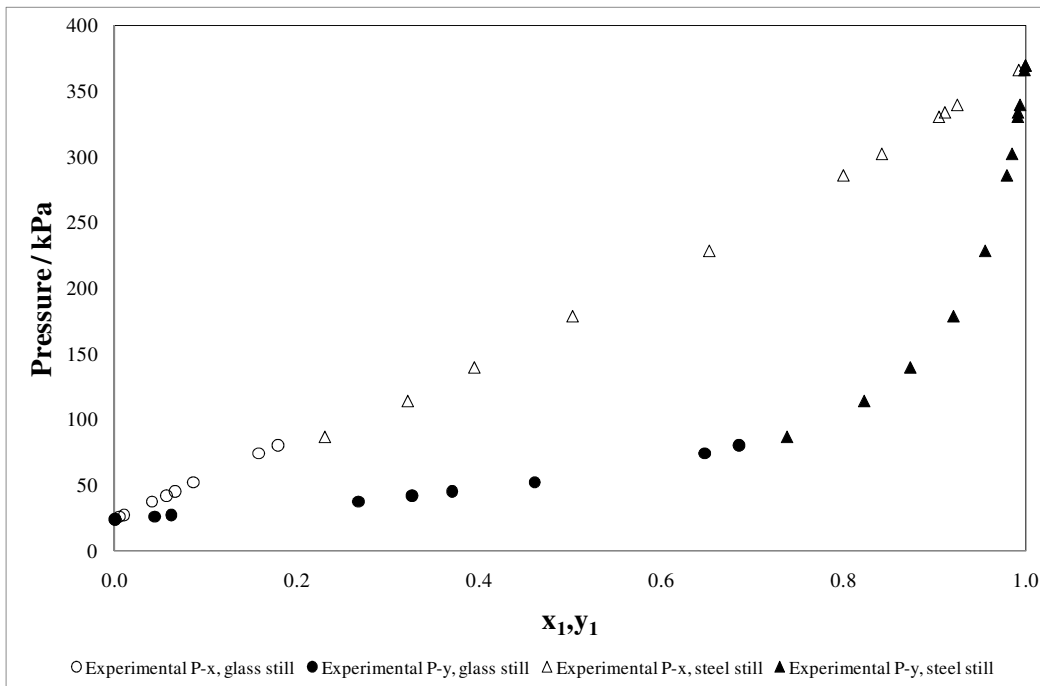
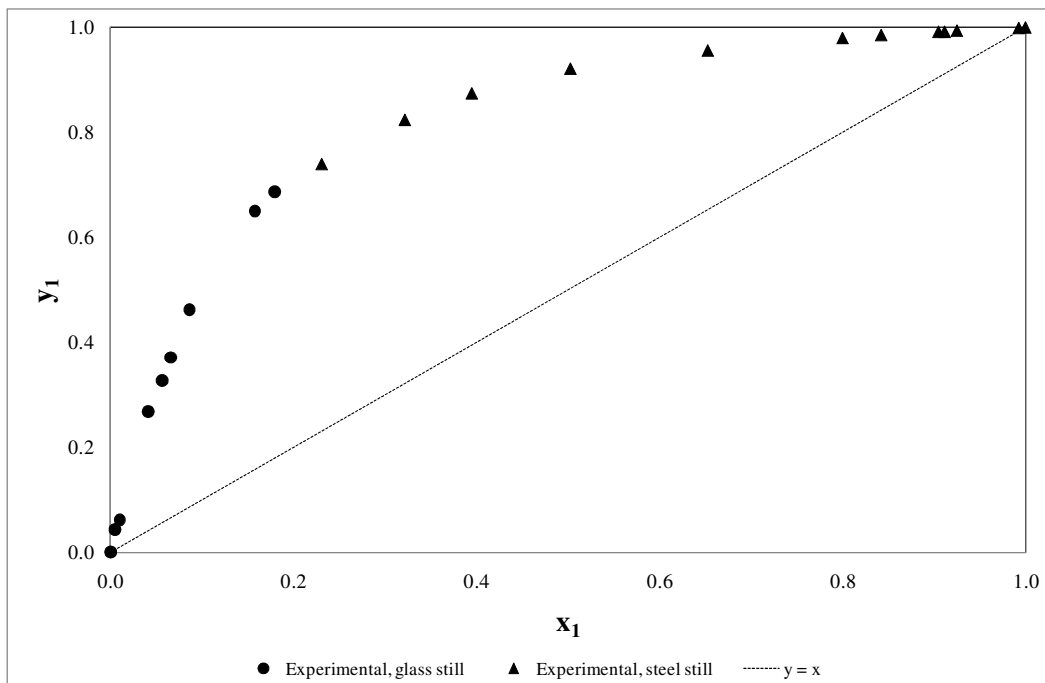


Figure 6-28  $x_1$ - $y_1$  data for the 2-propanone (1) + n-propanoic acid (2) system at 353.15K



**Figure 6-29 Experimental P- $x_1$ - $y_1$  data for the 2-propanone (1) + n-propanoic acid (2) system at 373.15K**



**Figure 6-30  $x_1$ - $y_1$  data for the 2-propanone (1) + n-propanoic acid (2) system at 373.15K**

#### 6.5.4. Results for the system: 1-propanol (1) + n-butanoic acid (2)

Isothermal measurements were performed at 333.15K and 353.15K which constitute new VLE data. The composition analysis was carried out using the Shimadzu 2014 GC fitted with the packed Porapak Q column (described in Tables 6-3 and 6-5). Two sets of calibration curves are presented here; Figures 6-31 and 6-32 illustrate the data fitted to a linear curve, and Figures 6-33 and 6-34 illustrate the calibration plots fitted with quadratic equations. It was discussed in Section 6.2.2 that for this system the linear relationship between the area ratios and mole fraction ratios is not valid and hence the quadratic relationships (Figures 6-33 and 6-34) were used in the composition determinations. The experimental VLE data points are listed in Table 6-23 for both isotherms and the equilibrium phase diagrams are presented in Figures 6-35 to 6-38.

**Table 6-23 P-x<sub>1</sub>-y<sub>1</sub> data for 1-propanol (1) + n-butanoic acid (2)**

Measurements on apparatus of Joseph (2001) T = 333.15K			Measurements on apparatus of Joseph (2001) T = 353.15K		
Pressure / kPa	x <sub>1</sub>	y <sub>1</sub>	Pressure / kPa	x <sub>1</sub>	y <sub>1</sub>
0.67	0.000	0.000	3.54	0.000	0.000
1.09	0.003	0.018	5.84	0.034	0.269
2.45	0.062	0.496	10.65	0.152	0.604
5.21	0.206	0.783	25.72	0.504	0.929
7.66	0.348	0.883	28.71	0.558	0.947
9.21	0.460	0.918	30.16	0.577	0.955
12.35	0.609	0.968	34.72	0.687	0.976
14.34	0.698	0.983	38.07	0.752	0.983
15.2	0.742	0.988	42.44	0.830	0.992
16.64	0.810	0.994	46.07	0.894	0.997
17.2	0.857	0.995	48.67	0.950	0.999
19.36	0.945	0.999	51.3	1.000	1.000
20.56	1.000	1.000			

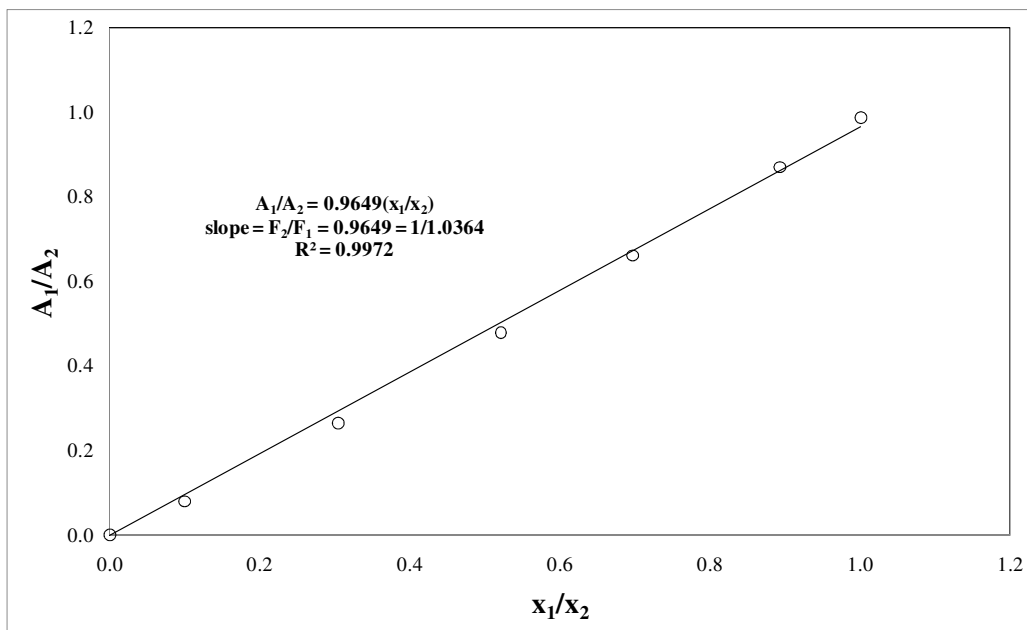


**Figure 6-31 GC calibration plot with a linear fit to the data for 1-propanol (1) + n-butanoic acid (2) in the n-butanoic acid rich region**

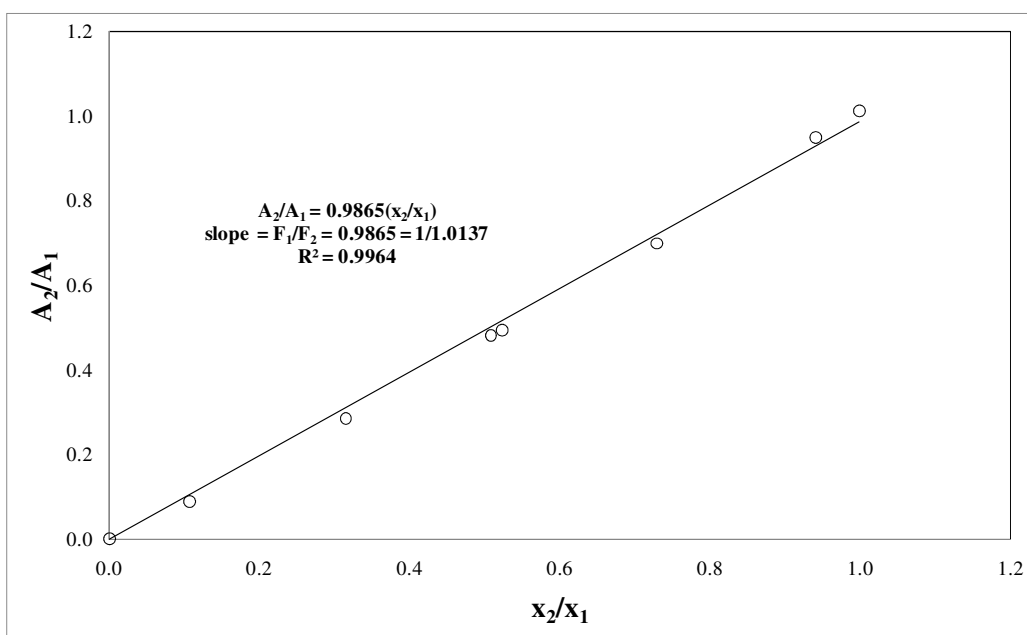


**Figure 6-32 GC calibration plot with a linear fit to the data for 1-propanol (1) + n-butanoic acid (2) in the 1-propanol rich region**

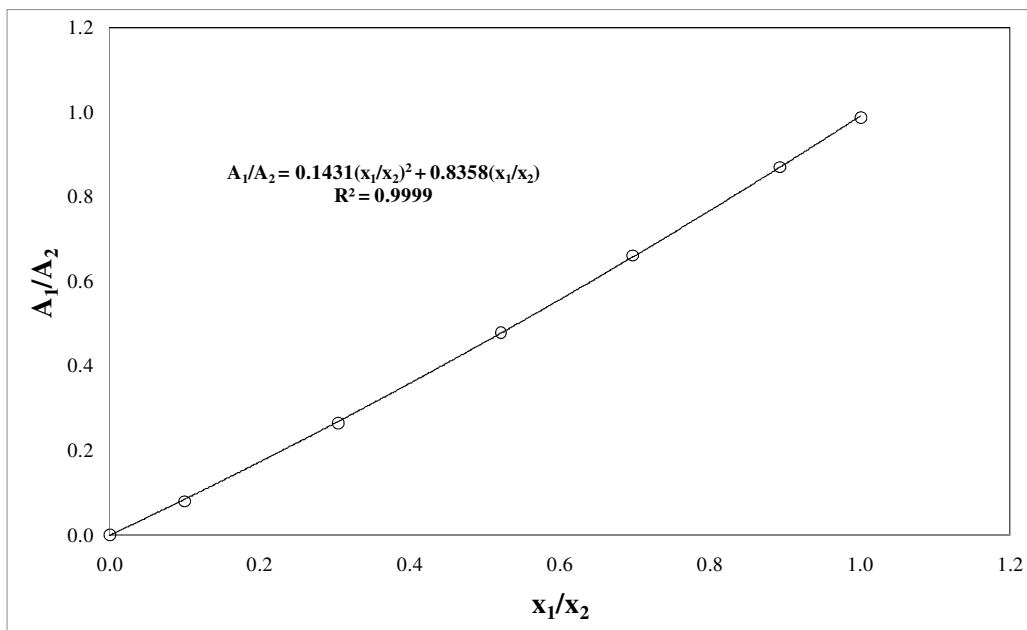


Figure 6-33 GC calibration plot with a quadratic fit to the data for 1-propanol (1) + n-butanoic acid (2) in the n-butanoic acid rich region

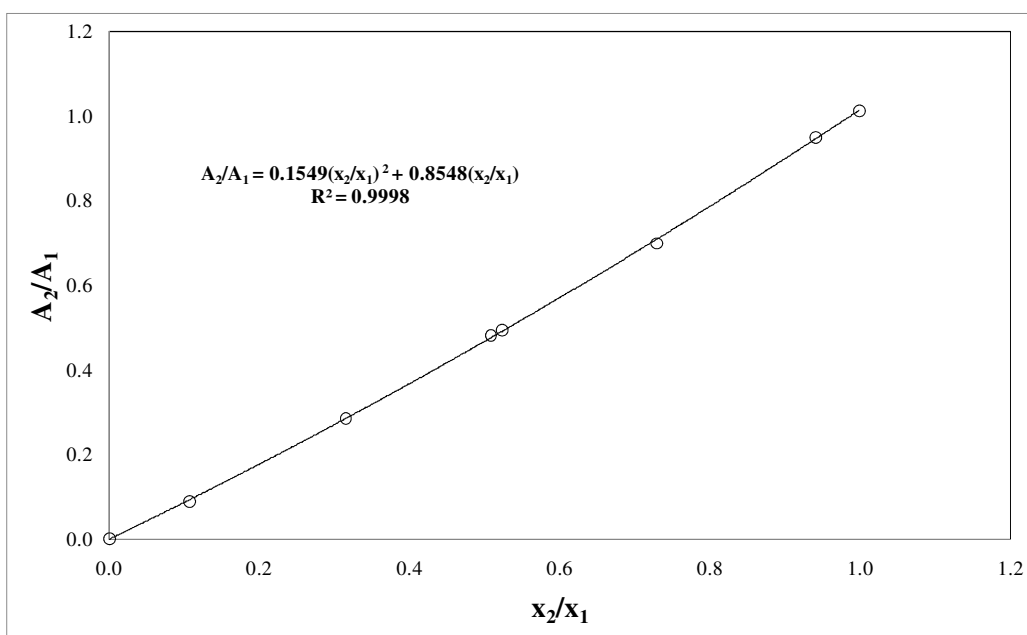
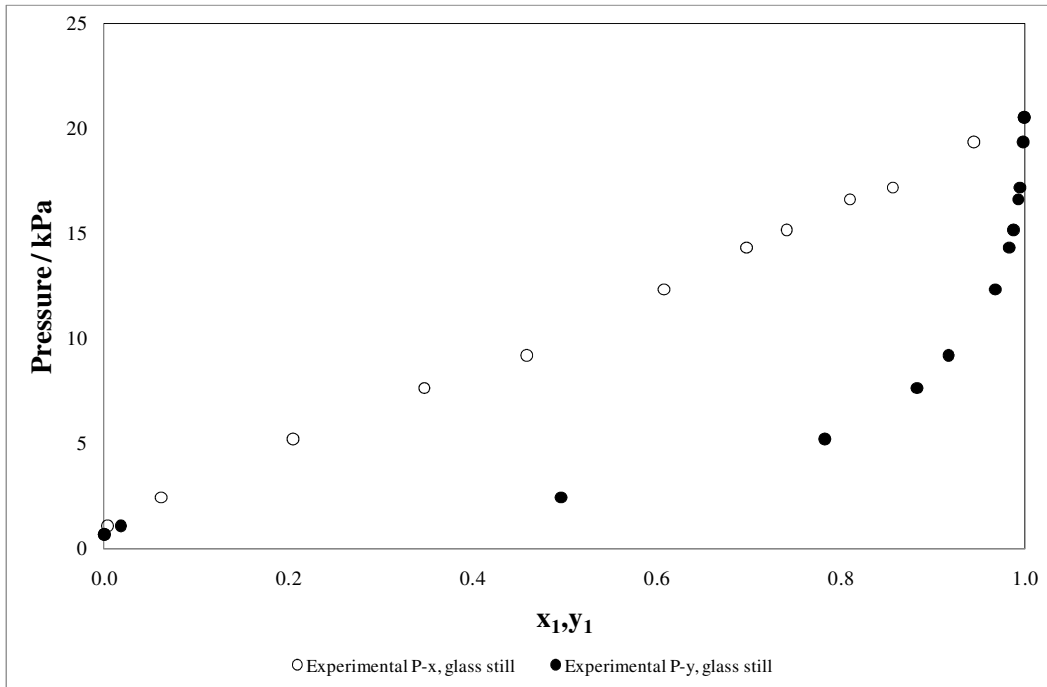
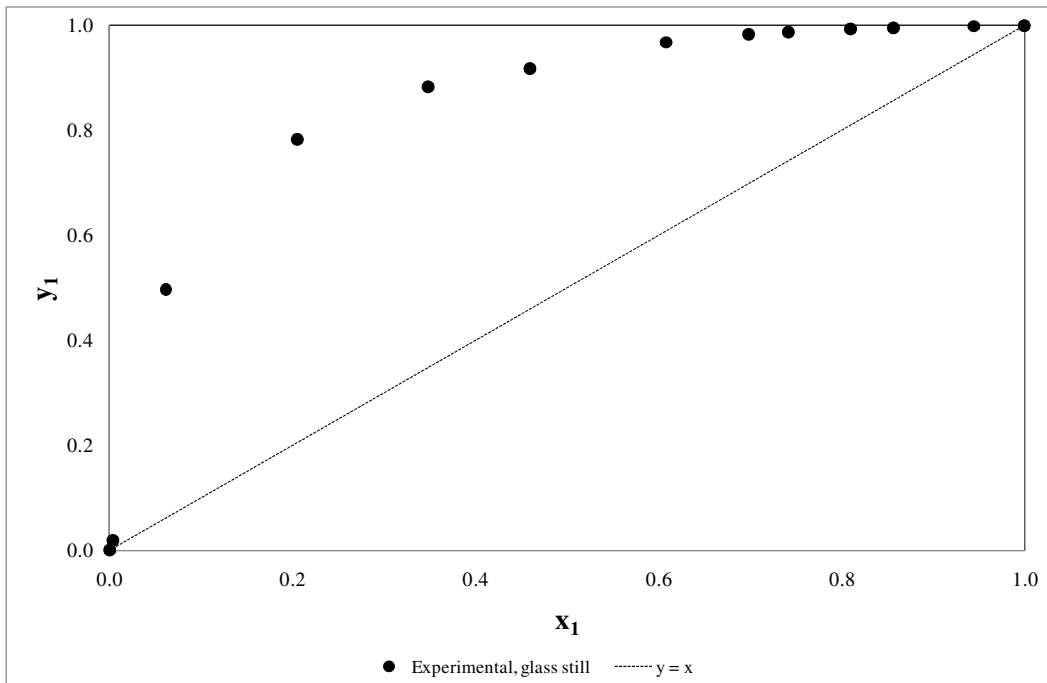


Figure 6-34 GC calibration plot with a quadratic fit to the data for 1-propanol (1) + n-butanoic acid (2) in the 1-propanol rich region



**Figure 6-35 Experimental P- $x_1$ - $y_1$  data for the 1-propanol (1) + n-butanoic acid (2) system at 333.15K**



**Figure 6-36  $x_1$ - $y_1$  data for the 1-propanol (1) + n-butanoic acid (2) system at 333.15K**

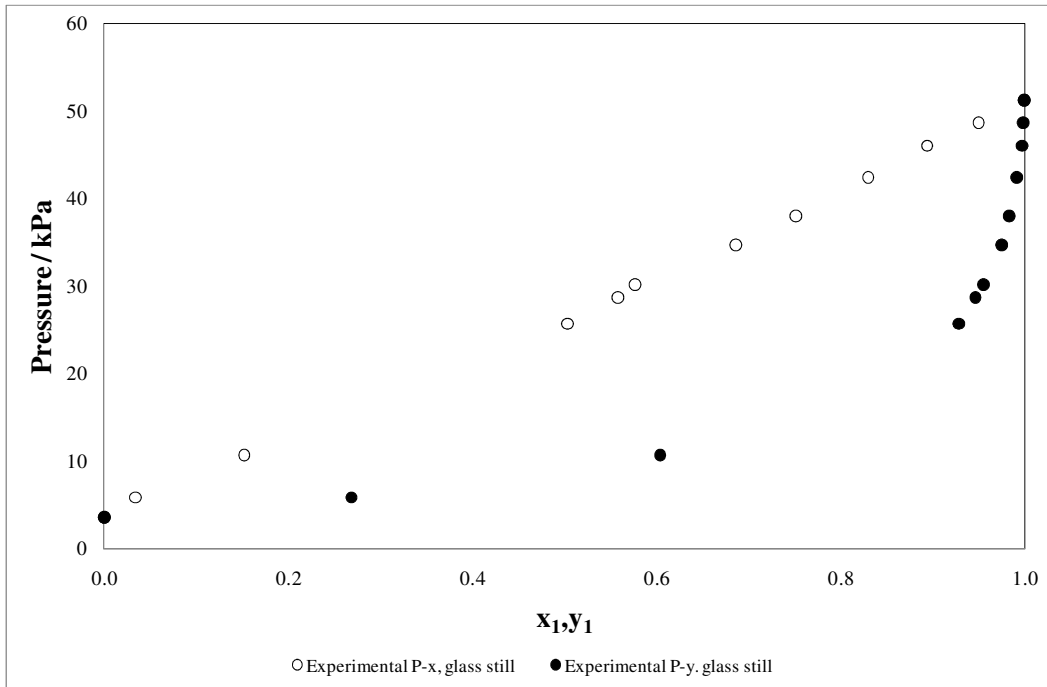


**Figure 6-37 Experimental P- $x_1$ - $y_1$  data for the 1-propanol (1) + n-butanoic acid (2) system at 353.15K**

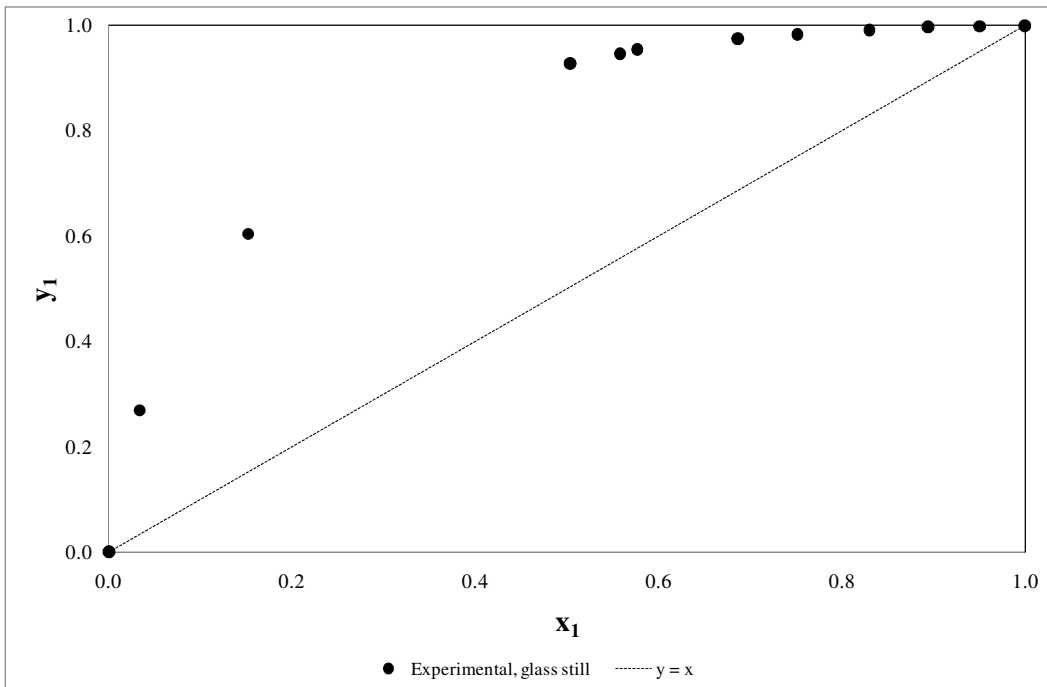


**Figure 6-38  $x_1$ - $y_1$  data for the 1-propanol (1) + n-butanoic acid (2) system at 353.15K**

## CHAPTER 7

### DATA ANALYSIS AND DISCUSSION

The theoretical aspects that are employed in data reduction and thermodynamic consistency testing of experimental data that are applicable to this project have been discussed in Chapter 3. This chapter deals with the results and discussion of the VLE data analysis performed.

#### 7.1. Experimental vapour pressure data for pure components

Accurate vapour pressure data are essential when modeling binary VLE systems. Vapour pressures were therefore measured for all the pure components that were used in this project (this data was tabulated and plotted in Section 6.4). Table 7-1 gives the average absolute pressure deviations and average absolute temperature deviations (as defined in Section 6.4) which provides, wherever possible, a comparison between the vapour pressure data measured in this project and the data available in Poling et al. (2001) and the DDB (2008).

**Table 7-1 Comparison between literature and experimental vapour pressure data.**

Component	$\Delta T_{\text{avg}} / ^\circ\text{C}$		$\Delta T_{\text{avg}} \%$		$\Delta P_{\text{avg}} / \text{kPa}$		$\Delta P_{\text{avg}} \%$	
	Ref 1 <sup>a</sup>	Ref 2 <sup>b</sup>	Ref 1 <sup>a</sup>	Ref 2 <sup>b</sup>	Ref 1 <sup>a</sup>	Ref 2 <sup>b</sup>	Ref 1 <sup>a</sup>	Ref 2 <sup>b</sup>
2-butanol	0.07	0.28	0.14	0.50	0.07	0.38	0.36	1.39
1-propanol	0.14	0.36	0.20	0.53	0.24	0.51	0.64	1.69
n-butanoic acid	0.32	*	0.41	*	0.06	*	4.30	*
n-propanoic acid	0.43	1.45	0.74	2.55	0.12	0.39	2.22	6.95
2-propanone	0.22	0.48	0.27	0.58	1.69	3.52	0.60	1.36
cyclohexane	0.30	0.30	0.43	0.42	0.83	0.87	0.97	0.96

<sup>a</sup>Poling et al., 2001

<sup>b</sup>DDB, 2008

\* no data available from this source to compare experimental data with

In general, the deviations between the vapour pressure data measured in this work and that of the literature sources were small. The deviations of measured data for each component were smaller (if not similar) from Poling et al.(2001) as compared to that of the DDB(2008). Using the data

from Poling et al.(2001), the average absolute temperature differences ( $\Delta T_{avg}$ ) were below 0.5 °C for all components and the average absolute pressure differences ( $\Delta P_{avg}$ ) were all below 1 kPa except for 2-propanone for which it was 1.69 kPa. This does however correspond to a  $\Delta P_{avg}$  % of 0.6 which is relatively low. In addition, the average absolute temperature deviation as a percentage was only 0.27% for 2-propanone indicating reasonable agreement with the data of Poling et al. (2001). Hence all the vapour pressures measured in this project were considered to agree reasonably well with the literature data. The vapour pressure determinations provide a simultaneous check on the following:

- temperature sensors (i.e. their calibration and operation)
- pressure sensors ( i.e. their calibration and operation)
- chemical reagents (purity)
- experimental apparatus
- experimental method

The vapour pressure data (excluding the components of the test system) were regressed to obtain the parameters for the Antoine equation:

$$\ln(P_i^{sat} / kPa) = A_i + \frac{B_i}{T / ^\circ C + C_i} \quad (7.1)$$

and the parameters obtained along with the  $\Sigma(\Delta P^2)$  for each set of data are given in Table 7-2 (with units as indicated in Equation 7.1 above). The low values for the expression  $\Sigma(\Delta P^2)$  show that the equation fitted the data exceedingly well.

**Table 7-2 Parameters for the Antoine equation (this work)**

	<b>2-butanol</b>	<b>1-propanol</b>	<b>n-butanoic acid</b>	<b>n-propanoic acid</b>	<b>2-propanone</b>
A	114.50	76.84	52.00	44.98	62.82
B	-9410.48	-7677.89	-489.16	-5277.91	-6157.00
C	-15.06	-13.38	-273.75	-53.13	18.14
$\Sigma(\Delta P^2)$	0.0280	0.0537	0.0079	0.0145	0.0366

## 7.2. Determination of experimental activity coefficients for binary systems

Experimental activity coefficients are usually obtained either by assuming ideal gas behaviour for the vapour phase ( $\Phi_i=1$ ) or evaluating the vapour phase correction term  $\Phi_i$  from a suitable model (usually the virial EOS) and substituting into:

$$y_i \Phi_i P = x_i \gamma_i P_i^{sat} \quad (3.38)$$

However, Clifford (2004) has shown that in the case of carboxylic acids this procedure produced extremely poor values for the experimental activity coefficients as a result of the high degree of association that occurs in carboxylic acids, even at low pressures. This was confirmed during this study since the activity coefficients calculated via the conventional method above were inconsistent with the normal trends expected for a binary system. An example of the sort of results that were obtained is given in Figure 7-1 which shows the experimental activity coefficients for the 2-propanone (1) + n-propanoic acid (2) system at 333.15K calculated using the conventional method. The unusual curves obtained are as a result of the strong association that occurs, even at low pressures. It is for this reason that it is important to make use of models that take association into account.

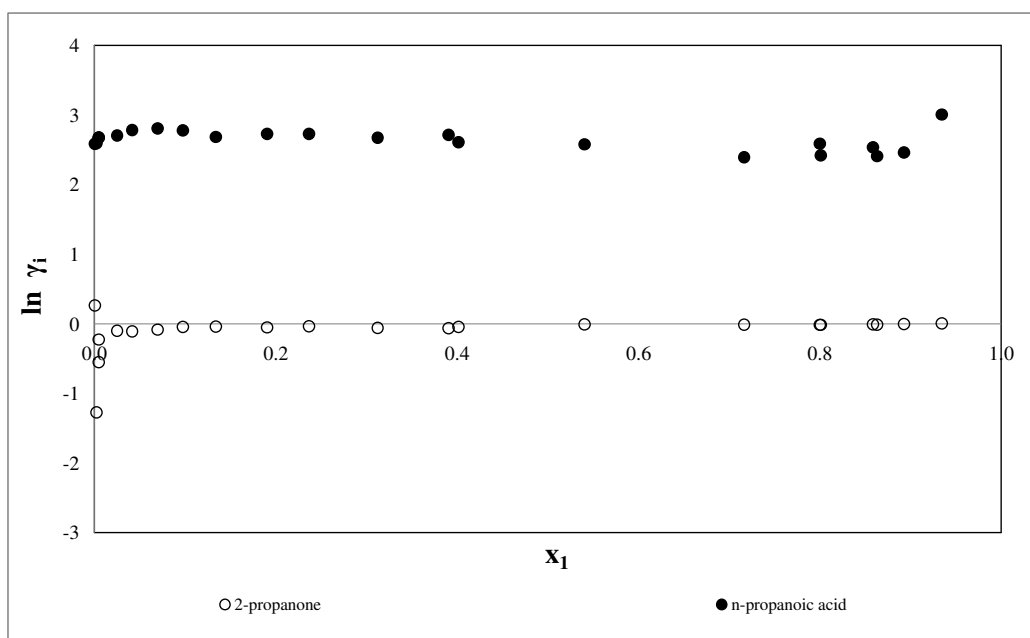


**Figure 7-1 Experimental liquid-phase activity coefficients for the 2-propanone (1) + n-propanoic acid (2) system at 333.15K using the conventional method**

### 7.3. Binary VLE data reduction

The use of process simulators such as Aspen Plus<sup>®</sup> is the most popular route taken to model and predict the performance of industrial processes. Therefore, for this study, Aspen Plus<sup>®</sup> was used as the data reduction tool with the combined method for VLE ( $\gamma$ - $\Phi$  method). The VLE data were correlated taking into consideration the non-ideality in both the liquid and vapour phases. The vapour phase fugacity coefficients were calculated using the methods capable of describing associating systems that were available in Aspen: viz. the method of Hayden and O'Connell (1974), Nothnagel et al. (1973) and the VPA/IK-CAPE EOS (Abbott and Van Ness, 1992). For the liquid phase, three local-composition based activity coefficient models were used to represent non-ideality: viz. Wilson (Wilson, 1964), NRTL (Renon and Prausnitz, 1968) and UNIQUAC (Abrams and Prausnitz, 1975). For the activity coefficient models, only the  $a_{ij}$  and  $b_{ij}$  parameters (in Equations 3.66, 3.70b and 3.79) were included in the regression. All others were set equal to zero and the NRTL  $\alpha$  parameter was fixed at 0.3 as discussed in Chapter 3.

The objective function used for the regression algorithm was the ordinary least squares which makes use of the pressure and vapour compositions for isothermal VLE data (reduces to Barkers method when only P- $x_i$  data is used). The Britt-Luecke algorithm, a rigorous maximum-likelihood method, was used as opposed to the approximate solution method of Deming which is also available in Aspen (usually used as a last resort when Britt-Luecke does not converge). For the initialization, the Deming method is recommended by Aspen and was used for this study but a weighted least-squares algorithm is also available.

### 7.4. Thermodynamic consistency testing

Thermodynamic consistency testing was carried out to assess the quality of the measured data before they were used to obtain model parameters. From the description of these tests in Section 3.7, it follows that the slope test, area test and direct test all require experimental activity coefficients. However, as mentioned earlier in this chapter, as a result of the high degree of association present, the experimental activity coefficient data obtained via the conventional calculation method cannot be used. Hence, the consistency tests for associating systems are not trivial; vapour phase non-idealities are significant even at low pressures and the ideal gas law or even the truncated virial EOS is no longer valid. With the direct test in particular, only an activity coefficient model can be used as opposed to the point test where an EOS and activity

coefficient model can be used. Therefore, only the stringent point test of Van Ness et al. (1973, 1975 & 1982) was used in this study.

As discussed in Section 3.7.4, the point test can be considered as a modeling test since a thermodynamically consistent model must be found that is capable of fitting the experimental data before the test can be applied. The model consists not only of the activity coefficient model, but also the vapour-phase EOS. In applying the point test, the mathematical model is regressed to the experimental P- $x_i$  data to obtain a set of values for the adjustable model parameters by minimizing the pressure deviations between the experimentally measured pressures and those calculated by the model. In doing so, the systematic errors are transferred to the vapour composition residual. The model, which is necessarily thermodynamically consistent since it satisfies the Gibbs-Duhem equation, is then used to calculate the  $y_i$  values which are compared to the experimentally measured values. As the experimental  $y_i$  data are not used in the regression, a comparison of the experimental  $y_i$  values with those predicted by the model represents a measure of thermodynamic consistency. The test relies on an appropriate model being employed for the regression. The model's fit to the data needs to be satisfactory then, the point test requires that the vapour composition display an average absolute deviation of less than 0.01 for the data set to be deemed consistent.

When applied to data, the results of the point test provide information on the data as well as the models used to fit them. It should be noted that these results are highly sensitive to the selection of the models. It is possible for data to pass a thermodynamic consistency test and still be erroneous. Similarly, good data may fail a thermodynamic consistency test whenever the standard assumptions that are embedded in most applications of thermodynamic consistency test are inappropriate. In general, it is not known when these assumptions begin breaking down for any given system, and, when they do, a systematic bias will be introduced in the results of the thermodynamic consistency tests. Nevertheless, applying thermodynamic consistency tests to VLE data provides a wealth of information that is difficult to obtain in any other way (Jackson & Wilsak, 1995).

Owing to the complexity of vapour phase for the binary systems in this project, the models used for the vapour phase were varied initially while consistently using the NRTL model for the liquid phase – i.e. model combinations applied first were NRTL-HOC, NRTL-VPA & NRTL-NTH. It

was observed that more often than not the NRTL-HOC gave the best fit to the  $P-x_i$  data based on the  $\Delta P_{avg}$ . Therefore, the subsequent model combinations applied fixed HOC for the vapour phase and only the liquid phase activity coefficient model was changed – i.e. the model combinations of NRTL-HOC, WILSON-HOC and UNIQUAC-HOC were then applied to check consistency.

The 333.15K data set for the 2-propanone (1) + 2-butanol (2) system was the only data set in this project for which the point test passed for all model combinations used (discussed in Section 7.4.1). For all the other data sets, Tables 7-4 to 7-10 summarise the results obtained. In these tables, the full set of measured data are provided in each table with the  $\Delta P_{avg}$  and  $\Delta y_{1avg}$  obtained when the full set of data is used in the regressions for the test. For model combinations for which the test failed, points with the highest  $y_i$ -residuals were excluded one at a time from the data regressions and the test re-evaluated until the test criterion ( $\Delta y_{1avg} < 0.01$ ) was satisfied. Points that needed to be excluded for a particular model combination in order for the test to pass are indicated by the “x” in the table in the relevant column. The  $\Delta P_{avg}$  and  $\Delta y_{1avg}$  are provided at the bottom of each table for the cases where the full set of data points were used as well as where only the data points for which the test passed were used. For the final data regression (discussed in Section 7.4), only data points for which the consistency test passed for at least one of the model combinations that were used in this project (discussed earlier) were included. Points that were excluded from the final data regression analyses are indicated by the “\*” in the Tables 7-4 to 7-10.

#### **7.4.1. Point test results: 2-propanone (1) + 2-butanol (2)**

The average absolute deviations for the pressure and vapour mole fractions for each of the five model combinations used for the are given in Tables 7-3 to 7-5 for the 333.15K, 353.15K and 373.15K data sets respectively. The pressure-residuals and  $y_i$ -residuals for this data set are plotted in Figures 7-2 to 7-5. Figures 7-2 and 7-3 give the results obtained when the NRTL model was fixed for the liquid phase but HOC, VPA & NTH were used for the vapour phase. Figures 7-4 and 7-5 give the results obtained when the HOC model was fixed for the vapour phase and the effect of the liquid phase activity coefficient model was investigated. Upon examination of the P-residual plots (Figures 7-2 and 7-4), all five model combinations fit the  $P-x_i$  data well for the 333.15K data set. The NRTL-HOC combination provides a slightly better fit than the other models (lowest  $\Delta P_{avg}$  in Table 7-3) but isn't significantly better than the others.

Changing the activity coefficient model for this isotherm (Figures 7-4 and 7-5) resulted in an almost negligible variation in the results obtained. Since the models fit the data without any anomalous behaviour, with a reasonably good scatter about the x-axis, it is possible to evaluate the data on the basis of the  $y_i$ -residuals. With all model combinations used for this data set the  $\Delta y_{1\text{avg}}$  was below 0.01 and the point-to-point  $y_i$ -residuals, like the pressure-residuals, are reasonably well scattered about the x-axis. This data set is therefore considered to be thermodynamically consistent and all points were included in the final regression analyses.

**Table 7-3 Average deviations for the point test: 2-propanone (1) + 2-butanol (2) at 333.15K**

	<b>NRTL-HOC</b>	<b>NRTL-VPA</b>	<b>NRTL-NTH</b>	<b>WILS-HOC</b>	<b>UNIQU-HOC</b>
$\Delta P_{\text{avg}}$ (kPa)	0.41	0.44	0.43	0.41	0.41
$\Delta y_{1\text{avg}}$	0.0054	0.0071	0.0043	0.0055	0.0054

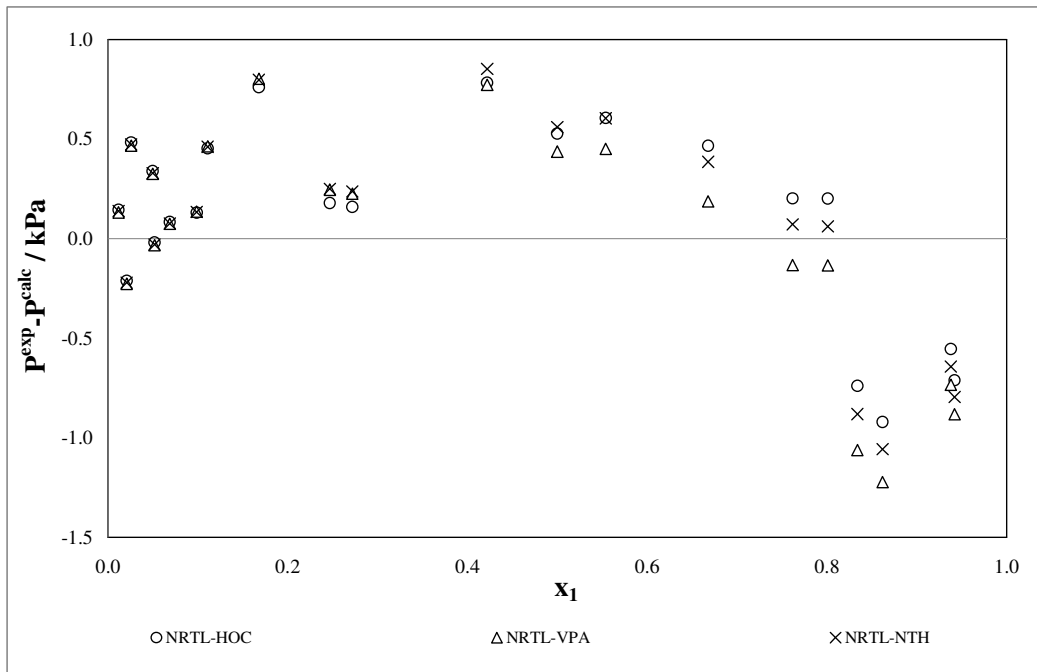


**Figure 7-2 Point test (varying EOS): pressure-residual for the 2-propanone (1) + 2-butanol (2) system at 333.15K**

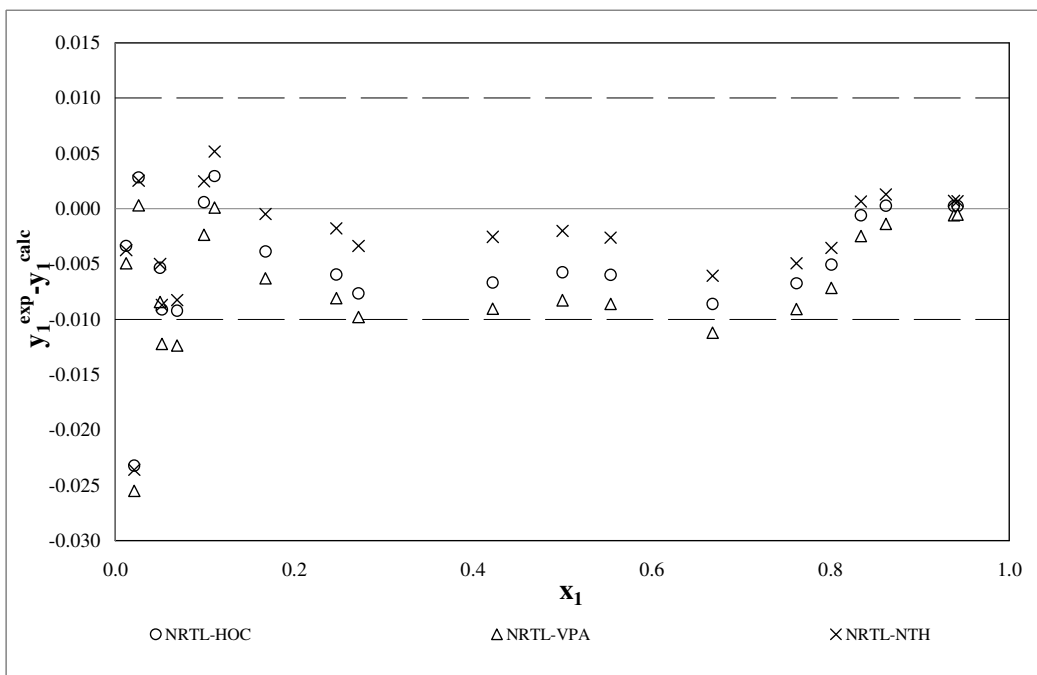


**Figure 7-3 Point test (varying EOS):  $\Delta y_1$  for the 2-propanone (1) + 2-butanol (2) system at 333.15K**

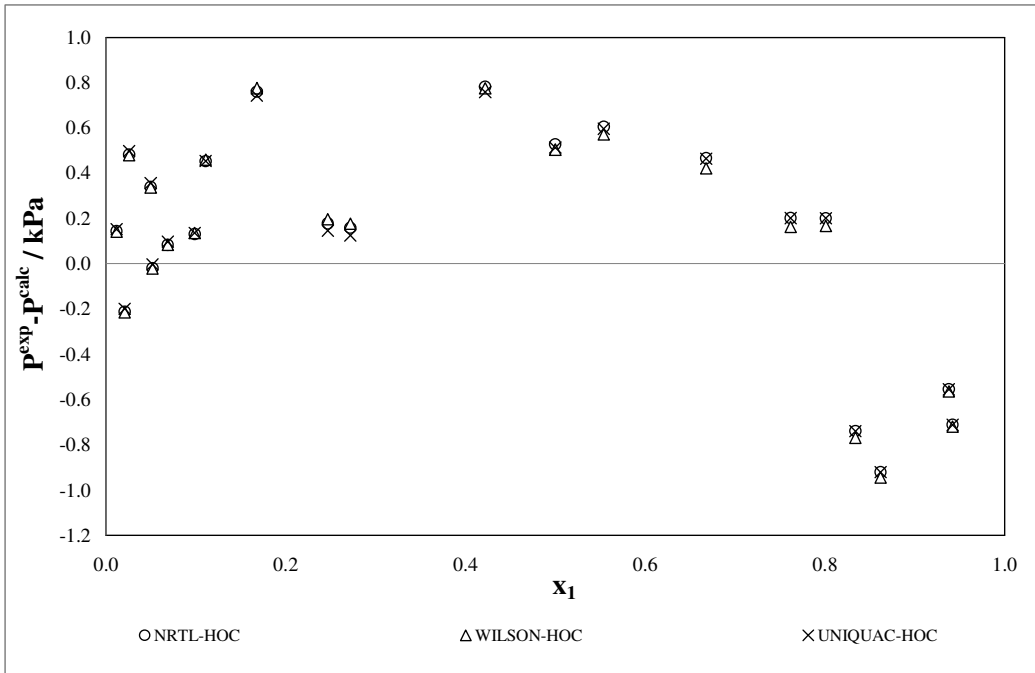


**Figure 7-4 Point test (varying activity coefficient model): pressure-residual for the 2-propanone (1) + 2-butanol (2) system at 333.15K**

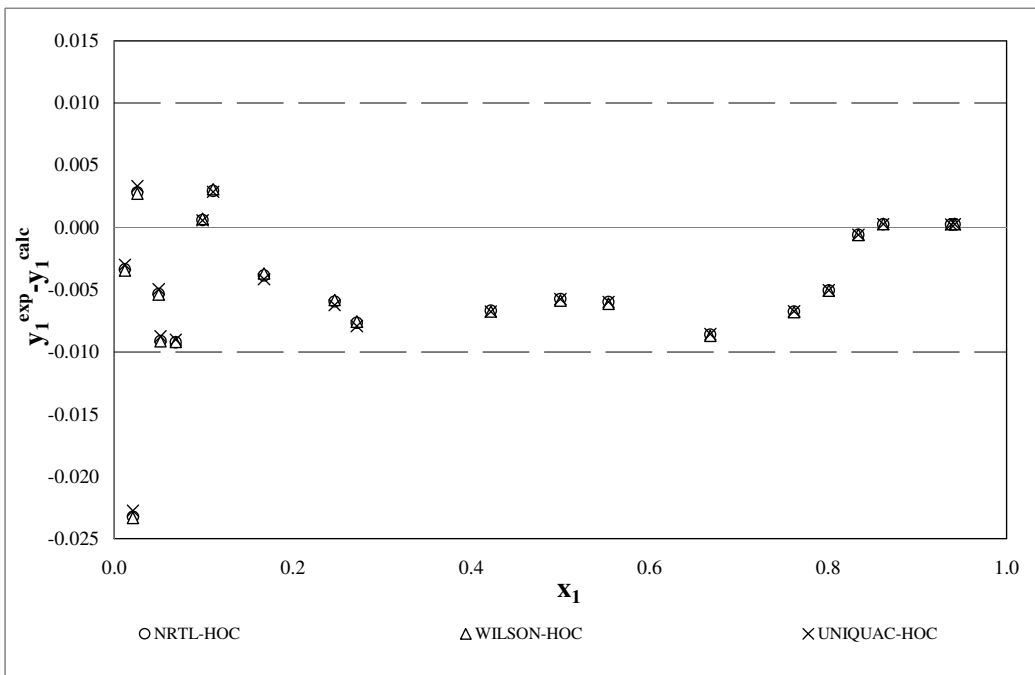


**Figure 7-5 Point test (varying activity coefficient model):  $\Delta y_1$  for the 2-propanone (1) + 2-butanol (2) system at 333.15K**

The pressure- and  $y_i$ -residual plots for all the remaining data sets can be found in Appendix B. For the 353.15K data set, the test passes for all model combinations used except when the NRTL-VPA model was (see Table 7-4). The  $\Delta P_{avg}$  however is the highest for this model combination which indicates that the model did not fit the P- $x_i$  data as well as the other model combinations and in this case the  $y_i$ -residuals should not even be looked at. This illustrates how good data points can be erroneously deemed incorrect if the test is not interpreted correctly. All data points from this set were included in the final regressions.

**Table 7-4 Average deviations for the point test: 2-propanone (1) + 2-butanol (2) – 353.15K**  
**NB: “x” indicates points which need to be excluded from the analysis in order for the remaining data to pass the point test with the model combination indicated by that particular column**

$x_1$	$y_1$	P / kPa	NRTL-HOC	NRTL-VPA	NRTL-NTH	WILS-HOC	UNIQ-HOC
0.000	0.000	46.38					
0.018	0.093	50.70					
0.020	0.107	51.29		x			
0.036	0.175	55.18		x			
0.057	0.258	60.18		x			
0.063	0.270	59.5		x			
0.089	0.355	67.19		x			
0.141	0.469	78.01		x			
0.151	0.489	80.26		x			
0.166	0.513	82.06		x			
0.214	0.576	92.24		x			
0.247	0.621	98.57		x			
0.440	0.761	129.30		x			
0.541	0.820	145.50		x			
0.632	0.859	160.20		x			
0.762	0.916	174.8		x			
0.829	0.943	185.1					
0.864	0.956	190.5					
0.937	0.981	202.6					
0.943	0.983	203.4					
1.000	1.000	213.8					
<b>Point test results using the full set of data</b>							
$\Delta P_{avg}$ (kPa)			1.02	1.13	1.11	1.02	1.00
$\Delta y_{1avg}$			0.0070	0.0107	0.0049	0.0070	0.0069
<b>Point test results with excluded data points</b>							
$\Delta P_{avg}$ (kPa)			1.02	0.63	1.11	1.02	1.00
$\Delta y_{1avg}$			0.0070	0.0091	0.0049	0.0070	0.0069

For the 373.15K data set, the test only passed when the NRTL-NTH combination was used. However, the average absolute pressure-residual for this combination was the highest indicating that this model fit the data for slightly worse than the others and the  $y_1$ -residual using this combination should not be looked at. This illustrates how a bad data point can be passed if the test is not interpreted properly. Only the one data point corresponding to P=245.2kPa from this

data set was excluded in the final regression analyses since the point test passes when this point is excluded for NRTL-HOC, WILS-HOC and UNIQUAC-HOC. For this data set the model combinations which include the HOC for the vapour phase fitted the data better than when the VPA or NTH was used. Once again, because the fit of the NRTL-VPA model was not as good as for the case when HOC was used and it requires more points to be excluded in order for the test criterion to be satisfied.

**Table 7-5 Average deviations for the point test: 2-propanone (1) + 2-butanol (2) – 373.15K**

**NB: an “x” in a particular column indicates that that point needs to be excluded from the analysis in order for the remaining data to pass the point test**

$x_1$	$y_1$	P / kPa	NRTL-HOC	NRTL-VPA	NRTL-NTH	WILS-HOC	UNIQUAC-HOC
0.000	0.000	102.9					
0.037	0.128	114.0					
0.069	0.219	123.7					
0.415	0.697	225.2		x			
0.495*	0.747*	245.2*	x	x		x	x
0.545	0.789	257.7					
0.618	0.819	272.3		x			
0.777	0.899	305.1		x			
0.829	0.928	321.0					
0.865	0.946	331.6					
0.925	0.972	347.2					
0.942	0.978	352.1					
1.000	1.000	369.4					
<b>Point test results using the full set of data</b>							
$\Delta P_{avg}$ (kPa)			2.69	2.81	3.06	2.69	2.52
$\Delta y_{1avg}$			0.0107	0.0165	0.0084	0.0107	0.0105
<b>Point test results with excluded data points</b>							
$\Delta P_{avg}$ (kPa)			2.63	2.56	3.06	2.64	2.47
$\Delta y_{1avg}$			0.0092	0.0087	0.0084	0.0092	0.0089
			* data not included in final regressions				

#### 7.4.2. Point test results: 2-propanone (1) + n-propanoic acid (2)

Tables 7-6 to 7-8 give the results for the 333.15K, 353.15K and 373.15K data sets respectively. For the final regression analyses, no data points were excluded from the 333.15K and 353.15K data sets, and two points had to be excluded from the 373.15K data set.

**Table 7-6 Average deviations for the point test: 2-propanone (1) + n-propanoic acid (2) – 333.15K**

**NB: an “x” in a particular column indicates that that point needs to be excluded from the analysis in order for the remaining data to pass the point test**

$x_1$	$y_1$	P / kPa	NRTL-HOC	NRTL-VPA	NRTL-NTH	WILS-HOC	UNIQU-HOC
0.000	0.000	3.64					
0.001	0.025	3.73					
0.002	0.022	3.74					
0.005	0.077	4.29		x			
0.005	0.103	4.43					
0.025	0.397	6.62	x	x		x	x
0.042	0.504	8.57		x			
0.070	0.637	11.65		x			
0.098	0.730	14.77		x			
0.134	0.810	18.32	x			x	x
0.191	0.860	24.26					
0.237	0.892	29.62					
0.313	0.926	36.75					
0.391	0.944	44.89					
0.402	0.952	46.51					
0.540	0.974	63.35					
0.717	0.990	82.41					
0.800	0.992	91.7					
0.801	0.993	91.70					
0.859	0.995	98.7					
0.863	0.996	98.89					
0.893	0.997	103.1					
0.935	0.997	108.9					
1.000	1.000	115.5					
<b>Point test results using the full set of data</b>							
$\Delta P_{avg}$ (kPa)			0.38	0.31	0.31	0.33	0.37
$\Delta y_{lavg}$			0.0125	0.0228	0.0073	0.0124	0.0125
<b>Point test results with excluded data points</b>							
$\Delta P_{avg}$ (kPa)			0.41	0.38	0.31	0.36	0.40
$\Delta y_{lavg}$			0.0098	0.0093	0.0073	0.0099	0.0098

**Table 7-7 Average deviations for the point test: 2-propanone (1) + n-propanoic acid (2) –  
353.15K**

**NB: an “x” in a particular column indicates that that point needs to be excluded from the analysis in  
order for the remaining data to pass the point test**

$x_1$	$y_1$	P / kPa	NRTL-HOC	NRTL-VPA	NRTL-NTH	WILS-HOC	UNIQ-HOC
0.000	0.000	9.97					
0.005	0.056	11.23		x	x		
0.023	0.230	14.65		x	x		
0.053	0.435	20.92		x	x		
0.079	0.551	25.67		x	x		
0.184	0.771	44.90		x	x		
0.260	0.849	60.75			x		
0.278	0.863	63.15		x	x		
0.317	0.863	64.8		x	x		
0.382	0.914	83.71			x		
0.396	0.908	80.7			x		
0.432	0.936	93.03			x		
0.508	0.944	104			x		
0.656	0.971	132.4			x		
0.818	0.988	165.6					
0.842	0.991	176.1					
0.893	0.994	189.3					
0.896	0.994	191.9					
1.000	1.000	213.8					
<b>Point test results using the full set of data</b>							
$\Delta P_{avg}$ (kPa)			1.94	2.99	2.05	2.04	1.96
$\Delta y_{avg}$			0.0083	0.0994	0.0123	0.0086	0.0084
<b>Point test results with excluded data points</b>							
$\Delta P_{avg}$ (kPa)			1.94	2.12	0.76	2.04	1.96
$\Delta y_{avg}$			0.0083	0.0093	0.0009	0.0086	0.0084

**Table 7-8 Average deviations for the point test: 2-propanone (1) + n-propanoic acid (2) –  
373.15K**

**NB: an “x” in a particular column indicates that that point needs to be excluded from the analysis in  
order for the remaining data to pass the point test**

$x_1$	$y_1$	P / kPa	NRTL-HOC	NRTL-VPA	NRTL-NTH	WLS-HOC	UNIQ-HOC
0.000	0.000	23.65					
0.005	0.043	25.89					
0.010	0.062	26.97		x	x		
0.041*	0.267*	37.44*	x	x	x	x	x
0.057*	0.327*	41.58*	x	x	x	x	x
0.066	0.371	44.99	x	x	x		x
0.086	0.462	52.02		x	x		
0.158	0.648	74.11		x	x		
0.180	0.686	80.42		x	x		
0.231	0.739	86.5		x	x		
0.322	0.823	113.8		x	x		
0.395	0.874	139.4			x		
0.503	0.921	178.4			x		
0.653	0.956	228.2			x		
0.800	0.980	285.7					
0.842	0.985	302.1					
0.905	0.992	330.3					
0.912	0.992	333.7					
0.925	0.994	339.4					
0.993	0.999	365.9					
1.000	1.000	369.4					
<b>Point test results using the full set of data</b>							
$\Delta P_{avg}$ (kPa)			2.04	1.51	3.94	2.50	2.14
$\Delta y_{1avg}$			0.0142	0.0494	0.0723	0.0152	0.0144
<b>Point test results with excluded data points</b>							
$\Delta P_{avg}$ (kPa)			2.17	1.18	0.95	3.92	3.90
$\Delta y_{1avg}$			0.0084	0.0090	0.0069	0.0088	0.0067

\*data not included in final regressions

### 7.4.3. Point test results: 1-propanol (1) + n-butanoic acid (2)

Tables 7-9 and 7-10 summarise the results for the point test for this system. The average absolute pressure residuals were below 0.8 kPa for all model combinations and for both isotherms. The p-residuals also scattered reasonably well around the x-axis. Four data points had to be excluded from the 333.15K data set and none were excluded from the 353.15K data set before the test criterion was satisfied. The test is extremely sensitive in the n-butanoic acid-rich region as the  $P$ - $y_i$  curve is almost horizontal in this region.

**Table 7-9 Average deviations for the point test: 1-propanol (1) + n-butanoic acid (2) – 333.15K**

**NB: an “x” in a particular column indicates that that point needs to be excluded from the analysis in order for the remaining data to pass the point test**

$x_1$	$y_1$	P / kPa	NRTL-HOC	NRTL-VPA	NRTL-NTH	WILS-HOC	UNIQ-HOC
0.000	0.000	0.67					
0.003*	0.018*	1.09*	x	x	x	x	x
0.062*	0.496*	2.45*	x	x	x	x	x
0.206*	0.783*	5.21*	x	x	x	x	x
0.348*	0.883*	7.66*	x	x	x	x	x
0.460	0.918	9.21					
0.609	0.968	12.35					
0.698	0.983	14.34					
0.742	0.988	15.20					
0.810	0.994	16.64					
0.857	0.995	17.20					
0.945	0.999	19.36					
1.000	1.000	20.56					

**Point test results using the full set of data**

$\Delta P_{avg}$ (kPa)	0.14	0.13	0.14	0.15	0.23
$\Delta y_{lavg}$	0.0396	0.0521	0.0491	0.0406	0.0389

**Point test results with excluded data points**

$\Delta P_{avg}$ (kPa)	0.15	0.12	0.17	0.11	0.13
$\Delta y_{lavg}$	0.0073	0.0082	0.0083	0.0071	0.0070

\*data not included in final regressions

**Table 7-10 Average deviations for the point test: 1-propanol (1) + n-butanoic acid (2)–  
353.15K**

**NB: an “x” in a particular column indicates that that point needs to be excluded from the analysis in  
order for the remaining data to pass the point test**

$x_1$	$y_1$	P / kPa	NRTL-HOC	NRTL-VPA	NRTL-NTH	WILS-HOC	UNIQ-HOC
0.000	0.000	3.54					
0.034	0.269	5.84		x	x	x	
0.152	0.604	10.65	x	x	x	x	
0.504	0.929	25.72			x		
0.558	0.947	28.71					
0.577	0.955	30.16	x				
0.687	0.976	34.72					
0.752	0.983	38.07					
0.830	0.992	42.44					
0.894	0.997	46.07					
0.950	0.999	48.67					
1.000	1.000	51.30					
<b>Point test results using the full set of data</b>							
$\Delta P_{avg}$ (kPa)			0.50	0.28	0.76	0.27	0.68
$\Delta y_{lavg}$			0.0110	0.0276	0.0889	0.0159	0.0093
<b>Point test results with excluded data points</b>							
$\Delta P_{avg}$ (kPa)			0.58	0.28	0.28	0.46	0.68
$\Delta y_{lavg}$			0.0096	0.0044	0.0042	0.0032	0.0093

## 7.5. Final data reduction analyses

The parameters obtained from the VLE data reduction for each model are presented here, along with the average deviations between the experimental pressures and vapour compositions and those calculated from the model. In addition, for each model the fit to the experimental data is displayed graphically. Points that were excluded from the regressions were pointed out in Section 7.4 and are indicated by hollow points in the graphs that follow – i.e. if there are no hollow points in a particular graph, this indicates that no data points were excluded from that data set in the final regressions. The best fit model combination was decided by choosing the model that provided the minimum for the  $\Delta P_{\text{avg}}$ .

### 7.5.1 Final regression results: 2-propanone (1) + 2-butanol (2)

The model parameters obtained for this system are given in Table 7-12. A summary of the best-fit models is given in Table 7-11. In general, all models fit the data quite well. For the 333.15 data set, the liquid phase activity coefficient model did not seem to have any effect on the fit to the data with models which used the HOC EOS for the vapour phase gave slightly better results than the others. For both the 353.15K and 373.15K data sets, the NRTL-VPA appears to provide the best fit to the data – but it is only marginally better than the other models except for the 353.15K data set where the NRTL-NTH faired poorly in estimating the vapour phase compositions.

**Table 7-11 Best fit models for the 2-propanone (1) + 2-butanol (2) system**

<b>T (K)</b>	<b>Best fit model</b>
	NRTL-HOC/WILSON-HOC/UNIQUAC-
333.15	HOC
353.15	NRTL-VPA
373.15	NRTL-VPA

**Table 7-12 Model Parameters for the 2-propanone (1) + 2-butanol (2) system**

Parameter	Component i	Component j	T=333.15K	T=353.15K	T=373.15K
			Value (SI units)		
<b>NRTL-HOC</b>					
a <sub>ij</sub>	ACETONE	2-BUOH	0.11	-3.70	-0.23
a <sub>ij</sub>	2-BUOH	ACETONE	0.31	0.36	0.09
b <sub>ij</sub>	ACETONE	2-BUOH	-44.11	1310.44	78.77
b <sub>ij</sub>	2-BUOH	ACETONE	85.78	-0.39	47.48
η <sub>ij</sub>	ACETONE	2-BUOH	0.90	0.77	1.53
average  ΔP  (kPa)			0.33	0.94	2.94
average  Δy <sub>1</sub>			0.005	0.006	0.005
Parameter	Component i	Component j	T=333.15K	T=353.15K	T=373.15K
			Value (SI units)		
<b>NRTL-VPA</b>					
A <sub>i</sub>	ACETONE		-0.01	0.11	-0.01
B <sub>i</sub>	ACETONE		-5405.72	-5009.60	-4832.52
A <sub>i</sub>	2-BUOH		-0.23	-4.28	-0.04
B <sub>i</sub>	2-BUOH		-3898.14	-3696.31	-5935.54
a <sub>ij</sub>	ACETONE	2-BUOH	1.16	-3.66	0.25
a <sub>ij</sub>	2-BUOH	ACETONE	1.38	0.34	0.20
b <sub>ij</sub>	ACETONE	2-BUOH	-441.60	1310.46	61.72
b <sub>ij</sub>	2-BUOH	ACETONE	-233.74	3.52	-31.22
average  ΔP  (kPa)			0.37	0.92	1.89
average  Δy <sub>1</sub>			0.006	0.007	0.009
<b>NRTL-NTH</b>					
A <sub>i</sub>	ACETONE		0	0	0
B <sub>i</sub>	ACETONE		0	0	0
A <sub>i</sub>	2-BUOH		0	0	0
B <sub>i</sub>	2-BUOH		0	-0.01	0
a <sub>ij</sub>	ACETONE	2-BUOH	0.75	3.95	1.43
a <sub>ij</sub>	2-BUOH	ACETONE	0.24	1.12	0.42
b <sub>ij</sub>	ACETONE	2-BUOH	-273.24	-1594.55	-555.44
b <sub>ij</sub>	2-BUOH	ACETONE	121.34	38.70	-64.66
average  ΔP  (kPa)			0.35	1.09	3.08
average  Δy <sub>1</sub>			0.005	0.091	0.008

			T=333.15K	T=353.15K	T=373.15K
<b>WILSON-HOC</b>					
a <sub>ij</sub>	ACETONE	2-BUOH	2.52	7.59	0.14
a <sub>ij</sub>	2-BUOH	ACETONE	0.43	-0.62	0.03
b <sub>ij</sub>	ACETONE	2-BUOH	-991.38	-2783.32	-113.39
b <sub>ij</sub>	2-BUOH	ACETONE	-174.26	190.01	-26.34
η <sub>ij</sub>	ACETONE	2-BUOH	0.86	0.75	1.52
average  ΔP  (kPa)			0.33	0.94	2.95
average  Δy <sub>1</sub>			0.005	0.007	0.005
<b>UNIQUAC-HOC</b>					
η <sub>ij</sub>	ACETONE	2-BUOH	0.89	0.78	-1.61
a <sub>ij</sub>	ACETONE	2-BUOH	0.01	0.11	0.06
a <sub>ij</sub>	2-BUOH	ACETONE	0.07	7.26	4.51
b <sub>ij</sub>	ACETONE	2-BUOH	81.14	41.77	24.19
b <sub>ij</sub>	2-BUOH	ACETONE	-199.74	-2713.22	-1778.05
average  ΔP  (kPa)			0.33	0.94	2.66
average  Δy <sub>1</sub>			0.005	0.006	0.010

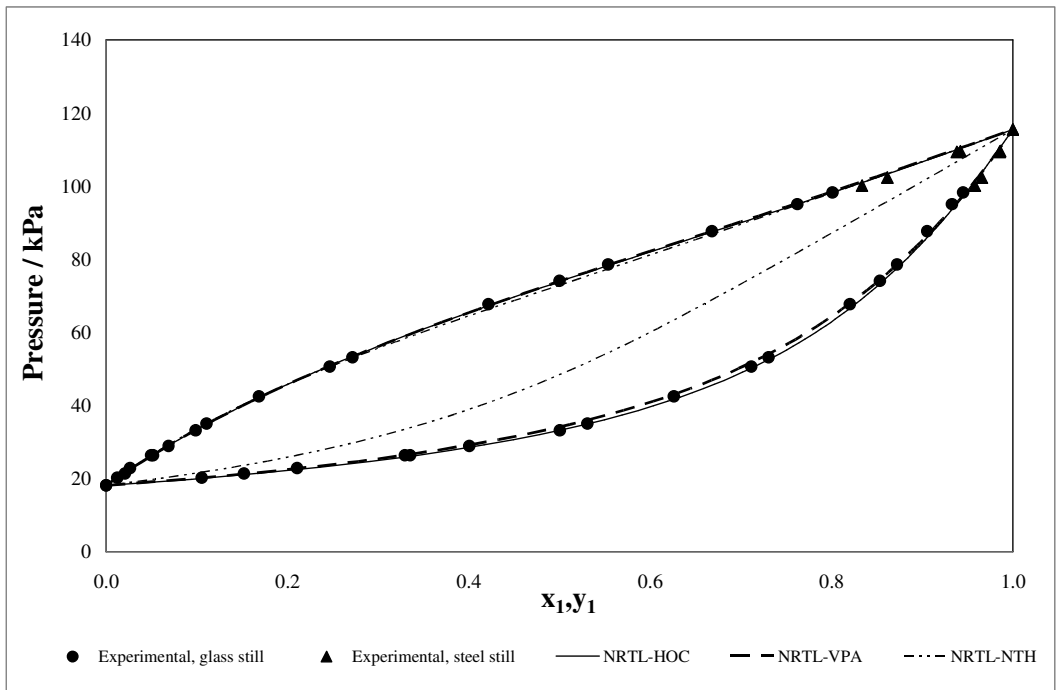


Figure 7-6 Comparison between HOC, VPA and NTH model fits to P- $x_1$ - $y_1$  data for the 2-propanone (1) + 2-butanol (2) system at 333.15K

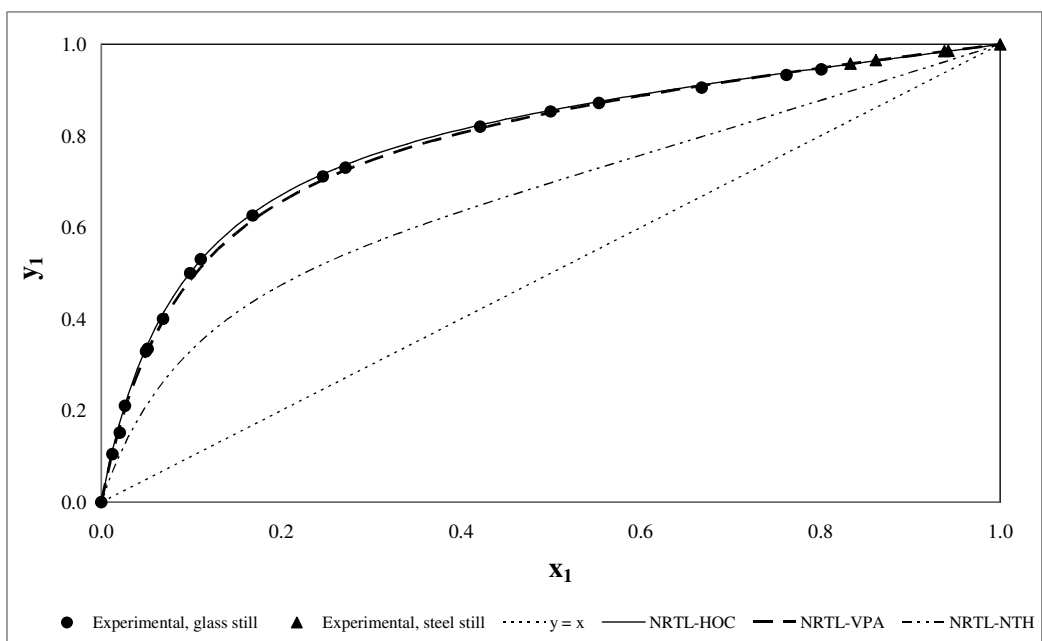
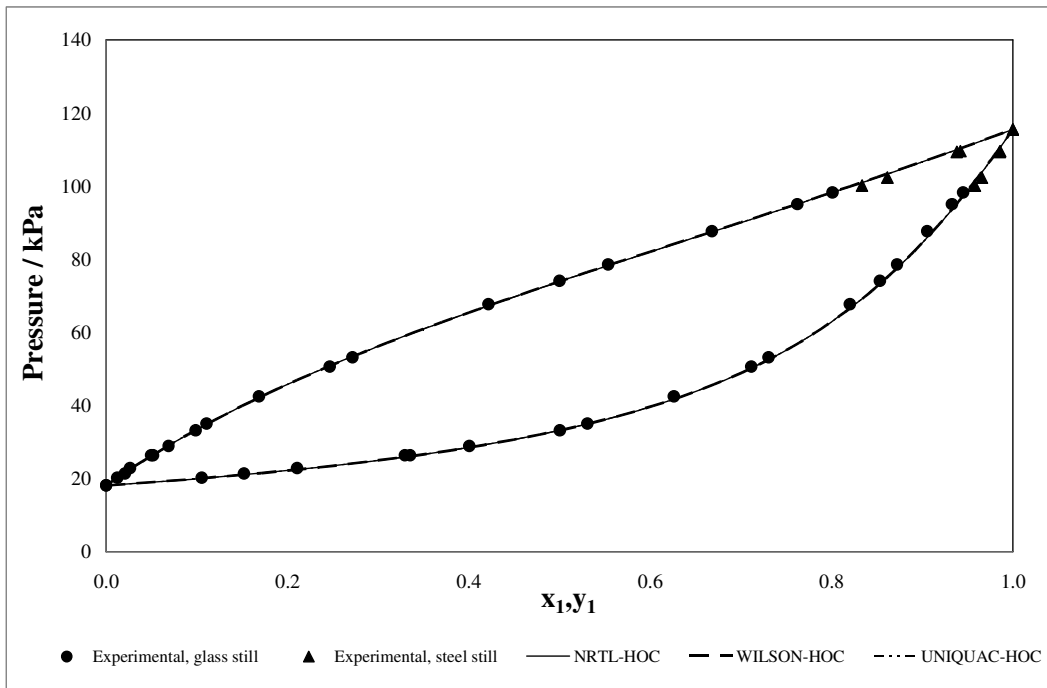
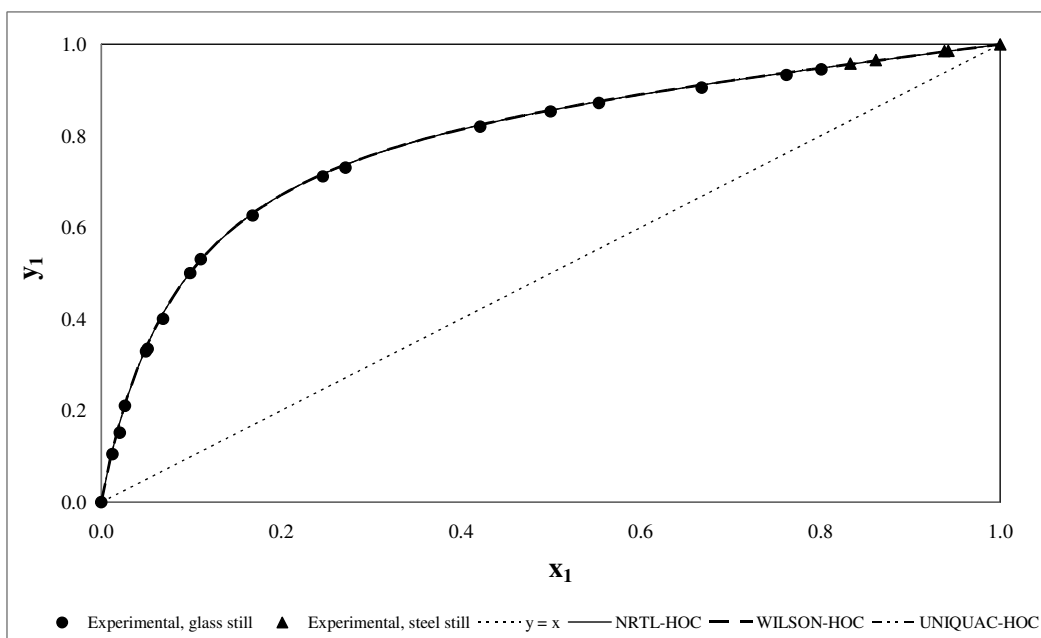


Figure 7-7 Comparison between HOC, VPA and NTH model fits to  $x_1$ - $y_1$  data for the 2-propanone (1) + 2-butanol (2) system at 333.15K



**Figure 7-8 Comparison between NRTL, WILSON and UNIQUAC model fits to P- $x_1$ - $y_1$  data for the 2-propanone (1) + 2-butanol (2) system at 333.15K**



**Figure 7-9 Comparison between NRTL, WILSON and UNIQUAC model fits to  $x_1$ - $y_1$  data for the 2-propanone (1) + 2-butanol (2) system at 333.15**

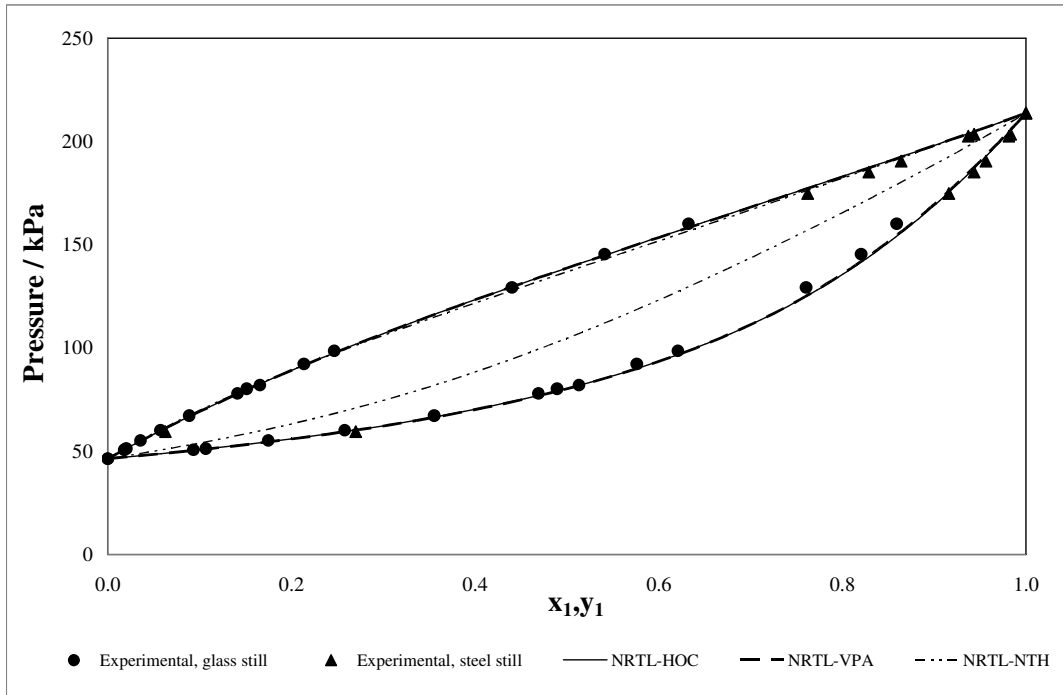


Figure 7-10 Comparison between HOC, VPA and NTH model fits to P- $x_1$ - $y_1$  data for the 2-propanone (1) + 2-butanol (2) system at 353.15K

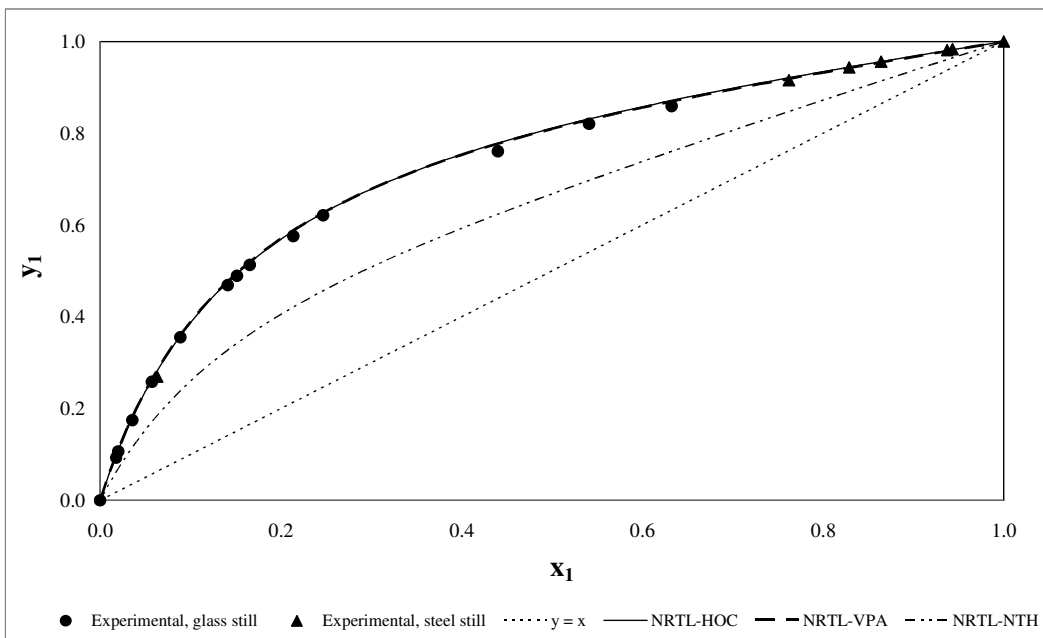
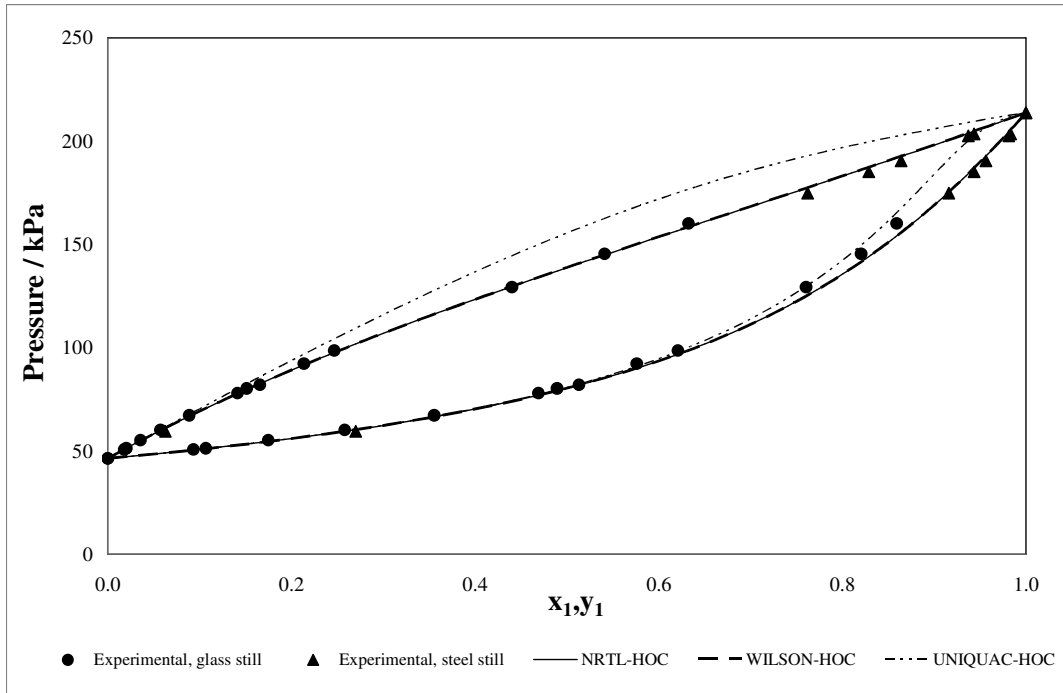
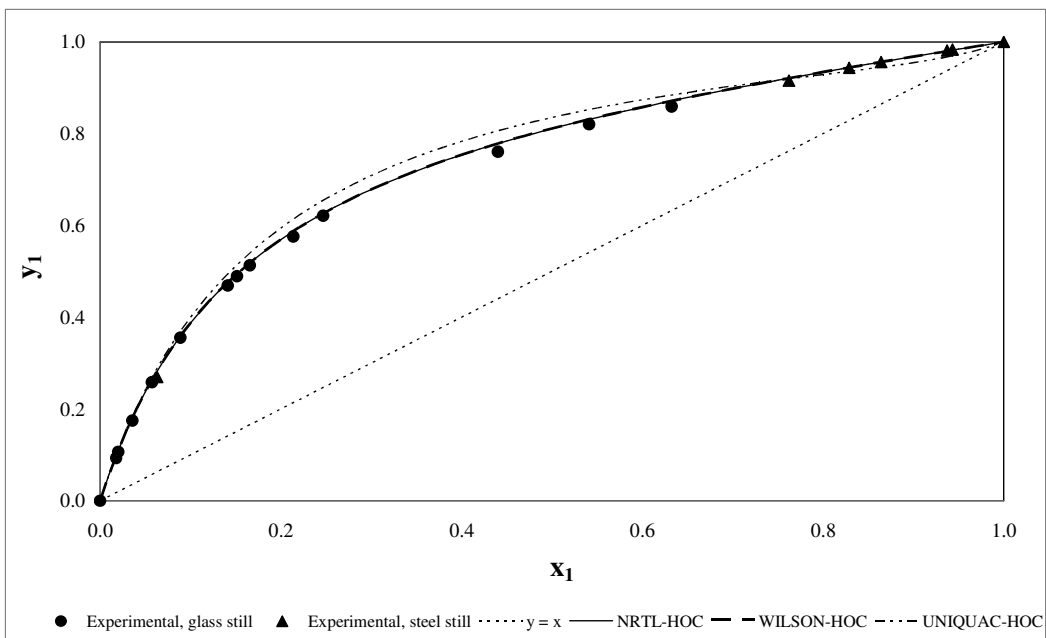


Figure 7-11 Comparison between HOC, VPA and NTH model fits to  $x_1$ - $y_1$  data for the 2-propanone (1) + 2-butanol (2) system at 353.15K



**Figure 7-12 Comparison between NRTL, WILSON and UNIQUAC model fits to experimental  $P$ - $x_1$ - $y_1$  data for the 2-propanone (1) + 2-butanol (2) system at 353.15K**



**Figure 7-13 Comparison between NRTL, WILSON and UNIQUAC model fits to experimental  $x_1$ - $y_1$  data for the 2-propanone (1) + 2-butanol (2) system at 353.15K**

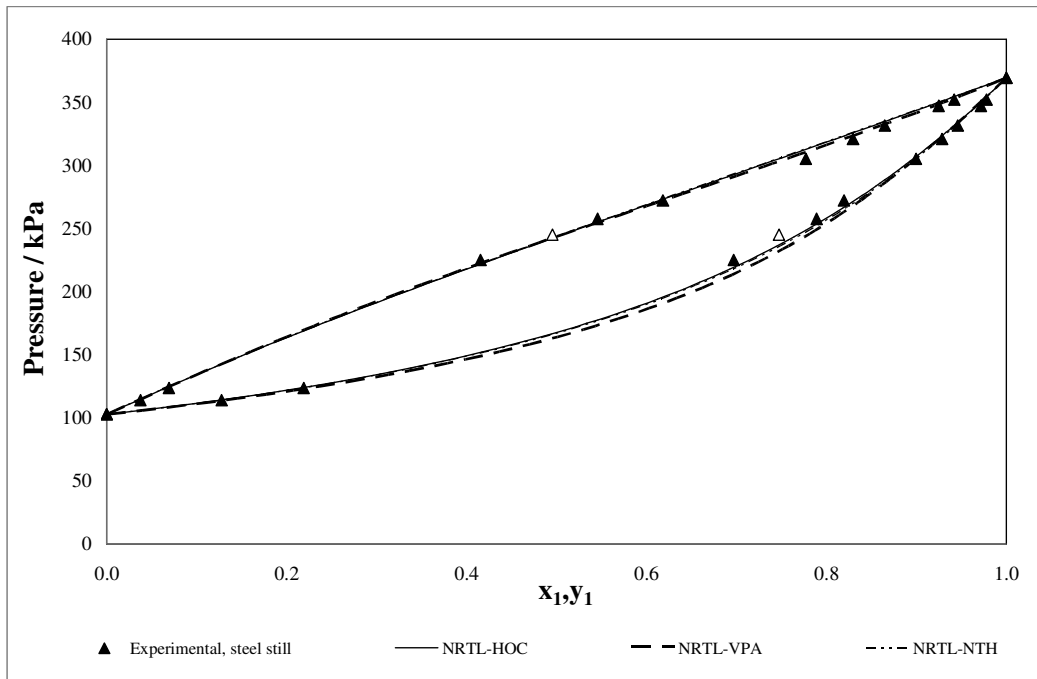


**Figure 7-14 Comparison between HOC, VPA and NTH model fits to  $P$ - $x_1$ - $y_1$  data for the 2-propanone (1) + 2-butanol (2) system at 373.15K**

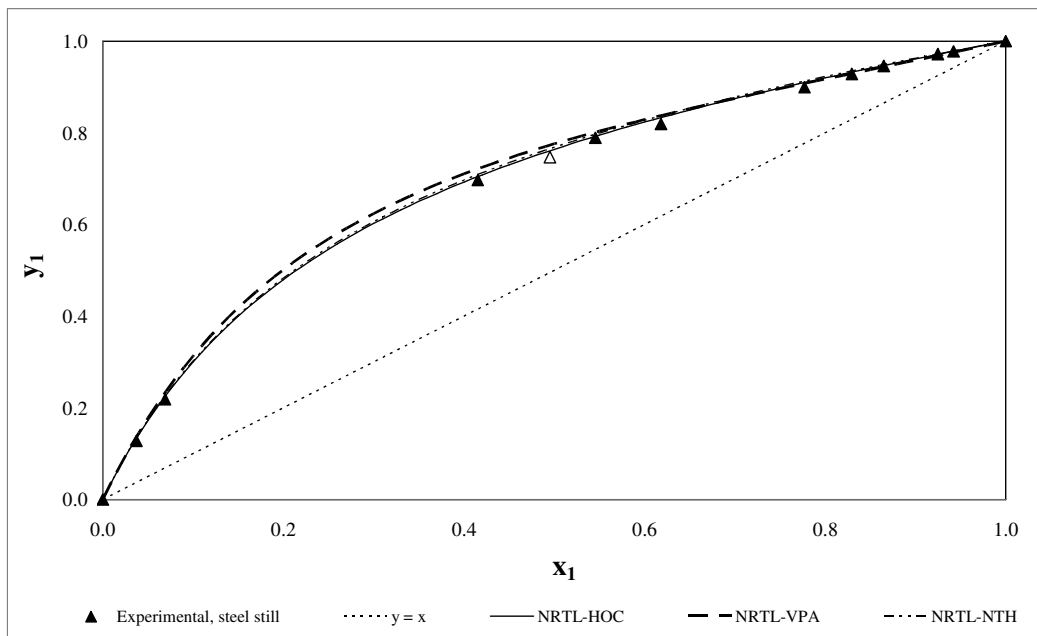


**Figure 7-15 Comparison between HOC, VPA and NTH model fits to  $x_1$ - $y_1$  data for the 2-propanone (1) + 2-butanol (2) system at 373.15K**

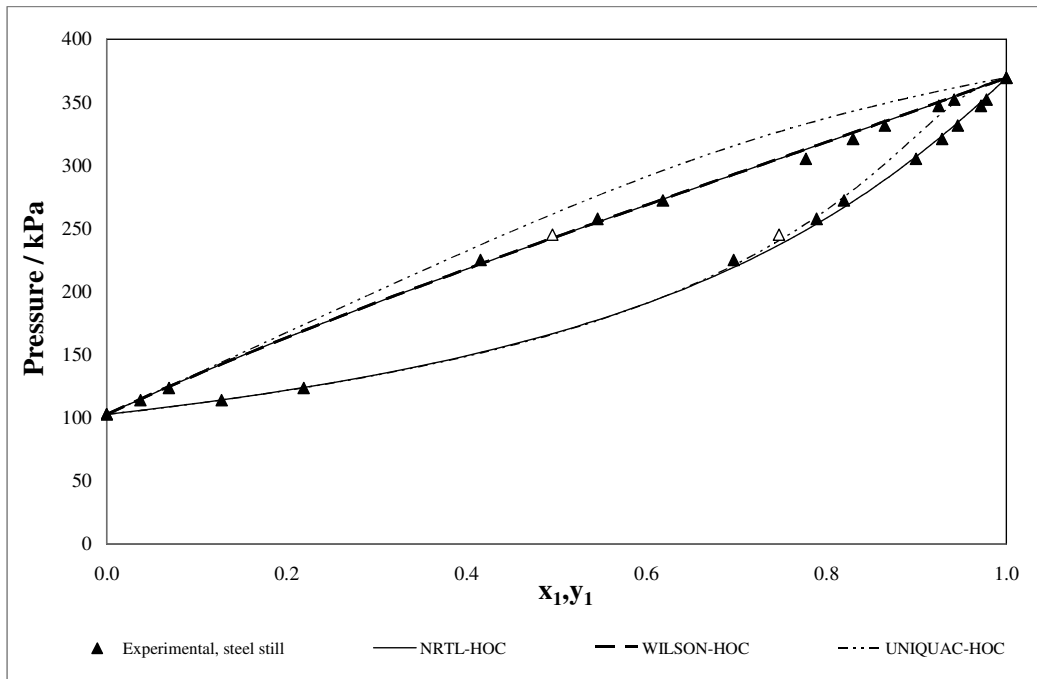


**Figure 7-16 Comparison between NRTL, WILSON and UNIQUAC model fits to experimental  $P$ - $x_1$ - $y_1$  data for the 2-propanone (1) + 2-butanol (2) system at 373.15K**

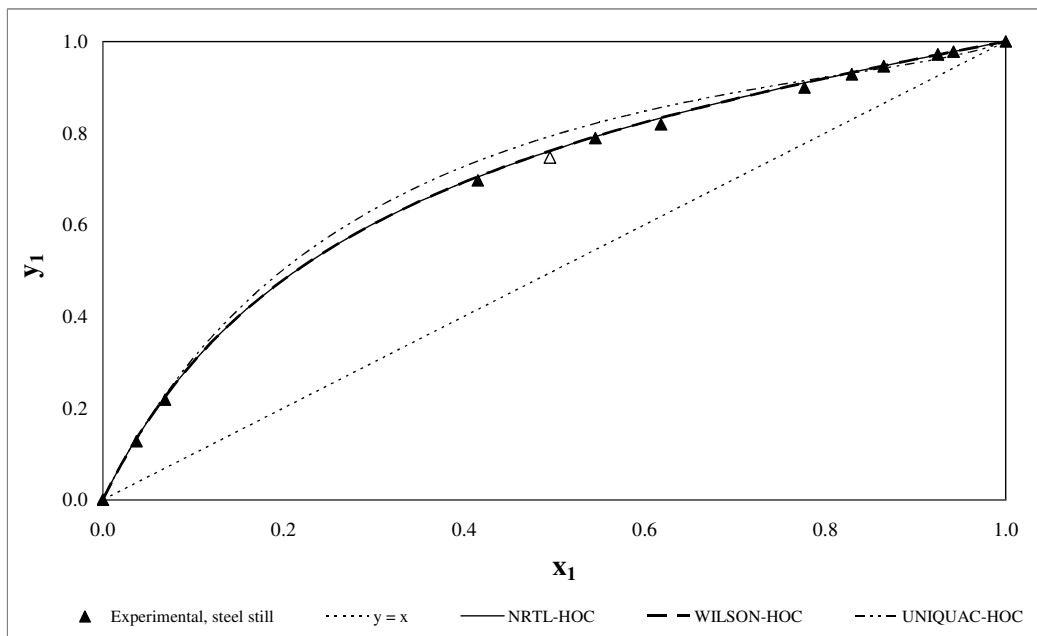


**Figure 7-17 Comparison between NRTL, WILSON and UNIQUAC model fits to experimental  $x_1$ - $y_1$  data for the 2-propanone (1) + 2-butanol (2) system at 373.15K**

### 7.5.2 Final regression results: 2-propanone (1) + n-propanoic acid (2)

The model parameters obtained for this system are given in Table 7-14. A summary of the best-fit models is given in Table 7-13. The NRTL-NTH model performed very poorly in fitting the vapour phase compositions for the 333.15K isotherm but was the best fit for the 353.15K and 373.15K data sets.

**Table 7-13 Best fit models for the 2-propanone (1) + n-propanoic acid (2) system**

T (K)	Best fit model
333.15	WILSON-HOC
353.15	NRTL-NTH
373.15	NRTL-NTH

**Table 7-14 Model Parameters for the 2-propanone (1) + n-propanoic acid (2) system**

Parameter	Component i	Component j	T=333.15K	T=353.15K	T=373.15K
			Value (SI units)		
<b>NRTL-HOC</b>					
a <sub>ij</sub>	ACETONE	C3OOH	-0.45	-0.88	-0.33
a <sub>ij</sub>	C3OOH	ACETONE	8.52	0.45	0.02
b <sub>ij</sub>	ACETONE	C3OOH	-145.60	358.35	1020.27
b <sub>ij</sub>	C3OOH	ACETONE	-2410.22	-209.83	-520.90
η <sub>ij</sub>	ACETONE	C3OOH	3.31	3.86	4.50
average  ΔP  (kPa)			0.37	2.32	6.99
average  Δy <sub>1</sub>			0.013	0.006	0.007
<b>NRTL-VPA</b>					
A <sub>i</sub>	ACETONE		0.00	0.00	0.00
B <sub>i</sub>	ACETONE		-5921.24	-5943.32	-5914.71
A <sub>i</sub>	C3OOH		0.00	-0.01	0.00
B <sub>i</sub>	C3OOH		-2509.70	-2962.58	10000.00
a <sub>ij</sub>	ACETONE	C3OOH	-0.55	-9.66	-1.21
a <sub>ij</sub>	C3OOH	ACETONE	14.19	1.34	0.15
b <sub>ij</sub>	ACETONE	C3OOH	-179.80	2950.70	689.86
b <sub>ij</sub>	C3OOH	ACETONE	-4200.97	233.06	-320.77
average  ΔP  (kPa)			0.36	2.41	5.23
average  Δy <sub>1</sub>			0.010	0.010	0.020

Parameter	Component i	Component j	T=333.15K	T=353.15K	T=373.15K
			Value (SI units)		
<b>NRTL-NTH</b>					
A <sub>i</sub>	ACETONE		0.00	0.00	0.00
B <sub>i</sub>	ACETONE		0.00	0.00	0.00
A <sub>i</sub>	C3OOH		0.00	0.00	0.00
B <sub>i</sub>	C3OOH		0.00	0.00	0.00
a <sub>ij</sub>	ACETONE	C3OOH	1.13	-11.66	-1.34
a <sub>ij</sub>	C3OOH	ACETONE	623.21	0.87	0.30
b <sub>ij</sub>	ACETONE	C3OOH	-461.90	3723.59	639.56
b <sub>ij</sub>	C3OOH	ACETONE	-207212.36	290.35	-261.73
average  ΔP  (kPa)			1.74	2.05	4.44
average  Δy <sub>1</sub>			0.097	0.012	0.019
<b>WILSON-HOC</b>					
a <sub>ij</sub>	ACETONE	C3OOH	-0.54	-0.19	-0.05
a <sub>ij</sub>	C3OOH	ACETONE	2.74	0.29	0.16
b <sub>ij</sub>	ACETONE	C3OOH	-176.29	117.61	387.65
b <sub>ij</sub>	C3OOH	ACETONE	-694.74	-154.67	-797.04
η <sub>ij</sub>	ACETONE	C3OOH	3.30	3.88	4.50
average  ΔP  (kPa)			0.33	2.32	5.29
average  Δy <sub>1</sub>			0.013	0.006	0.006
<b>UNIQUAC-HOC</b>					
η <sub>ij</sub>	ACETONE	C3OOH	3.31	3.88	4.50
a <sub>ij</sub>	ACETONE	C3OOH	2.25	0.22	0.00
a <sub>ij</sub>	C3OOH	ACETONE	-0.39	-0.17	-0.01
b <sub>ij</sub>	ACETONE	C3OOH	-566.54	-102.69	-551.82
b <sub>ij</sub>	C3OOH	ACETONE	-130.52	83.17	316.20
average  ΔP  (kPa)			0.36	2.32	6.56
average  Δy <sub>1</sub>			0.013	0.006	0.007

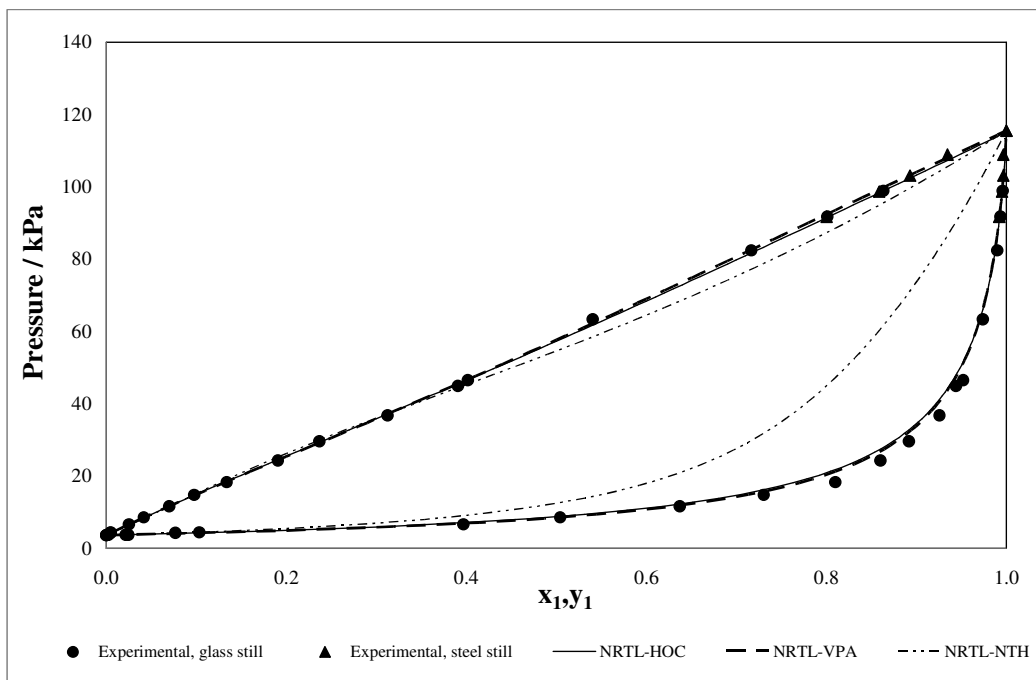


Figure 7-18 Comparison between HOC, VPA and NTH model fits to  $P$ - $x_1$ - $y_1$  data for the 2-propanone (1) + n-propanoic acid (2) system at 333.15K

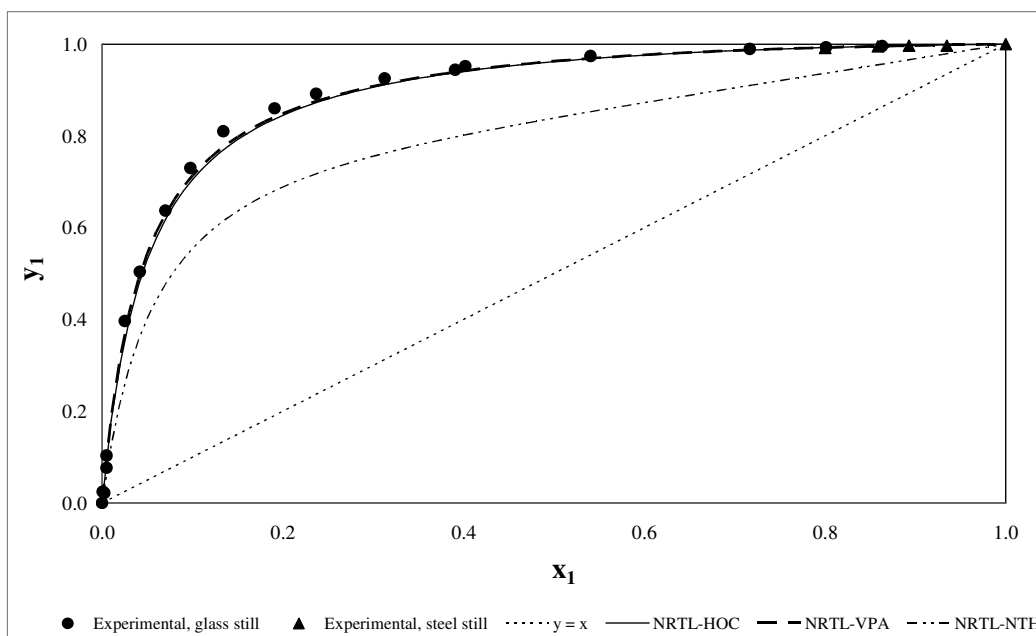
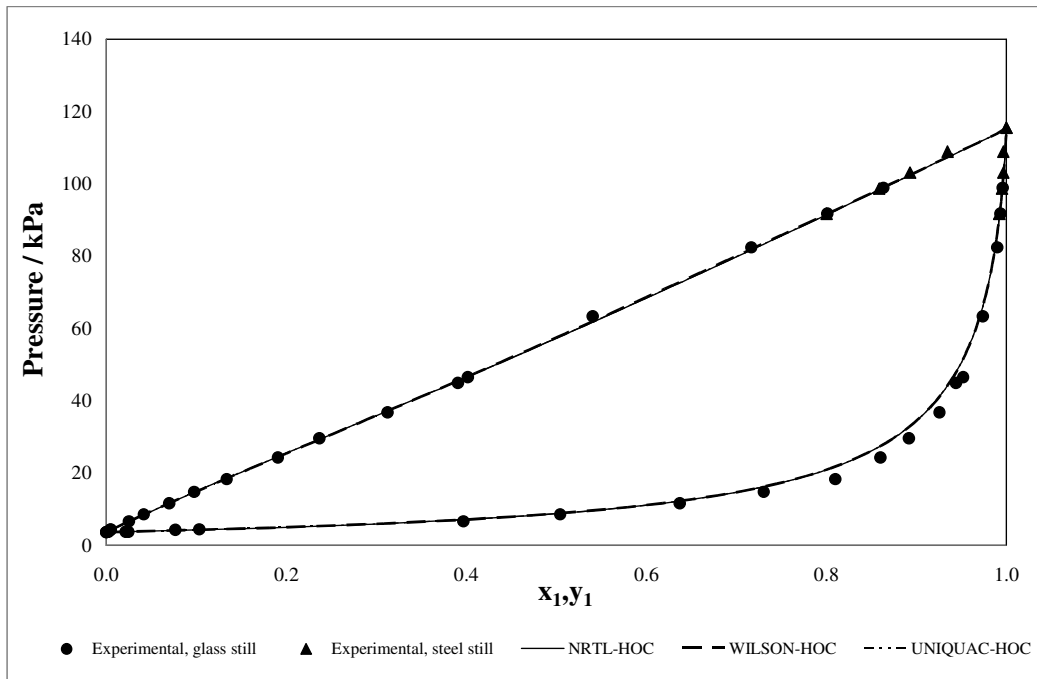
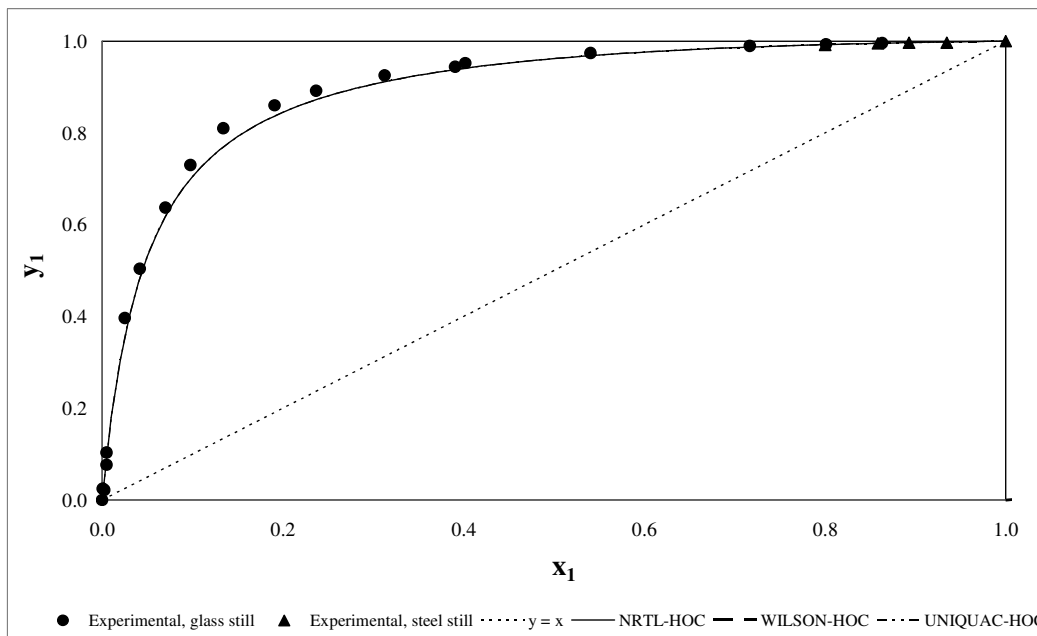


Figure 7-19 Comparison between HOC, VPA and NTH model fits to  $x_1$ - $y_1$  data for the 2-propanone (1) + n-propanoic acid (2) system at 333.15K



**Figure 7-20 Comparison between NRTL, WILSON and UNIQUAC model fits to experimental  $P$ - $x_1$ - $y_1$  data for the 2-propanone (1) + n-propanoic acid (2) system at 333.15K**



**Figure 7-21 Comparison between NRTL, WILSON and UNIQUAC model fits to experimental  $x_1$ - $y_1$  data for the 2-propanone (1) + n-propanoic acid (2) system at 333.15K**

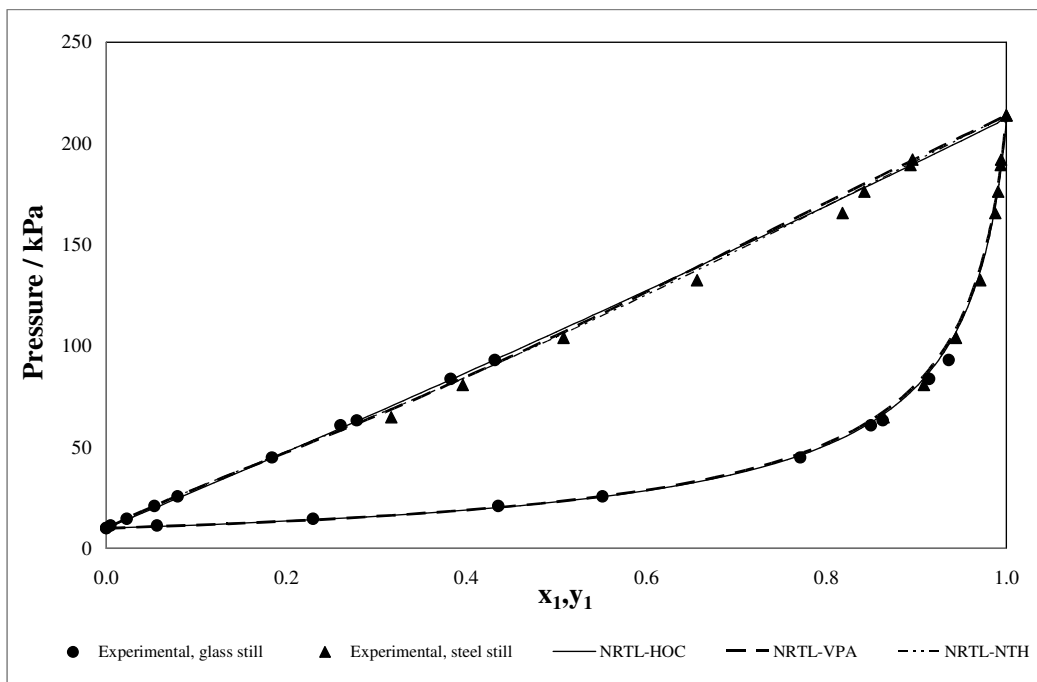


Figure 7-22 Comparison between HOC, VPA and NTH model fits to  $P$ - $x_1$ - $y_1$  data for the 2-propanone (1) + n-propanoic acid (2) system at 353.15K

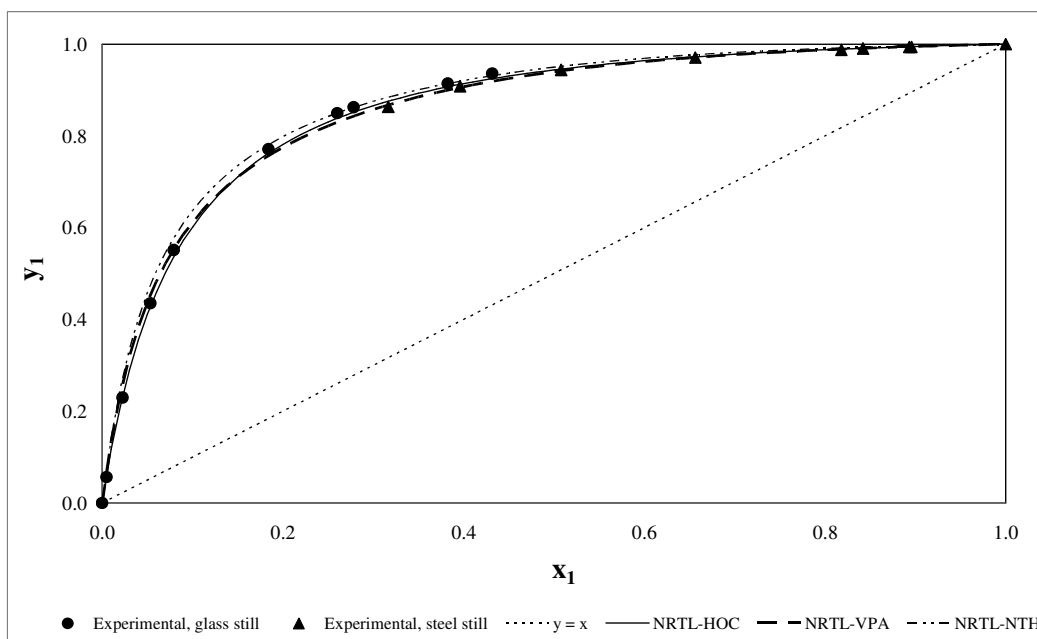
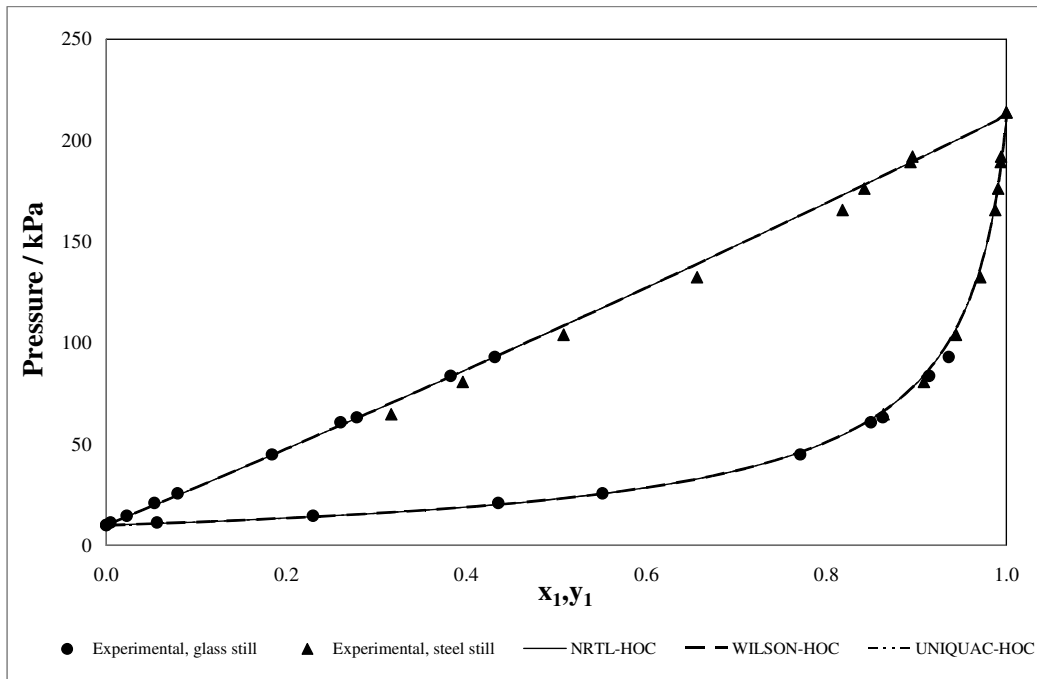
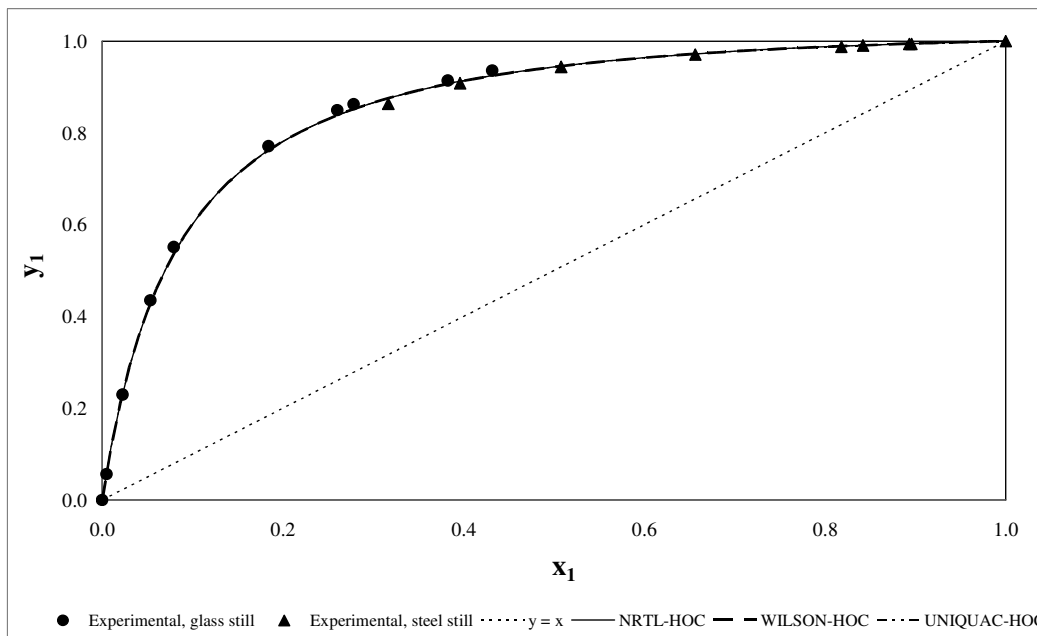


Figure 7-23 Comparison between HOC, VPA and NTH model fits to  $x_1$ - $y_1$  data for the 2-propanone (1) + n-propanoic acid (2) system at 353.15K



**Figure 7-24 Comparison between NRTL, WILSON and UNIQUAC model fits to experimental  $P$ - $x_1$ - $y_1$  data for the 2-propanone (1) + n-propanoic acid (2) system at 353.15K**



**Figure 7-25 Comparison between NRTL, WILSON and UNIQUAC model fits to experimental  $x_1$ - $y_1$  data for the 2-propanone (1) + n-propanoic acid (2) system at 353.15K**

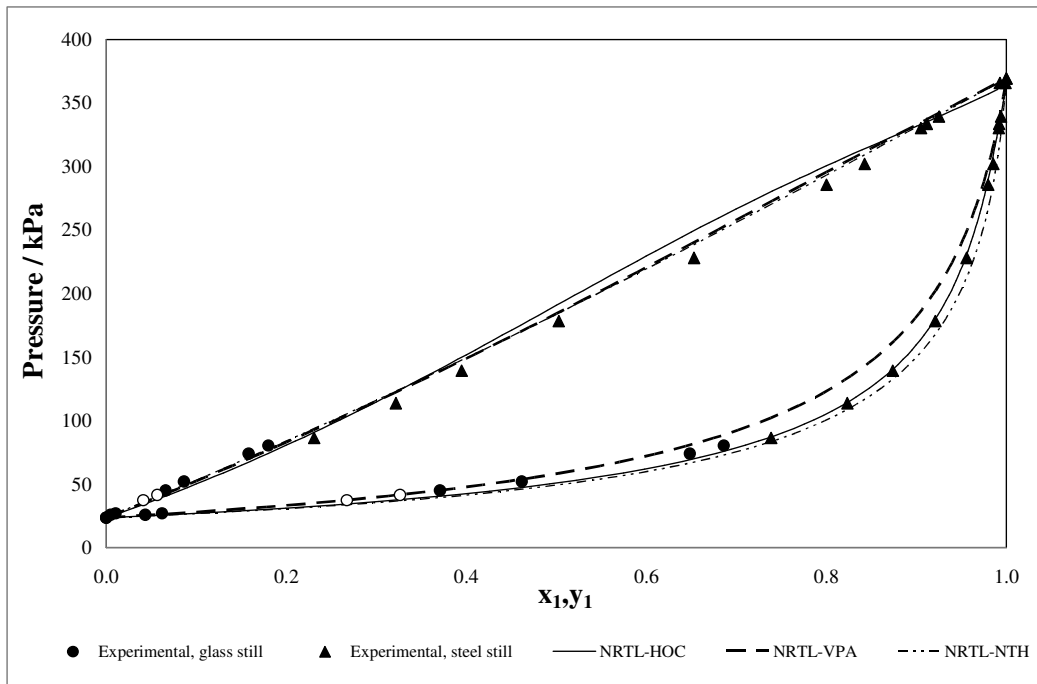


Figure 7-26 Comparison between HOC, VPA and NTH model fits to  $P$ - $x_1$ - $y_1$  data for the 2-propanone (1) + n-propanoic acid (2) system at 373.15K

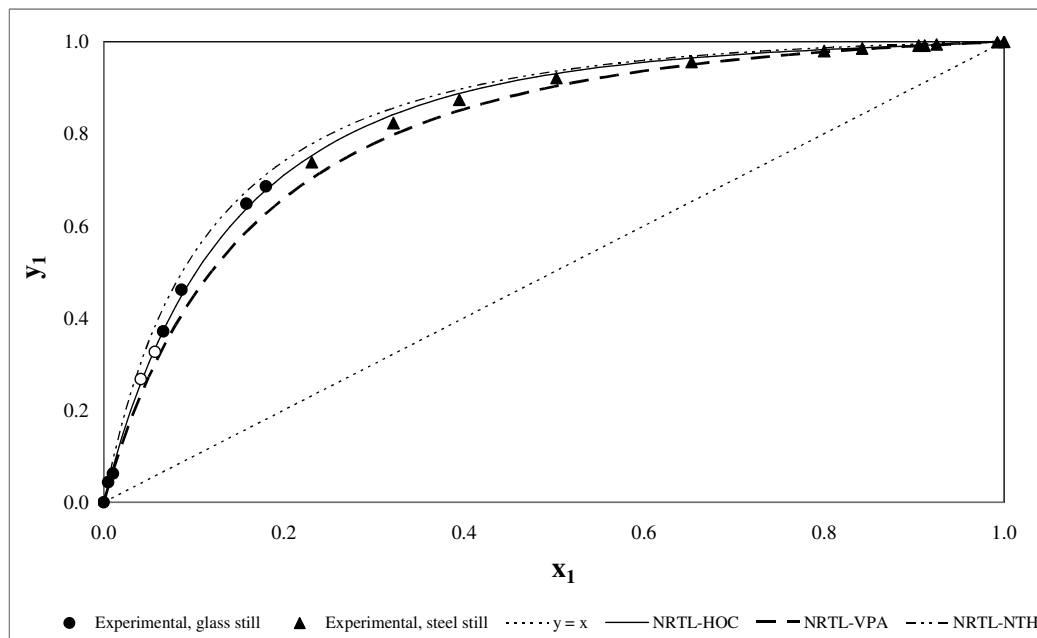


Figure 7-27 Comparison between HOC, VPA and NTH model fits to  $x_1$ - $y_1$  data for the 2-propanone (1) + n-propanoic acid (2) system at 373.15K

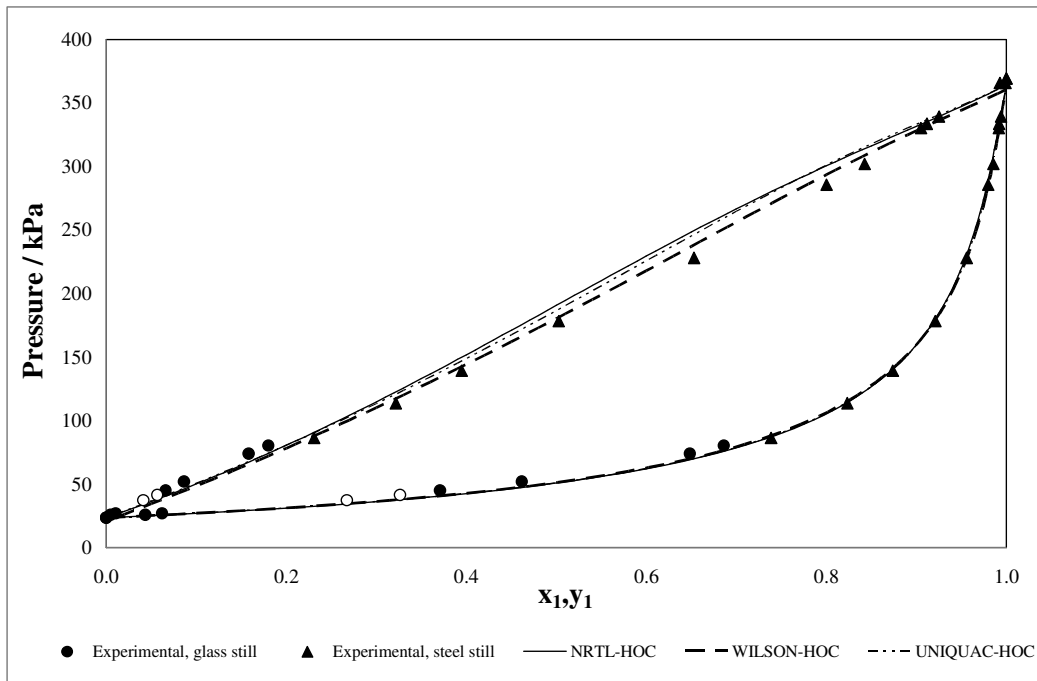


Figure 7-28 Comparison between NRTL, WILSON and UNIQUAC model fits to experimental  $P$ - $x_1$ - $y_1$  data for the 2-propanone (1) + n-propanoic acid (2) system at 373.15K

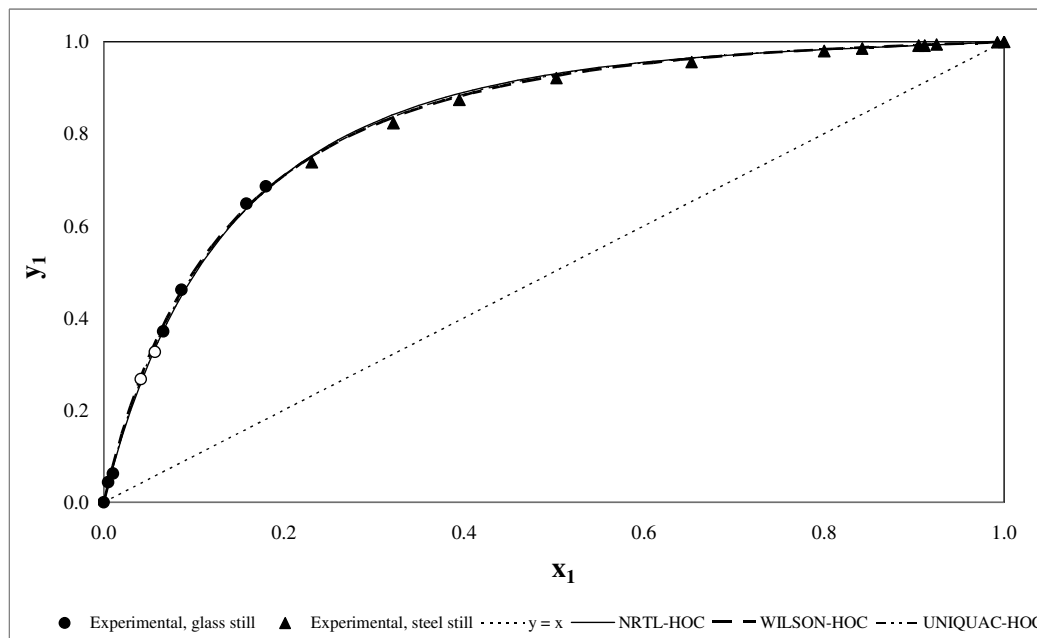


Figure 7-29 Comparison between NRTL, WILSON and UNIQUAC model fits to experimental  $x_1$ - $y_1$  data for the 2-propanone (1) + n-propanoic acid (2) system at 373.15K

### 7.5.3 Final regression results: 1-propanol (1) + n-butanoic acid (2)

The model parameters obtained for this system are given in Table 7-16 and a summary of the best-fit models for each isotherm is provided in Table 7-15. The WILSON-HOC model provided the best fit for both data sets of this system. In order to satisfy the consistency test criterion four data points from the n-butanoic acid-rich region had to be excluded from the final regression analyses and hence the model accuracy is highly skewed towards the 1-propanol-rich region for the 333.15K data set. The “bump” in the model predictions in the n-butanoic acid-rich region should therefore not be considered a true description of the system as there is a lack of experimental evidence in this region to confirm this; more data point are required in the sparse region. The results do however show that the WILSON-HOC model combination not only fits the experimental data better than the NRTL and UNIQUAC model combinations, but it is also better suited to data extrapolation. Without accurate experimental data in the sparse regions, the NRTL and UNIQUAC models fail in this instance to adequately describe this alcohol + carboxylic acid system.

**Table 7-15 Best fit models for the 1-propanol (1) + n-butanoic acid (2) system**

<b>T (K)</b>	<b>Best fit model</b>
333.15	WILSON-HOC
353.15	WILSON-HOC

**Table 7-16 Model parameters for the 1-propanol (1) + n-butanoic acid (2) system**

Parameter	Component i	Component j	<b>T=333.15K</b>	<b>T=353.15K</b>
			Value (SI units)	
<b>NRTL-HOC</b>				
$a_{ij}$	1PROH	1-C4OOH	-0.24	-0.18
$a_{ij}$	1-C4OOH	1PROH	-14.19	-12.36
$b_{ij}$	1PROH	1-C4OOH	-335.52	-451.78
$b_{ij}$	1-C4OOH	1PROH	6102.15	5323.75
$\eta_{ij}$	1PROH	1-C4OOH	-11.68	-7.13
average $ \Delta P $ (kPa)			0.31	0.56
average $ \Delta y_i $			0.003	0.013

			<b>T=333.15K</b>	<b>T=353.15K</b>
<b>NRTL-VPA</b>				
A <sub>i</sub>	1PROH		0.00	0.00
B <sub>i</sub>	1PROH		-9481.14	-10000.00
A <sub>i</sub>	1-C4OOH		0.00	0.00
B <sub>i</sub>	1-C4OOH		-1076.92	-10000.00
a <sub>ij</sub>	1PROH	1-C4OOH	-0.16	1.64
a <sub>ij</sub>	1-C4OOH	1PROH	-14.12	7.81
b <sub>ij</sub>	1PROH	1-C4OOH	-309.10	-1150.45
b <sub>ij</sub>	1-C4OOH	1PROH	6125.54	-1661.11
average  ΔP  (kPa)			0.23	0.67
average  Δy <sub>1</sub>			0.002	0.024
Parameter	Component i	Component j	Value (SI units)	
<b>NRTL-NTH</b>				
A <sub>i</sub>	1PROH		0	0
B <sub>i</sub>	1PROH		0	0
A <sub>i</sub>	1-C4OOH		0	0
B <sub>i</sub>	1-C4OOH		0	0
a <sub>ij</sub>	1PROH	1-C4OOH	-1.20	-0.86
a <sub>ij</sub>	1-C4OOH	1PROH	-155.31	54.67
b <sub>ij</sub>	1PROH	1-C4OOH	-60.79	-244.12
b <sub>ij</sub>	1-C4OOH	1PROH	53074.16	-18272.16
average  ΔP  (kPa)			0.38	0.68
average  Δy <sub>1</sub>			0.004	0.017
<b>WILSON-HOC</b>				
a <sub>ij</sub>	1PROH	1-C4OOH	-209.56	20.27
a <sub>ij</sub>	1-C4OOH	1PROH	55.07	-6.36
b <sub>ij</sub>	1PROH	1-C4OOH	-100916.30	-8109.77
b <sub>ij</sub>	1-C4OOH	1PROH	-18039.97	2624.41
η <sub>ij</sub>	1PROH	1-C4OOH	-7.13	-7.13
average  ΔP  (kPa)			0.13	0.29
average  Δy <sub>1</sub>			0.006	0.011
<b>UNIQUAC-HOC</b>				
η <sub>ij</sub>	1PROH	1-C4OOH	-3.70	-7.13
a <sub>ij</sub>	1PROH	1-C4OOH	-12.59	-22.42
a <sub>ij</sub>	1-C4OOH	1PROH	-1.54	-0.98
b <sub>ij</sub>	1PROH	1-C4OOH	4531.52	8260.55
b <sub>ij</sub>	1-C4OOH	1PROH	-503.85	-328.42
average  ΔP  (kPa)			0.35	0.81
average  Δy <sub>1</sub>			0.00	0.01

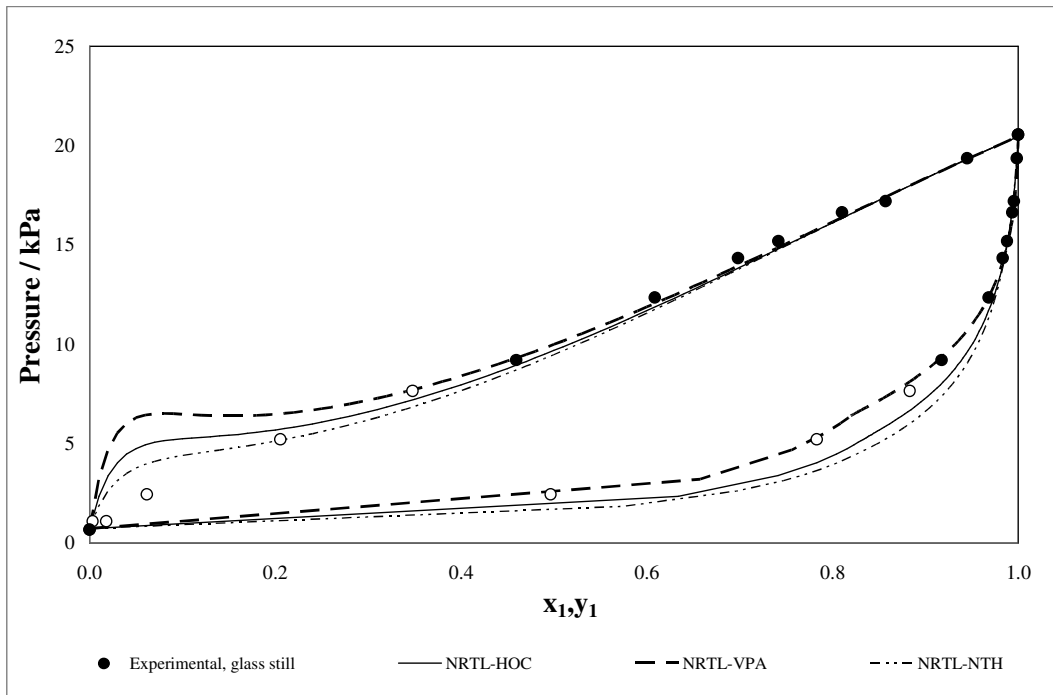


Figure 7-30 Comparison between HOC, VPA and NTH model fits to  $P$ - $x_1$ - $y_1$  data for the 1-propanol (1) + n-butanoic acid (2) system at 333.15K

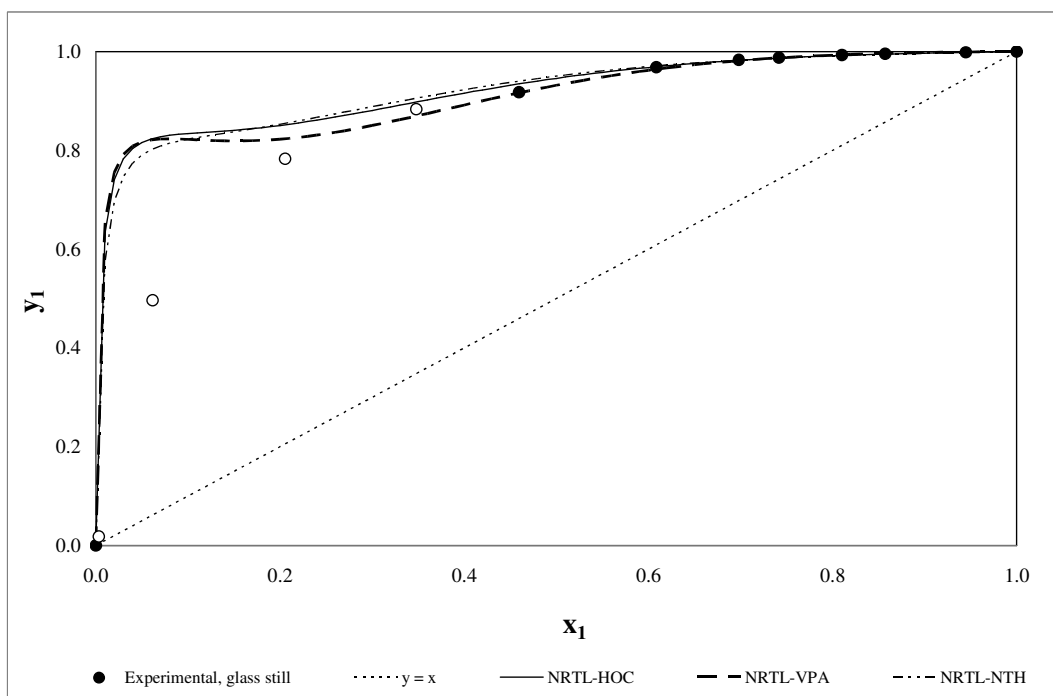
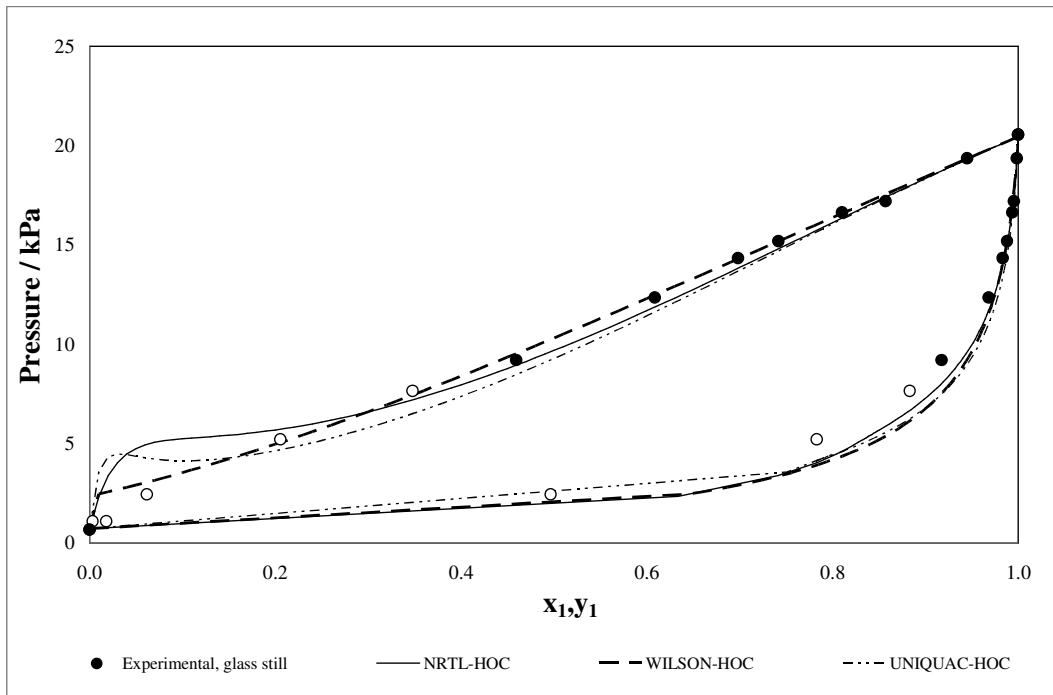
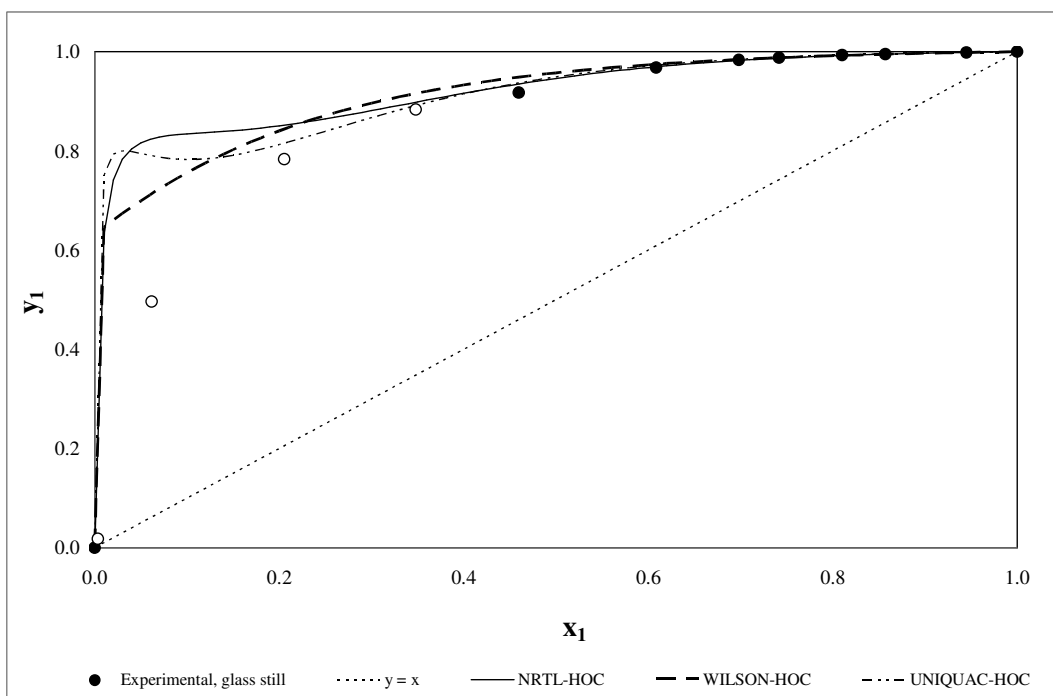


Figure 7-31 Comparison between HOC, VPA and NTH model fits to  $x_1$ - $y_1$  data for the 1-propanol (1) + n-butanoic acid (2) system at 333.15K



**Figure 7-32 Comparison between NRTL, WILSON and UNIQUAC model fits to experimental  $P$ - $x_1$ - $y_1$  data for the 1-propanol (1) + n-butanoic acid (2) system at 333.15K**



**Figure 7-33 Comparison between NRTL, WILSON and UNIQUAC model fits to experimental  $x_1$ - $y_1$  data for the 1-propanol (1) + n-butanoic acid (2) system at 333.15K**

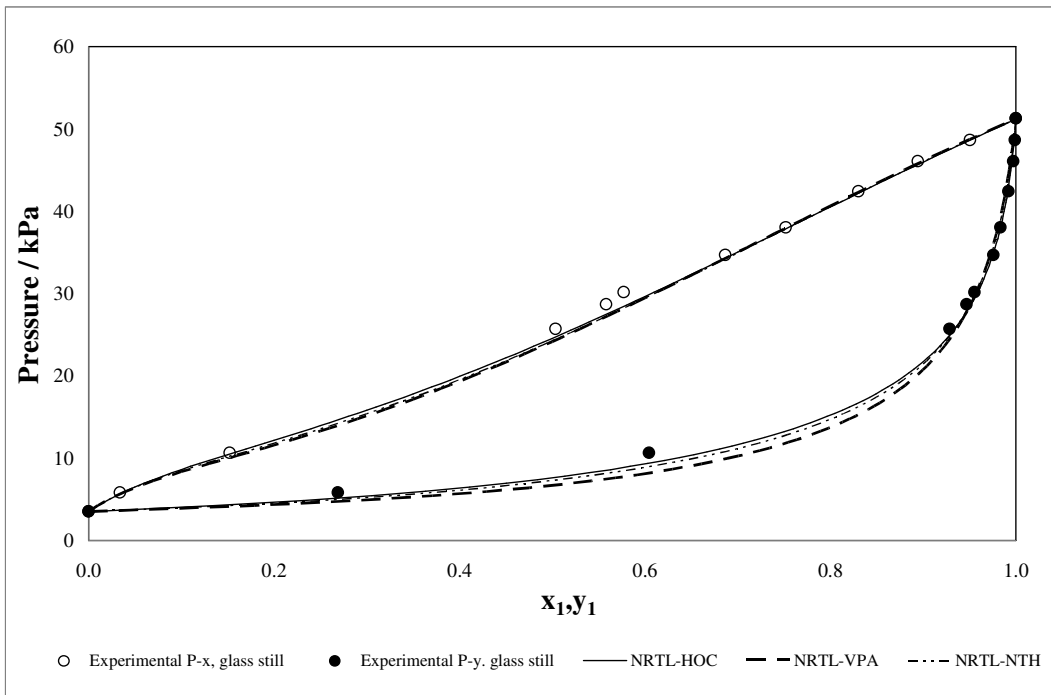


Figure 7-34 Comparison between HOC, VPA and NTH model fits to  $P$ - $x_1$ - $y_1$  data for the 1-propanol (1) + n-butanoic acid (2) system at 353.15K

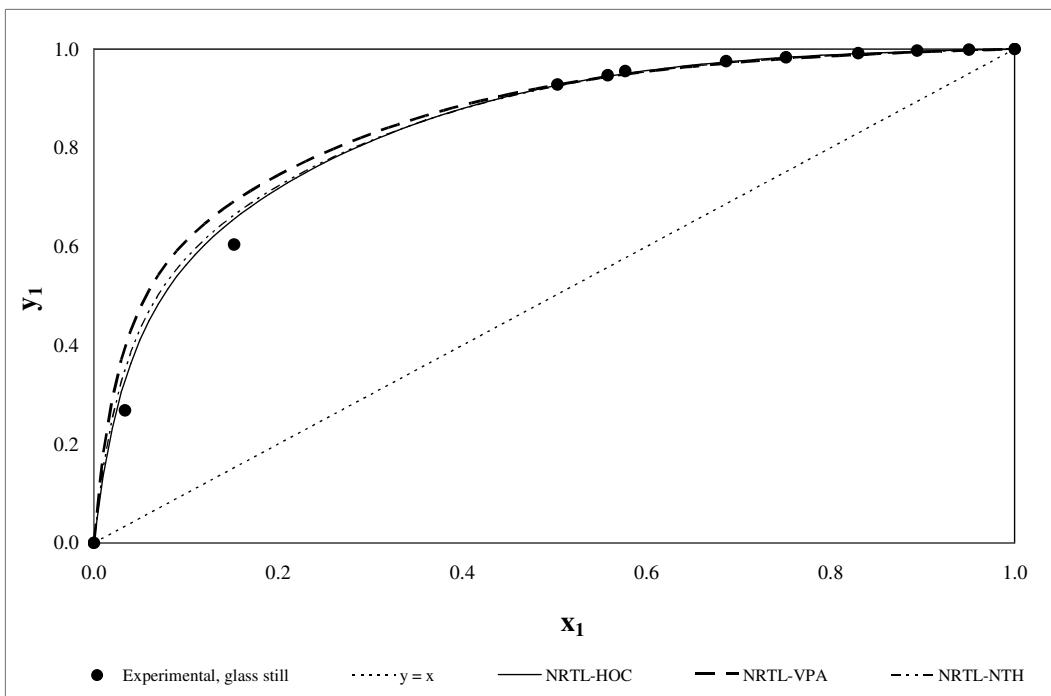
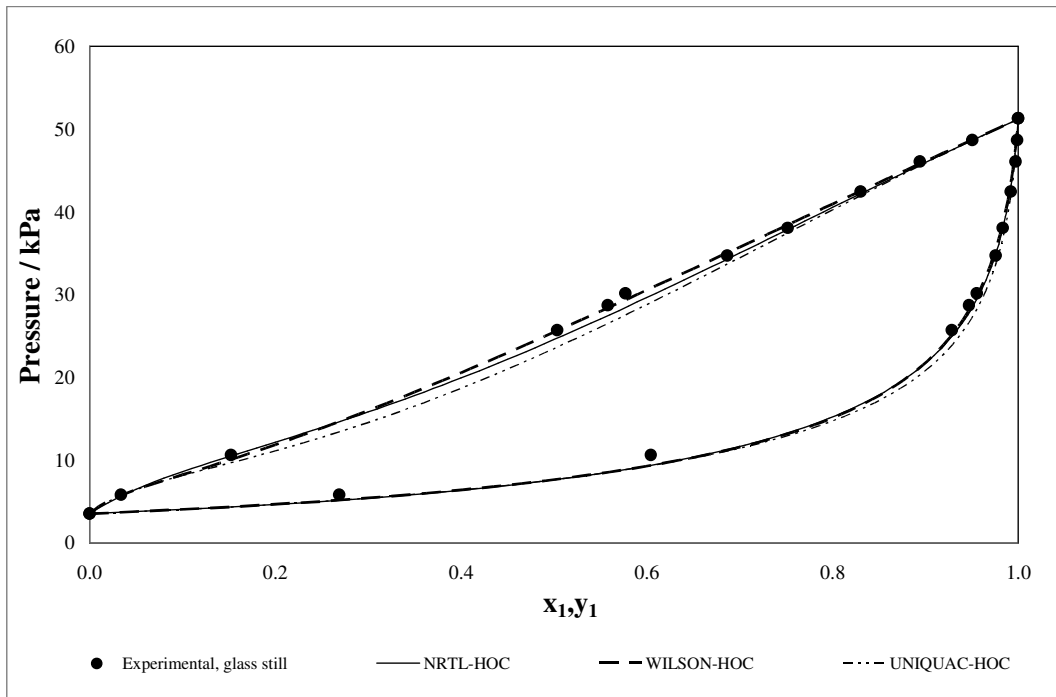
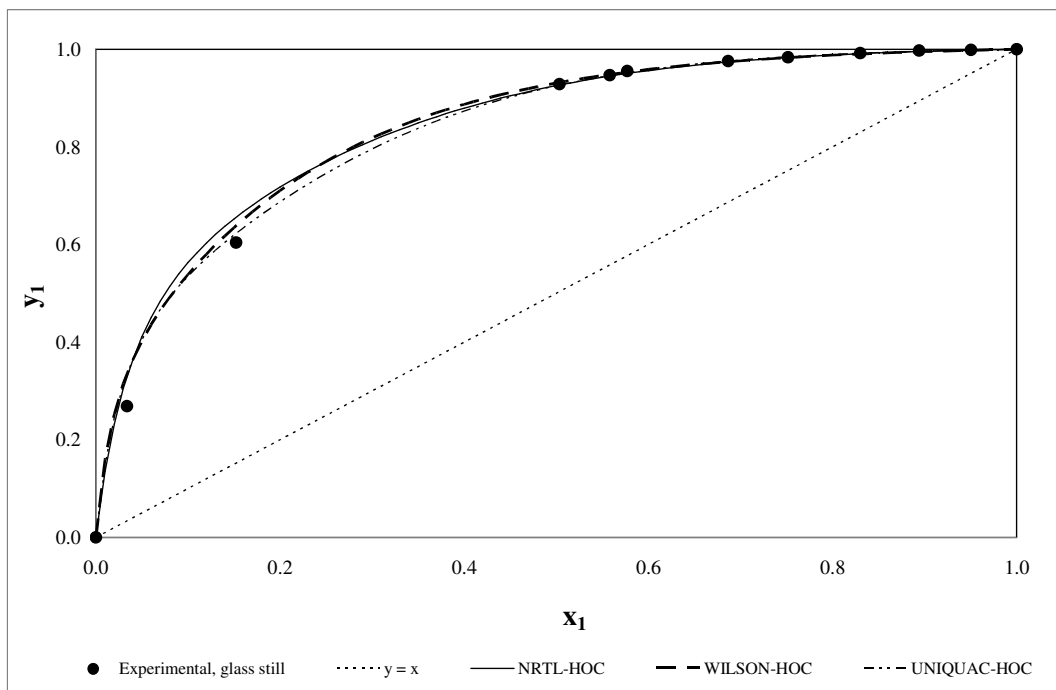


Figure 7-35 Comparison between HOC, VPA and NTH model fits to  $x_1$ - $y_1$  data for the 1-propanol (1) + n-butanoic acid (2) system at 353.15K



**Figure 7-36 Comparison between NRTL, WILSON and UNIQUAC model fits to experimental  $P$ - $x_1$ - $y_1$  data for the 1-propanol (1) + n-butanoic acid (2) system at 353.15K**



**Figure 7-37 Comparison between NRTL, WILSON and UNIQUAC model fits to experimental  $x_1$ - $y_1$  data for the 1-propanol (1) + n-butanoic acid (2) system at 353.15K**

## 7.6. The effect of excluded data points on model parameters obtained

Table 7-17 summarises the number of data points that were excluded for each binary system in order for the consistency test criterion to be satisfied. The full set of data was used in the final regression analyses for five of the eight data sets measured. Seven data points in total were left out of the final regressions across the remaining three sets of data.

**Table 7-17 Number of data points not included in final regression analyses**

System	Temperature / K	Number of data points excluded from final regression analyses
2-propanone + 2-butanol	333.15	0
	353.15	0
	373.15	1
2-propanone + n-propanoic acid	333.15	0
	353.15	0
	373.15	2
1-propanol + n-butanoic acid	333.15	4
	373.15	0

Tables 7-18 to 7-20 gives the model parameters obtained when the full set of data is used in the regression as well as those obtained when only the data points for which the consistency test criterion is satisfied are used in the regression. For the 2-propanone + 2-butanol and 2-propanone + n-propanoic acid systems, the model parameters obtained in both cases are for the most part quite similar. For the 1-propanol + n-butanoic acid system, however, there is a huge difference in the model parameters obtained when the full set of data is used. The “bump” in the phase diagrams for this system is also eliminated when all the data points are utilised in the regression.

**Table 7-18 Model Parameters obtained for the 2-propanone (1) + 2-butanol (2) system at 373.15K using the full set of data and only those for which the point test passes**

<b>Parameter</b>	<b>Component i</b>	<b>Component j</b>	<b>using only points for which the point test passes</b>	<b>using full set of data</b>
<b>NRTL-HOC</b>				
a <sub>ij</sub>	ACETONE	2-BUOH	-0.23	-1.05
a <sub>ij</sub>	2-BUOH	ACETONE	0.09	0.29
b <sub>ij</sub>	ACETONE	2-BUOH	78.77	402.62
b <sub>ij</sub>	2-BUOH	ACETONE	47.48	-40.94
η <sub>ij</sub>	ACETONE	2-BUOH	1.53	1.52
<b>NRTL-VPA</b>				
A <sub>i</sub>	ACETONE		-0.01	-0.01
B <sub>i</sub>	ACETONE		-4832.52	-4914.55
A <sub>i</sub>	2-BUOH		-0.04	-0.02
B <sub>i</sub>	2-BUOH		-5935.54	-5791.62
a <sub>ij</sub>	ACETONE	2-BUOH	0.25	0.00
a <sub>ij</sub>	2-BUOH	ACETONE	0.20	-0.07
b <sub>ij</sub>	ACETONE	2-BUOH	61.72	141.84
b <sub>ij</sub>	2-BUOH	ACETONE	-31.22	58.60
<b>NRTL-NTH</b>				
A <sub>i</sub>	ACETONE		0.00	0.00
B <sub>i</sub>	ACETONE		0.00	0.00
A <sub>i</sub>	2-BUOH		0.00	0.00
B <sub>i</sub>	2-BUOH		0.00	-0.09
a <sub>ij</sub>	ACETONE	2-BUOH	1.43	0.97
a <sub>ij</sub>	2-BUOH	ACETONE	0.42	1.54
b <sub>ij</sub>	ACETONE	2-BUOH	-555.44	-555.44
b <sub>ij</sub>	2-BUOH	ACETONE	-64.66	-219.40
<b>WILSON-HOC</b>				
a <sub>ij</sub>	ACETONE	2-BUOH	0.14	1.16
a <sub>ij</sub>	2-BUOH	ACETONE	0.03	0.46
b <sub>ij</sub>	ACETONE	2-BUOH	-113.39	-488.83
b <sub>ij</sub>	2-BUOH	ACETONE	-26.34	-193.59
η <sub>ij</sub>	ACETONE	2-BUOH	1.52	1.52
<b>UNIQUAC-HOC</b>				
η <sub>ij</sub>	ACETONE	2-BUOH	-1.61	-1.61
a <sub>ij</sub>	ACETONE	2-BUOH	0.06	0.06
a <sub>ij</sub>	2-BUOH	ACETONE	4.51	4.39
b <sub>ij</sub>	ACETONE	2-BUOH	24.19	22.86
b <sub>ij</sub>	2-BUOH	ACETONE	-1778.05	-1729.35

**Table 7-19 Model Parameters obtained for the 2-propanone (1) + n-propanoic acid (2) system at 373.15K using the full set of data and only those for which the point test passes**

<b>Parameter</b>	<b>Component i</b>	<b>Component j</b>	<b>using only points for which the point test passes</b>	<b>using full set of data</b>
<b>NRTL-HOC</b>				
a <sub>ij</sub>	ACETONE	C3OOH	-0.33	-0.33
a <sub>ij</sub>	C3OOH	ACETONE	0.02	0.03
b <sub>ij</sub>	ACETONE	C3OOH	1020.27	1017.21
b <sub>ij</sub>	C3OOH	ACETONE	-520.90	-517.26
η <sub>ij</sub>	ACETONE	C3OOH	4.50	4.50
<b>NRTL-VPA</b>				
A <sub>i</sub>	ACETONE		0.00	0.00
B <sub>i</sub>	ACETONE		-5914.71	-5933.99
A <sub>i</sub>	C3OOH		0.00	0.00
B <sub>i</sub>	C3OOH		10000.00	19551.08
a <sub>ij</sub>	ACETONE	C3OOH	-1.21	-1.22
a <sub>ij</sub>	C3OOH	ACETONE	0.15	0.21
b <sub>ij</sub>	ACETONE	C3OOH	689.86	683.50
b <sub>ij</sub>	C3OOH	ACETONE	-320.77	-331.18
<b>NRTL-NTH</b>				
A <sub>i</sub>	ACETONE		0.00	0.00
B <sub>i</sub>	ACETONE		0.00	0.00
A <sub>i</sub>	C3OOH		0.00	0.00
B <sub>i</sub>	C3OOH		0.00	0.00
a <sub>ij</sub>	ACETONE	C3OOH	-1.34	1.02
a <sub>ij</sub>	C3OOH	ACETONE	0.30	1.64
b <sub>ij</sub>	ACETONE	C3OOH	639.56	-657.47
b <sub>ij</sub>	C3OOH	ACETONE	-261.73	-6.11
<b>WILSON-HOC</b>				
a <sub>ij</sub>	ACETONE	C3OOH	-0.05	-0.05
a <sub>ij</sub>	C3OOH	ACETONE	0.16	0.15
b <sub>ij</sub>	ACETONE	C3OOH	387.65	385.98
b <sub>ij</sub>	C3OOH	ACETONE	-797.04	-800.04
η <sub>ij</sub>	ACETONE	C3OOH	4.50	4.50
<b>UNIQUAC-HOC</b>				
η <sub>ij</sub>	ACETONE	C3OOH	4.50	4.50
a <sub>ij</sub>	ACETONE	C3OOH	0.00	0.02
a <sub>ij</sub>	C3OOH	ACETONE	-0.01	-0.01
b <sub>ij</sub>	ACETONE	C3OOH	-551.82	-545.22
b <sub>ij</sub>	C3OOH	ACETONE	316.20	316.25

**Table 7-20 Model Parameters for the 1-propanol (1) + n-butanoic acid (2) system at  
333.15K using the full set of data and only those for which the point test passes**

<b>Parameter</b>	<b>Component i</b>	<b>Component j</b>	<b>using only points for which the point test passes</b>	<b>using full set of data</b>
<b>NRTL-HOC</b>				
a <sub>ij</sub>	1PROH	1-C4OOH	-0.24	2.83
a <sub>ij</sub>	1-C4OOH	1PROH	-14.19	0.72
b <sub>ij</sub>	1PROH	1-C4OOH	-335.52	-1304.89
b <sub>ij</sub>	1-C4OOH	1PROH	6102.15	323.15
η <sub>ij</sub>	1PROH	1-C4OOH	-11.68	4.22
<b>NRTL-VPA</b>				
A <sub>i</sub>	1PROH		0.00	0.00
B <sub>i</sub>	1PROH		-9481.14	-4740.70
A <sub>i</sub>	1-C4OOH		0.00	0.00
B <sub>i</sub>	1-C4OOH		-1076.92	-678.30
a <sub>ij</sub>	1PROH	1-C4OOH	-0.16	-0.09
a <sub>ij</sub>	1-C4OOH	1PROH	-14.12	-12.11
b <sub>ij</sub>	1PROH	1-C4OOH	-309.10	-318.19
b <sub>ij</sub>	1-C4OOH	1PROH	6125.54	4622.50
<b>NRTL-NTH</b>				
A <sub>i</sub>	1PROH		0	0
B <sub>i</sub>	1PROH		0	0
A <sub>i</sub>	1-C4OOH		0	0
B <sub>i</sub>	1-C4OOH		0	0
a <sub>ij</sub>	1PROH	1-C4OOH	-1.20	1.47
a <sub>ij</sub>	1-C4OOH	1PROH	-155.31	0.97
b <sub>ij</sub>	1PROH	1-C4OOH	-60.79	-840.33
b <sub>ij</sub>	1-C4OOH	1PROH	53074.16	211.30
<b>WILSON-HOC</b>				
a <sub>ij</sub>	1PROH	1-C4OOH	-209.56	-1.14
a <sub>ij</sub>	1-C4OOH	1PROH	55.07	1.16
b <sub>ij</sub>	1PROH	1-C4OOH	-100916.30	45.02
b <sub>ij</sub>	1-C4OOH	1PROH	-18039.97	-174.94
η <sub>ij</sub>	1PROH	1-C4OOH	-7.13	4.13
<b>UNIQUAC-HOC</b>				
η <sub>ij</sub>	1PROH	1-C4OOH	-3.70	4.30
a <sub>ij</sub>	1PROH	1-C4OOH	-12.59	0.34
a <sub>ij</sub>	1-C4OOH	1PROH	-1.54	7.44
b <sub>ij</sub>	1PROH	1-C4OOH	4531.52	188.82
b <sub>ij</sub>	1-C4OOH	1PROH	-503.85	-3048.42

## CHAPTER 8

### CONCLUSIONS

The objective of this study was to investigate the phase equilibrium behaviour of systems involving oxygen-containing compounds. A literature survey was undertaken to determine binary systems of industrial significance for which data were unavailable and hence, VLE measurements were required. In addition to the measurement of the pure component vapour pressures and the test system (cyclohexane + ethanol at 323.15K); isothermal VLE data were obtained for the following previously unmeasured binary systems:

1. 2-propanone (1) + 2-butanol (2) at 333.15K, 353.15K and 373.15K
2. 2-propanone (1) + n-propanoic acid (2) at 333.15K, 353.15K and 373.15K
3. 1-propanol (1) + n-butanoic acid (2) at 333.15K and 353.15K

The VLE data were modelled and tested using the thermodynamic relationships discussed. The conclusions of this study are presented in this chapter.

#### 8.1. Experimental aspects

VLE measurements on oxygen-containing compounds were performed on two dynamic recirculating stills, developed by Joseph (2001) and Reddy (2006). The measurements ranged from 1.59kPa to 479.7kPa and from 313.30K to 390.79K. The pressure accuracy of glass apparatus of Joseph (2001) was estimated as  $\pm 0.03$  kPa and it was controlled to within 0.01 kPa for isobaric operation. The accuracy of the measured temperature was estimated as  $\pm 0.02$ K and the temperature control varied between  $\pm 0.01$ K and  $\pm 0.05$ K depending on the chemical system being investigated and the composition range. The pressure accuracy of the VLE apparatus of Reddy (2006) was estimated as  $\pm 0.1$ kPa and it was controlled to within 0.1kPa for isobaric operation. The accuracy of the measured temperature on the apparatus of Reddy (2006) was estimated as  $\pm 0.02$ K and was controlled to within  $\pm 0.01$ K. The composition of the equilibrium phases were obtained via gas chromatography and the calculated species compositions were estimated to be accurate to  $\pm 0.002$  mole fraction. A full description of the VLE stills is presented in Chapter 4.

The results obtained for the vapour pressures and the highly non-ideal test system were in excellent agreement with the literature data. From this it was concluded that the apparatus and operating procedures used were capable of producing highly accurate VLE data and confidence in the new data measured was obtained.

## **8.2. Theoretical aspects**

The measured vapour pressure data were regressed to obtain parameters for the Antoine equation. These parameters were utilised in the binary VLE data regression. It was confirmed that the experimental activity coefficients could not be obtained via the conventional calculation procedure due to the strong association that occurs, even at low pressures. Thermodynamic models incorporating association were therefore used to model the systems in this study. The vapour phase fugacity coefficients were calculated using the methods capable of describing associating systems that were available in Aspen: viz. the method of Hayden and O'Connell (1974), Nothnagel et al. (1973) and the VPA/IK-CAPE EOS (Abbott and Van Ness, 1992). For the liquid phase, three local-composition based activity coefficient models were used: viz. Wilson (Wilson, 1964), NRTL (Renon and Prausnitz, 1968) and UNIQUAC (Abrams and Prausnitz, 1975).

The binary VLE systems were modelled successfully via the combined method ( $\gamma$ - $\Phi$ ) approach (Smith et al., 2001). The optimization of all model parameters was accomplished via the ordinary least squares regression algorithm, utilising the experimental pressure and vapour compositions in the objective function. The data were smooth and well-fitted by the models in most cases, which were judged by the deviations between the measured values and those calculated from the model. Table 8-1 summarises the best-fit models for the systems worked with in this study. The parameters obtained for the various models are presented in Section 7.5.

Thermodynamic consistency testing was carried out on all measured data to assess their quality. Most of the common tests cannot be used for associating systems since they usually require experimental activity coefficients, which cannot be obtained due to the complex vapour phase behaviour. The point test of Van Ness et al. (1973, 1975 & 1982) was used in this study and it was found that seven data points in total had to be excluded in order for the test to be satisfied. If the test criterion is not met, then the data are inconsistent, the models used in the test are

erroneous or inapplicable to the systems, or a combination of both. Nevertheless, data points that needed to be excluded in order for the point test to pass were not used in the final regression analyses to obtain the model parameters.

**Table 8-1 Best-fit models for the systems in this study**

System	Temperature / K	Best fit model
2-propanone + 2-butanol	333.15	NRTL-HOC/WILSON-HOC/UNIQUAC-HOC
	353.15	NRTL-VPA
	373.15	NRTL-VPA
2-propanone + n-propanoic acid	333.15	WILSON-HOC
	353.15	NRTL-NTH
	373.15	NRTL-NTH
1-propanol + n-butanoic acid	333.15	WILSON-HOC
	353.15	WILSON-HOC

## CHAPTER 9

### RECOMMENDATIONS AND FUTURE WORK

As discussed, it is relatively difficult to measure and analyse data involving associating systems and considerable room for improvement exists in both the experimental techniques adopted, the models, and the techniques used for correlating and regressing the measured data.

Recommendations pertaining to this study are:

1. Although the equipment design of Reddy (2006) is a great improvement to that of Harris (2004), the VLE apparatus of Reddy (2006) takes a relatively long time to heat up and attain a state of thermodynamic equilibrium within. A smaller still design (with less stainless steel to heat up) or a more efficient heating system should be investigated to improve on this aspect.
2. A further comment regarding the VLE apparatus of Reddy (2006) is that the manner of charging the sample to the still is somewhat inconvenient. The sample was charged to the still by creating a vacuum within the still and introducing the sample through the valve used to drain the reboiler. It is suggested that a small dropping funnel or something similar be added to the equipment and utilised for this purpose.
3. Due to time limitations, it was not possible to investigate all the available thermodynamic models with both the direct and combined methods. It is recommended that alternative models be applied (via the direct and combined methods) to the systems in this study and their applicability assessed thereafter. Models that can account for the association of polar compounds in particular should be investigated.
4. In addition, the type of regression used in this study to obtain the parameter estimates does not take into account the experimental uncertainty in the independent variables. As this can influence the interpretation of the results, it would be useful to switch the regression algorithms to those based on the principles of maximum likelihood. The maximum likelihood regression technique takes into account errors in all the experimental points as opposed to other methods which assume that one or more experimental values are known exactly.

5. With regards to the thermodynamic consistency tests, different results are obtained with different models for either the activity coefficient expressions or the EOS. Inappropriate choices for models will bias the results and lead to incorrect conclusions. It was recommended by Jackson and Wilsak (1995) that statistical procedures be utilized to account for the effects of experimental uncertainty in all the measured variables and to propagate these uncertainties in order to bound the final test results. This would greatly aid in interpreting the results.
6. Another recommendation for future work is to use multi-property regression in the parameter regression. That is, instead of using VLE data alone, one should make use of heat capacity or heat of mixing data as well. This will greatly improve the reliability of the results obtained.
7. This study dealt with short-chain associating compounds. VLE systems involving longer-chain compounds ( $>C_6$ ) at varying conditions of temperature and pressure should be investigated. A correlation could exist between members of the same homologous series for example.

## REFERENCES

- Abbott, M.M. and Van Ness, H.C., 1992. Thermodynamics of Solutions Containing Reactive Species, a Guide to Fundamentals and Applications. *Fluid Phase Equilibria*, 77, 53–119.
- Abrams, D.S., and Prausnitz, J.M., 1975. Statistical Thermodynamics of Liquid Mixtures: A New Expression for the excess Gibbs Energy of Partly or Completely Miscible Systems. *American Institute of Chemical Engineers Journal*, 21(1), 116-127.
- Alpert, N., Elving, P.J., 1949. Vapor-Liquid Equilibria in Binary Systems Ethylene Dichloride-Toluene and Formic Acid-Acetic Acid. *Industrial and Engineering Chemistry*, 41(12), 2864-2867.
- Anderson, T.F., and Prausnitz, J.M., 1978. Application of the UNIQUAC Equation to Calculation of Multicomponent Phase Equilibria. 1: Vapour-liquid Equilibria; 2: Liquid-Liquid Equilibria. *Industrial and Engineering Chemistry, Process Design and Development*, 17, 552-567.
- Barker, J.A., 1953. Determination of Activity Coefficients from Total Pressure Measurements. *Australian Journal of Chemistry*, 6, 207-210.
- Barnicki, S.D., June 2002. *How Good are Your Data? Some thoughts on the measurement and interpretation of vapor-liquid equilibrium.* [www.cepmagazine.org](http://www.cepmagazine.org)
- Bradshaw, S.M., 1985. *A Static Equilibrium Cell for High Pressure and Temperature Vapour-Liquid Equilibrium Measurement.* Dissertation (MSc). University of Natal, Durban, South Africa.
- Carlson, H.C. and Colburn A.P., 1942. Vapor-Liquid Equilibria of Nonideal Solutions. Utilization of Theoretical Methods to Extend Data. *Industrial and Engineering Chemistry*, 34(5), 581-589.
- Chapman, W.G., Gubbins, K.E., Jackson, G. and Radosz, M., 1990. New Reference Equation of State for Associating Liquids. *Industrial and Engineering Chemistry Research*, 29, 1709.
- Christian, S. D., 1957. Liquid-Vapour Equilibrium in the System Acetic Acid-Propionic Acid at 20 °C. *Journal of Physical Chemistry*, 61, 1441-1442.
- Christian, S.D., Neparko, E. and Affsprung, H.E., 1960. A New Method for Determination of Activity Coefficients of Components in Binary Liquid Mixtures. *Journal of Physical Chemistry*, 64, 442-440.

- Christiansen, L.J. and Fredenslund, A., 1975. Thermodynamic Consistency using Orthogonal Collocation or Computation of Equilibrium Vapor Compositions at High Pressures. *The American Institute of Chemical Engineers Journal*, 21(1), 49-57.
- Clifford, S.L., 2004. *Low-Pressure Vapour-Liquid Equilibrium and Molecular Simulation of Carboxylic Acids*. Dissertation (MSc). University of Natal, Durban, South Africa.
- Clifford, S.L., 2006. *Molecular Simulation and Modeling of the Phase Equilibria of Polar Compounds*. Thesis (PhD). University of KwaZulu-Natal, Durban, South Africa.
- Clifford, S.L., Ramjugernath, D and Raal, J.D., 2005. Vapour-Liquid Equilibrium of Carboxylic Acid Systems: Propionic Acid+Valeric Acid and Isobutyric Acid+Valeric Acid. *Fluid Phase Equilibria*, 237, 89-99.
- Curtiss, L.A., Foster, J.P. and Weinhold, F., 1980. *Journal of the American Chemical Society*, 88, 899.
- Dolezalek, F., 1908. *Z. Phys. Chem.*, 64, 727.
- Dortmund Data Bank, Purchased 2008. *DDBST Software and Separation Technology GmbH*, Oldenburg.
- Fredenslund, A., Gmehling, J. and Rasmussen, P., 1977. *Vapor-Liquid Equilibria using UNIFAC*. Elsevier, Amsterdam.
- Gess, M.A., Danner, R.P., and Nagvekar, M., 1991. *Thermodynamic Analysis of Vapor-Liquid Equilibria: Recommended Models and a Standard Data Base*. Design Institute for Physical Property Data, American Institute of Chemical Engineers.
- Gillepsie, D.T.C., 1946. Vapor-Liquid Equilibrium Still for Miscible Liquids. *Industrial and Engineering Chemistry Analytical Edition*, 18(9), 575-577.
- Gilliland, E.R. and Scheeline, H.W., 1940. High-Pressure Vapor-Liquid Equilibrium for the Systems Propylene-Isobutane and Propane-Hydrogen Sulfide. *Industrial and Engineering Chemistry*, 32(1), 48-54.
- Gmehling, J. and Onken, U., 1977. *Vapour Liquid Equilibrium Data Collection. Organic Hydroxy Compounds: Alcohols*. DECHEMA Chemistry Data Series. Frankfurt/Main, W. Germany.
- Griswold, J., Andres, D. and Klein, V.A., 1943. Determination of High-Pressure Vapor-Liquid Equilibrium. The vapor-liquid equilibrium of benzene-toluene. *Transactions of the American Institute of Chemical Engineers*, 39(2), 223-246.

- Gross, J. and Sadowski, G., 2001. Perturbed-Chain SAFT: An Equation of State Based on a Perturbation Theory for Chain Molecules. *Industrial and Engineering Chemistry Research*, 40, 1244-1260.
- Hansen, R.S. and Miller, F.A., 1954. A New Method for Determination of Activities of Binary Solutions of Volatile Liquids. *The Journal of Physical Chemistry*, 58(3), 193-196.
- Hansen, R.S., Miller, F.A. and Christian, S.D., 1955. Activity Coefficients of Components in the Systems Water-Acetic Acid, Water-Propionic Acid and Water-*n*-Butyric Acid at 25°. *Journal of Physical Chemistry*, 59, 391-395.
- Hansen, R.S., Miller, F.A., Christian, S.D., 1955. Activity Coefficients of Components in the Systems Water-Acetic Acid, Water-Propionic Acid and Water-*n*-Butyric Acid at 25°. *Journal of Physical Chemistry*, 59, 391-395.
- Harris, R.A., 2004. *Robust Equipment for the Measurement of Vapour-Liquid Equilibrium at High Temperatures and High Pressures*. Thesis (PhD). University of KwaZulu-Natal, Durban, South Africa.
- Hayden, J.G. and O'Connell, J.P., 1975. A Generalized Method for Predicting Second Virial Coefficients. *Industrial and Engineering Chemistry, Process Design and Development*, 14, 209-216.
- Huang, S.H. and Radosz, M., 1990. Equation of State for small, large, polydisperse and associating molecules. *Industrial and Engineering Chemistry Research*, 29, 2284.
- Hwengwere, A.P., 2005. *Vapour-Liquid Equilibrium of Carboxylic Acids*. Dissertation (MSc). University of KwaZulu-Natal, Durban, South Africa.
- Jackson, P.L. and Wilsak, R.A., 1995. Thermodynamic consistency tests based on the Gibbs-Duhem equation applied to isothermal, binary vapor-liquid equilibrium data: data evaluation and model testing. *Fluid Phase Equilibria*, 103(2), 155-197.
- Johnson, E.W. and Nash, L.K., 1950. *Journal of the American Chemical Society*, 74, 743.
- Jones, C.A., Schoenborn, E.M. and Colburn, A.P., 1943. Equilibrium Still for Miscible Liquids. Data on Ethylene Dichloride-Toluene and Ethanol-Water. *Industrial and Engineering Chemistry*, 35(6), 666-672.
- Joseph, M.A., 2001. *Computer-Aided Measurement of Vapour-Liquid Equilibria in a Dynamic Still at Sub-Atmospheric Pressures*. Dissertation (MSc). University Natal, Durban, South Africa.

- Joseph, M.A., Raal, J.D. and Ramjugernath, D., 2001. Phase Equilibrium Properties of Binary Systems with Diacetyl from a Computer Controlled Vapour-Liquid Equilibrium Still. *Fluid Phase Equilibria*, Vol. 182, pp. 157-176.
- Karle, J. and Brockway, L.O., 1944. An Electron Diffraction Investigation of the Monomers and Dimers of Formic, Acetic and Trifluoroacetic Acids and the Dimer of Deuterium Acetate. *Journal of the American Chemical Society*, 66, 574.
- Kneisl, P., Zondlo, J.W., and Whiting, W.B., 1989. The Effect of Fluid Properties on Ebulliometer Operation. *Fluid Phase Equilibria*, 46, 85-94.
- Kontogeorgis, G.M., Voutsas, E.C., Yakoumis, L.V. and Tassios, D.P., 1996. An Equation of State for Associating Fluids. *Industrial Engineering and Chemical Research*, 35, 4310-4318.
- Landee, F.A. and Johns, I.B., 1941. The Electron-Sharing Ability of Organic Radicals. XII. The Effect of the Radicals on the Degree of Association of Polar Molecules. *Journal of the American Chemical Society*, 63, 2891-2895.
- Langdon, W.M. and Keyes, D.B., 1942. Vapor-Liquid Equilibrium Data on Ethyl Alcohol-Water and on Isopropyl Alcohol-Water. *Industrial and Engineering Chemistry*, 34(8), 938-942.
- Lewis, G.N. and Randall, M., 1923. *Thermodynamics and the Free Energy of Chemical Substances*, McGraw-Hill, New York.
- Lide, D.R., 2005. *CRC Handbook of Chemistry and Physics. 86th Edition 2005-2006*. CRC Press Taylor & Francis group, Boca Raton.
- Lundin, R.E., Harris, F.E. and Nash, L.K., 1952. The Vapor Phase Association of Butyric and Heptanoic Acids. *Journal of the American Chemical Society*, 74(3), 743-745.
- Macdougall, F.H., 1936. The Molecular State of the Vapor of Acetic Acid at Low Pressures at 25, 30, 35, and 40°. *Journal of the American Chemical Society*, 58, 2585-2591.
- Macdougall, F.H., 1941. A Study of the Vapor of Propionic Acid at 45, 50, 55, 60 and 65°. *Journal of the American Chemical Society*, 63, 3420-3424.
- Maher, P.J. and Buford, D.S., 1979. Infinite Dilution Activity Coefficients Values from Total Pressure VLE Data. Effect of Equation of State Used. *Industrial and Engineering Chemistry Fundamentals*, 18(4), 354-357.
- Malanowski, S. and Anderko, A., 1992. *Modelling Phase Equilibria: Thermodynamic Background and Practical Tools*. John Wiley, New York.

- Meng, L., Duan, Y.Y. and Li, L., 2004. Correlations for Second and Third Virial Coefficients of Pure Fluids. *Fluid Phase Equilibria*, 226, 109-120.
- Narasigadu, C., 2006. *Phase Equilibrium Investigation of the Water and Acetonitrile Solvent with Heavy Hydrocarbons*. Dissertation (MSc). University of KwaZulu-Natal, Durban, South Africa.
- Ndlovu, M., 2005. *Development of a Dynamic Still for Measuring Low Pressure Vapour-Liquid-Liquid Equilibria (Systems of Partial Liquid Miscibility)*. Dissertation (MSc). University of KwaZulu-Natal, Durban, South Africa.
- Nothnagel, K.H., Abrams, D.S. and Prausnitz, J.M., 1973. Generalized Correlation for Fugacity Coefficients in Mixtures at Moderate Pressures. Application of Chemical Theory of Vapor Imperfections. *Industrial and Engineering Chemistry Process Design and Development*, 12(1), 25-35.
- Othmer, D.F. and Benenati, R.F., 1945. Composition of Vapors from Boiling Binary Systems. Aqueous Systems of Acetone, Methanol, and Methyl Ethyl Ketone; and Other Systems With Acetic Acid As One Component. *Industrial and Engineering Chemistry*, 37(3), 299-303.
- Othmer, D.F., 1928. Composition of Vapors from Boiling Binary Solutions. *Industrial and Engineering Chemistry*, 20(7), 743-746.
- Othmer, D.F., 1932. Composition of Vapors from Boiling Binary Solutions. *Industrial and Engineering Chemistry. Analytical Edition*, 4(2), 232-234.
- Perry, R.H. and Green, D.W., 1998. *Perry's Chemical Engineers' Handbook. 7th Edition*. McGraw-Hill, New York.
- Poling, B.E., Prausnitz, J.M. and O'Connell, J.P., 2001. *The Properties of Gases and Liquids*. 5<sup>th</sup> Edition. New York: McGraw-Hill.
- Prausnitz, J.M., 1969. *Molecular Thermodynamics of Fluid Phase Equilibria*. Prentice-Hall, Englewood Cliffs, New Jersey.
- Prausnitz, J.M., Anderson, T.F., Grens, E.A., Eckert, C.A., Hsieh, R. and O'Connell, J.P., 1980. *Computer Calculations for Multicomponent Vapour-Liquid and Liquid-Liquid Equilibria*. Prentice-Hall, Englewood Cliffs, New Jersey.
- Prausnitz, J.M., Rüdiger, N.L., and Gomez de Azevedo, E., 1999. *Molecular Thermodynamics of Fluid Phase Equilibria, 3rd Edition*, Prentice Hall.
- Raal, J.D. and Mühlbauer, A.L., 1998. *Phase Equilibria: Measurement and Computation*. Taylor and Francis, Bristol, PA.

- Rackett, H.G., 1970. Equation of State for Saturated Liquids. *Journal of Chemical and Engineering Data*, 15(4), 514-517.
- Reddy, P., 2006. *Development of a Novel Apparatus for Vapour-Liquid Equilibrium Measurements at Moderate Pressures*. Thesis (PhD). University of KwaZulu-Natal, Durban, South Africa.
- Redlich, O. and Kister, A.T., 1948. On the Thermodynamics of Solutions. IV. The Determination of Liquid-Vapor Equilibria by Measuring the Total Pressure. *Journal of the American Chemical Society*, 71, 505-507.
- Reid, R.C., Prausnitz, J.M. and Polling, B.E., 1988. *The Properties of Gases and Liquids*. 4th Edition. New York: McGraw-Hill.
- Renon, H. and Prausnitz, J.M., 1968. Local Compositions in Thermodynamic Excess Functions for Liquid Mixtures. *American Institute of Chemical Engineers Journal*, 14, 135-144.
- Ritter, H.L. and Simons, J.H., 1945. The Molecular State of Acetic Acid Vapor. *Journal of the American Chemical Society*, 67, 757-762.
- Sandler, S.I., 1999. *Chemical and Engineering Thermodynamics*. 3<sup>rd</sup> Edition John Wiley and Sons, New York.
- Scatchard, G. and Ticknor, L.B., 1952. Vapor-Liquid Equilibrium. IX. The Methanol-Carbon Tetrachloride-Benzene System. *Journal of the American Chemical Society*, 74, 3724-3729.
- Scatchard, G., 1938. Vapor-Liquid Equilibrium. II. Chloroform-Ethanol Mixtures at 35, 45 and 55°. *Journal of the American Chemical Society*, 60, 1278-1287.
- Scheeline, H.W. and Gilliland, E.R., 1939. Vapor-Liquid Equilibrium in the System Propane-Isobutylene. *Industrial and Engineering Chemistry*, 31(8), 1050-1057.
- Scott, R.L., 1956. Corresponding States Treatment of Nonelectrolyte Solutions. *J. Chem. Phys.*, 25, 193-205.
- Sebastiani, E. and Lacquaniti, L., 1967. Acetic Acid-Water System Thermodynamical Correlation of Vapor-Liquid Equilibrium Data. *Chemical Engineering Science*, 22, 1155-1162.
- Soave, G., 1972. Equilibrium Constants from a Modified Redlich-Kwong EOS. *Chemical Engineering Science*, 39, 357.
- Smith, J.M., Van Ness, H.C. and Abbott, M.M., 1996. *Introduction to Chemical Engineering Thermodynamics*, 5th Edition. McGraw-Hill, Singapore.

- Smith, J.M., Van Ness, H.C. and Abbott, M.M., 2001. *Chemical Engineering Thermodynamics, 6th Edition*. McGraw-Hill, Singapore.
- Soni, M., 2003. Vapour-Liquid Equilibria and Infinite Dilution Activity Coefficients Measurements of Systems Involving Diketones. Dissertation (MSc). University of KwaZulu-Natal, Durban, South Africa.
- Spencer, C.F. and Adler, S.B., 1978. A Critical Review of Equations for Predicting Saturated Liquid Density. *Journal of Chemical and Engineering Data*, 23(1), 82-89.
- Spencer, C.F. and Danner, R.P., 1972. Improved Equation for Prediction of Saturated Liquid Density. *Journal of Chemical and Engineering Data*, 17(2), 236-241.
- Taylor, M.D. and Bruton, J., 1952. *Journal of the American Chemical Society*, 74, 4151.
- Tsonopoulos, C. and Prausnitz, J.M., 1970. Fugacity Coefficients in Vapour-Phase Mixtures of Water and Carboxylic Acids. *The Chemical Engineering Journal*, 1, 273-277.
- Tsonopoulos, C. and Prausnitz, J.M., 1970. Fugacity Coefficients in Vapor-Phase Mixtures of Water and Carboxylic Acids. *The Chemical Engineering Journal*, 1, 273-278. (NB: correction in 1972, *The Chemical Engineering Journal*, 4)
- Valderrama, J.O., 2003. The State of the Cubic Equations of State. *Industrial and Engineering Chemistry Research*, 42, 1603-1618.
- Van Dyk, B., 2005. Practical Thermodynamics for Simulations. Theory and Model Selection. Process Development/Sasol Technology R&D (internal Sasol Limited document).
- Van Ness, H.C. and Abbott, M.M., 1982. *Classical Thermodynamics of Nonelectrolyte Solutions: With Applications to Phase Equilibria*. McGraw-Hill, New York.
- Van Ness, H.C., 1995. Thermodynamics in the Treatment of Vapor/Liquid Equilibria (VLE) Data. *Pure and Applied Chemistry*, 67(6), 859-872.
- Van Ness, H.C., Byer, S.M. and Gibbs, R.E., 1973. Vapour-Liquid Equilibrium: Part I. An Appraisal of Data Reduction Methods. *American Institute of Chemical Engineers Journal*, 19, 238-244.
- Van Ness, H.C., Pedersen, F. and Ramussen, P., 1978. Part V. Data Reduction by Maximum Likelihood. *American Institute of Chemical Engineers Journal*, 24, 1055-1063.
- Vawdrey, A.C., Oscarson, J.L., Rowley, R.L. and Wilding, W.V., 2004. Vapor-Phase Association of *n*-Aliphatic Carboxylic Acids. *Fluid Phase Equilibria*, 222-223, 239-245.
- Walas, S.M., 1985. *Phase Equilibria in Chemical Engineering*, Butterworth.
- Weltner, W., 1955. *Journal of the American Chemical Society*, 77, 3941.

- Wilson, G.M., 1964. Vapor-Liquid Equilibrium. XI. A New Expression for the Excess Free Energy of Mixing. *Journal of the American Chemical Society*, 86, 127-130.
- Wolbach, J.P. and Sandler, S.I., 1997. Using Molecular Orbital Calculations to Describe the Phase Behavior of Hydrogen-Bonding Fluids. *Industrial and Engineering Chemistry Research*, 36, 4041-4051.
- York, R. and Holmes, R.C., 1942. Vapor-Liquid Equilibria of the System Acetone-Acetic Acid-Water. *Industrial and Engineering Chemistry*, 34(3), 345-350.

## Appendix A

### A.1. The criterion for equilibrium:

Consider a closed system consisting of two phases, say  $\alpha$  and  $\beta$ , which are in thermodynamic equilibrium. From Equation 3.8 (Chapter 3), for a closed system the Gibbs free energy is related to temperature and pressure by the following expression (for  $n$  moles of material):

$$d(nG) = (nV)dP - (nS)dT \quad (\text{A.1})$$

Each individual phase in the closed system may still exchange mass with each other through the common interface and is therefore each an open system having  $n^\alpha$  and  $n^\beta$  moles respectively. For an open system, in addition to temperature and pressure, the Gibbs free energy is also a function of the mole numbers  $n_1, n_2, \dots, n_N$  (for  $N$  components), that is,

$$(nG) = f(P, T, n_1, n_2, \dots, n_N) \quad (\text{A.2})$$

The total differential of  $(nG)$  is:

$$d(nG) = \left( \frac{\partial nG}{\partial P} \right)_{T,n} dP + \left( \frac{\partial nG}{\partial T} \right)_{P,n} dT + \sum \left( \frac{\partial nG}{\partial n_i} \right)_{P,T,n_j} dn_i \quad (\text{A.3})$$

where the subscript  $n$  indicates that *all* mole numbers are held constant, and subscript  $n_j$  that all mole numbers *except*  $n_i$  are held constant. The first two terms on the right hand side of Equation A.3 is for a system of constant composition and from Equation A.1 it can be seen that:

$$\left( \frac{\partial nG}{\partial P} \right)_{T,n} = nV \quad (\text{A.4})$$

$$\left( \frac{\partial nG}{\partial T} \right)_{P,n} = -nS \quad (\text{A.5})$$

By definition in terms of the Gibbs free energy,

$$\left( \frac{\partial(nG)}{\partial n_i} \right)_{P,T,n_j} = \mu_i \quad (\text{A.6})$$

Assuming uniform temperature and pressure, Equation A.3 can therefore be rewritten for each of the phases as:

$$d(nG)^\alpha = (nV)^\alpha dP - (nS)^\alpha dT + \sum \mu_i^\alpha dn_i^\alpha \quad (\text{A.7})$$

$$d(nG)^\beta = (nV)^\beta dP - (nS)^\beta dT + \sum \mu_i^\beta dn_i^\beta \quad (\text{A.8})$$

Equations A.7 and A.8 may be added to obtain the change in the total Gibbs energy for the two-phase (closed) system:

$$d(nG) = (nV)dP - (nS)dT + \sum \mu_i^\alpha dn_i^\alpha + \sum \mu_i^\beta dn_i^\beta \quad (\text{A.9})$$

Where each total-system property is obtained using an equation of the form:

$$nM = (nM)^\alpha + (nM)^\beta \quad (\text{A.10})$$

Since Equation A.1 and A.9 are both applicable to the two-phase closed system, a comparison of the two implies that at equilibrium:

$$\sum \mu_i^\alpha dn_i^\alpha + \sum \mu_i^\beta dn_i^\beta = 0 \quad (\text{A.11})$$

For systems without chemical reaction, the changes  $dn_i^\alpha$  and  $dn_i^\beta$  are due solely to the mass transfer of the components between the phases and the law of conservation of mass requires that:

$$dn_i^\alpha = -dn_i^\beta \quad (\text{A.12})$$

Therefore, it follows that Equation A.11 reduces to:

$$\sum (\mu_i^\alpha - \mu_i^\beta) dn_i^\alpha = 0 \quad (\text{A.13})$$

The quantities of  $dn_i$  are independent and arbitrary and Equation A.13 must hold for any value of  $dn_i$ . It therefore implies that for Equation A.13 to hold true, each term in the parenthesis must separately be equal to zero. Hence,

$$\mu_i^\alpha = \mu_i^\beta \quad (i = 1, 2, \dots, N) \quad (\text{A.14})$$

Equation A.14 can be shown to hold true for more than two phases in equilibrium by successively considering the phases in pairs. The general criterion for equilibrium for  $\pi$  phases with  $N$  chemical components is:

$$\mu_i^\alpha = \mu_i^\beta = \dots = \mu_i^\pi \quad (i = 1, 2, \dots, N) \quad (\text{A.15})$$

The equality of temperature and pressure at equilibrium (intuitively assumed here) can also be shown using a similar derivation.

## A.2. Fugacity of a pure liquid:

For a pure liquid, considering a phase change from a saturated liquid to a saturated vapour at the saturation pressure and constant temperature, the following expression results from Equation 3.20 (Chapter 3):

$$f_i^V = f_i^L = f_i^{sat} \quad (\text{A.16})$$

The corresponding fugacity coefficient at saturated pressure is:

$$\phi_i^{sat} = \frac{f_i^{sat}}{P_i^{sat}} \quad (\text{A.17})$$

This leads to the following relation:

$$\phi_i^V = \phi_i^L = \phi_i^{sat} \quad (\text{A.18})$$

Combining Equations 3.8 and 3.13 (Chapter 3) to eliminate  $dG_i$  gives:

$$dG_i = V_i dP - S_i dT = RT d \ln f_i \quad (\text{A.19})$$

At constant temperature,

$$d \ln f_i = \frac{V_i}{RT} dP \quad (\text{A.20})$$

Integrating (isothermally) from the initial state of a saturated liquid ( $P_i^{sat}$ ) to the final state of a compressed liquid at pressure  $P$  gives the fugacity:

$$f_i^L = f_i^{sat} \exp \left[ \int_{P_i^{sat}}^P \frac{V_i}{RT} dP \right] \quad (\text{A.21})$$

Substituting for  $f_i^{sat}$ ,

$$f_i^L = \phi_i^{sat} P_i^{sat} \exp \left[ \int_{P_i^{sat}}^P \frac{V_i}{RT} dP \right] \quad (\text{A.22})$$

$V_i$  represents the liquid molar volume. At temperatures well below the critical temperature,  $T_c$ , the liquid molar volume is a weak function of pressure and hence can be considered approximately constant when evaluating the integral in Equation A.22.  $V_i$  is assumed to be constant at the saturated liquid molar volume,  $V_i^L$ . Hence, Equation A.22 becomes:

$$f_i^L = \phi_i^{sat} P_i^{sat} \exp \left[ \frac{V_i^L (P - P_i^{sat})}{RT} \right] \quad (\text{A.23})$$

## Appendix B: (Residuals for the point test)

### B.1. Results for the system: 2-propanone (1) + 2-butanol (2)

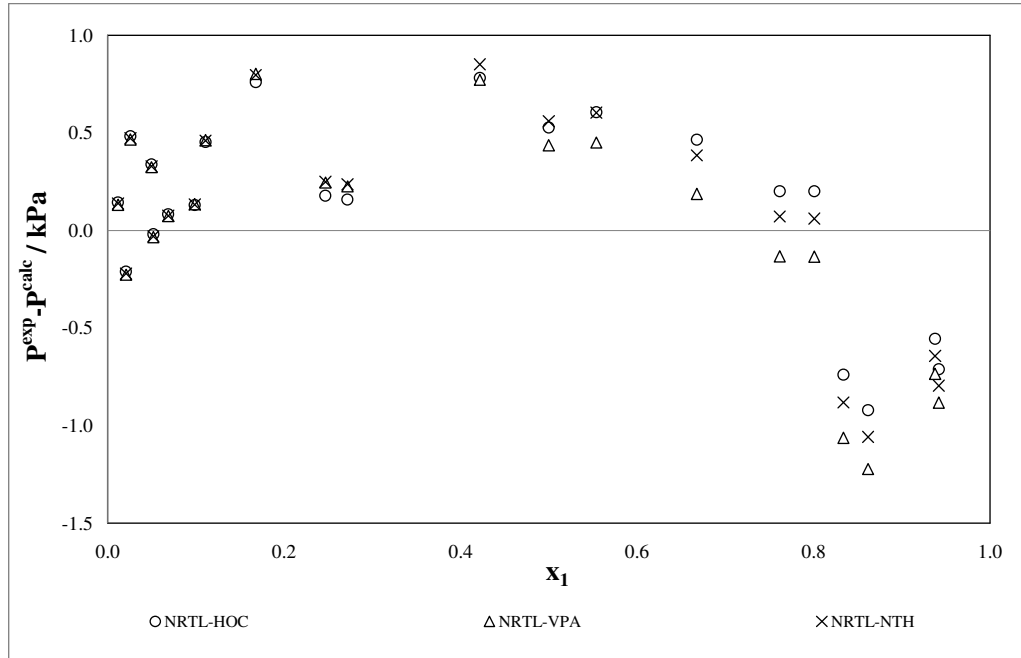


**Figure B-1 Point test (varying EOS): pressure-residual for the 2-propanone (1) + 2-butanol (2) system at 333.15K**

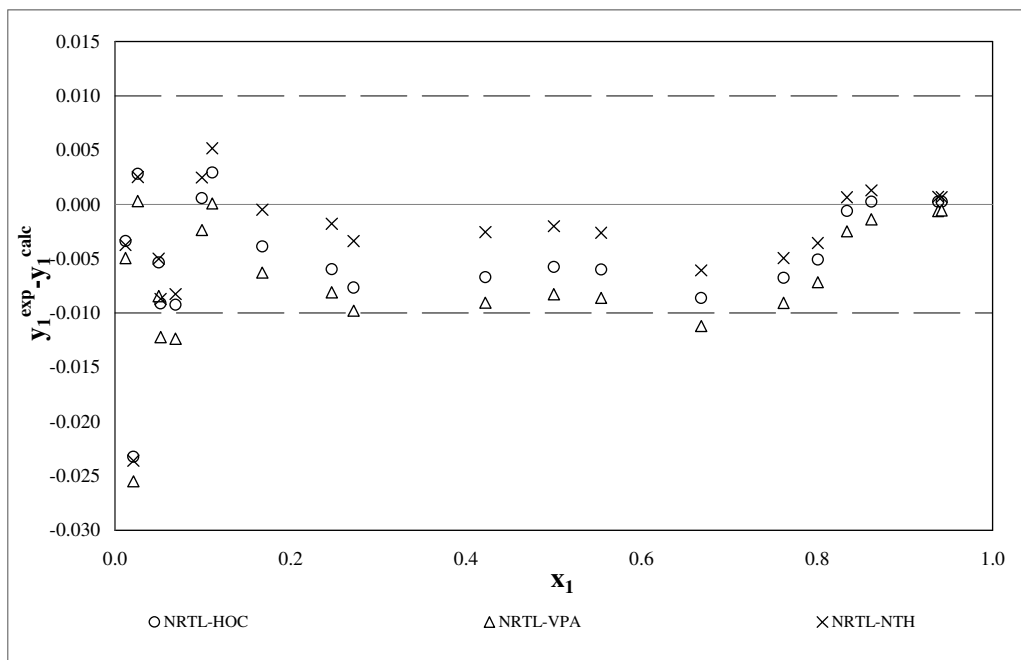


**Figure B-2 Point test (varying EOS):  $\Delta y_1$  for the 2-propanone (1) + 2-butanol (2) system at 333.15K**

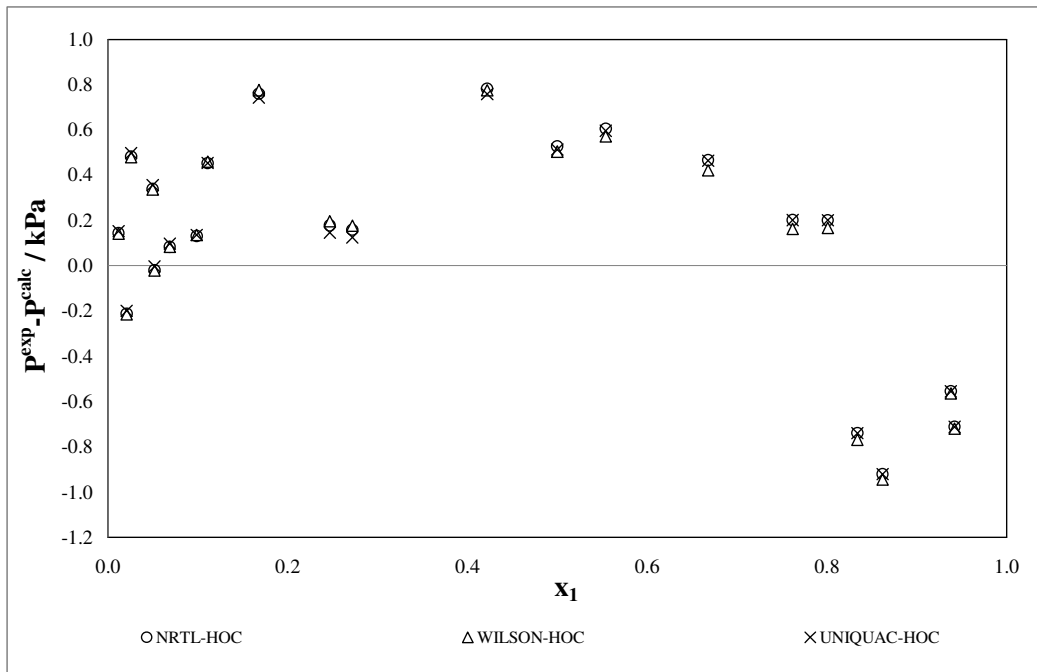


**Figure B-3 Point test (varying activity coefficient model): pressure-residual for the 2-propanone (1) + 2-butanol (2) system at 333.15K**

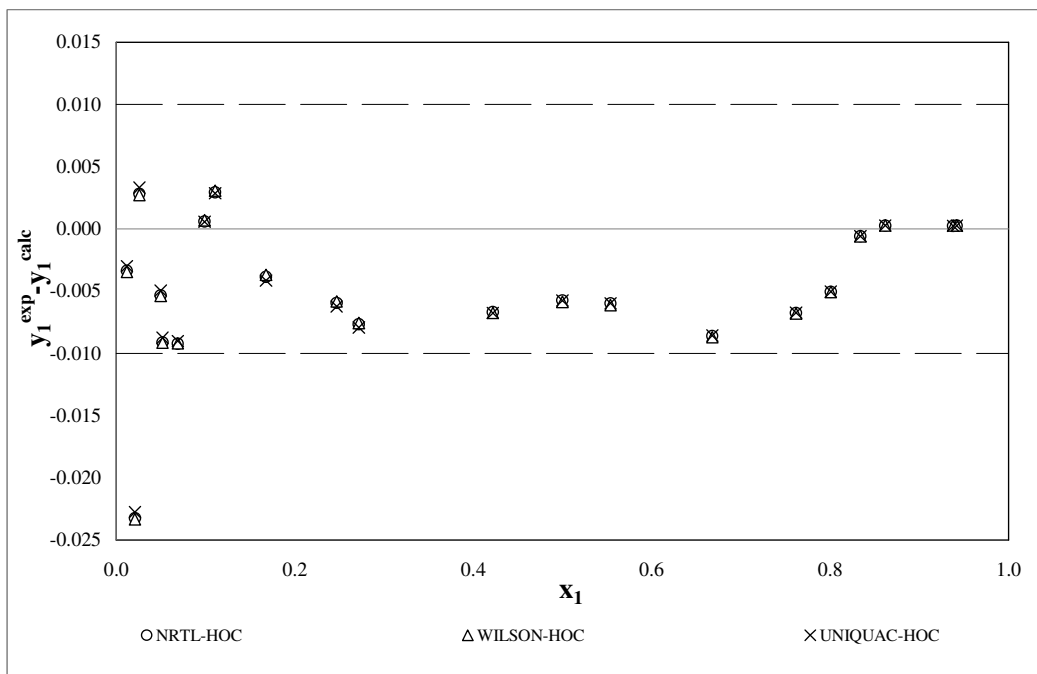


**Figure B-4 Point test (varying activity coefficient model):  $\Delta y_1$  for the 2-propanone (1) + 2-butanol (2) system at 333.15K**

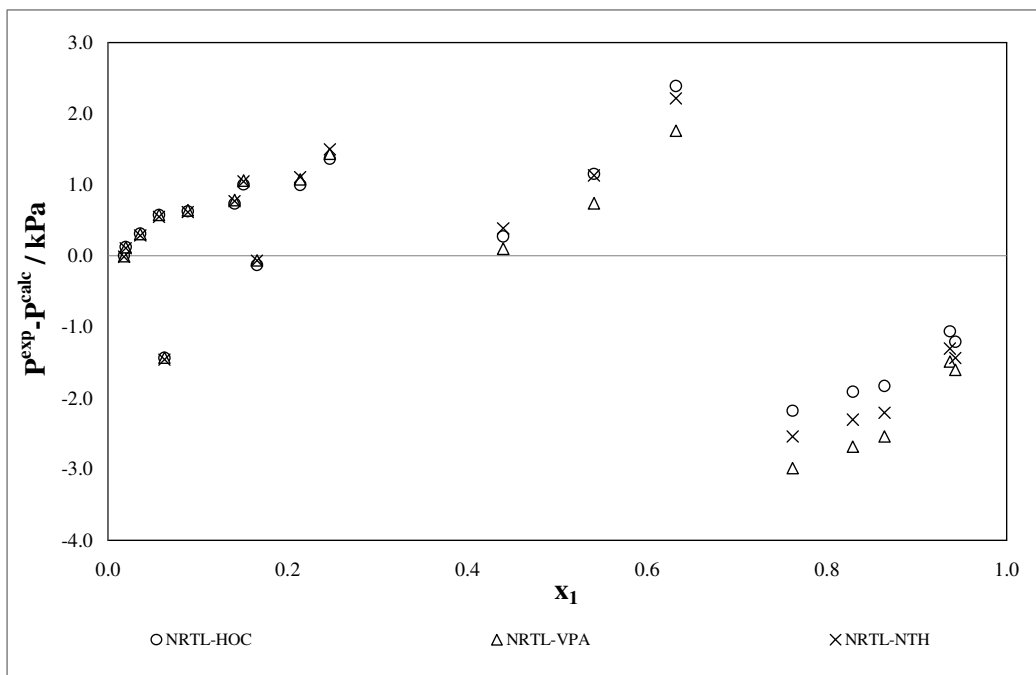


**Figure B-5 Point test (varying EOS): pressure-residual for the 2-propanone (1) + 2-butanol (2) system at 353.15K**

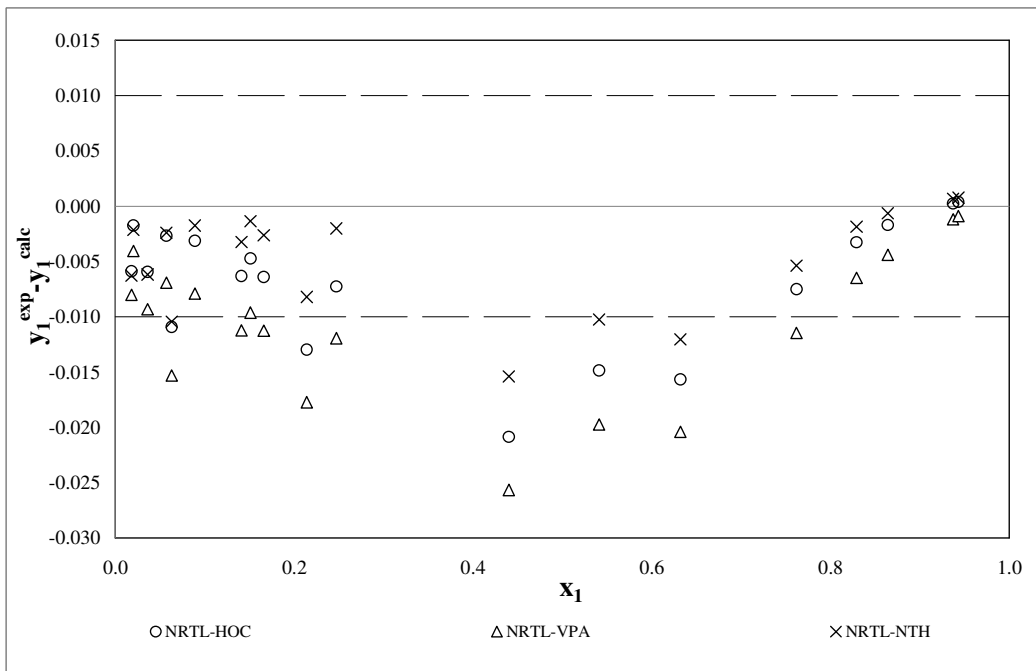


**Figure B-6 Point test (varying EOS):  $\Delta y_1$  for the 2-propanone (1) + 2-butanol (2) system at 353.15K**

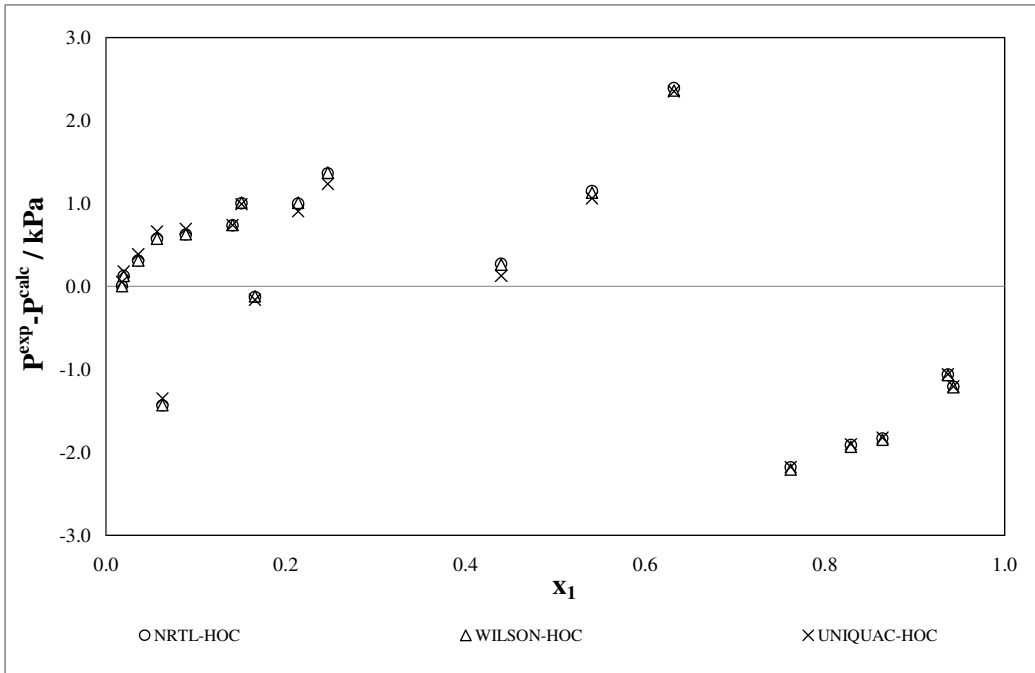


**Figure B-7 Point test (varying activity coefficient model): pressure-residual for the 2-propanone (1) + 2-butanol (2) system at 353.15K**

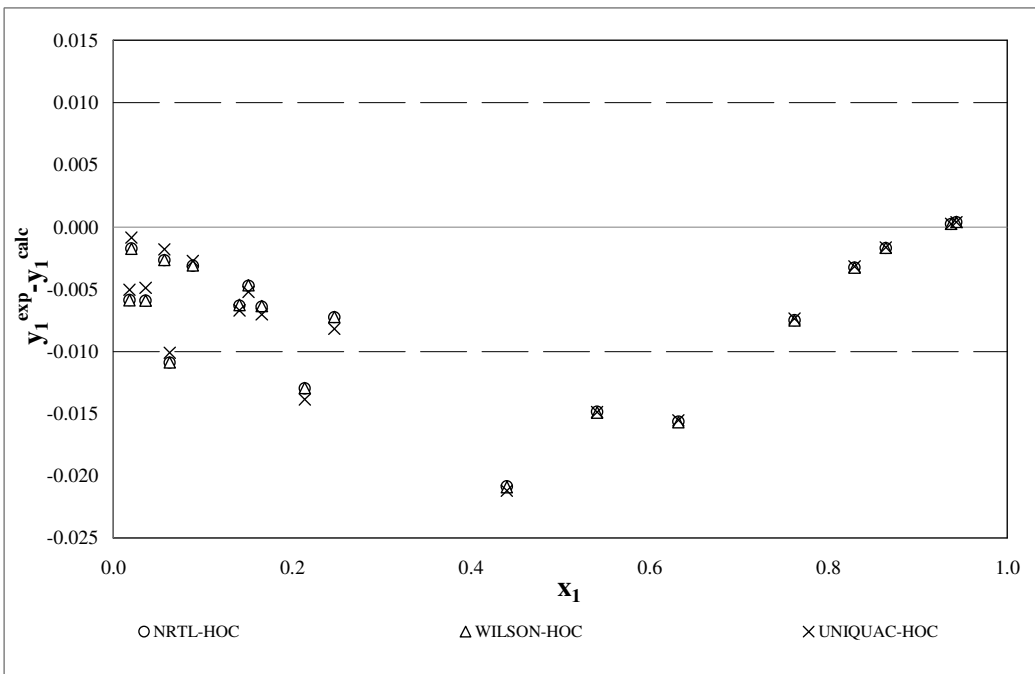


**Figure B-8 Point test (varying activity coefficient model):  $\Delta y_1$  for the 2-propanone (1) + 2-butanol (2) system at 353.15K**

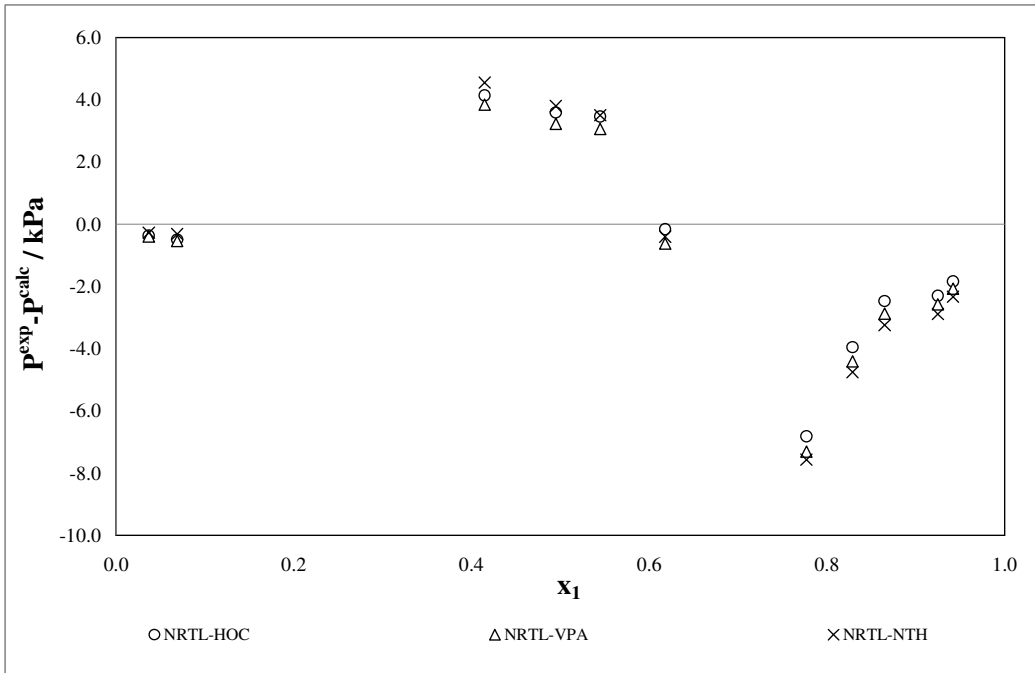


**Figure B-9 Point test (varying EOS): pressure-residual for the 2-propanone (1) + 2-butanol (2) system at 373.15K**

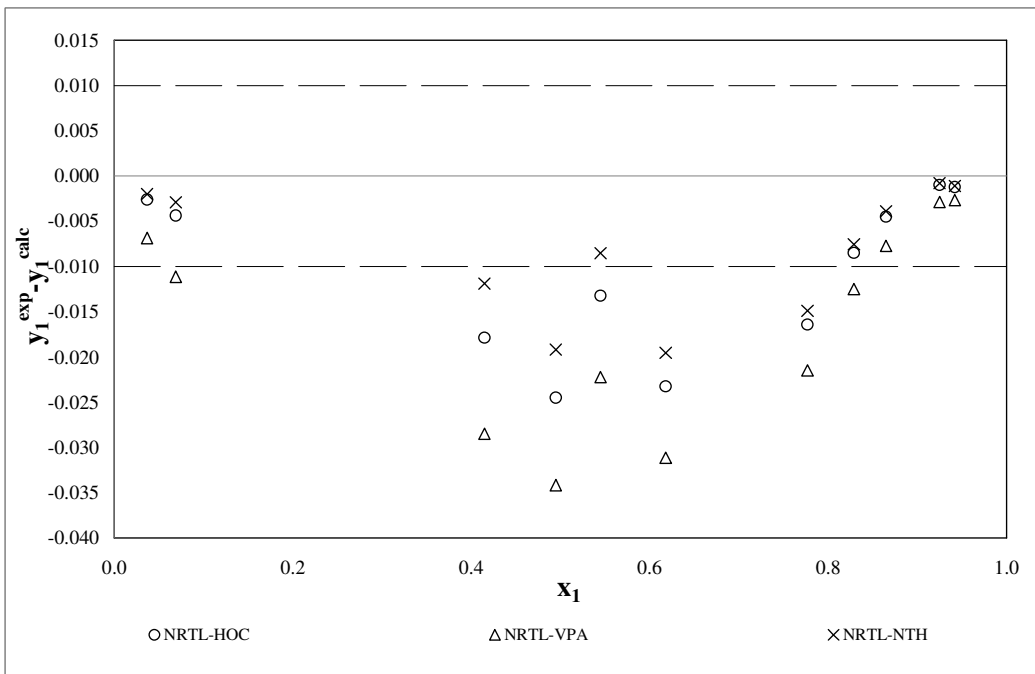


**Figure B-10 Point test (varying EOS):  $\Delta y_1$  for the 2-propanone (1) + 2-butanol (2) system at 373.15K**

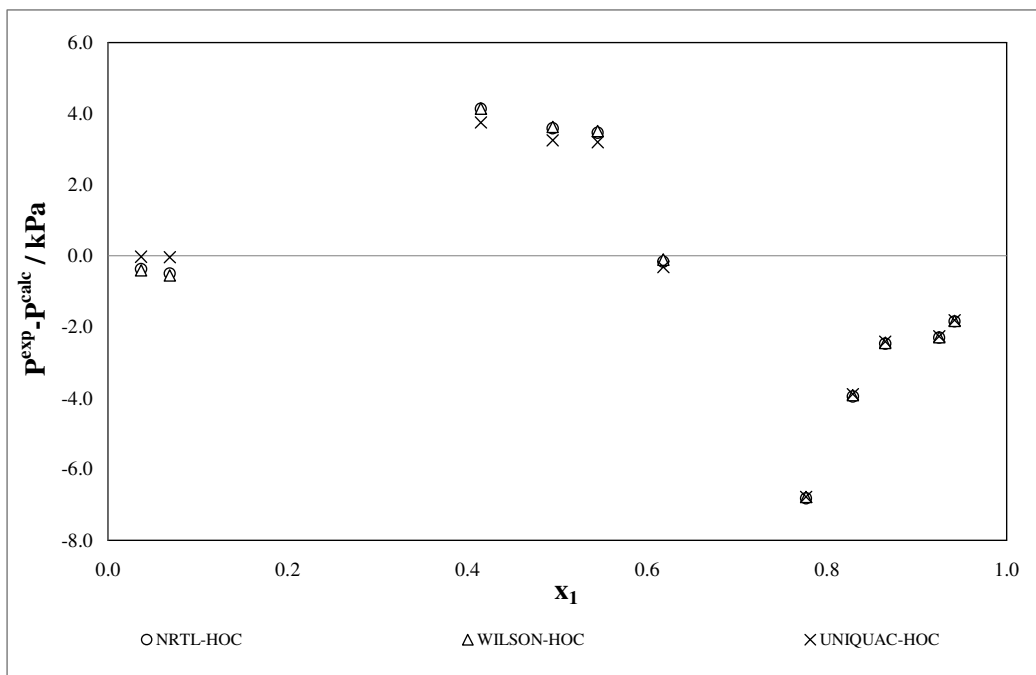


**Figure B-11 Point test (varying activity coefficient model): pressure-residual for the 2-propanone (1) + 2-butanol (2) system at 373.15K**

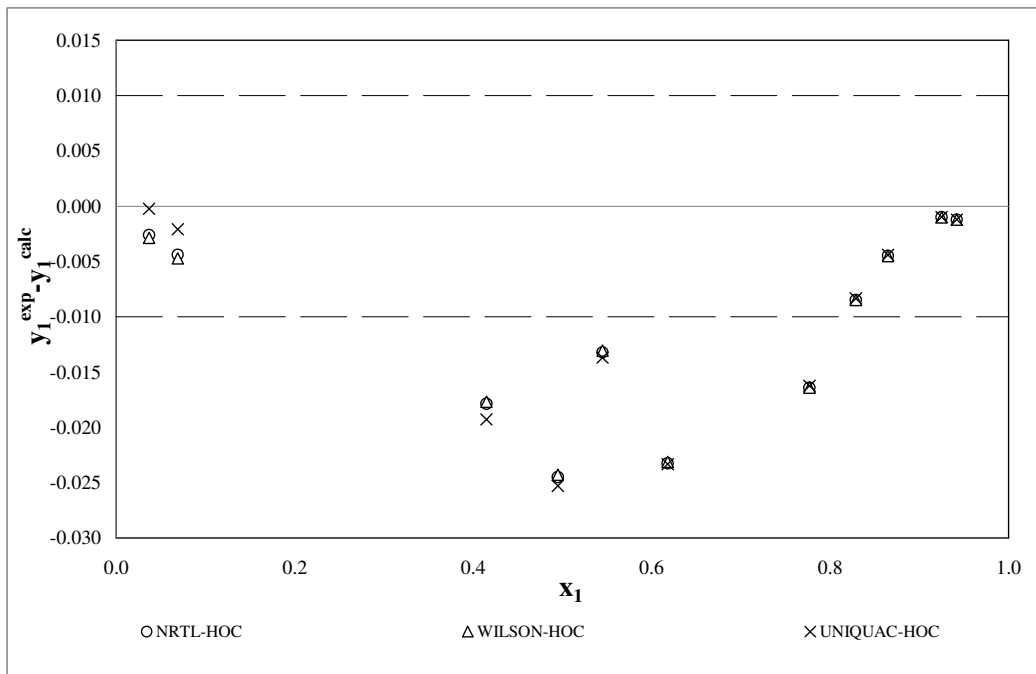


**Figure B-12 Point test (varying activity coefficient model):  $\Delta y_1$  for the 2-propanone (1) + 2-butanol (2) system at 373.15K**

**B.2. Results for the system: 2-propanone (1) + n-propanoic acid (2)**

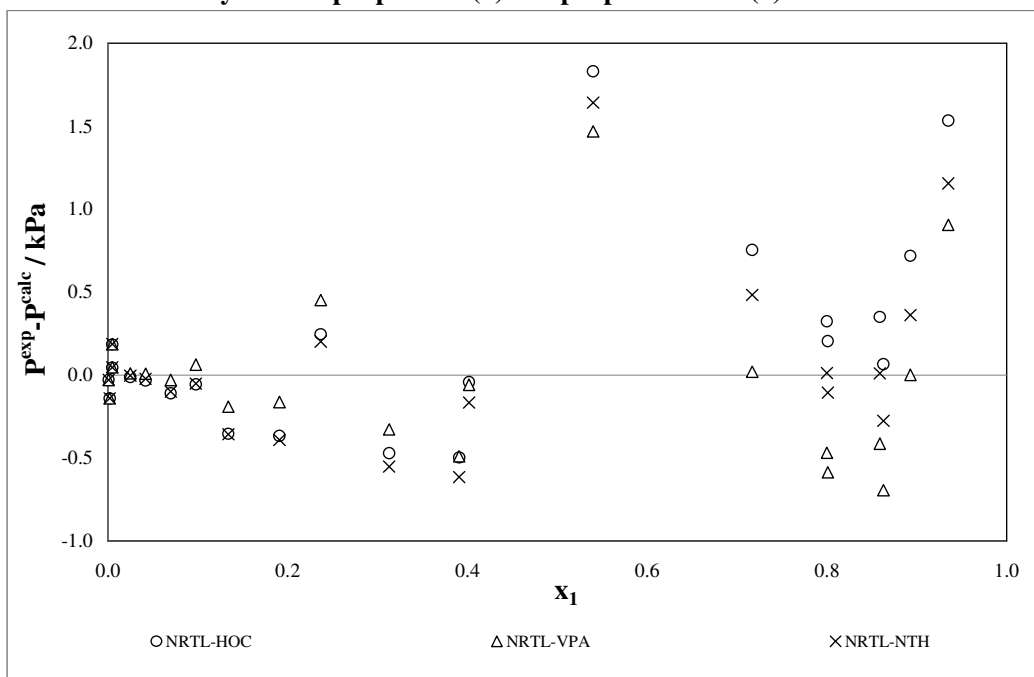


**Figure B-13 Point test (varying EOS): pressure-residual for the 2-propanone (1) + n-propanoic acid (2) system at 333.15K**

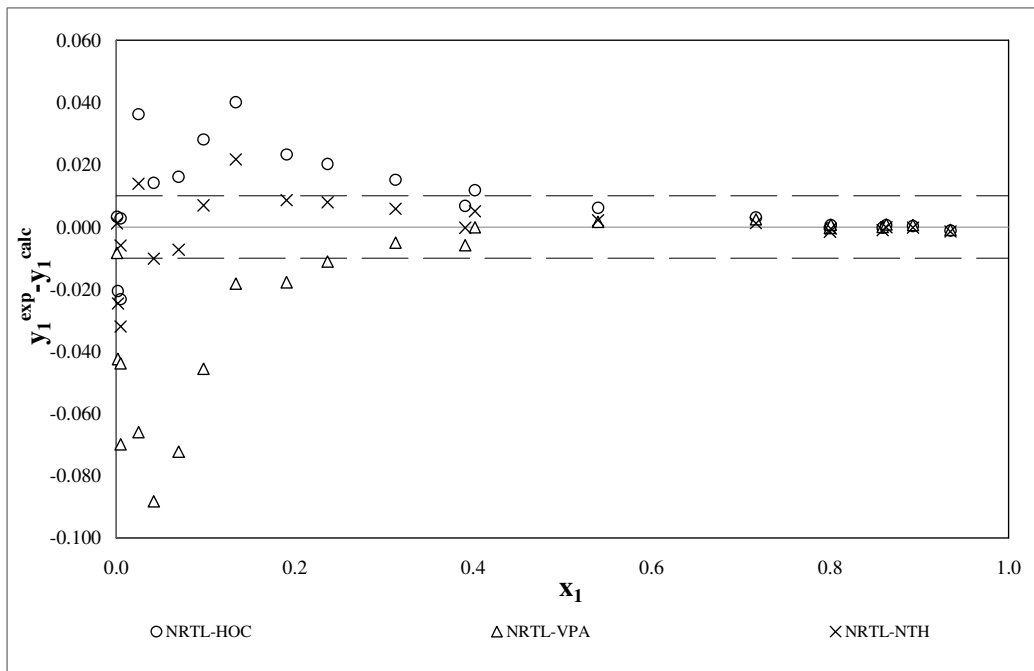


**Figure B-14 Point test (varying EOS):  $\Delta y_1$  for the 2-propanone (1) + n-propanoic acid (2) system at 333.15K**

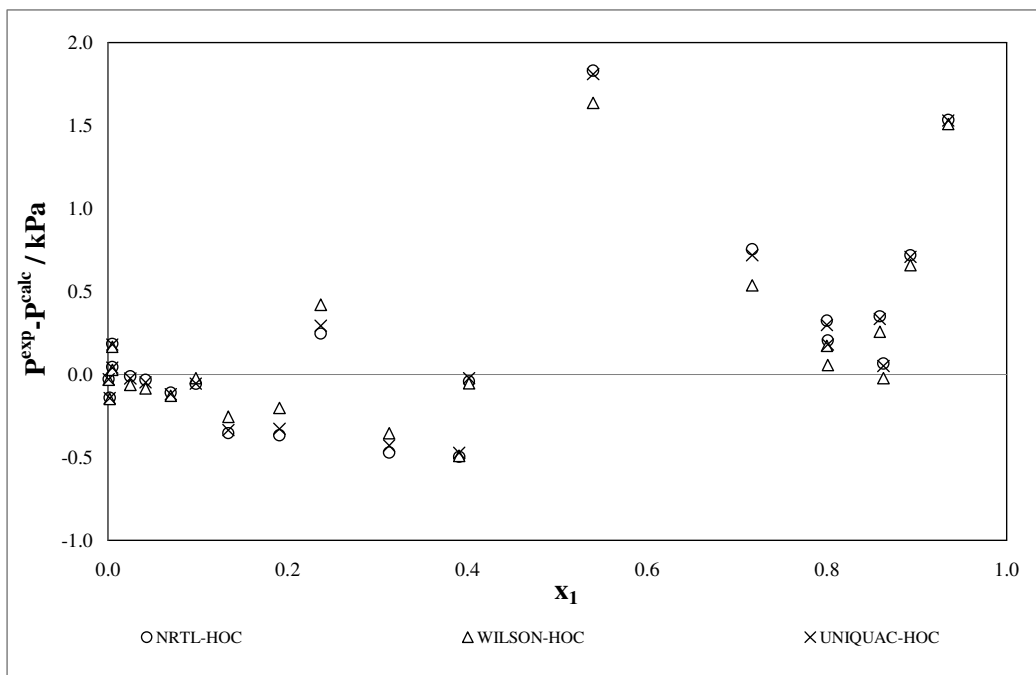


**Figure B-15 Point test (varying activity coefficient model): pressure-residual for the 2-propanone (1) + n-propanoic acid (2) system at 333.15K**

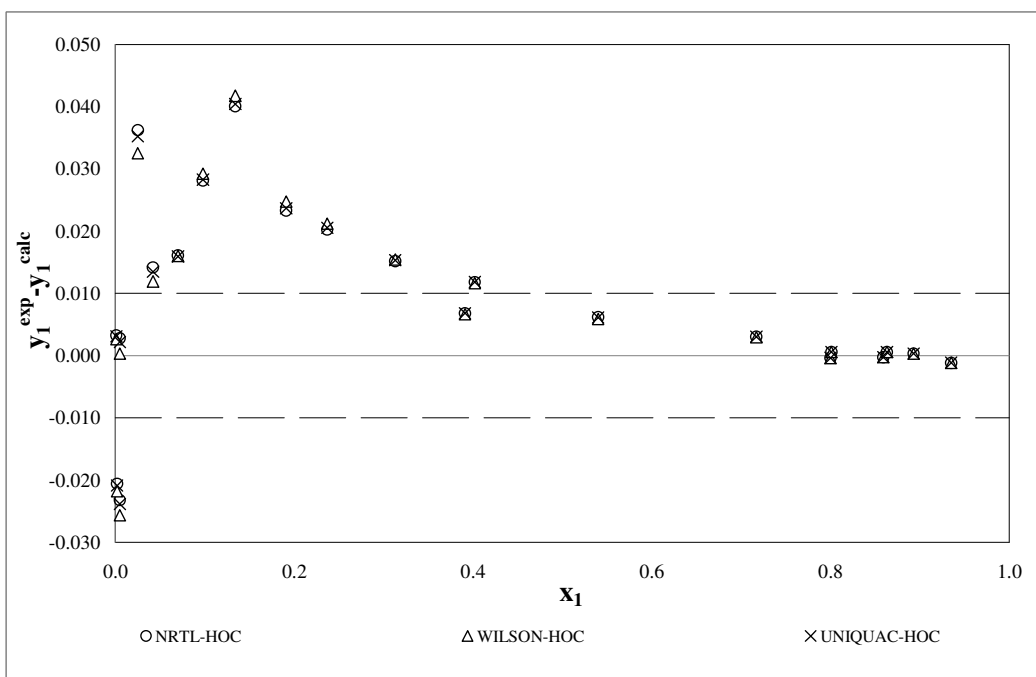


**Figure B-16 Point test (varying activity coefficient model):  $\Delta y_1$  for the 2-propanone (1) + n-propanoic acid (2) system at 333.15K**

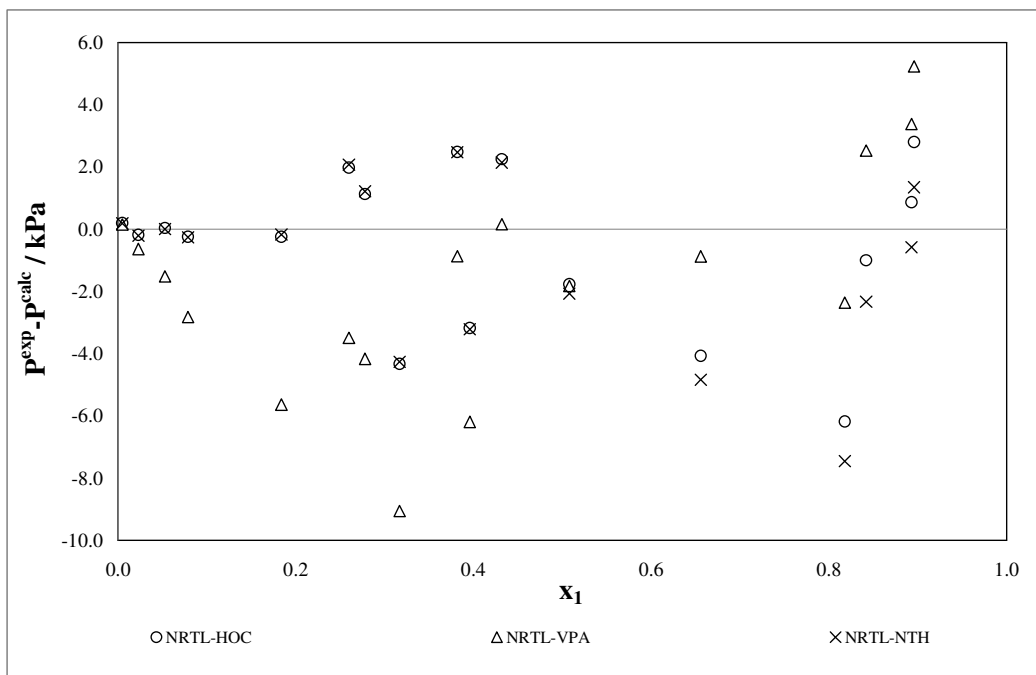


**Figure B-17 Point test (varying EOS): pressure-residual for the 2-propanone (1) + n-propanoic acid (2) system at 353.15K**

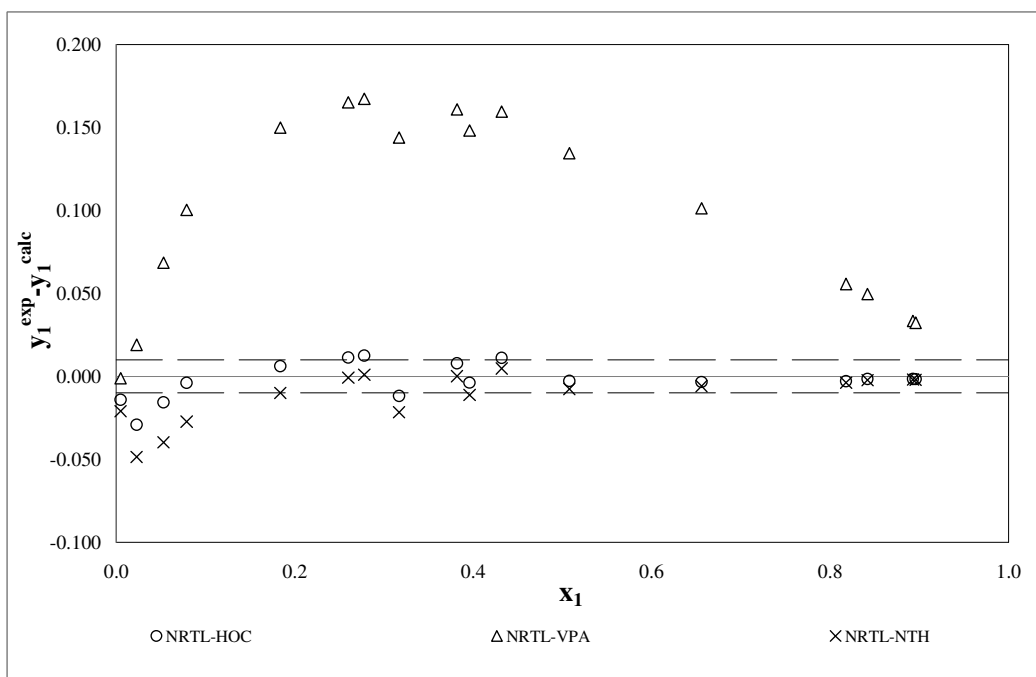


**Figure B-18 Point test (varying EOS):  $\Delta y_1$  for the 2-propanone (1) + n-propanoic acid (2) system at 353.15K**

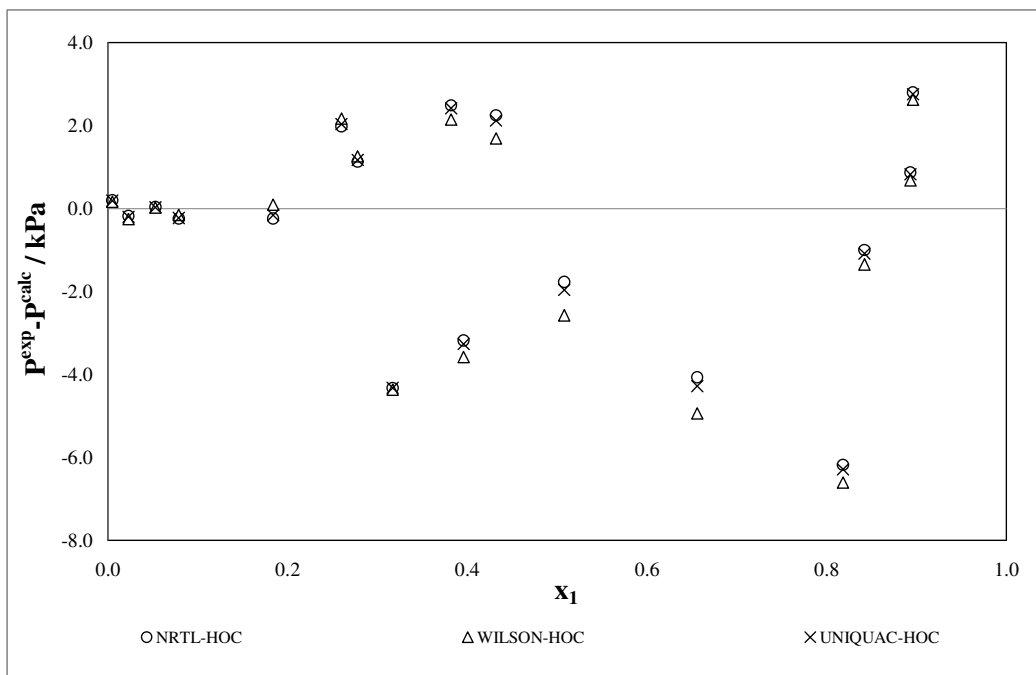


**Figure B-19 Point test (varying activity coefficient model): pressure-residual for the 2-propanone (1) + n-propanoic acid (2) system at 353.15K**

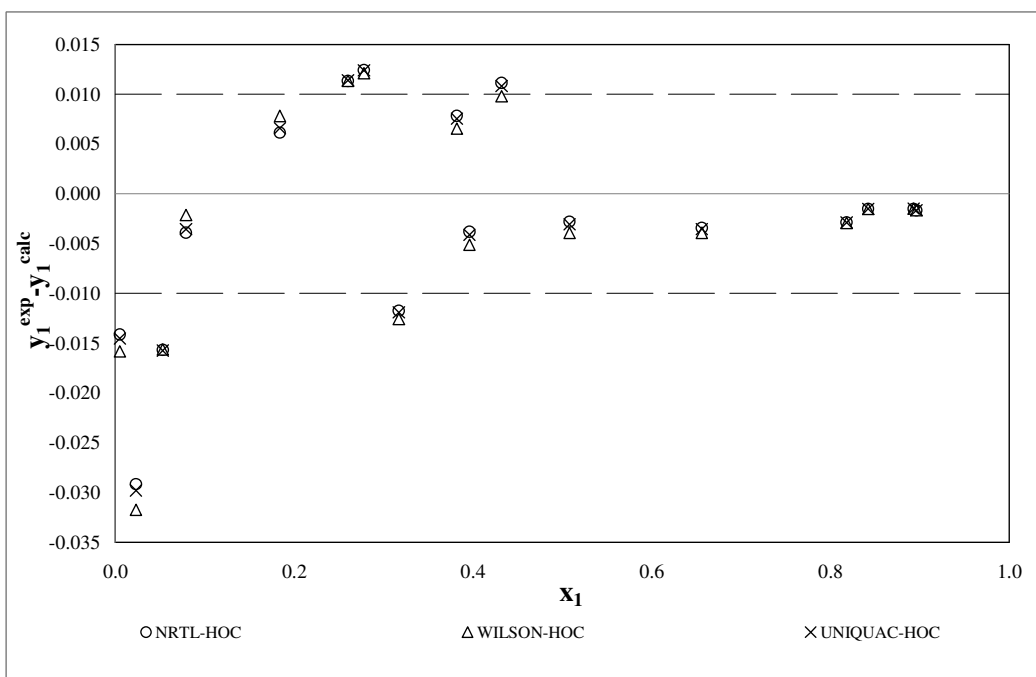


**Figure B-20 Point test (varying activity coefficient model):  $\Delta y_1$  for the 2-propanone (1) + n-propanoic acid (2) system at 353.15K**

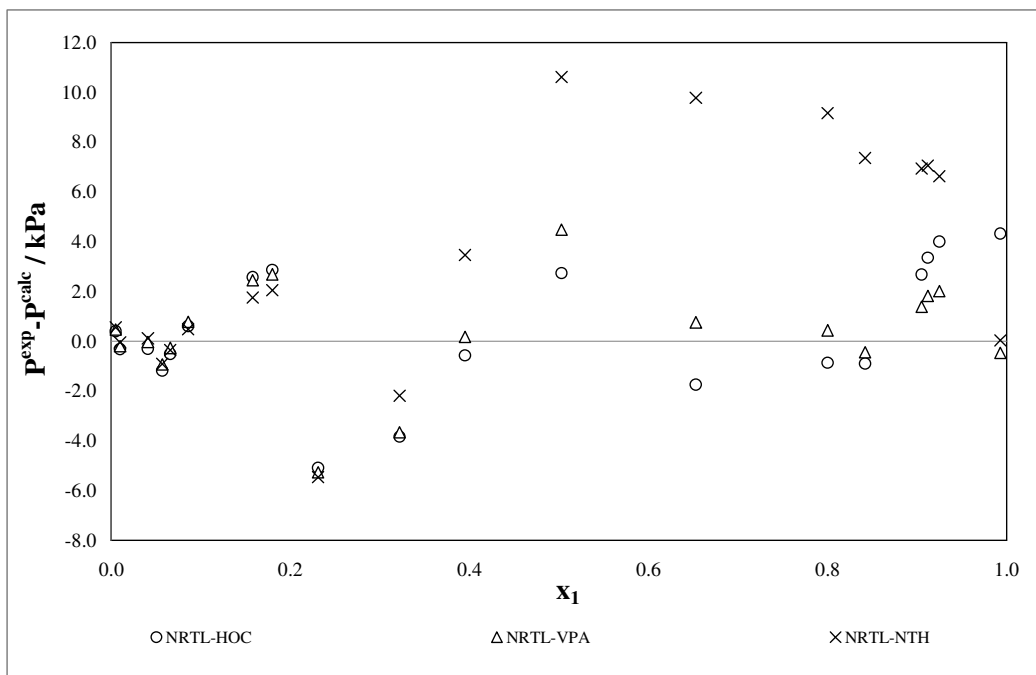


**Figure B-21 Point test (varying EOS): pressure-residual for the 2-propanone (1) + n-propanoic acid (2) system at 373.15K**

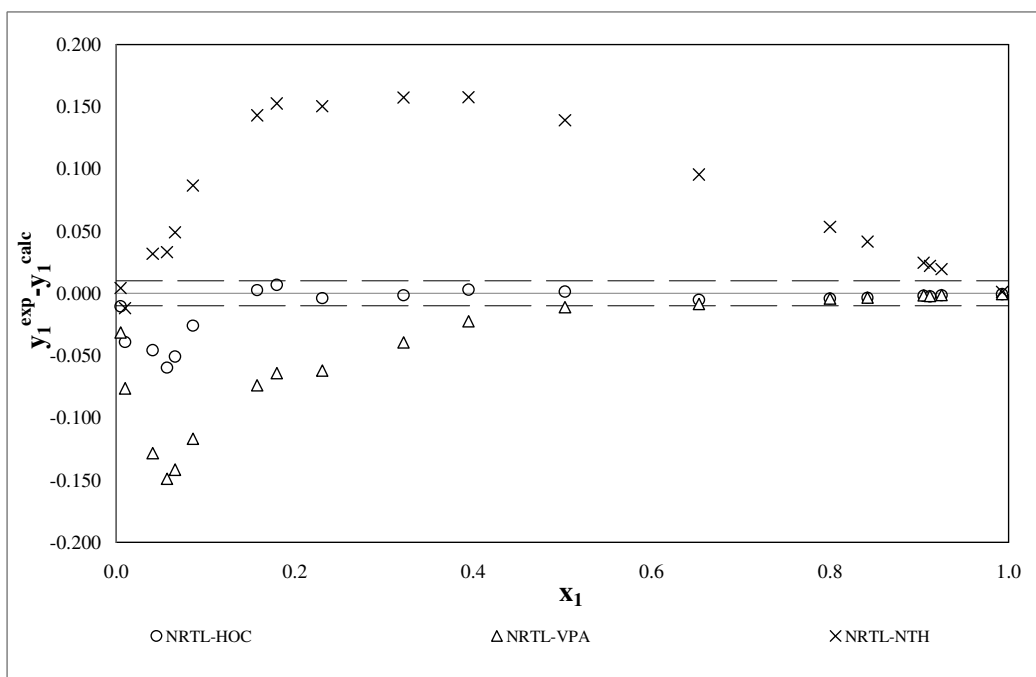


**Figure B-22 Point test (varying EOS):  $\Delta y_1$  for the 2-propanone (1) + n-propanoic acid (2) system at 373.15K**

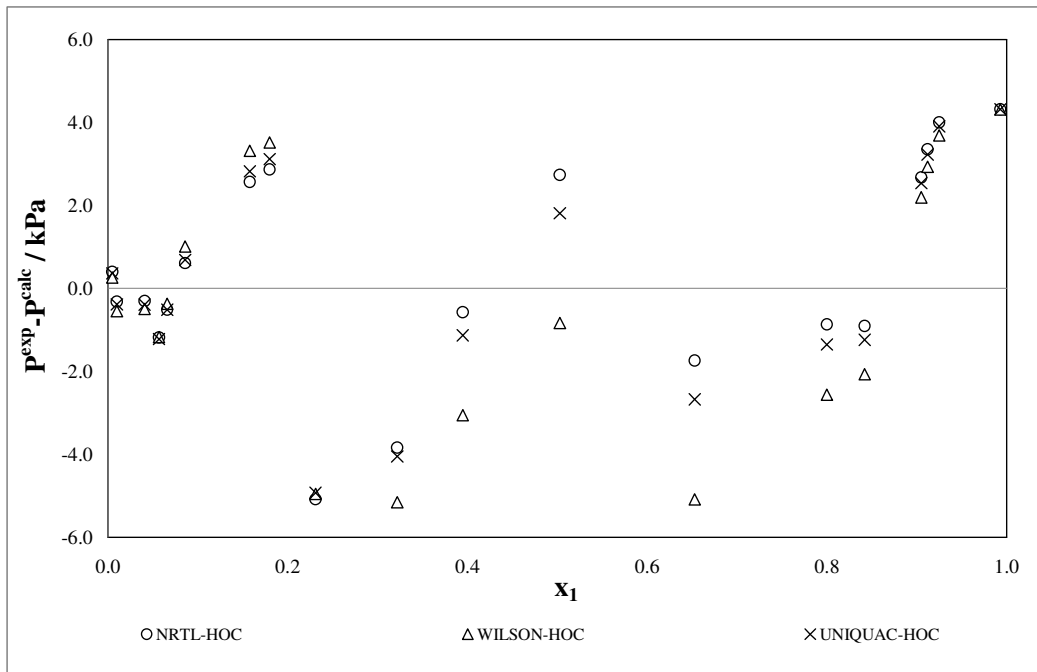


**Figure B-23 Point test (varying activity coefficient model): pressure-residual for the 2-propanone (1) + n-propanoic acid (2) system at 373.15K**

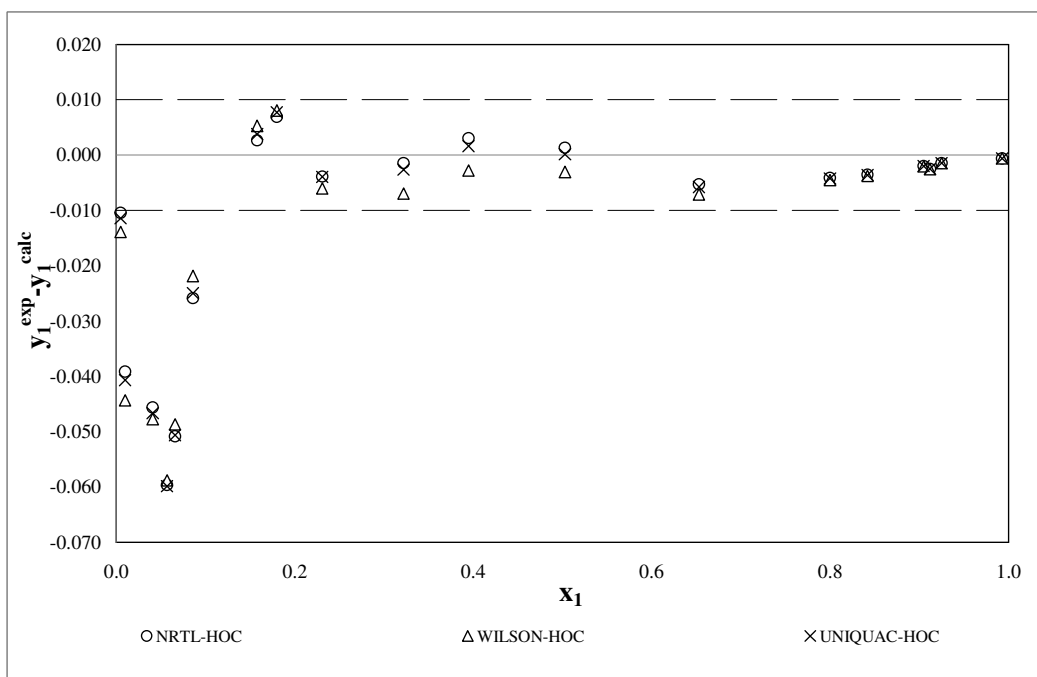


**Figure B-24 Point test (varying activity coefficient model):  $\Delta y_1$  for the 2-propanone (1) + n-propanoic acid (2) system at 373.15K**

**B.3. Results for the system: 1-propanol (1) + n-butanoic acid (2)**

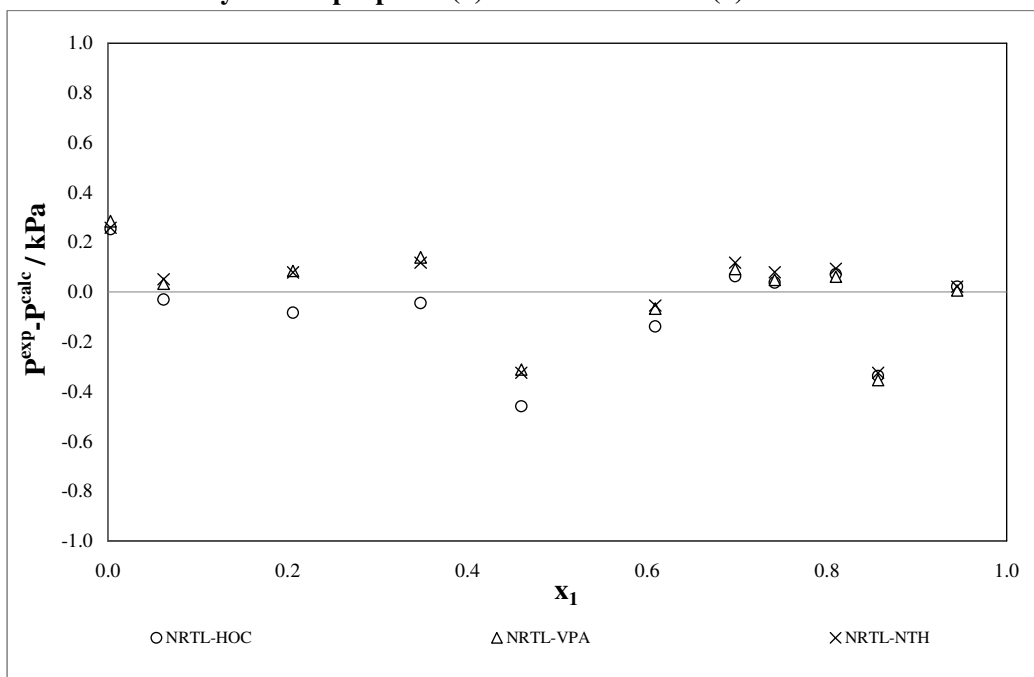


**Figure B-25 Point test (varying EOS): pressure-residual for the 1-propanol (1) + n-butanoic acid (2) system at 333.15K**

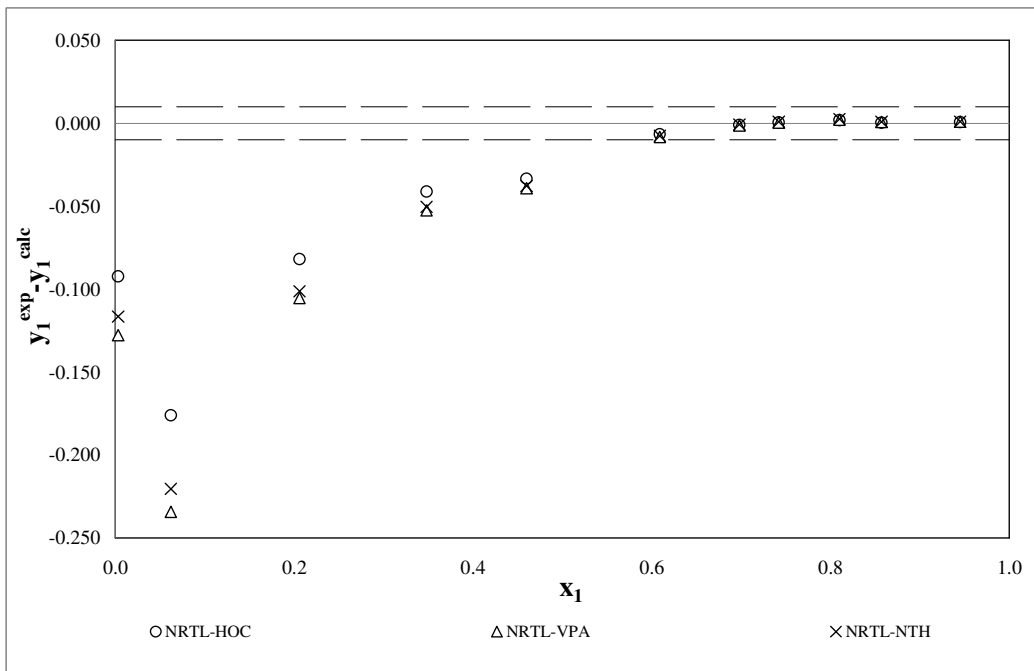


**Figure B-26 Point test (varying EOS):  $\Delta y_1$  for the 1-propanol (1) + n-butanoic acid (2) system at 333.15K**

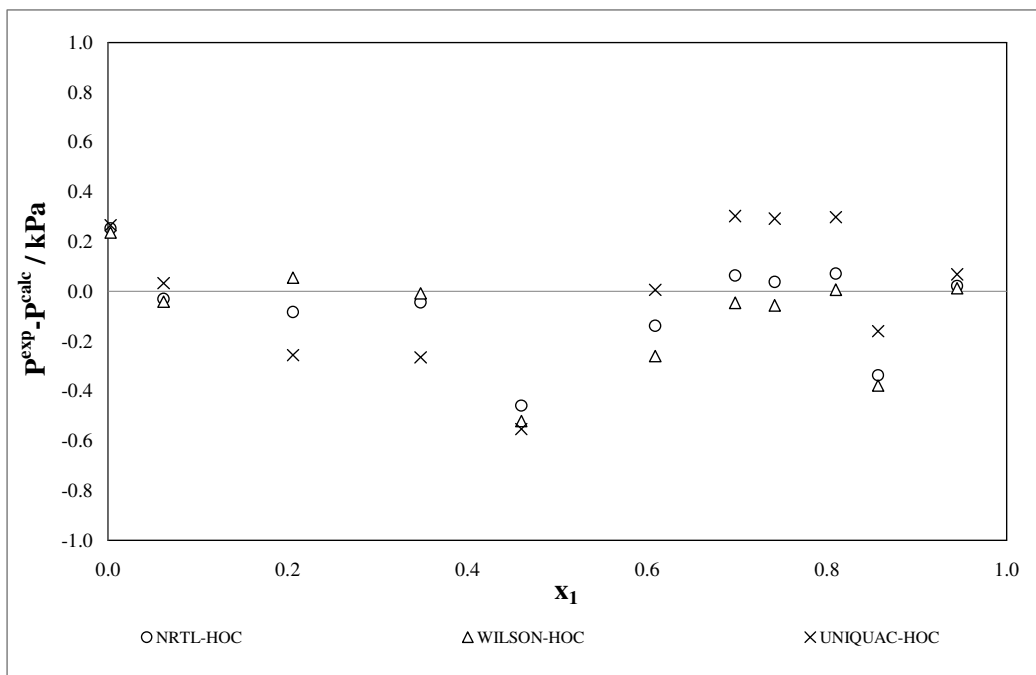


**Figure B-27 Point test (varying activity coefficient model): pressure-residual for the 1-propanol (1) + n-butanoic acid (2) system at 333.15K**

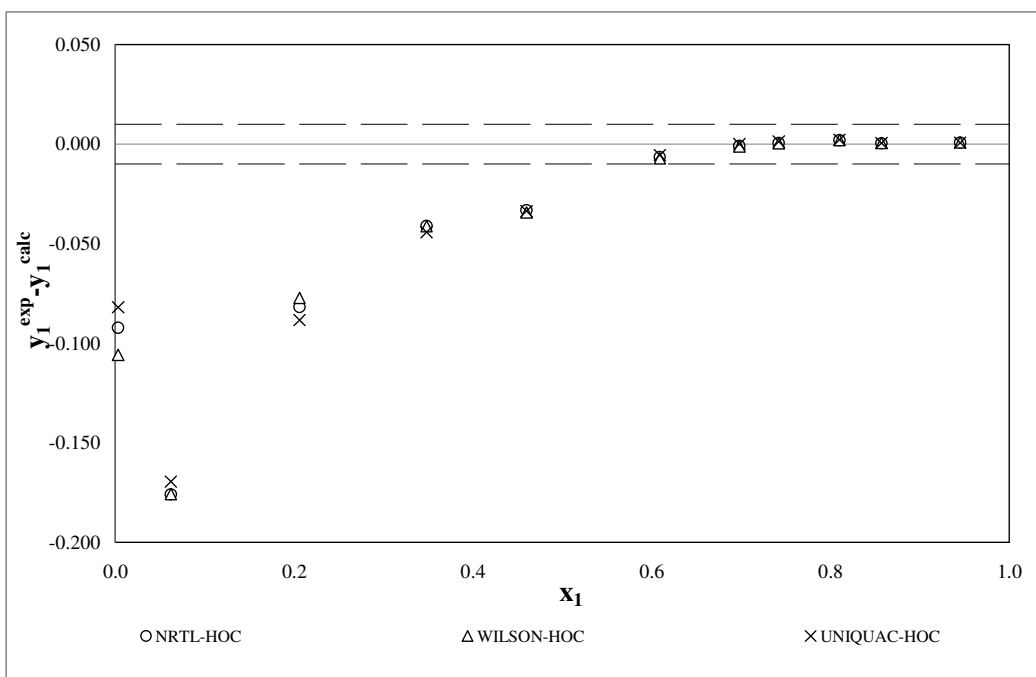


**Figure B-28 Point test (varying activity coefficient model):  $\Delta y_1$  for the 1-propanol (1) + n-butanoic acid (2) system at 333.15K**

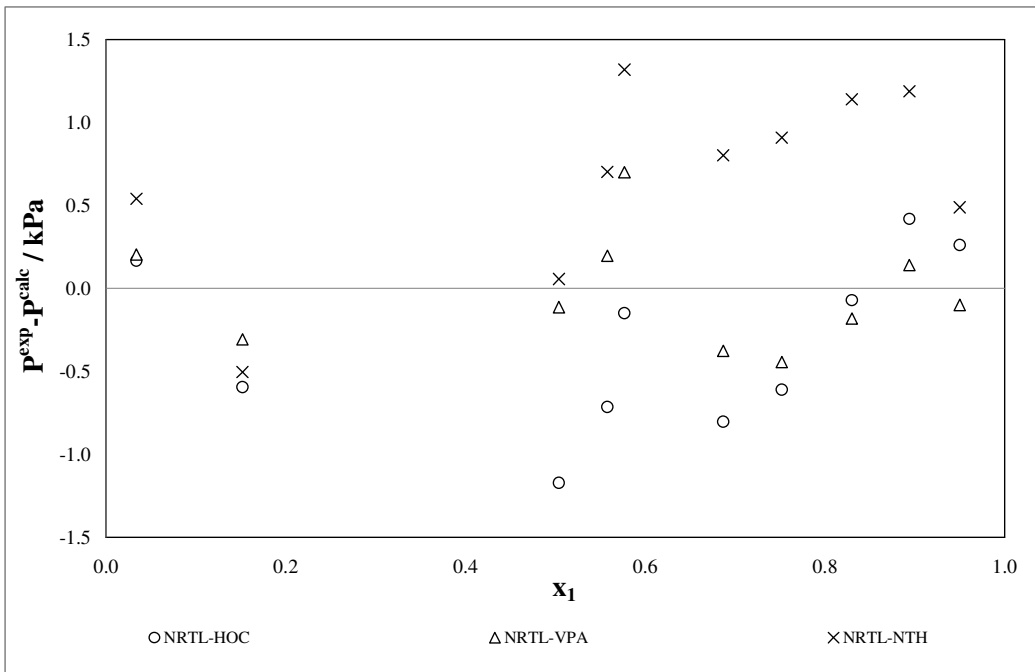


**Figure B-29 Point test (varying EOS): pressure-residual for the 1-propanol (1) + n-butanoic acid (2) system at 353.15K**

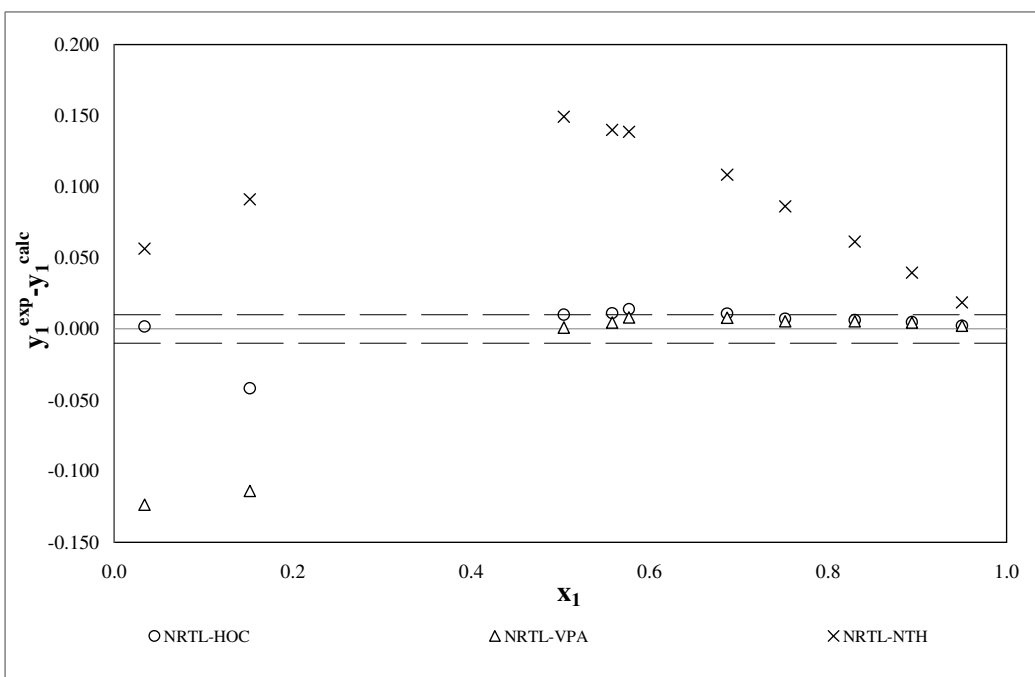


**Figure B-30 Point test (varying EOS):  $\Delta y_1$  for the 1-propanol (1) + n-butanoic acid (2) system at 353.15K**

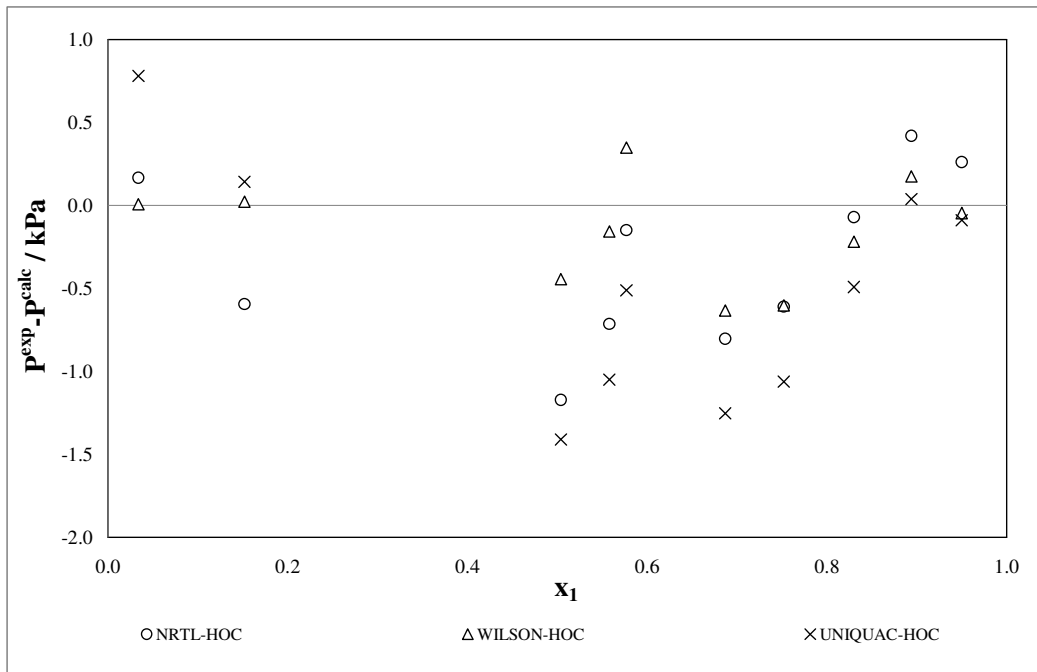


**Figure B-31 Point test (varying activity coefficient model): pressure-residual for the 1-propanol (1) + n-butanoic acid (2) system at 353.15K**

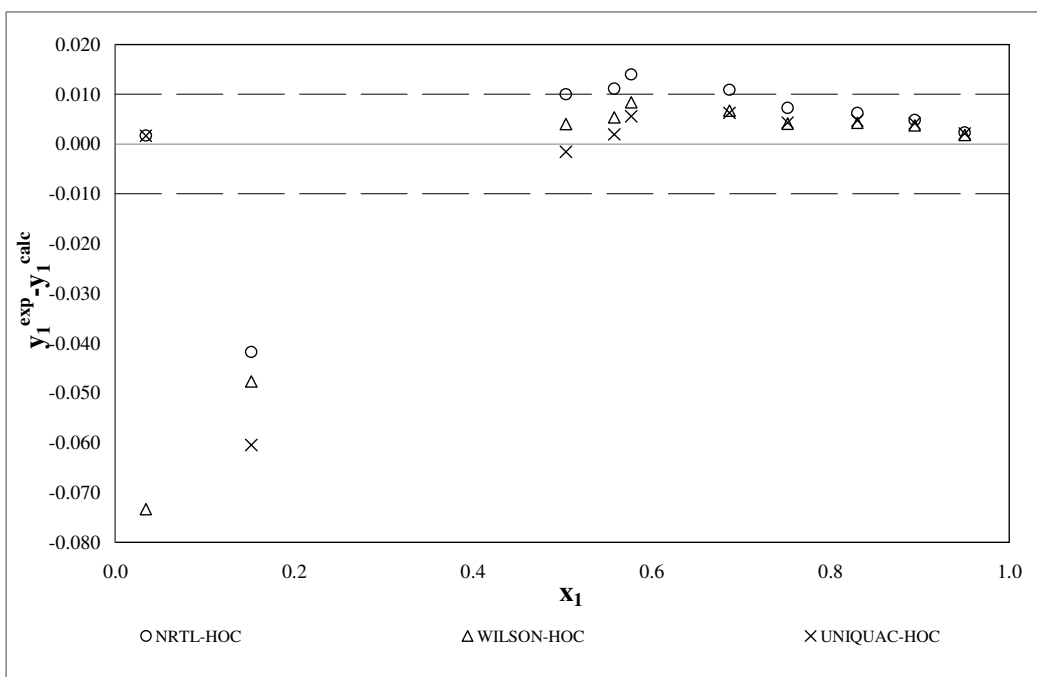


**Figure B-32 Point test (varying activity coefficient model):  $\Delta y_1$  for the 1-propanol (1) + n-butanoic acid (2) system at 353.15K**